# TRIFLING MATTERS: DIFFERENTIAL REGULATION OF FEEDFORWARD AND FEEDBACK INTERNEURONS OF THE DENTATE GYRUS BY RELEASE OF ENDOGENOUS NOREPINEPHRINE



ROBERT ARTHUR BROWN

*Your file Votre référence*
*ISBN: 0-612-93077-7*
*Our file Notre référence*
*ISBN: 0-612-93077-7*

# TRIFLING MATTERS: DIFFERENTIAL REGULATION OF FEEDFORWARD AND FEEDBACK INTERNEURONS OF THE DENTATE GYRUS BY RELEASE OF ENDOGENOUS NOREPINEPHRINE

by

© Robert Arthur Brown

A thesis submitted in partial fulfillment of
the requirements for the degree of

Doctor of Philosophy

Department of Psychology

Memorial University of Newfoundland

June 2003

St. John's Newfoundland

# Abstract

TRIFLING MATTERS: DIFFERENTIAL REGULATION OF FEEDFORWARD AND FEEDBACK INTERNEURONS OF THE DENTATE GYRUS BY RELEASE OF ENDOGENOUS NOREPINEPHRINE

Norepinephrine is known to play an important role in hippocampal function. Norepinephrine is required for long-term potentiation in dentate gyrus, and norepinephrine blockade or depletion can interfere with acquisition and retrieval in hippocampal dependent tasks. While gross measures of hippocampal function such as evoked potentials demonstrate plastic changes under the influence of norepinephrine, single unit studies to date report suppression of principle cell firing and increased firing rates for inhibitory interneurons. Such changes should reflect an increase in inhibition and would predict a decrease in plasticity.

In this thesis I examine the effect of "natural" synaptic release of norepinephrine on spontaneous firing rates of cells in dentate gyrus, with concomitant electroencephalographic recording. Physiologically identified interneurons are classified as either feedforward or feedback depending on whether they were activated prior to, or after, the perforant path evoked population spike. Principle cells are identified by their characteristic firing properties and a firing latency within the window of the perforant path evoked population spike.

In this study feedforward interneurons virtually cease firing in response to synaptic release of norepinephrine, producing a period of disinhibition which lasts several minutes. Simultaneously, cells identified as principle cells increase their firing rates. Feedback interneurons demonstrated a mixed profile with some cells increasing their firing rates and others decreasing their firing rates.

Fast Fourier analysis of the electroencephalographic recordings revealed a increase in relative power in the theta band as reported previously, together with a decrease in overall power and a decrease in relative power of the gamma band. These data are compared to previous studies of noradrenergic effects on single unit, evoked potential, and electroencephalography measures in the literature. The results are also compared to existing models of plasticity such as long-term potentiation and gamma power regulated acquisition and recall of hippocampal representations. Finally a new framework is proposed as to how norepinephrine may play a role in plasticity by allowing new information to be bound to mature hippocampal representations.

hilum:

(ˈhaɪləm) [L. *hīlum* little thing, trifle; according to Festus, thought to have orig. meant 'that which adheres to a bean'; hence in modern Botanical use (see 2).]

**1.** Something very minute. *Obs.*

**1659** D. PELL *Impr. Sea* 44 Unhewn Sailors, that have no more than a meer hilum of goodness in them.

**2.** *Bot.* The point of attachment of a seed to its seed-vessel; the scar on the ripe seed.

**1753** CHAMBERS *Cycl. Supp.*, *Hilum*, a word used by botanists to express the blackish spot in beans, commonly called by us the eye of the bean. **1830** LINDLEY *Nat. Syst. Bot.* 115 Seeds..with a smooth shining coat, and a broad pale hilum. **1880** GRAY *Struct. Bot.* vi. §8. 277 In the simplest form of ovule, hilum and chalaza are one.

**b.** A similar mark on a starch-granule. **c.** 'The aperture in the extine of a pollen grain' (*Syd. Soc. Lex.*).

**1867** J. HOGG *Microsc.* II. i. 341 Most of the granules [of starch] have a circular spot, termed the hilum, around which a large number of curved lines arrange themselves.

**3. a.** *Anat.* = hilus 'Applied also to certain small apertures and depressions' (*Syd. Soc. Lex.*). **b.** *Path.* 'A term for a small flattened staphyloma of the iris from corneal perforation, in consequence of its likeness to the hilum of the garden bean' (*Syd. Soc. Lex.*). **c.** A little opening in the statoblast of a sponge.

**1887** SOLLAS in *Encycl. Brit.* XXII. 424 (*Sponges*) On one side of the capsule is a hilum which leads into the interior.

The Oxford English Dictionary 2nd ed. 1989, Oxford University Press

TABLE OF CONTENTS

# LIST OF FIGURES

LIST OF TABLES

# ACKNOWLEDGMENTS

A great many people, all of whom deserve high praise here at the beginning, have contributed to the completion of my program. I have benefited from the collective wisdom and enthusiasm of my colleagues, professors, family and friends. Without their support this process would never have been brought to fruition. .

My supervisor, Dr. Carolyn Harley, has been encouraging of all my endeavors, whether or not they were related to my program of study. I only hope that I can emulate her warmth and genuine personal regard with my own students.

Dr. John Evans has been an inspiration. His passion for science is eclipsed perhaps only by his desire to see paperwork completed accurately and in a timely fashion. His confidence has helped carry me through my own periods of doubt. Dr. Detlef Bieger spent many patient hours reading papers with me, translating gnarled German into elegant English prose. Dr. Gilbert Kirouac has been a great resource for the manipulation of the axoclamp 2a in particular and everything else in general.

My lab-mates have endured my music, musings, and occasionally erratic behaviour with good grace. In particular I wish to thank Susan Walling, whose graduate career has paralleled my own, and Cordell Clarke, who taught me the basics of cell recording. Data would have never been collected without the advice and trouble-shooting expertise of Mr. Steve Milway. Mr. Avery Earle scripted the custom data analysis routines, solved many a problem with hardware, software, sometimes wetware and has shown me that 1 and 0 do more than add to 1.

The staff at Bitter's (sometimes referred to as my living room) have both aided and impeded my progress by treating me as one of the family. A special thank you to Doug Gorman for keeping the place running so I could have somewhere to go after journal club.

No list of thank-yous would be complete without acknowledging Drs. Paul Frankland and John Yeomans whose tutelage pushed me towards graduate school..

My parents, Eleanor and Roy Brown, and my siblings have been full of enthusiasm and encouragement. I believe that in their eyes this degree is the equivalent of the Nobel Prize, and almost as unlikely. Marina Osborne has been invaluable for her unflagging interest in my progress, in addition to her assistance with the more mundane tasks of helping my wife and I keep house and amuse the dog.

My wife, Sheila Osborne-Brown, has of course borne the brunt of these years in graduate school. She has supported me in every way and has never stopped believing that this path was the right one for us to travel; even when it has meant sacrifices in her own career as she follows me about the continent. Her belief in me has allowed me to do things I might never have otherwise attempted. If she had not come into my life all those years ago I might still be nailing shingles.

# LIST OF ABBREVIATIONS

| | |
|---|---|
| A | amperes |
| AHP | afterhyperpolarization |
| AMPA | alpha-amino-3-hydroxy-5-methylisoxazole-4-propionate |
| ASCII | american standard code for information interchange |
| CA | cornu ammonis |
| cAMP | cyclic-adenosine-mono-phosphate |
| DAB | diamino benzene(?) |
| DG | dentate gyrus |
| DSP-4 | N- (2-chlorethyl)-ethyl-2-bromobenzylamine |
| EEG | electroencephalograph |
| EP | evoked potential |
| EPSP | excitatory post-synaptic potential |
| GABA | gamma-aminobutryric acid |
| Ga | gauge |
| Hz | Hertz |
| IPSP | inhibitory post-synaptic potential |
| LTP | long-term potentiation |
| M | mol |
| ml | millilitre |
| mm | millimetre |
| ms | millisecond |
| NA | noradrenaline |
| nA | nanoampere |
| NMDA | n-methyl-D-aspartate |
| PBS | phosphate buffered saline |
| PKA | protein kinase A |
| s | seconds |
| SLM | stratum lacunosum moleculare |
| UFF | universal file format |
| V | volts, voltage |
| Ω | ohm |

*Microelectrode recording during stimulation of the NA [noradrenaline] system in the mesencephalon or elsewhere will become possible as soon as the course and origin of the fibres are defined. The hilus, where the amount of NA fibres is highest, should be the place of choice to start such attempts.*

*--Blackstad, Fuxe and Hökfelt 1967*

## Introduction

Blackstad et al. believed that noradrenaline, or norepinephrine, fibres regulated excitability in the hippocampus, a role distinct from the glutamate containing fibres. As the quotation suggests they assumed that norepinephrine effects would be particularly distinct in the hilar segment of the dentate gyrus of hippocampus. Several laboratories have investigated the effect of norepinephrine on firing rates of single cells in the hippocampus using electrical stimulation of norepinephrine fibers (Segal and Bloom 1974b), or application of exogenous norepinephrine (Segal and Bloom 1974a, Pang and Rose 1987, Rose and Pang

1989, Bijak and Misgeld 1995, Bergles et al. 1996, Parra et al. 1998) and these studies have agreed that norepinephrine, in general, inhibits principal cells of the hippocampus and excites interneurons. While consistent with each other, these conclusions are at odds with biochemical measures (Parfitt et al. 1991) and evoked potential recordings in the hippocampus (Neuman and Harley 1983) that suggest norepinephrine promotes excitation of principal cells. The present thesis characterizes the effects of release of endogenous norepinephrine on interneurons of the hilar region subjacent to the dentate gyrus. Norepinephrine release is evoked using glutamate applied to the norepinephrine cells of origin, the locus coeruleus, to produce a pattern that mimics the burst release pattern of norepinephrine in the behaving animal. In setting the context for these investigations, I review the structure and connectivity of the hippocampus and the locus coeruleus and previous investigations of norepinephrine effects, with a particular focus on the hilar region.

The hippocampus is involved in the integration of information originating in sensory and associational cortices. Numerous studies have hypothesized a role for the hippocampus in learning and the formation of memory traces. Current models of learning mechanisms such as long-term potentiation (LTP) were developed in hippocampus (Bliss and Lømø 1973).

The hippocampus is driven by afferent systems carrying information from three major sources. The perforant path carries information from two of these sources. Polymodal sensory information is conveyed from the lateral entorhinal

cortex via the lateral perforant path, and cortical-associational information is conveyed by the medial perforant path (Burwell 2000), which originates in medial entorhinal cortex. In addition to these glutamatergic projections, subcortical neuromodulatory pathways influence the processing of the hippocampal network depending upon the motivational, emotional, and autonomic state of the animal. The norepinephrine system arising from the locus coeruleus is one such system (Harley 1998). Despite consisting of only a few thousand cells, the locus coeruleus is able to influence the functioning of the hippocampal network as indexed through behavioural (e.g. Sara et al. 1995), electrophysiological (e.g. Harley and Milway 1986) and biochemical (e.g. Parfitt et al. 1991) assays. The locus coeruleus responds to a variety of environmental stimuli and the activity of locus coeruleus neurons correlates with the animal's level of arousal (Aston-Jones and Bloom 1981a). In particular the locus coeruleus responds to novelty and environmental change (Sara and Segal 1991).

Learning is considered to be mediated by a change in synaptic weights resulting from the coincident activity of neurons (Bailey et al. 2000). A critical feature of this type of plasticity is the pairing of postsynaptic depolarization with synaptic activation (Deisseroth et al. 1996). Synaptic activation causeing a long slow depolarization event which maximizes inward $Ca^{++}$ flow (Mermelstein et al. 2000). Events or compounds which depolarize neurons are considered to promote synaptic efficacy while hyperpolarizing agents decrease efficacy (Wigström and Gustafsson 1983a, b). Current theories hold that synaptic weight can be altered in

the short term by kinase activity phosphorylating local proteins in the synaptic region to alter their efficacy (Malenka and Siegelbaum 2000). Both the activity of neuromodulatory receptors and the translation of new proteins are required for changes of synaptic weight that last several hours (Kandel 2001). The role that neuromodulators play within these theories is more controversial than the role of new proteins.

Synaptic modification that is long lasting requires the translation of proteins that are believed to play a role in remodeling the synapse. Frey and Morris (1997) have proposed that neuromodulators binding to their receptors set a "tag" that marks a synapse as requiring proteins. Abel et al. (1998) have suggested that neuromodulators play a role in relieving inhibitory constraints on transcription. Neuromodulatory receptors may also play a role in disinhibition, which would allow prolonged depolarization and repeated firing of principal cells, conducive to LTP, by decreasing the GABAergic drive from inhibitory interneurons (Wigström and Gustafsson 1983c, Buzsaki 1984) and decreasing the after hyperpolarization (Haas and Rose 1987).

A disinhibitory role of neuromodulators is consistent with two new and complementary views of synaptic plasticity. First, it has been proposed by Pike et al. (1999) that long-term changes require bursting of the postsynaptic cell. Bursting produces a prolonged depolarization with different dynamics than the dendritic spike produced by a single back-propagating action potential. Other work has shown that repeated synaptic activation is necessary for the

phosphorylation of cyclic adensosine-monophosphate binding protein (CREB) (Deisseroth et al. 1996).

The second view (Bailey et al. 2000) proposes that all associative potentiation requires a heterosynaptic component. In contrast to classical Hebbian potentiation where increases in synaptic strength is a result of coincident pre and postsynaptic activity, late phase LTP requires the activation of a modulatory input in addition to glutamatergic synaptic activity. The modulatory input in most systems travels in the same fiber bundle as the glutamatergic fibres, and so high frequency electrical stimulation of the fibre bundle induces modulator release in addition to evoking glutamate release. Blockade of neuromodulator receptors prevents late phase LTP in a variety of preparations.

Norepinephrine is known to both increase bursting of target cells (Madison and Nicoll 1986) and significantly depolarize principal cells in the hippocampus (Lacaille and Schwartzkroin 1988). Although such a role for norepinephrine is consistent with the enhancement of evoked potentials by norepinephrine (e.g. Harley and Sara 1992) and with paired pulse evidence of decreased inhibition in the presence of norepinephrine (Leung and Miller 1988), unit recording studies to date agree that norepinephrine increases the activity of interneurons (Pang and Rose 1987, Rose and Pang 1989, Bijak and Misgeld 1995, Bergles et al. 1996, Parra et al. 1998, see also review of Buzsaki 1984). Increased inhibition would be expected to decrease synaptic efficacy (Wigström and Gustafsson 1983a-c).

Behavioral evidence and electrophysiological evidence supports a role for norepinephrine in promoting neural plasticity in the hippocampus. This role of norepinephrine appears inconsistent with the evidence from single unit recordings in the hippocampal circuit which have identified increased inhibitory activity as a primary action of norepinephrine. The present study investigates the response of single units in the hippocampus in the area of densest norepinephrine innervation to release of endogenous norepinephrine elicited by glutamatergic excitation of the locus coeruleus. A brief review of hippocampal anatomy and of the properties of the locus coeruleus and its relationship to the hippocampus and to behavior follows: What is known of noradrenergic modulation in the dentate gyrus specifically and what is known of hilar interneurons is addressed subsequently.

### *Hippocampal Anatomy*

Hippocampal anatomy has traditionally focused on the connections of principal cells. The hippocampus consists of two enfolded cell sheets differing in their organization and principal cell types. Ammon's horn (Cornu Ammonis or CA) is a laminar cortex with the pyramidal cell being the principal cell type. The pyramidal cells occur in a densely packed layer. Pyramidal cells have two dendritic systems: short basal dendrites branch in stratum oriens, whereas a long primary dendrite extends and produces short side branches in strata radiatum and lacunosum moleculare. The dentate gyrus is also a laminar structure with the principal cell being the granule cell. Granule cells occur in a densely packed

layer, but their dendritic arbor projects in a single direction into the molecular layer (see Figure 1).

The hippocampus is classically considered to consist of a trisynaptic loop (Andersen et al. 1971). The entorhinal cortex is the origin of most of the extra-hippocampal afferents and projects to all major subfields of the hippocampus (Witter et al. 2000). Granule cells project to the CA3 pyramidal cells via the mossy fibres, although CA3 receives a direct input from layer II of entorhinal cortex as well. CA3 pyramidal cells project in turn to CA1 pyramidal cells via the Schaffer collaterals with a smaller projection to the septum. CA1 also receives a direct projection from entorhinal cortex, although from layer III. CA1 is considered to be the output of the hippocampus proper. CA1 projects to subiculum and entorhinal cortex with minor projections to higher cortical areas. The glutamatergic afferents to the hippocampal formation are summarized in Figure 2.

*Dentate Gyrus*

The primary input to the dentate gyrus is layer II of entorhinal cortex. Entorhinal cortex projects to the molecular layer of dentate gyrus in a lamellar fashion. Lateral entorhinal cortex projections terminate on the outer one third of the granule cell dendrites; medial entorhinal cortex projections terminate on the middle one third of the dendritic tree (Witter 1993). The inner third of the molecular layer is innervated by interneuron projections arising from the contralateral hippocampus (Amaral et al. 1995) in a point-to-point fashion

(Zappone and Sloviter 2001), back projections from CA3 pyramidal cells (Wu et al. 1998) and hilar mossy cells (Scharfman 1995a) and input from the submammillothalamic nucleus (Pasquier and Reinoso-Suarez 1976, 1978; Harley et al. 1983) (see Figure 3). Recently it has been reported that deeper layers of entorhinal cortex (IV-VI) also send a light projection to dentate gyrus (Deller et al. 1996). These deep fibres travel within the perforant path, but differ in that they lack a laminar distribution in dentate gyrus. The deep fibres drop collaterals from the molecular layer, enter stratum granulosum, and terminate in the subgranular region. The deep fibres form synapses with a variety of cells in all layers that they traverse.

There is a second dimension to the organizational structure of the entorhinal cortex projection to dentate gyrus. The terminal zones of entorhinal cortex layer II cell projections also have a strip or slab-like architecture, in which cells originating from lateral entorhinal cortex project most heavily to the septal pole, with cells originating from the medial entorhinal cortex projecting preferentially to the temporal pole. There is an intermediate entorhinal cortex zone that projects to an intermediate region between the septal and temporal poles of the hippocampus (reviewed by Witter et al. 2000).

*Hilus*

The hilus has been controversial with respect to both its boundaries and relationship to the principal cell sheets. Early investigators could not agree whether the polymorphic region enclosed by the blades of the dentate gyrus

consisted of modified pyramidal cells (with associated Schaffer collaterals) and was thus part of CA3, or whether the region represented a plexiform layer of dentate gyrus analogous to stratum oriens. Indeed one of the earliest review articles regarding the hippocampus was an attempt to reconcile contrasting views of the hilus (Smith 1896). Lorente de No (1934) ascribed the hilus to the pyramidal cell sheet and designated the region CA4. It was not until Amaral's (1978) exhaustive Golgi study that the hilus was generally accepted to be associated with dentate gyrus. Some recent authors (e.g. Mott et al. 1997) skirt the issue by referring to the hilus border or some other finessing term. For the purpose of this thesis we shall consider the pyramidal cells enclosed by the blades of dentate gyrus to be CA3. The borders proposed by Amaral shall be adopted for hilus and CA3 as depicted in Figure 1.

Hilus has a great diversity of cell types; Amaral (1978) identified 21 distinct types using the Golgi preparation. Little is known about the physiology on connections of many of these cell types, and it is possible that Amaral overestimated the number of distinct cell types since his focus was to stress the differences between hilus and CA3. The two cell types that receive the most attention in hilus are the mossy cell and the spiny stellate or HIPP cell discussed below. Hilus also receives the densest norepinephrine innervation in hippocampus (Oleskevich et al. 1989).

*CA3*

The perforant path fibres that innervate the infrapyramidal blade of dentate gyrus continue into CA3. The medial and lateral perforant path fibres mingle somewhat as they enter CA3 and so the perforant path does not have a strict laminar profile in CA3 as it does in dentate gyrus. The perforant path fibres synapse in deep radiatum and stratum lacunosum moleculare before terminating in CA2 (Tamamaki and Nojyo 1993, Witter 1993). In addition to these extra-hippocampal projections, the CA3 pyramidal neurons receive two intrinsic glutamatergic projections.

Axons of dentate gyrus granule cells make contact with CA3 pyramidals in the stratum lucidum, although some collaterals cross stratum pyramidale to make contact in stratum oriens (Henze et al. 2000). Stratum oriens is also the lamina where recurrent axon collaterals originating from other CA3 pyramidal cells terminate. Axons emerging from CA3 pyramidal cells send collaterals along the length of the septo-temporal axis (Witter 1993). See Figure 4 for a summary diagram.

There is evidence that the mossy fibres only sparsely innervate CA3 pyramidal cells, and that mossy fibres form five times as many contacts with interneurons as they do with principal cells (Amaral 1990, Acsády et al. 1998). There is some physiological support for this as sharp electrode recordings from CA3 pyramidal soma show a massive and prolonged hyperpolarization associated with stimulation of the granule cell layer (Reid et al. 2001).

*CA2*

CA2 can be demarcated by a slight change in the morphology of pyramidal cells, and there are a number of molecular markers that delineate this small transitional region including positive staining for the monoclonal antibody TOR-23 (Stephenson and Kushner 1989) and an absence of the tyrosine kinase receptor c-kit (Motro et al. 1991). After a period of neglect CA2 is again receiving some attention as it has recently been reported that neurofibrillary tangles associated with rodent models of early Alzheimer's disease occur first in CA2 (Takayama et al. 2002). The pyramidal cells of CA2 may also express potassium channels distinct from the rest of Ammon's Horn (Talley et al. 2001). Even though there is a molecular and morphological identity for this region, present theory has yet to establish a distinct role for CA2. Since it can be difficult to unambiguously identify the boundaries of CA2 without immunocytochemistry performed distinctly for the purpose, the majority of authors simply choose to ignore this sub-field.

*CA1*

Field CA1 receives input from several sources. The Shaffer collateral projection originating from the CA3 pyramidal cells is perhaps the best studied. These fibres originate from the basal end of CA3 pyramidal cells and travel through stratum oriens before crossing the pyramidal cell layer and ascending through CA3. As they enter CA1 these fibres turn and follow stratum lucidum, dropping collaterals to make contact with dendrites of CA1 pyramidal cells in

strata oriens and radiatum. There is a topographic organization to this projection, with CA3 pyramidal cells closest to CA1 innervating the CA2 border region most heavily, and tending to make more synaptic contacts in stratum oriens or shallow radiatum (Amaral and Witter 1989). CA3 pyramidal cells distal from the CA1 border region tend to innervate cells towards the subiculum, and project most heavily to deep radiatum, with few or no collaterals projecting to stratum oriens. This projection figures prominently in the LTP literature.

CA1 receives other glutamatergic input however. Layer III of the entorhinal cortex projects directly to CA1 (Witter and Amaral 1991), as do a few layer II collaterals (Lingenhöhl and Finch 1991). The direct perforant path projection also enters CA1 through stratum radiatum, and sends collaterals to stratum lacunosum moleculare, where they terminate on both the distal apical dendrites of pyramidal cells and stratum lacunosum-moleculare interneurons. See Figure 5 for a summary diagram. This projection follows the slab architecture proposed by Witter et al. (2000), with lateral entorhinal cortex projecting most heavily to temporal CA1, and medial entorhinal cortex projecting most heavily to septal CA1. Although the direct perforant path projection has been considered to be of minor importance in rat, recently this projection has been proposed as the major excitatory input to CA1 in monkey on the basis of 2-deoxyglucose uptake (Sybirska et al. 2000). Whether there is a prominent role for this projection in rat, or indeed in monkey, is not known at this time. The direct perforant path projection to CA1 has a distinct termination pattern. Rather than the laminar

termination pattern associated with CA3 and dentate gyrus, in CA1 the two components of the perforant path contact distinct populations of cells in a topographic fashion. The medial entorhinal cortex contacts cells proximal to CA2, and lateral entorhinal cortex contacts cells distal to CA2 (Witter and Amaral 1991).

Both perirhinal and postrhinal cortex send minor glutamatergic projections to CA1, although the perirhinal projection to CA1 is disputed (Canning et al. 2000). Perirhinal cortex projections predominate in the CA1 region distal to the CA1/CA2 border. The projection is relatively sparse in CA1, but is heavier in subiculum (Witter et al. 2000). Current source density analysis suggests that the current sink in subiculum occurs in deep radiatum or stratum lacunosum moleculare (Naber et al. 1999). In contrast, postrhinal cortex projects primarily to the proximal region of CA1, and little to not at all to the distal portions of the CA1 field (Witter et al. 2000).

### *Locus Coeruleus Anatomy*

The locus coeruleus in rat is a compact nucleus comprising approximately 1400-1800 cells (Aston-Jones et al. 1995) located just lateral to the fourth ventricle, and medial to the mesencephalic nucleus. Despite being small in number these cells innervate virtually every region of the forebrain, in addition to substantial spinal and cerebellar projections. There is some confusion over the precise boundaries of the locus coeruleus. The name comes from the blue-black

colour of tyrosine-hydroxylase: in primates the locus coeruleus is literally a blue spot (Cooper et al. 1996). Examination of the region with a variety of techniques has revealed several norepinephrine positive nuclei that differ in their cell types and orientations of dendrites. These nuclei have been designated A4 through A7 and locus coeruleus is A6 (Dahlström and Fuxe 1964).

The locus coeruleus proper is a compact nucleus of mostly fusiform cells mixed with small rounded cells and medium ovoid cells (Swanson 1976, Shimizu and Imamoto 1970). Some two hundred large multipolar cells are also present in the ventral portion, or subcoerulear zone, of the nucleus (Björklund and Lindvall 1979, Swanson 1976). The subcoeruleus is a less densely packed region of biochemically heterogeneous cells (Aston-Jones et al. 1995). There are approximately 130 norepinephrine containing cells in the region (Grzanna et al. 1980) and Amaral and Sinnamon (1977) have suggested that the term subcoeruleus be reserved for the norepinephrine containing cells of the region. The boundaries of the subcoeruleus are unclear because the norepinephrine cells are part of a sparsely continuous sheet of norepinephrine cells that extends from A7 to A5 (Aston-Jones et al. 1995) and is sometimes referred to as the pontine lateral tegmental system (Bjorklund and Lindvall 1979). A5 shares some terminal sites with the locus coeruleus proper (Aston-Jones et al. 1995): its axons travel a ventral pathway to the forebrain which may include some fibres from A7 and the anterior portion of the locus coeruleus (Maeda and Shimizu 1972). A4 is contiguous with the locus coeruleus but extends dorsolaterally from the

periaqueductal grey to curve along the roof of the 4th ventricle (Björklund and Lindvall 1979, Foote et al. 1980b). A4 is also sometimes treated as part of the locus coeruleus (Aston-Jones et al. 1995). The dendrites of A4 extend medially and ventrally towards the ventricular surface (Aston-Jones et al. 1995).

The locus coeruleus lacks a clear internal structure such as layers or columns that are associated with cortical structures. There are groups of cells whose dendrites differ in the plane of orientation (Swanson 1976). The dendrites of the locus coeruleus extend preferentially to four zones and some authors argue that the locus coeruleus may be divided on the basis of these dendritic fields (Foote et al. 1995, Shipley et al. 1996), but a functional reason for such a division has yet to be elucidated.

Virtually all cells of the locus coeruleus express dopamine β-hydroxylase with the exception of a population of small round cells, which express gamma-amino-butyric acid (GABA) (Anima et al. 1987, Swanson 1976). Locus coeruleus neurons co-express a variety of peptides including galanin (Skofitsch and Jakobowitz 1985), neuropeptide Y (Everitt et al. 1984, Sutin and Jakobowitz 1988), vasopressin (Caffe et al 1985, 1988), vasoactive intestinal peptide (Sutin and Jakobowitz 1988), atrial natiuretic factor (Sutin and Jakobowitz 1988) and possibly corticotropin releasing factor (Valentino et al. 1992), and enkephalin (Finley et al. 1981). Locus coeruleus neurons have also been reported to co-localize the amino acids glutamate (Fung et al. 1994) and N-acetylaspartylglutamate (Forloni et al. 1987).

The locus coeruleus receives a limited set of inputs. The nucleus paragigantocellularis provides the majority of glutamatergic input to the locus coeruleus (Aston-Jones et al. 1986, Ennis and Aston-Jones 1997). Minor glutamate projections are received from the periaqueductal grey (Ennis et al. 1991), frontal cortex (Luppi et al. 1995, Jodo and Aston-Jones 1997), medial preoptic area (Ennis et al. 1991), dorso-medial hypothalamus (Aston-Jones et al. 2001) and the central nucleus of the amygdala (Luppi et al. 1995). A prominent inhibitory projection arises from the prepositus hypoglossi (Aston-Jones et al. 1986).

There is a more defined organization of the locus coeruleus with respect to the targeting of its efferents (Loughlin et al. 1986). Ventral regions give rise to descending projections to cerebellum and spinal cord. Dorsal regions project rostrally. The anterior regions tend to innervate the hypothalamus and thalamus. The posterior regions tend to project to hippocampus, cortex, and other forebrain sites. Individual cells project to multiple zones. Retrograde tracing studies have shown that projections to cerebellum originate throughout the locus coeruleus (Room et al. 1981) and a single locus coeruleus cell can project to both cerebellum and amygdala (Dietrichs 1985). Double injections of retrograde tracers in spatially separated sites will converge on common cells (Room et al. 1981, Ader et al. 1980, Nagai et al. 1981). The notion of diffuse zonal borders is supported by electrophysiological evidence showing that single locus coeruleus

cells can be antidromically activated from multiple sites (Nakamura and Iwama 1975, Takigawa and Mogenson 1977).

*Locus Coeruleus Projections to Hippocampus*

There is presently no consensus on which group forms the projection to hippocampus. Both the large multipolar (Loy et al. 1980, Loughlin et al. 1986) and fusiform cells have been proposed (Haring and Davis 1983).

Norepinephrine fibres reach Ammon's horn through three primary routes (Loy et al. 1980). The fibres that ascend to hippocampus travel a common route as they exit the locus coeruleus, traveling via the dorsal tegmental bundle and the medial forebrain bundle. Beyond the medial forebrain bundle some fibres split to form a ventral projection to Ammon's Horn. From the medial forebrain bundle these fibres turn ventrally and laterally eventually entering the hippocampus from the temporal pole.

The dorsal fibres continue in a rostral direction after exiting the medial forebrain bundle. Another set of fibres splits and enters the hippocampus through the fornix to innervate CA3. These fibres run in strata oriens and pyramidale, with the oriens fibres sending collaterals to innervate the pyramidal cell layer particularly in the CA3/CA2 border region. Additional collaterals from both groups of fibres form a relatively dense plexus in radiatum.

The remaining fibres form the cingular pathway that enters the dorsal hippocampus moving in a septal to temporal direction. One branch of this

projection runs in the alveus and stratum oriens of CA1, ramifying in the oriens to send collaterals to stratum pyramidale. The remaining branch travels orthogonal to the septal/temporal axis (in a subiculo-dentate direction) in the stratum lacunosum moleculare of CA1 and drops collaterals into radiatum.

Dentate gyrus receives norepinephrine fibres from all three of these projections. Both the cingular pathway, and the ventral pathway send collaterals from stratum lacunosum moleculare of CA3/CA1 across the hippocampal fissure to innervate the molecular layer of dentate gyrus, particularly towards the temporal end. The temporal molecular layer also receives an input as the ventral CA3 stratum lacunosum moleculare fibres continue to run into dentate gyrus, coursing close to stratum granulosum as far as the apex of dentate. At the septal end the dentate gyrus molecular layer is innervated predominantly by fibres coursing through the hilus and crossing stratum granulosum. These latter fibres may arise from the cingulum norepinephrine fibres continuing to run into hilus from stratum lacunosum moleculare of CA3 enclosed between the granular blades (Loy et al. 1980). The hilus receives the densest input, and all three systems appear to contribute to this innervation.

Locus coeruleus projections are bilateral, although the extent of the bilaterality depends upon the particular structure innervated. Locus coeruleus projections to cortex have been estimated to be 90% ipsilateral (Ader et al. 1980, Room et al. 1981). In hippocampus the locus coeruleus afferents in CA1 are

estimated to be 80% ipsilateral, and perhaps as low as 70% ipsilateral in the dentate gyrus and hilar regions (Loy et al. 1980).

### *Norepinephrine Content in Hippocampus*

Norepinephrine content in hippocampus has been assessed by several methods. Koda and Bloom (1977) and Koda et al. (1978) used light microscopy to visualize glyoxylic acid induced fluorescent varicosities and electron microscopy to visualize small granular vesicles in the dentate gyrus. They observed the highest fluorescence levels in the hilus, followed by the molecular layer, with little fluorescence in the stratum granulosum. A unilateral cut to the dorsal tegmental bundle, in which the locus coeruleus fibres run, depleted the supply of catecholamines to the hippocampus and decreased both the fluorescent varicosities and the small granular vesicles in the hilus. The decrease was greatest ipsilateral to the cut indicating a larger ipsilateral innervation from locus coeruleus.

Oleskevich et al. (1989) used uptake of tritiated norepinephrine to quantify the distribution of norepinephrine varicosities in autoradiographs. The highest density of varicosities was located in dentate gyrus ($2.4 \times 10^6/mm^3$). Within the dentate gyrus the ventral blade had a larger innervation than the dorsal blade, and the crests of the blades contained more varicosities than either the apex or the medial ends. The hilus showed strong radioactivity, while the molecular layer had a lighter innervation. The granule layer itself had only sparse innervation. After

dentate gyrus, CA3 had the next highest number of varicosities ($1.9 \times 10^6/mm^3$), followed by CA1 ($1.2 \times 10^6/mm^3$). Curiously, because of the difference in the numbers of cells in the regions, the authors estimate that each CA3 pyramidal cell receives 180 synapses from norepinephrine fibres, versus only 20 synapses per cell for granule cells in dentate gyrus, and 10 synapses per cell for a CA1 pyramidal cell. If interneurons were primary targets, however, the ratio would be highest in the hilus.

Direct measurements of norepinephrine content in hippocampus parallel the anatomical studies. Crutcher and Davis (1980) found the amount of norepinephrine in the dentate gyrus to be $0.57 \pm 0.07$ μg/g and in the rest of the hippocampus to be $0.30 \pm 0.05$ μg/g.

*Locus Coeruleus Efferents and Receptors in Hippocampus*

To date it has been difficult to describe the postsynaptic targets of norepinephrine fibres in hippocampus for several reasons. Firstly immunocytochemistry permits the visualization of fibres, but not their postsynaptic target. It is therefore possible to quantify the dopamine beta-hydroxylase-positive fiber density among hippocampal regions, without distinguishing between fibres of passage and fibres with functional synapses. Complicating this picture is the possibility that some of norepinephrine's effects may come, not through traditional synapses, but rather through volume transmission via release in interstitial space. Some estimates suggest that fewer than 15% of locus coeruleus terminals form traditional synapses with postsynaptic

cells in cortex (Séguéla et al. 1990, Umbracio et al. 1995). Volume transmission is widely accepted, although there are opposing viewpoints. Serial reconstruction of thin sections has yielded estimates of synaptic connectivity from norepinephrine fibres as high as 90% in hippocampus (Olschowka et al. 1981, Papadopoulos and Parnavelas. 1991). Differences in technique may account for part of the discrepancy. Umbriaco et al. (1995) rely on stereological assumptions derived from observations of acetylcholine varicosities in parietal cortex, which may or may not be of general utility. Umbracio et al. (1995) also explicitly looked for postsynaptic specializations on spines and dendritic shafts. Milner and Bacon (1989) report that although only 25% of tyrosine hydroxylase terminals make synaptic contact with dendrites or cell soma, a full 33% of norepinephrine varicosities form axo-axonic synapses with GABA-ergic terminals. Investigators have adopted the approach of localizing adrenoceptors with immunohistochemistry, sometimes identifying norepinephrine terminals with a second immunohistochemical label (using antibodies to intermediate enzymes in the biosynthetic pathway for norepinephrine, typically tyrosine hydroxylase or dopamine-β-hydroxylase) or induced fluorescence using glyoxylic acid (e.g. Aoki et al. 1994, Milner et al. 2000)

Noradrenergic receptors themselves are divided into two major families termed α and β. The α-receptor family is larger and consists of two subtypes α1 and α2. These subtypes are further subdivided, α1 divided into α1a, α1b, and α1d (the α1c subtype is homologous to α1a) (Cooper et al. 1996). α2 receptors are

clustered into three types termed α2a through α2c. It is possible that the α2a and α2b subtypes could be further divided into α2a1 and 2, and α2b1 and 2, although the evidence for this division is not compelling at this time (Clarke et al. 1995, Bylund et al. 1995, Wikberg-Matsson et al. 1995). Not all of these subtypes are present in the central nervous system.

Likewise, β-receptors are divided into three subtypes: β1, β2, β3. Of these receptors only β1 and β2 are found in the central nervous system (Cooper et al. 1996). A putative β4 receptor has been identified, but not yet localized to brain (Galitsky et al. 1997).

Norepinephrine varicosities appear to appose dendrites of CA3 pyramidal cells, with the heaviest innervation of CA3 occurring in the region of the cell bodies. Varicosities occasionally appose interneuron dendrites in CA3 radiatum. In CA1 varicosities appose pyramidal cell soma and stratum radiatum dendrites. In dentate gyrus varicosities are sometimes adjacent to molecular layer interneurons (Loy et al. 1980). In hilus the norepinephrine fibres branch to form a dense plexus that appears to form both axo-dendritic and axo-somatic contacts (Loy et al. 1980).

Milner and Bacon (1989) characterized the postsynaptic targets of norepinephrine fibres in hippocampus using combined immunohistochemistry for tyrosine hydroxylase, an intermediate enzyme in the norepinephrine biosynthetic pathway, and γ-aminobutyric acid (GABA), the primary transmitter of inhibitory interneurons. They observed no instance of a tyrosine hydroxylase positive

terminal innervating a GABA positive cell body or dendrite, although approximately one third of tyrosine hydroxylase positive terminals appeared to form axo-axonic contact with a GABA positive terminal, suggesting that norepinephrine and GABA may modulate each other's release. Approximately 25% of the terminals formed synapses with putative granule cell soma or dendrites (tyrosine hydroxylase and GABA negative) and the remaining 40% of terminals did not have a relationship with other processes. The large number of "dangling" terminals does not necessarily imply that a substantial proportion of norepinephrine effects occur through extra-synaptic volume conduction (Agnati et al. 1992). Identifying synaptic contact through light or electron microscopy, especially when used in combination with opaque visualizers such as immunohistochemistry or Golgi stain, depends critically upon both the plane of section and the reconstruction technique. Serial reconstruction suggests that approximately 90% of norepinephrine terminals in dentate gyrus have identifiable synapses (Papadopoulos and Parnavelas 1991). Norepinephrine is also known to modulate the activity of glial cells (Magistretti 1994) and these cells are known to express β-receptors (Fillenz 1990, Salm and McCarthy 1992).

Crutcher and Davis (1980) compared the fields of α and β receptors to the amount of norepinephrine innervation in the hippocampus of adult rats using tritiated compounds to identify receptors. α-receptor binding by WB-4101 was found to be similar between dentate gyrus, CA3 and CA1. β-receptor binding by dihydro-alprenolol was 30% higher in dentate gyrus than in Ammon's horn.

*α-Receptor Distribution*

Young and Kuhar (1980) used tritiated WB-4101 (selective for αl adrenoceptors) and tritiated p-aminoclonidine (selective for α2 adrenoceptors) to locate and differentiate fields of α-adrenergic receptors in the rat brain. They found high levels of αl-receptors in the molecular layer of the dentate gyrus and also high levels in the caudal dentate. High levels of α2-receptors were seen in the locus coeruleus.

Milner et al. (1998) used an antibody to study the distribution of the $\alpha 2_a$ receptor in hippocampus. Strong immunoreactivity was seen in the pyramidal and granule cell layers. Scattered reaction product was seen in interneurons in stratum oriens and in the hilus of dentate gyrus. Diffuse product was also seen in stratum lacunosum moleculare of both CA1 and CA3, and was stronger in ventral hippocampus. Stratum lucidum of CA3 showed diffuse reaction. Electron microscopic examination revealed that $\alpha 2_a$ immunoreactivity is largely presynaptic. Reaction product was located on both tyrosine hydroxylase positive and negative terminal endings, suggesting that they may modulate the release of both norepinephrine and other transmitters or modulators. Postsynaptic receptors were located on primary cell dendrites, and were generally apposed to tyrosine hydroxylase positive terminals. Some glia in the principal cell layers were $\alpha 2_a$ reactive. In the hilus and stratum lucidum of CA3 α2a reaction product was seen in glia and unmyelinated axons. Very rarely was reaction product seen in a mossy fiber terminal or apposed to a mossy fiber terminal. In the molecular layer of

dentate gyrus staining was lighter in the inner third. In hilus staining was stronger in the central, or deep, hilus, lighter in the subgranular region. Few dendritic profiles were seen in hilus.

### *β-receptor Distribution*

The hippocampus and the rest of the limbic system has a high density of β receptors in comparison to neocortex and brain stem as measured with tritiated alprenolol, a β-receptor agonist (Alexander et al. 1975). In hippocampus both β1 and β2 receptors are present, although not in equal numbers. Studies with a tritiated non-selective β-agonist (iodocyanopindolol) in combination with selective β-antagonists suggest that over 70% of β-receptors in hippocampus are of the β1 type. The remainder are of the β2 subtype (Rainbow et al. 1984, Tiong and Richardson 1990).

Milner et al. (2000) used immunohistochemistry to study the distribution of the β1 receptor in the dentate gyrus. Reactivity was seen in soma of the pyramidal cell layer and granule cell layer, in addition to scattered interneuron profiles in stratum radiatum and stratum lacunosum moleculare of CA1 and the molecular layer and hilus in dentate gyrus. Subgranular soma also stained positive for parvalbumin, marking these cells as basket or chandelier cells. These same cells were the only cells that showed somatic profiles. Granule cells stain heavily for postsynaptic β-receptors in dendrites, particularly in the inner two-thirds of the molecular layer, occasionally in spines. Presynaptic profiles were rare. Reaction

product was common in astrocytes. Tyrosine hydroxylase positive axons and terminals were generally apposed by β-receptor immunoreactivity through out the dentate gyrus.

### *Responses of Locus Coeruleus to Environmental Stimuli*

The locus coeruleus displays a strong circadian rhythm. Locus coeruleus activity in the rat is highest during the active phase (dark) of the light/dark cycle, and lowest during slow wave sleep. The locus coeruleus is inactive during paradoxical sleep (Aston-Jones and Bloom 1981). Locus coeruleus activity is modulated by the suprachiasmatic nucleus via a connection through the dorso-medial hypothalamus, and locus coeruleus plays a role in scheduled protein synthesis (Aston-Jones et al. 2001, Cirelli et al. 1996). The changes in locus coeruleus activity precede shifts in behavioural states, and therefore locus coeruleus has been implicated in driving circadian changes in other systems. During the waking state the locus coeruleus has two distinct firing modes. When the animal is engaged in stereotyped behaviour (consummatory, grooming, light sleep), slow rhythmic activity dominates. Cells fire at rates from 0.5-4 Hz in an uncoordinated fashion (Aston-Jones and Bloom 1981b). In contrast during anomalous sensory stimuli the locus coeruleus fires in a phasic burst pattern.

Bursts are seen during spontaneous waking, during interruptions of stereotyped behaviour, and in response to noxious stimuli (Foote et al. 1980a, Aston-Jones and Foote 1980, Hirata and Aston-Jones 1994). In addition to

unexpected sensory events, bursting can occur in response to cognitively complex stimuli. In monkey, the locus coeruleus bursts in response to the presentation of a preferred food item (Foote et al. 1980a). In rat, locus coeruleus bursting occurs in response to salient stimuli during classical conditioning, but bursting ceases when the conditioning is well-established behaviourally (Sara and Segal 1991). Alteration of contingencies, such as extinction or reversal, causes a renewed bursting response (Sara and Segal 1991). Reversal of contingencies has also been shown to result in norepinephrine efflux at sites efferent to the locus coeruleus (Dalley et al. 2001).

Bursts are therefore not simple responses to unexpected stimuli, but are instead complex events that fire during a mismatch of expectations, or in response to stimuli during periods of increased saliency in specific tasks. In monkey, locus coeruleus cells display bursts in response to the presentation of a target stimulus in both auditory and visual oddball tasks (Aston-Jones et al. 1994, Swick et al. 1994, Usher et al. 1999). The presence of a locus coeruleus burst predicts performance on individual oddball trials, and pharmacological manipulation to decrease firing rates degrades performance (Aston-Jones et al. 1997, Aston-Jones et al. 1998, Rajkowski et al. 1998), which suggests a role for locus coeruleus in attention and vigilance (Usher et al. 1999).

A role for the locus coeruleus in attention is supported by studies in rat showing that both novelty seeking and behavioural responses to novelty are dependent on the integrity of the locus coeruleus. Either blockade of β-receptors

or activation of α2-receptors blocks investigatory behaviour (Sara et al. 1995). The locus coeruleus responds to novelty with a burst (Kitchigina et al. 1997), and this burst results in an increased population spike in dentate gyrus that is blocked by the β-receptor antagonist propranolol (Kitchigina et al. 1997). Burst activity of locus coeruleus neurons has been shown to result in increases in norepinephrine levels at target sites efferent to the locus coeruleus (Florin-Lechner et al. 1996, Dalley et al. 2001).

### *Norepinephrine Effects on Behaviour*

There have been numerous studies of norepinephrine effects on learning and memory, although the results have not always been clear. Investigators have primarily used two approaches: locus coeruleus lesion (electrolytic or chemical) and pharmacological manipulation of norepinephrine-receptors.

#### *Lesion of Locus Coeruleus*

Lesions of locus coeruleus using N- (2-chlorethyl)-ethyl-2-bromobenzylamine (DSP-4) have been shown to disrupt temporal conditioning tasks (Al-Zaharani et al. 1998), step through inhibitory avoidance tasks (Moran et al. 1992), and decrease spontaneous alternation (Pisa et al. 1988). DSP-4 lesions are reported to not affect performance on an 8 arm radial maze (Luine 1990, Chrobak 1985). DSP-4 lesions do not appear to impair performance on the Morris water maze task (Valjakka et al. 1990, Sirviö et al. 1991, 1994, Björklund et al. 2000, although Selden et al. (1990) reported an impairment in navigation

using local but not distal cues) and in some cases lesioned animals learn more quickly than sham controls. This paradoxical effect may indicate an interaction of task requirements and stress brought on by housing conditions (Lapiz et al. 2000, 2001).

*Pharmacological Manipulations*

A common strategy in pharmacological studies is blockade or activation of α-receptors. Since α2 receptors are inhibitory autoreceptors at both the soma and release sites, blockade of α2 receptors can serve to increase norepinephrine release in addition to blocking postsynaptic effects of α2 receptors. As a result it can be difficult to interpret behavioural effects using compounds that are active at α2 sites. For instance Haller et al. (1997) reported that atipamezole increases activity in the open field and impairs performance in the shuttle box. The increase in open field activity could be blocked by both β- and α1 receptor antagonists leading to the interpretation that the atipamezole mediated effect was occurring through an increase in norepinephrine release, which activated postsynaptic α1 and β-receptors. In contrast, α1 and β-receptor antagonists could not block the impairment of shuttle box performance, leading to the interpretation that the atipamezole impairment was mediated by postsynaptic α2 receptors. α2 antagonists have been reported to enhance spatial performance in mice, rats, and humans (Tanila et al. 1998, Carlson et al. 1992, Jakala et al. 1999) and performance in a complex maze task in rats (Devauges and Sara 1991, Sara and Devauges 1989). The role of α2 receptor blockade in water maze tasks is not

clear. It is possible that the manipulation may differentially affect young and old animals (Sirviö et al. 1991, 1992a, 1992b) or that the action of ligand on specific receptor subtypes is important; animals which over express α2c receptors are reported to be impaired in the water maze (Björklund et al. 2000). Recently atipamezole administration has been reported to result in an increased stability of place fields in familiar environments. Administration of the α2 agonist dexmedetomidine results in rotations or new place fields in familiar environments (Tanila 2001).

There is also evidence for a role of norepinephrine in long-term memory in humans (Cahill et al. 1994, Nielson and Jensen 1994) and rodents (e.g. Izquierdo 1998, Kobayashi 2000, Clayton and Williams 2000). The effects of norepinephrine in promoting long-term memory seem to be mediated primarily by β-receptors (Cahill et al. 1994, Nielson and Jensen 1994, Izquierdo et al. 1998). Only a few studies have localized this action of norepinephrine to the hippocampus (e.g., Izquierdo et al. 1998); or to hippocampally dependent tasks, e.g.. Kobayashi et al. 2000).

### *Norepinephrine Effects on Electrophysiology in Dentate Gyrus*

#### *Evoked Potential Studies*

Norepinephrine has a profound effect on evoked potentials in the hippocampus. Neuman and Harley (1983) first reported that iontophoresed norepinephrine increases the population spike evoked in dentate gyrus by

perforant path stimulation. The effect could be long lasting (> 30 min), with a single norepinephrine application enhancing evoked potentials for up to eleven hours, and was termed norepinephrine long-lasting potentiation. Norepinephrine long-lasting potentiation is robust when it occurs, since short-term effects are also common, and can be induced in a variety of ways including exogenous norepinephrine applied to the ventricles (Chaulk and Harley 1998) or evoked release of endogenous norepinephrine by glutamate in both the anaesthetized preparation (Harley and Milway 1986) and the behaving animal (Klukowski and Harley 1994). Electrical stimulation of the major glutamatergic input to locus coeruleus, the nucleus paragigantocellularis, produces short but not long-term changes in dentate gyrus (Babstock and Harley 1992). Norepinephrine long-lasting potentiation is also observed in vitro where norepinephrine enhances the efficacy of the medial perforant path stimulation (Lacaille and Harley 1985), although norepinephrine is reported to depress the lateral perforant path projection to dentate gyrus (Dahl and Sarvey 1989).

Norepinephrine is required for LTP in dentate gyrus. Norepinephrine depletion and blockade of β-receptors reduces the probability of LTP induction and LTP magnitude in vitro for both EPSP slope and population spike (Stanton and Sarvey 1985c, Swanson-Park et al. 1999). A similar reduction by norepinephrine depletion is seen in vivo (Bliss et al. 1983). Unlike norepinephrine long-lasting potentiation, the effect of norepinephrine on LTP is identical in the medial and lateral perforant path with β-receptor blockade blocking the induction

of LTP for both medial and lateral perforant pathways (Bramham et al. 1997). Norepinephrine depleted rats also show reduced LTP in the awake behaving preparation (Robinson and Racine 1985), although under these conditions norepinephrine depletion increased the magnitude of the population spike and decreased EPSP slope under control conditions. High frequency tetanus of the perforant path is known to increase norepinephrine levels in freely behaving rats (Bronzino et al. 2001). Norepinephrine long-lasting potentiation is also dependent on protein synthesis (Stanton and Sarvey 1985a) as is late-phase LTP (Stanton and Sarvey 1984). This pattern of electrophysiological effects with norepinephrine is consistent with an early hypothesis by Seymour Kety that norepinephrine's role is to favor facilitatory change in recently active synapses (Harley 1987).

*Paired Pulse Studies*

The paired pulse technique is used to assess the dynamics of local circuit neurons in dentate gyrus. If a second pulse is delivered to the perforant path shortly after a first pulse, the second evoked potential is altered compared to the first. Typically the population spike is small or nonexistent, the amplitude of the evoked potential may be reduced, and sometimes the -*EPSP slope is diminished. The effect is attributed to the recruitment of both feedforward and feedback interneurons by the first perforant path pulse and resultant evoked potential.

Sara and Bergis (1991) used the α2 receptor antagonist idazoxan to increase tonic norepinephrine release. When probed with paired-pulses, five of

eight animals showed enhanced inhibition that was independent of granule cell excitability. An earlier study had shown that the idazoxan enhancement of the first evoked potential was blocked by prior lesion of the locus coeruleus by DSP-4 (Richter-Levin et al. 1991).

*Single Unit Studies*

Evoked potentials are a secondary indicator; they are summed responses of thousands of cells. In order to understand the effects of norepinephrine on network functioning, it is necessary to evaluate the responses of individual cells.

*Principle Cells*

Several studies have reported that exogenous norepinephrine can both excite and inhibit spontaneous firing of granule cells, although papers differ as to which effect predominates.

Gray and Johnston (1987) recorded granule cell activity in whole cell and patch clamp configurations in slices of rat hippocampus in vitro. Potassium ($K^+$) and sodium ($Na^+$) currents were blocked with tetrodotoxin and 3,4-diaminopyridine (3,4-DAP) in both the bath and electrode solutions. Pressure ejection of either norepinephrine or the β-receptor agonist isoprenaline increased the amplitude of an inward calcium ($Ca^{++}$) current with a delay of approximately 20 seconds. The increase of the $Ca^{++}$ current was not blocked by application of the α2-receptor clonidine suggesting that norepinephrine was acting through the β-receptor. Norepinephrine also increased the amplitude and duration of $Ca^{++}$ action potentials. Direct application of both the cyclic-adenosine-mono-phosphate

(cAMP) activator forskolin and the cAMP analogue 8-bromo-cAMP also increased the inward $Ca^{++}$ current. Single $Ca^{++}$ channel recording showed an increase in the probability of channel opening and increased open time in the presence of norepinephrine, isoprenaline, and 8-bromo-cAMP.

Lacaille and Schwartzkroin (1988) reported that iontophoresed norepinephrine excited the majority of responsive granule cells in vitro. Recordings were attempted from 34 cells, of which 16 responded to norepinephrine. Twelve of these cells depolarized an average of 10.4 mV for approximately 17 seconds. The depolarization was associated with an increase in membrane resistance attributed to the closing of a $Ca^{++}$ dependent $K^{+}$ channel which has the effect of blocking both the after hyperpolarization and spike accommodation (Haas and Rose 1987). A minority of granule cells had a smaller hyperpolarizing response (-6.9 mV), which was transient (average duration 6.7 seconds). Lacaille and Schwartzkroin observed that both excitatory and inhibitory responses could be elicited by adjusting the position of the iontophoresis pipette, and that the effects were postsynaptic since they could be produced in slices perfused in low $Ca^{++}$ and high $Mg^{++}$ solutions that blocked synaptic transmission.

Pang and Rose (1989) reported that 18 of 21 granule cells were inhibited by pressure ejection of norepinephrine into dentate gyrus in vivo. Of the three other cells one was excited, and the other two had a biphasic response. Granule cell inhibition was mimicked by pressure ejection of the α1-agonist phenylephrine

(5/7, 2 excited) although granule cells could be excited by pressure ejection of either an α2 agonist (A60884) or β agonist (isoproterenol).

Bijak and Misgeld (1995) recorded inhibitory postsynaptic potentials (IPSPs) from granule cells in slices of guinea pig hippocampus. Both norepinephrine and isoproterenol (a β-receptor agonist) increased the frequency of IPSPs in the majority of recorded granule cells (9/14 and 8/12 respectively) even after blockade of glutamatergic synaptic transmission by CNQX (AMPA receptor blocker) and CGP 37849 (NMDA receptor blocker) (10/12 cells). The α-receptor agonists phenylephrine (α1) and clonidine (α2) were ineffective at increasing IPSP frequency. The IPSPs could be either $K^+$ dependent or $Cl^-$ dependent. $K^+$ dependent IPSPs occurred in approximately 50% of granule cells and appeared to be mediated by GABA receptors since they occurred in the presence of picrotoxin and bicuculline but not CGP 55845A. Application of norepinephrine or isoproterenol both increased the frequency of $K^+$ dependent IPSPs, and induced $K^+$ dependent IPSPs in granule cells which had been previously unresponsive. Although a number of these IPSP events were dependent on activity of interneurons, norepinephrine and isoproterenol also increased IPSPs in granule cells when action potentials were blocked by teterodotoxin. The increase could be blocked by bicuculline leading to the conclusion that norepinephrine is partially active on terminals of GABAergic cells.

*Interneurons*

Several studies have investigated the effect of norepinephrine on interneurons of the dentate gyrus and hilar regions. There is less variability in these results with the majority of authors agreeing that application of norepinephrine increases the activity of interneurons.

Pang and Rose (1987) recorded principal cells and interneurons in the hippocampus of anaesthetized rats. While recordings took place in both CA1 and the subgranular and hilar zones of dentate gyrus, the results are combined across regions in the results section of the paper. Norepinephrine and related compounds were administered by microinjection and iontophoresis. Application of norepinephrine increased the firing rates of the majority of interneurons (79/94) by approximately 300%. The norepinephrine associated increase in firing was blocked by both the α2 receptor antagonist rauwolscine and the β-receptor antagonist timolol. Agonists of all adrenoceptors increased the firing of interneurons (α1 phenylephrine, α2 clonidine and A-60889, β isoproterenol). Rose and Pang (1989) revisited the issue reporting only recordings in dentate gyrus. The majority of interneurons (19/24) increased their firing rates in response to the pressure ejection of norepinephrine, the α1-receptor agonist phenylephrine, or the β-receptor agonist isoproterenol.

Bijak and Misgeld (1995) recorded from hilar interneurons in slices of guinea pig hippocampus. They distinguished two cell types on the basis of their after-hyperpolarization and spike frequency adaptation. Type I cells had a large

after-hyperpolarization and little discharge frequency adaptation. Type II had a small after-hyperpolarization, some spike frequency adaptation and had a slower spontaneous firing rate than type I. Both bath applied norepinephrine and isoproterenol had small effects on membrane potential (less than 5 mV in either direction). Norepinephrine and isoproterenol reduced the amplitude and duration of slow after-hyperpolarizations in type I cells. Isoproterenol increased spontaneous discharge rate of type I cells, but not the number of APs elicited by depolarizing pulses.

Type II cells responded to norepinephrine and isoproterenol with an increased spontaneous discharge rate, and more action potentials during depolarizing pulses. Alpha agonists had no effect on the after-hyperpolarization.

Addition of the α-receptor agonist phenylephrine increased a $K^+$ leak conductance, while addition of the β-receptor agonist isoproterenol decreased a $K^+$ leak conductance in both type I and II cells. Isoproterenol also induced an increase in the frequency of both EPSPs and IPSPs presumably by increasing the spontaneous release of transmitter from presynaptic terminals.

*Electroencephalography (EEG)*

Rhythmic activity of principal cells can be assessed by EEG. The frequency bands that have received the majority of attention are theta and gamma. Theta rhythm is slow activity (6-12 Hz) that governs spiking activity of principal cells. In behaving preparations principal spikes are known to occur in the positive phase of theta rhythm (Fox et al. 1986). Theta rhythm LTP protocols mimic this

tendency by applying several tetanic bursts within a single theta peak with a period of no stimulation corresponding to the negative phase of the theta rhythm. Theta rhythms are generated both within the hippocampus, and imposed externally by the neocortex via the entorhinal cortex (Vanderwolf 1969, Vanderwolf and Leung 1982). Entorhinal theta (sometimes called walking theta) is also referred to as type I and is distinguished by a slightly faster rate (9-12 Hz) and being insensitive to atropine. Type I theta is attenuated by urethane anaesthesia with the result that the majority of theta in the preparations in this study is type II (Fox et al. 1986). Type II (or immobility theta) theta is slower (5-9 Hz) rhythm generated within the hippocampus that is atropine sensitive (Vanderwolf and Leung 1982, Fox et al. 1986).

Gamma rhythms (40-90 Hz) are generated by coupled networks of interneurons. Gamma rhythm has recently garnered much attention since they have the ability to control spiking activity of principal cells on a much smaller time scale (Traub et al. 1998) than theta rhythms. Gamma has been proposed as a physiological marker of both storage and recall of information as the small time windows of coincident spiking activity of the principal cells allow efficient binding of information into cohesive representations (reviewed by Traub et al. 1998, and McBain and Fishahn 2001).

Activation of locus coeruleus by the cholinergic agonist bethanechol has profound effects on EEG recorded in hippocampus and cortex. Bethanechol increases the firing rates of locus coeruleus neurons to 3-5 times basal rates

In cortex activation of the locus coeruleus produced a significant decrease power in all bands of the power spectrum. However both theta and gamma bands were decreased less relative to other power bands as a result the relative power of these two bands increased significantly. In contrast the theta power recorded in hippocampus did not decrease although all other power bands, including gamma, did decrease. As a result theta dominated the hippocampal EEG records of post-infusion animals. The effect on EEG lasted approximately 15 minutes consistent with washout of the drug and a return to basal firing rates in the locus coeruleus.

### *Classifying Cells of the Dentate Gyrus*

There are several schemes of classifying interneuronal cells in the hippocampus and the literature is substantial. The majority of classification has been done on the basis of the size, shape, and location of the cell body and dendritic arbor (see for example Amaral 1978). Some authors have classified cells solely on the pattern of axonal arborization (Mott et al. 1997). Other systems rely upon classifying cells by co-localization of peptides (Miettinen and Freund 1992), or by calcium binding proteins (Miettinen et al. 1992). Combinations of these approaches are possible (Parra et al. 1991). Freund and Buzsaki (1995) addressed some of the relationships among the classification systems in an extensive review of the interneuron literature.

Broadly speaking, interneurons receive glutamatergic input from either the perforant path (feedforward interneurons) or from recurrent mossy fibres

(feedback interneurons). In turn, interneurons project primarily to either the molecular layer of dentate gyrus, indicative of dendritic inhibition, or the stratum granulosum, indicative of somatic inhibition. Feedforward cells have activation thresholds below that of granule cells (Scharfman 1991) and so can be activated at perforant path stimulation levels that are subthreshold for evoking a population spike in the evoked potential. Feedforward inhibition has been highlighted as a mechanism for enhancing signal to noise in the hippocampus (Buzsaki 1984) since inhibition of principle cells would occur together with direct excitation of principle cells and only those cells most strongly activated would fire against a quiet background of other principle cell activity. Feedback interneurons will not be driven until the appearance of a population spike in the evoked potential. Feedback interneurons will also have longer latencies measured from the perforant path stimulation. Feedback inhibition would oppose bursting in the principle cells and regulate timing at sites efferent to the principle cells. There are of course exceptions to this gross simplification of interneuron physiology.

The glutamatergic mossy cell is the most common non-granule cell in the dentate gyrus, numbering approximately 30, 000 (Patton and McNaughton 1994). The mossy cells receive excitatory input from both granule cells and CA3 pyramidal cells (Scharfman et al. 1990, Scharfman 1994) and the mossy cell provides extensive excitatory inputs to parvalbumin positive basket cells (Blasco-Ibáñez et al. 2000) in addition to contacting granule cells (Scharfman 1995a, Wenzel et al. 1997). Mossy cells can be activated in both a feed-forward or feed-

back manner in an idiosyncratic fashion (Scharfman and Schwartzkroin 1990, Scharfman et al. 1990); as a result, their firing thresholds can range from 0.5 to 2 times the current necessary to evoke a population spike (Buckmaster and Schwartzkroin 1995). Because these cells may be activated by either the perforant path or by granule cell or CA3 activity, estimates of the mossy cell latency in response to perforant path stimulation also varies greatly, from 2.5 ms (Scharfman and Schwartzkroin 1990) to over 20 ms (Scharfman 1995b). The mossy cell has a broad intracellular action potential which ranges from 1.5 to 2.6 ms (Scharfman and Schwartzkroin 1990, Buckmaster and Schwartzkroin 1995). The mossy cell generally fires single action potentials although the occasional doublet can be observed (Buckmaster and Schwartzkroin 1995).

The basket cell and the similar chandelier or axo-axonic cell are common interneurons numbering approximately 10, 000 (Patton and McNaughton 1994). The basket cells provide powerful shunting inhibition at the soma of the post-synaptic granule cells. They too fire in both a feed-forward and feed-back fashion (Sik et al. 1997). While basket cells are generally considered to have thresholds far below that necessary to evoke a population spike (Buckmaster et al. 2002) there may be a functional subdivision of the basket cells. Immunocytochemistry has identified at least two groups of basket cells which differ in their expression of calcium binding proteins (Freund and Buzsaki 1995). The typical basket cells express parvalbumin and have short latencies to perforant path stimulation which ranges from 1.5 to 5.5 ms (Buckmaster et al. 2002, Scharfman 1995b, Mizumori

et al 1989, Han et al. 1993, Han 1994). Atypical basket cells are far less numerous and express calbindin. The electrophysiology of atypical basket cells has not been extensively studied, but the spike latency in response to perforant path stimulation has been reported as 10-15 ms (Sik et al. 1997). The basket cells have moderately wide intracellular action potentials which range from 0.7 to 1.1 ms (Buckmaster et al. 2002, Scharfman 1995). Basket cells typically fire single action potentials (Buckmaster et al. 2002) although it is possible that these cells may fire trains of action potentials in response to suprathreshold stimulation (Buzsaki et al. 1983). Basket cells are estimated to have a baseline firing rate of approximately 5 Hz (Mizumori et al. 1989).

The chandelier or axo-axonic cell is similar to the basket cell in most respects (Freund and Buzsaki 1995). The chandelier cell is distinguished primarily by its innervation of the initial and proximal segments of granule cell axons rather than the soma proper (Martinez et al. 1996; Han 1994, Soriano et al. 1990). It is less common than the basket cell with approximately 1000 chandelier cells per hippocampus (Patton and McNaughton 1994). Since electron microscopy is often required to make the distinction, chandelier cells are often treated as basket cells (Freund and Buzsaki 1995).

The hilar interneuron forming a dense axonal plexus in the commissural and association pathway terminal field (HICAP cell) is a pure feed-forward cell and as a result it fires at intensities below that required for a population spike and has a short latency of approximately 4 ms (Sik et al. 1997). The HICAP cell has a

very narrow intracellular action potential width of 0.5 ms (Han et al. 1993) and fires single action potentials (Sik et al. 1997).

The hilar interneuron with its axon ramifying in the perforant path terminal field (HIPP cell; also called the spiny stellate) is a pure feedback cell that is common in the hilus, numbering approximately 4800 per hippocampus (Buckmaster et al. 2002). These cells co-express somatostatin and have the high activation thresholds and long latencies (6-7 ms) associated with feedback cells (Buckmaster et al. 2002, Scharfman 1993). These cells have moderate to wide intracellular action potentials of 0.8 to 1.8 ms (Buckmaster et al. 2002, Buckmaster and Schwartzkroin 1995). Although these cells fire single action potentials they have exceptionally high baseline firing rates of approximately 20 Hz (Han et al. 1993, Scharfman 1993). HIPP and HICAP cells are often classified together with other cells as GABAergic polymorphic cells (Freund and Buzsaki 1995). The total number of polymorphic cells is estimated to be approximately 15, 000 per hippocampus (Patton and McNaughton 1994).

There has been no attempt to identify interneuron types on the basis of their extracellular waveforms, although it is common in extracellular recording to report whether an interneuron was activated in a feed-forward or feed-back fashion. A problem every extracellular recording study needs to address is that of separating waveforms of interneurons from the waveforms of principal cells, and separating the target cell from other unit waveforms and system noise. The former problem is one of discriminating units, the latter of cluster cutting. Since the

present investigation relies on extracellular recording methodology a brief review of the issues in cell isolation and identification follows.

*Cluster Cutting*

Waveform separation is accomplished almost exclusively by cluster cutting. Various waveform parameters such as spike width, time of peak, amplitude, time of valley, are measured, and then plotted pairwise. The experimenter selects and modifies the boundaries of clusters in sequential pairings. Harris et al. (2000) observe that this method is prone to experimenter bias, and error rates soar anytime two spikes appear closely in time. Automated cluster cutting outperforms manual cuts substantially.

The error associated with cluster cutting error is not a major concern in the present study. Cluster cutting techniques were designed to solve the problem of multiple units recorded from a single low impedance electrode or electrode assembly. In the case of low impedance recording the experimenter is attempting to maximize the number of units recorded from a single electrode. In the present study I am attempting to isolate a single unit by using high impedance electrodes. The cluster cutting task in this case is not to separate units from similar unit events, but rather to cut units from random threshold crossings or stereotyped background noise. Although the reduced cluster cutting procedure in high impedance recording may still discard spikes that are very dissimilar from the typical waveform for that unit, the procedure likely results in less than 1 lost spike

per 1000. In the low impedance electrode data set of Harris all of the extreme outliers identified by Mahalanobis distance (4 spikes per 1000) would be counted as part of the unit cluster since they are identifiable as cellular waveforms rather than as noise. It is also not likely that clusters in this thesis represent multiple cells. The high impedance of the recording electrode necessitates that the unit be exceptionally close to the pore of the electrode tip to be seen. In the rare case where more than one unit was seen during recording, one was generally half the amplitude of the other, allowing the threshold to be set such that only one unit was recorded. Autocorrelograms were examined to ensure that the time during the refractory period was empty of spikes, bolstering the argument that clusters represent a record from a single cell.

*Discriminating Cells*

The identification of a cell as an interneuron as opposed to a principal cell is more problematic than ensuring a clean cluster. Pang and Rose (1987) distinguished units on the total widths of their unfiltered action potentials. Waveform widths shorter than 400 μs were considered to be interneurons, widths wider than 600 μs were considered to be granule cells. The hilus was localized by proceeding 150 μm ventral from the depth at which the perforant path evoked response was biphasic. They note that interneurons tended to fire faster, and responded to perforant path stimulation with multiple action potentials.

Tomasulo and Steward (1996) used slightly more stringent criteria in their classification of interneurons and principal cells. In order for a cell to be classified

as an interneuron in their study, it was required to have a total filtered (1-3 kHz) action potential width of less than 800 μs and fire spontaneously, at least occasionally, at 10 Hz or faster. Additional criteria that were used less stringently included firing multiple spikes to a single perforant path stimulus, the first spikes occurred with a latency of 4 and 6 ms to perforant path and commissural stimulation respectively, and the first spike generated by perforant path stimulation occurred prior to the population spike. Electrode placements were localized to the hilus by first placing the recording electrode to obtain a positive going evoked potential, and then advancing the electrode below the granule cell layer as judged by the occurrence of multiple units in audio/visual monitoring.

Csicsvari et al. (1999b) adapted the cluster cutting approach in assigning cells to pyramidal or interneuron categories in CA1 tetrode recordings. All discriminable units were recorded and cluster cut. The resulting cell clusters were analyzed for three parameters: average firing rate, average width, and the first moment of the autocorrelogram (corresponding to the mean). These attributes were then projected in three-dimensional plots. Although any given cell could overlap categories in a single dimension, two clear clusters were formed in the three dimensional plot.

Wiebe and Stäubli (2001) further adapted this procedure to microwire recordings in the dentate gyrus and CA1. Cells were recorded and cluster cut, and analyzed for negative going cell width, mean firing rate, and autocorrelations. The results from each cell were then run through the following decision process; if the

average rate in Hz < 0.04 (cell width in μs) –3.5 *and* there was an initial peak in the autocorrelogram at 3-5 ms, then the cell was a principal cell. If the average rate in Hz > 0.04 (cell width in μs) –3.5 *and* the autocorrelogram displayed a secondary peak in the 80-200 ms range, then the cell was an interneuron. Presumably all cells fell into one category or the other, since no mention is made of intermediate cases.

In the present study rates of firing, frequency of bursting, response to perforant stimulation with attention to the current required to evoke a unit relative to the current required for a population spike, the latencies of firing with respect to the evoked potential stimulus, autocorrelograms of the interspike intervals, and a symmetry ratio characterizing relative widths of the spike waveform (see Methods) are used to in the discrimination and classification of cell types.

### *Mechanisms of Norepinephrine Potentiation*

Pharmacological studies agree that the β-receptor plays the dominant role in norepinephrine dependent plasticity of evoked potentials (Neuman and Harley 1983, Stanton and Sarvey 1987, Bramham et al. 1997). The β-receptor is a $G_s$-protein receptor positively coupled to adenylyl cyclase and stimulation of the β-receptor increases cyclic-adenosine-mono-phosphate (cAMP) in hippocampus (Stanton and Sarvey 1985b, Dunwiddie et al. 1992). cAMP has several intracellular effects, one of which is activation of the cAMP dependent kinase (PKA) by separating the catalytic subunits from the regulatory subunits (Li et al.

2000). The catalytic subunits of PKA have both direct and indirect effects on cell excitability. PKA has been shown to decrease the dendritic A current (Hoffman and Johnson 1998) possibly through the phosphorylation of the Kv4.2 $K^+$ channel (Anderson et al. 2000). PKA also decreases the magnitude of the $Ca^{++}$-dependent $K^+$ current AHP (Madison and Nicoll 1986) which can increase bursting of the postsynaptic cell (Madison and Nicoll 1982). PKA increases the conductance of the L type voltage gated $Ca^{++}$ channel via phosphorylation (Davare et al. 2000). PKA also regulates the conductance of the N-methyl-D-aspartate (NMDA) receptor increasing the $Ca^{++}$ conductance through this channel when the cell is depolarized (Leonard and Hell 1997). The NMDA channel has a unique coincidence detection property. The NMDA receptor consists of a ion channel directly gated by glutamate. Under basal conditions the channel pore is blocked by a magnesium ion, which attenuates influx of $Ca^{++}$ and other cations even when the receptor binds glutamate (Nowak et al. 1984). The magnesium ion is expelled from the channel during postsynaptic depolarization permitting $Ca^{++}$ influx. Activation of the NMDA channel requires both presynaptic release of glutamate and postsynaptic depolarization. The NMDA channel is known to be modulated by other protein kinases including calcium/calmodulin kinase II and protein kinase C (Leonard and Hell 1997).

PKA also has indirect effects on cell excitability through its repression of protein phosphatase I (Woo et al. 2002). Protein phosphatase I dephosphorylates proteins, including receptors and ion channels, returning them to their basal states.

By opposing the actions of protein phosphatase I, PKA further enhances both $Ca^{++}$ flows and cell excitability by amplifying the actions of calcium/calmodulin kinase II (Wang and Kelly 1996).

Norepinephrine long-lasting potentiation is likely to be dependent on calcium influx since norepinephrine increases NMDA induced currents, and blockade of NMDA receptors blocks norepinephrine induced long-lasting potentiation (Stanton et al. 1989; Burgard et al. 1989).

### *Summary*

The hippocampus is a model system for the study of learning and memory, and many behavioural tasks are dependent on the integrity of the hippocampus. Norepinephrine is released in hippocampus during the performance of cognitive tasks and disruption of the norepinephrine system by lesion or pharmacological manipulation can degrade task performance. Norepinephrine has been shown to modulate activity of the hippocampal network as indexed by evoked potential and paired pulse recording. Evoked potential evidence demonstrates that norepinephrine application results in the increased efficacy of a constant stimulation, and that LTP is more easily induced in the presence of norepinephrine. In contrast, paired pulse evidence suggests that norepinephrine increases feedback inhibition.

Unit recording studies also show that both principal cells and interneurons have their activity modulated by norepinephrine. The direction of the modulation

however is consistent with paired pulse evidence and contrary to what models of plasticity would predict. Thus we come to a conundrum: how can a modulator that unambiguously enhances evoked potentials in the dentate gyrus do so by inhibiting principal cells and enhancing interneuron responses? There are several possibilities that could explain the discrepancies.

Exogenous application of norepinephrine may not replicate endogenous release. Both Lacaille and Schwartzkroin (1988) and Parra et al. (1991) reported that both excitatory and inhibitory responses to norepinephrine can be recorded from the same cell, depending on the location of the norepinephrine application. Furthermore, Curet and de Montmigny (1988a) report that exogenous norepinephrine application is biased towards activation of the α2-receptor. In contrast, release of endogenous norepinephrine tends to activate α1 and β-receptors (Curet and de Montmigny 1988b). These results are consistent with Bijak and Misgeld (1991) who reported an increase in the frequency of both spontaneous EPSPs and IPSPs after bath application of norepinephrine or noradrenergic compounds. Exogenous application of norepinephrine or receptor agonists may contact extra-synaptic receptors rather than receptors that are enclosed by a synapse.

Release of endogenous norepinephrine driven by pharmacological manipulations does not mimic the phasic burst of norepinephrine associated with cognitive tasks. Instead the bath applied, intracerebroventricular administered, or peripherally injected pharmacological agent is likely to cause an increase in the

tonic release of norepinephrine from terminals. Rather than mimicking the bursting of locus coeruleus during complex tasks, exogenous norepinephrine more closely mimics the difference in basal activity associated with a transition from slow wave sleep to a waking state (less the burst of locus coeruleus activity associated with the waking event itself).

Characterization of extracellularly recorded units may not accurately reflect the diversity of interneuron types that exist in dentate gyrus. Previous in vivo studies have focused on short latency, feedforward driven interneurons with high spontaneous firing rates. This selection bias may not accurately reflect the balance of interneuron activity in dentate gyrus. In addition the in vivo work has used low impedance electrodes or microwires for recordings, which compound the problem of identifying a clear record of a single cell from other units.

### *The Present Study*

This study designed to reconcile noradrenergic modulation of interneurons and principal cells in the dentate gyrus with the evoked potential data. Cells will be recorded with minimal criteria for inclusion in the study. To be included cells must be driven by perforant path stimulation, either in a feedforward or feedback fashion, and must be discriminable in the evoked potential. There is no selection for cells on the basis of baseline rate. The hilar placement of the electrode will be assured by both a positive going evoked potential record and histological verification of the pipette tip aided by iontophoresis of the neuronal tracer

biocytin. Norepinephrine modulation of unit and evoked potentials will be induced by release of endogenous norepinephrine, driven by glutamate activation of locus coeruleus using parameters that have been shown to mimic locus coeruleus burst activity associated with cognitive tasks. This study differs from the majority of the literature in that:

i) it is performed in vivo

ii) cell sampling is not selected on the basis of rate

iii) endogenous norepinephrine is released

iv) norepinephrine release is driven in a pattern resembling that observed in behaving animals

v) all recorded cells must be discriminable in the evoked potential.

## Methods

### *Surgical Procedures*

Subjects were 19 male Sprague-Dawley rats obtained from the Memorial University Vivarium. Animals weighed from 250 to 700 (60-360 days old) grams. In order to minimize animal use some animals had been used in previous experiments. Two animals had been used as stimuli in a social memory task when they were 20-30 day old juveniles. One animal had been exposed to peppermint odour as an odour alone control in a conditioned place preference task. Animals were anaesthetized with 1.5 g/kg of urethane and fixed in a stereotaxic apparatus. A subdural injection of Marcaine (0.2 ml) with epinephrine was injected into the scalp to provide additional local anaesthesia and control bleeding. A rectal temperature probe was inserted and rectal temperature was maintained between 36.5-37.5 °C. A single incision was made on the midline and the skin was retracted to expose the skull. Holes were drilled over three locations; hippocampus (-3.5 mm posterior, 2.0 mm lateral to bregma), perforant path (-7.2 mm posterior, 4.1 mm lateral to bregma), and the locus coeruleus (-12.6 mm posterior, 1.3 mm lateral to bregma). Bone flakes were removed, and dura retracted using a 26 Ga needle. The brain surface was kept moist using heavy mineral oil regularly applied to the skull openings.

### *Electrode Placements*

*Placement of Stimulating Electrode*

A low impedance recording electrode (0.5-1.0 MΩ) was lowered to an initial depth of 1.5 mm ventral to brain surface. The electrode was pulled from standard non-filament glass (#6280, A-M Systems Inc) on a vertical puller (700C, David Kopf Instruments) and filled with normal saline. The recording electrode was aimed at the hippocampus and lowered to an initial depth of 1.5 mm ventral to brain surface. A concentric bipolar stimulating electrode (SNEX-100, David Kopf Instruments) was aimed at the angular bundle and lowered to an initial depth of 2.0 mm ventral to brain surface. A stainless steel skull screw inserted anterior to bregma, in the hemisphere opposite to the recording and stimulating electrodes provided a ground connection.

Stimulation was controlled by software (*Experimenter's Workbench*, Datawave Systems). Trigger pulses were 0.2 ms applied at 0.1 Hz to a constant current stimulator (SIU90, Neuro Data Instruments Corp.) at an initial current of 400 μA, which was varied as necessary. The recording electrode was advanced until the point of maximum positivity of the waveform between depths of 2.2-3.5 mm ventral to brain surface. When the recording electrode was in place the stimulating electrode was advanced through tissue until the maximal population spike amplitude was obtained. The evoked potential was monitored in both *Workbench* and on a Gould 420 digital oscilloscope. The signal from the recording electrode was fed into a HIP5 headstage (Grass Instruments) that was

connected to a P5 amplifier (Grass Instruments). The signal was band pass filtered at 1 Hz-3 kHz and amplified 50-200x as necessary to fill a reasonable portion of the ±2.5V range of the analog/digital conversion (A/D) board. The signal was digitized at 148 kHz by a DT 2821 F-DI A/D board (Data Translation) before being collected by *Workbench*. A brief input/output (I/O) curve was collected to select currents suitable for driving interneurons. The low current required a positive going EPSP with no trace of a population spike, including a deflection in slope between 4-5 ms. The EPSP peak had to occur prior to 6 ms post-stimulation. The high current required a positive going EPSP with a clear medial perforant path population spike. The population spike had to be at least 1 mV in size, and occur between 4 and 5 ms post-stimulation. The low impedance recording electrode was then withdrawn.

*Ejection Pipette Placement*

The pressure ejection pipette was pulled from non-filament glass (G-2, Narashige Ltd.) on a two-stage vertical puller (PE-2, Narashige Ltd.). The pipette was filled with a combination of 500 mM glutamate (l-glutamic acid, Sigma-Aldrich) and 2% of either biocytin (biocytin hydrochloride, Sigma-Aldrich) or neurobiotin (N-(2-aminoethyl) biotinamide hydrochloride, Vector Laboratories). Pipettes were mounted in pressure tubing modified by the addition of a recording wire and amphenol pin inserted and epoxyed to the tubing. The tubing was connected to a pressure ejector (Neuro Phore BH-2, Medical Systems Corp.). Biocytin/glutamate was ejected using medical nitrogen (Canada Liquid Air) at a

constant pressure of 40 psi. Tip sizes were adjusted so that a pressure pulse with a duration of 2-15 ms yielded a volume of 70-250 nl measured in air. Tips were typically 25-50 μm, with impedances below 3 MΩ. The pipette was advanced on a 20° angle from the vertical to by-pass the sagittal sinus. Electrophysiological signals were band-passed filtered (600 Hz-10 kHz low pass, 60 Hz comb filter in) and amplified 20 000x on a Grass P5 amplifier. The signal was monitored on the Gould digital oscilloscope, and on an audio analyzer (Fredrick Haer Inc.). Locus coeruleus was generally found 6-6.5 mm ventral to brain surface. The locus coeruleus was identified by the characteristic silence that occurred after proceeding through the very active cerebellum. Individual locus coeruleus units were slow (approximately 1-2 Hz) and wide (approximately 1ms wide waveforms). Identification was aided by the presence of "jaw cells" of the mesencephalic tract of the trigeminal nerve that respond to stretching of the jaw with high frequency firing. These cells were are located dorsal to the locus coeruleus at the most anterior extent of the locus coeruleus , and lateral to the locus coeruleus for the remainder of the nucleus and provide an accurate marker for depth and medio-lateral placement of the ejection pipette. Localization of the locus coeruleus was also aided by the characteristic "burst-pause" response to tail or paw pinch.

*Single Unit Recording Electrode Placement*

Unit recording was performed with high impedance electrodes pulled from glass embedded with a capillary filament (#6020, A-M Systems). Electrodes were filled with 2% biocytin (biocytin hydrochloride, Sigma-Aldrich) dissolved in 0.5 M potassium acetate. Electrodes were not broken back and had an approximate tip size of 0.5-2 μm. Impedances ranged from 5-25 MΩ using an impedance meter (either an "Impedance Check", Frederick Haer, or a BL-1000, Winston Electronics). Electrodes with impedances over 25 MΩ were discarded. The electrodes were mounted and connected via shielded lead to either an x0.1L HS-2 headstage (Axon Instruments) or dual Grass HIP5 high impedance headstages (Grass Instruments). The signal from the HS-2 headstage was fed into an Axoclamp 2A amplifier in bridge mode (Axon Instruments). The gating input for the Axoclamp amplifier was provided by the digital to analog clock function (DAC) of *Workbench*. The electrodes were lowered 1.0-1.5 mm into the brain, and the bridge was balanced using 0.1-0.3 nA of current. Typically the impedance remained unchanged for electrodes towards the lower end of the impedance range (5-10 MΩ); impedances would often climb by 10-50 MΩ (30-70 MΩ final impedance) for electrodes that tested 20 MΩ or higher in the impedance meter. Output from the Vx10 port of the Axoclamp amplifier was split and fed into dual P511 low impedance headstages (Grass Instruments), which were in turn connected to Grass P5 amplifiers. One channel was filtered and amplified for units; the second channel was filtered and amplified for either EEG or EP's as

explained below. The unit amplifier bandpass filtered the signal (high pass 600 Hz, low pass 10 kHz, 60 Hz in) and further amplified the signal 50-1000x as necessary for the resulting unit waveforms to fill a reasonable portion of the ± 2.5 V range of the A/D board. Units were isolated by slowly advancing the stereotaxic arm in 2-3 μm increments. If several mm of tissue had been traversed without isolating a unit the bridge was balanced again, and if the impedance had climbed unreasonably the electrode was cleared using the buzz or clear buttons of the Axoclamp amplifier and the bridge rebalanced. When a unit was isolated it was first recorded in conjunction with evoked potentials.

Alternatively the HIP-5 headstages were connected directly to the P5 amplifiers and filtered as above. Amplification was adjusted to fill the ± 2.5 V range of the A/D board. Cell isolation and recording proceeded without a bridge, and the impedance of these electrodes in tissue was unknown during recording. Prior to passing current to mark the recording site (see below) the electrode lead was removed from the HIP-5 headstages and inserted in a x1 HS-2 headstage (Axon Instruments) with other connections being identical to the connections described above. Electrode impedance was determined prior to the passing of current to mark the recording site.

***Recording Evoked Potentials***

Stimulation was delivered as in the stimulating electrode placement, 0.1 Hz pulses delivered to the constant current stimulator by *Workbench*. Signals

were digitized at 148 kHz and 50.625 ms events were captured in *Workbench* (7500 A/D values, 3750 A/D values per channel). One channel was filtered for evoked potentials (band pass filtered at 1 Hz and 3 kHz, 60 Hz out) while the other was band pass filtered for units (600 Hz and 10 kHz, 60 Hz in). At least one minute was recorded at each of the high and low current conditions. If the evoked potential characteristics appeared to have changed since the current levels were determined a small I/O curve was done, consisting of 1 minute of recording at four or five different current levels. Recording often continued at the high current level for several minutes until the unit spontaneously fired in the pre-stimulation portion of the record so that the waveform was available for comparison purposes. The same procedure was followed after the glutamate ejection, either at 5 minutes post-ejection, or when the unit was deemed to have returned to its baseline firing rate.

***Recording EEG and Single Units***

No electrical stimulation was delivered during the glutamate ejection. The evoked potential channel was altered to record EEG by changing the high pass setting to 0.1 Hz, and the low pass setting to 300 Hz, 60 Hz filter in. Amplification was adjusted so that most of the A/D range was used (typically 500-1000x). The unit recording settings were unchanged. Data was collected in buffered 499.395 ms sweeps at 30,769.23 Hz, with points being alternately collected between the channels (15366 total points, 7683 points per channel). The

unit channel was monitored for threshold crossings, and when one was detected 6 ms (92 A/D values) of the crossing waveform was extracted and recorded to disc with the timestamp of the event. EEG was signal conditioned by discarding 59 out of every 60 points collected. The result was an EEG signal recorded at 256 Hz (128 A/D values per data sweep) suitable for fast Fourier analysis. One minute of EEG data prior to and following the locus coeruleus glutamate ejection was analyzed. The values used for theta power were 4-9 Hz and the values used for gamma power were 40-80 Hz.

A minimum of 5 minutes of spontaneous unit activity was recorded. After the baseline period a pressure pulse was applied to the glutamate containing pipette and recording continued until either the unit returned to baseline firing rate, or 5 minutes had elapsed, whichever was longer. If the unit did not change its firing rate the unit was followed for 5 minutes post-ejection.

After the post-ejection recording period evoked potentials were collected again using the same settings and protocol that was used in the pre-ejection period. If there had been no change in the firing rate of the unit, and there was no observable change in the evoked potential, the unit and EEG was recorded again with a longer pressure pulse of glutamate in the locus coeruleus. If there was no change in the firing rate of the unit, but there was a change in the evoked potential, then recording was terminated.

At the termination of all recordings, the site was marked with an extracellular ejection of biocytin. The x0.1L headstage was exchanged for an

x1.0L HS2 headstage (Axon Instruments) and biocytin was iontophoresed with199.99 nA, 200 ms depolarizing current pulses at 50% duty cycle for 30 minutes. Triggering stimuli were provided by Workbench. No recording was done during this process. After the termination of iontophoresis the electrode was withdrawn. Another electrode penetration could be made if the penetration was no closer than 300 μm to the earlier track. No more than three sites were marked per animal, and no more than 3 units were isolated from the same animal.

***Perfusion***

At the conclusion of the experiment, animals were removed from the apparatus and transcardially perfused with 300 ml of room temperature heparinized 0.1 M PBS followed by 200-300 ml of fixative consisting of 0.5% glutaraldehyde and 4% formaldehyde or paraformaldehyde mixed in 0.1 M PBS. The brain was removed from the skull and post fixed overnight in the same fixative with the addition of 30% sucrose at 4°C. The following day the brainstem was removed from the forebrain, and the pieces were placed in 30% sucrose in 20 mls 0.1 M PBS at 4°C until the pieces sank to the bottom of the container. Brains were then blocked for sectioning and frozen in methylbutane at –70°C and stored frozen at -70°C for later histology.

***Histology***

Brains were transferred from the freezer to the cryostat and mounted for sectioning. The brainstem containing the locus coeruleus was mounted in the sagittal plane, and the forebrain was mounted in the coronal plane. Hippocampal sections were cut at 80 microns, and collected from approximately where the cell layers begin to appear in the fimbria at 1.5-2.0 mm posterior to bregma. Sections were cut using the roll plate, and dropped into ice-cold 0.1 M PBS. Approximately 36 hippocampal sections were collected per animal.

Locus coeruleus sections were saved beginning from where the $4^{th}$ ventricle begins to take on an elongated shape at approximately 1.8 mm lateral from the midline. Sectioning continued until the cerebellum had completely detached from the brain stem, typically about 18 sections.

Sections were washed in 0.1 M phosphate buffered saline (pH 7.4) three times for at least 10 minutes per wash. Following this sections were incubated with the avidin-biotin complex (Vectastain Elite, Vector Laboratories) in 0.2% Triton-X (Sigma-Aldrich) for 16 hours at 4°C. Sections were again washed 3 times for at least 10 minutes in 0.1 M phosphate buffered saline and then developed with diamino-benzedene (DAB substrate kit, Vector Laboratories). Sections were washed 3 times for 10 minutes in distilled water and then mounted on gelatin coated slides. After air-drying sections were either further dehydrated in a graded series of alcohols, then cleared in xylene and cover slipped. Some

sections were rehydrated and counter-stained with a monochromatic cresyl violet procedure prior to being dehydrated and mounted.

### *Data Analysis*

*Unit Data*

Unit waveforms were cluster cut using the Common Processing package included with *Experimenter's Workbench*. Waveform attributes were plotted in a pairwise fashion and the cell firing events were cut from the noisy threshold events. Occasionally a manual parameter such as voltage at time was necessary to completely cut a cluster.

Unit data was assembled into a rate meter histogram using the plotting utility in *Common Processing*. Units firing rates for each one-second period were summed. Data were then exported to *Prism* (Graphpad Software) for graphing. The timestamps of unit events were exported to an ASCII file and run through a custom script to look for burst events (*count-bursts* App. A). *Count-bursts* looked for spike events that occurred within 6 ms of each other The script returns the number of spike events, the number of burst events, the number of spikes associated with each burst, and the average number of spikes per burst for the pre and post ejection periods. Interspike intervals were also described using autocorrelations. Autocorrelations were plotted using the correlation utility in *Common Processing*. Spikes were grouped in two ms bins over the period of 0-1000 ms and exported for graphing.

Amplitudes and widths of unit waveforms were determined by averaging all units within a cluster and examining the average waveform. Width was taken to be the time between the peak positivity and the peak negativity of the waveform (see Figure 6). Waveform amplitudes were taken as the voltage difference between the peak positivity and the peak negativity of the waveform divided by the amplification (See Figure 6).

The averaged waveform was also used to calculate the waveform asymmetry ratio (Henze et al. 2002) of the leading peak or valley for each cell (see Figure 7). The amplitude of the cell was plotted as a percent of total voltage change and shifted such that the baseline equaled 0%. The positive and negative components were approximately equal for all cells and the neither the positive nor the negative components represented more than 60% of the total voltage swing. Asymmetry was analyzed at the 20% level of maximum voltage. Asymmetry was expressed at the ratio of the rise time from 20% maximum to maximum divided by the fall time from maximum voltage to 20% (see Figure 7).

*Evoked Potentials*

EPSP slope and population spike changes were assessed using 1 minute averaged waveforms from the pre- and post-ejection period. Averages were chosen since the effect of norepinephrine on evoked potentials was not being investigated for its own interest, but rather being used as an index of the adequacy of the ejection pipette's placement and function. As such the variability of the

response was not quantified. Slopes were determined by exporting these averaged waveforms to *Excel* and calculating $\Delta V/\Delta t$ for the linear portion of the EPSP rise. Population spike was taken as the voltage difference between the leading peak and the trough of the population spike. Measurements of a typical evoked potential are depicted in Figure 8.

*EEG*

The EEG records were analyzed using the fast Fourier transform utility included with *Common Processing*. The analysis returned power in the theta range (4-9 Hz) and gamma ranges (40-80 Hz) as a percentage of total power. The theta values were also used in a scatter plot to investigate theta control of unit firing. Because of a discrepancy between real-time and the computer's processing time during data acquisition binning utilities in *Common Processing* were inappropriate. A custom script *fix-this-mess* (see Appendix B.) was written to determine how many times a unit had fired during a given EEG data sweep. Briefly the header files and timestamps were exported to an ASCII file using the *Data Edit* module of *Common Processing*. In the resultant files spike events had a universal file format record type (UFF) of 120, EEG sweeps had a UFF of 98. Data Edit sorted the output files on the time that processing was completed so that each EEG record was preceded by the spikes that had been detected during that EEG sweep collection. *Fix-this-mess* simply counted 120s preceding 98s, and returned that value. The spike count could be matched with the theta power output for graphing or further processing.

## Results

Stable recordings from the hilar region of the dentate gyrus were obtained from 27 cells. Placements were recovered for 19 biocytin injections as summarized in Figure 9A. Associated locus coeruleus placements were recovered for 14/19 animals and are shown in Figure 10. All cells could be driven by perforant path stimulation representing 18 feedforward, 7 feed-back cells and two putative granule cells. Feedforward cells were defined as those with a threshold below that required for a population spike (n=16). All but one of these cells could be shown to fire prior to the population spike at higher currents. Two additional cells included in this category had supraspike thresholds and latencies similar to the population spike, but had baseline rates exceeding 5 Hz in some intervals. Putative granule cells were defined as cells with a threshold at the level of the population spike and latencies in the window of the population spike, but with slow firing patterns. Feedback cells were defined as cells which had a threshold higher than that required for a population spike and which fired after the population spike. Twenty-three of the cells significantly changed their spontaneous firing rate in response to the glutamate ejection with 14/18 of the feedforward cells and 4/7 of the feedback cells decreasing their firing rates, while 3/7 feedback cells and the two putative granule cells increased their firing rates. Table 1 summarizes the firing characteristics of individual feedforward and feedback interneurons and putative granule cells.

Figure 11 shows the averaged inhibition of normalized firing rates for the 13 feedforward cells with baseline rates exceeding 1 Hz that decreased their firing rates. The period of inhibition began immediately, was maximal from 2-60 seconds post locus coeruleus activation and recovered within 2-3 minutes post activation. The group data suggest an apparent rebound.

Figure 12A shows the averaged response of the 3 feedback interneurons that were excited in response to the glutamate release. The maximal phasic response was seen within 10 seconds and recovered to baseline by 2-4 min post locus coeruleus activation, although one cell maintained some elevated activity through the recording period. Figure 12B shows the pattern of firing of the two feedback interneurons with a baseline of more than 1 Hz than were inhibited by locus coeruleus activation. The inhibition pattern is similar to that seen for the feedforward inhibition although rebound activity was not evident.

Figure 13 shows the responses of the two putative granule cells. These cells had very low firing rates and locus coeruleus activation induced a substantial burst.

Evoked potential recordings from before and 5 min following the locus coeruleus glutamate ejection were available for 25 of the cell recordings, one of which did not display a population spike. See Table 2. The population spike increased (more than 110% of baseline) for 9 cells and decreased (less than 90% of baseline) following the ejection for 8 cells. In 7 cases the population spike did not change. The evoked potential slope increased (greater than 5% over baseline)

for 8 cells, and decreased (less than 5% of baseline) in 8 cases. In 9 cases the slope did not change. Neither the slope ($t(24)=0.298$, $p=0.76$) nor the population spike ($t(24)=0.622$, $p=0.54$) were significantly different with all glutamate ejections treated as a group.

In rats with multiple injections there was a tendency for population spike changes to repeat with successive injections. Of the 3 rats with population spike increases, the increase was replicated in two and was followed by a decrease after a large increase in baseline in 1 rat. Two rats showed an approximately 10% decrease with each ejection. One rat didn't change on either ejection and a final rat showed a decrease followed by no change after a large increase in baseline. EPSP slope effects were more variable with increases, decreases or no changes seen successively in any given rat (see Table 2).

EEG was recorded simultaneously with spontaneous unit activity. Total power decreased in 22 of the 27 ejections. In the remaining cases there was no difference between power pre- and post ejection. Taken as a group power significantly decreased to 80% of the baseline value ($t(25)=2.28$,$p=0.03$). Two power bands were further examined. The percentage of power occurring in the theta band (4-8 Hz) increased in 18 cases, and decreased in 9 cases. Overall the increase of theta power to 116% of baseline was significant ($t(26)=-3.09$, $p=0.005$). The percentage of total power occurring in the gamma band (40-80 Hz) decreased in 22 cases, and increased in 5 cases. The group decrease to 73% of baseline following the ejection was significant ($t(26)=2.58$, $p=0.016$). The effects

of multiple glutamate ejections showed a similar pattern for EEG as for evoked measures. Four rats increased theta power and decreased gamma power repeatedly with glutamate activation while one rat decreased power in both domains repeatedly and two rats showed clear effects on 1 ejection but not on another. See Table 3 for a summary of individual experiments for EEG power and theta and gamma percentages of total power. Theta power was not predictive of interneuron firing rates on a sweep by sweep basis.

All recovered recording placements were located in the dentate gyrus. Seventeen of the 19 placements were in the granular/subgranular zone. These placements include one associated with a putative granule cell. Three placements were recovered in the lower blade which included two feedback cells. Three placements were recovered in the most medial portion of the hilus. Of the two placements outside the granule zone one was a slow firing feedback cell, the other could not associated with a single type. No placements were recovered in the molecular layer.

All of the recovered ejection placements were within 500 μm of the edge of the locus coeruleus. Four placements were within the locus coeruleus itself, while another five were ventromedial to locus coeruleus in the perisubcoerulear area. Two placements were anteromedial to locus coeruleus, two were dorsal and one was on the posterior margin. The most distant recovered placement was in the magnocellular portion of the medial vestibular nucleus approximately 400 μm ventral and 300 μm posterior to the locus coeruleus. Spike increases at ~10 min

post-ejection were observed for sites bordering the locus coeruleus in the anterior, posterior and ventral regions (n=4). Two placements centrally located in the locus coeruleus were not associated with spike increases. Increases in theta power were associated with sites within the locus coeruleus or on the dorsal posterior margin. Anterior and ventral placements were not associated with theta power increases. See Figure 10. Changes in cell firing patterns were elicited more frequently than evoked potential or EEG changes suggesting that there are different thresholds for recruiting effects on the network. Prior studies comparing norepinephrine levels and evoked potential change have also suggested threshold effects dependent on norepinephrine release pattern and level (Harley et al. 1996).

The recorded cells differed in a number of respects, which offer some opportunities for classifying them. Cell types have typically been distinguished by their firing rates and their action potential widths. The first moment of the autocorrelogram has also been used (Harris et al. 2000). One additional parameter that can be used is the asymmetry ratio (Henze et al. 2002). Asymmetry describes the difference between the rise from baseline to peak as a ratio of the fall time peak to baseline (see Figure 7). Plotting the cell width against asymmetry yields three distinct clusters in the current data set (see Figure 14). One cluster is distinguished by narrow extracellular action potential widths. The remaining clusters have roughly similar cell widths, but one cluster has a symmetry ratio centered about 1 (symmetrical cells), while the third cluster's symmetry ratio is

below 0.75 indicating a slow decay from peak relative to the rapid rise. See Figure 14.

The clustering appears valid to delineate functional categories of neurons as the majority of recorded feedback cells (5 of 7) fell into the symmetrical cluster. A single feedback cell fell into the narrow and into the wide category.

There appears to be no relationship between the recording placement and the properties of the recorded cell. It is difficult to determine whether the lack of a relationship truly means that physiologically distinguishable cell types are evenly distributed within the dentate gyrus for two reasons: first the majority of the recording placements were clustered in the peri-granular region and so other locations may not have been sufficiently sampled to observe a trend. Second it was unusual to recover more than one recording site from an animal from which multiple cells had been recorded. In those cases it was impossible to assign the recording site to a recorded cell.

Glutamate ejection into the locus coeruleus had a large effect on the recorded cells. The most common effect was for a decrease in the spontaneous firing rate following the ejection. This pattern was associated with all, but one of the feed-forward cells and a few of the feedback cells. Much less common was an increase in spontaneous firing rate, although this pattern occurred with three feedback cells and two putative granule cells. The single feed-forward cell that displayed an increased firing rate following the ejection (4022A see text below) could be considered anomalous due to a variable baseline period. During the

baseline recording the cell varied from 0 to 20 Hz. A six-minute average baseline rate of 8.7 Hz was more than double the 4 Hz rate of the cell in the one minute immediately preceding the ejection. This cell had returned to it's typical rate in the 20 seconds immediately preceding the ejection although this is not reflected in the one minute average used for comparison. A few other cells did not significantly alter their discharge pattern following glutamate ejection.

The following section reviews the firing characteristics of the cell types examined when categorized by firing on the evoked potential and by symmetry of the extracellular waveform using the clusters identified on the basis of waveform analysis.

### ***Feedforward Cells***

#### *Narrow Cells*

##### *Single spiking*

There were five feed-forward cells (Figures 15-19) with a narrow waveform. Four of these had similar baseline firing characteristics (4-10 Hz) with a mean rate of 7.5 Hz prior to locus coeruleus activation and little or no evidence of bursts during the pre or post recording periods. The 5$^{th}$ cell had a slower firing rate (.5 Hz) and showed some bursts. These cells exhibited the shortest latencies to perforant path activation seen for any of the cells recorded (3 ms or less; 4/5). A group of three fired only single spikes to perforant path stimulation and had no evidence of theta frequencies in the autocorrelation patterns (Fig. 15-17) while

two cells fired multiple spikes to perforant path stimulation and did show evidence of firing in the theta range (Fig. 18-19). The single spiking cells were inhibited by locus coeruleus activation while the multiple spiking cells showed no clear change. The individual cells and the associated locus coeruleus evoked responses are described in more detail.

*Cell JCR 4018A* (see Figure 15)

This cell was isolated 3.1 mm ventral from brain surface. The cell waveform was of the typical peak-valley form with a width of 203 μs and amplitude of 593 μV. This cell fired moderately fast with a baseline rate of 5.6 Hz and virtually no empty bins. The peak firing rate during the baseline period was 9 Hz. The cell did not burst. The ISI distribution revealed a very late primary peak between 100-120 ms with no activity occurring inside the 25 ms mark. The cell responded to 300μA of stimulation of the perforant path which was sufficient to elicit a very small population spike. The cell's firing latency was very short, in some cases the cell waveform appeared to partially overlap with the stimulation artifact. For spikes that were clearly separated from the stimulation artifact the mean latency was 1.1 ms.

Immediately following the pressure pulse the cell ceased firing for 35 seconds, and its activity remained below baseline for another 50 seconds. Following this period of suppression the cell appeared to fire at a new higher baseline with the final minute of recording producing an average rate of 9.8 Hz. The ISI distribution for this cell also shifted dramatically for this cell with the new

peak centered around 80 ms with some suggestion of a secondary peak appearing where the baseline peak had occurred.

The evoked potential slope increased to 106% of baseline, from 1.7 mV/ms to 1.8 mV/ms. The population spike also increased from 0.3 mV to 0.5 mV, an increase of 164%.

The overall power in the EEG record did not change for this cell although theta power increased significantly and gamma power decreased.

*Cell JCR 4006 B* (see Figure 16)

This cell was isolated 3.2 mm from brain surface in the hilus proper of dorsal dentate gyrus. The cell waveform was of the valley-peak form, with an amplitude of 579.23 μV, and a width of 458.1 μs. The cell fired regularly at 10 Hz and did not burst. Firing rates varied from 2 to 18 Hz during the baseline period (mean 11.07 Hz, stdev 2.73). The cell could be driven by low current stimulation of the perforant path. The cell fired in feed-forward mode, as the current was sub-threshold for a population spike. The cell responded with single action potentials with 100% reliability. The cell firing varied in time from 2.55 ms to 2.97 (mean 2.72 ms). The autocorrelation showed a peak at 30 ms with a smooth logarithmic-like decay pattern.

The cell responded to the pressure pulse with a transient increase to 14 Hz for three seconds. Firing then steadily decreased to reach 0 Hz at 23 s post ejection. Firing was suppressed for approximately eight minutes. The cell briefly returned to baseline rates before returning to a decreased firing rate of 6 Hz for

the duration of record. The decrease in firing from 10.05 Hz to 3.47 Hz was significant at $p<0.0001$ ($t=59$) for one minute means.

The evoked potential increased in slope from 5.97 mV/ms to 6.67 mV/ms approximately 18 minutes post ejection. There was an increase in the population spike from 2.21 mV to 2.47 mV.

There was a significant increase in the percentage of theta power in the EEG record (36.86 % pre, 41.28 % post, $p=0.032$). Total power in the EEG record decreased significantly (56297.11417 $mV^2$ pre ejection, 21117.13985 $mV^2$ post ejection, $p<0.0001$).

*Cell JCR 4024A* (see Figure 17)

This cell was isolated 3 mm ventral from brain surface. The cell was of the expected peak-valley form with a width of 725 μs and amplitude of 314 μV. The cell had a slow baseline firing rate of 0.5 Hz. The peak rate was only 4 Hz with a large number of empty bins. The cell did not burst frequently with only 2% of spikes occurring in bursts. Neither the autocorrelation nor the ISI distribution was of interest given the low number of spikes in the record. The cell could be driven with 100 μA of current delivered to the perforant path, which was subthreshold for a population spike. The latency of 3.8 ms resulted in the spikes appearing just following the crest of the evoked potential. At higher currents the cell fired with a latency of approximately 3 ms, well before the population spike.

Following the pressure pulse the cell ceased to fire for over one minute, with 90 seconds passing before the cell fired in consecutive bins. The cell

continued to increase its firing rate to reach a new baseline of 1.8 Hz by the end of recording. The slope increased over 10% from baseline recording from 3.0 mV/ms to 3.5 mV/ms. The population spike also increased over 10% from 1.9 mV to 2.1 mV.

All three EEG parameters were significantly altered following the ejection. The percentage of power present in theta frequencies increased, while overall power and the percentage of power in gamma frequencies decreased.

*Multiple spiking*

*JCR 4009B* (see Figure 18)

This cell was isolated 3.4 mm ventral from brain surface in the lower blade near the medial point of the dentate gyrus. The cell waveform was of the standard peak-valley form with an amplitude of 73.8 μV and a width of 461.5 μs. The cell fired rapidly during the baseline period at an average rate of over 10 Hz with a peak rate of 18 Hz. There were no empty bins after the first 10 seconds of the baseline period although the cell dipped below 5 Hz on several occasions. The cell could be driven with 70 μA of current which was below the threshold for a population spike. The cell fired several action potentials in response to perforant path stimulation, all of which occurred later than the latency of a population spike. The first spike occurred at an average latency of 5.1 ms, although it could be as early as 4 ms or as late as 6 ms. The second spike would typically follow the first with a delay of 1.3 ms. If there were a third spike it would follow the second with a further delay of 2.5 ms. The spiking activity seemed to be depressed by

turning the current past the threshold for a population spike, although it is unclear whether this was due to the cell being inhibited by granule cell firing, or whether the units were simply obscured by the larger voltage swings associated with higher stimulation currents. Despite the high baseline rate, and the bursts to afferent stimulation, the cell did not burst during the free recording period.

Both the autocorrelation and the ISI distribution plots show a strong primary peak in the 12-14 ms range with a weaker secondary peak at approximately 200 ms.

Following the pressure pulse in the locus coeruleus there was not a clear effect, the cell slowed briefly for several seconds before speeding up to slightly above baseline. The cell stopped firing at 52 seconds following the ejection, likely due to electrode movement as firing did not return by the end of the recording period and the cell did not appear in the final evoked potentials.

*Cell JCR 4022A* (see Figure 19)

This cell was isolated 2.5 mm ventral from brain surface. The cell was of the typical peak-valley form with a width of 329 μs and amplitude of 105 μV. The cell was very erratic during baseline recording with a peak rate of 20 Hz but also with 10 seconds or more of silence. Although the overall baseline rate was 8.7 Hz, the minute immediately preceding ejection had a rate of only 4 Hz, compared to an average rate of over 11 Hz for the first four minutes of recording. Firing during the last minute was also highly variable with a full quarter of the bins being empty and another quarter of the bins containing 10 spikes or more. The cell did not

burst. The ISI distribution reflects this erratic firing pattern with a very broad peak primary peak stretching from 20-80 ms. The autocorrelation is skewed, flattening slightly past 300 ms. The cell responded to stimulating current as low as 30 μA and fired with 100% efficiency. At this current level no population spike occurred. The latency was very early, approximately 2.5 ms. A slight increase of the current to 50 μA reduced the latency of spikes to 2 ms and also produced trailing spikes, which occurred on the down slope of the evoked potential, with a mean latency of 5.3 ms.

There was little response immediately following the pressure pulse. The cell continued firing at approximately 7 Hz, close to it's early baseline rate. Although using one minute pre-post comparisons suggests an increase of firing rate this does not appear to be the case. The cell began the final minute of baseline firing very slowly with periods of silence extending several seconds. The cell increased it's rate during the minute and the last 20 seconds yield a rate of 7.5 Hz. The cell did not appear to change it's rate immediately following the ejection. The variability of the cell continued during the post-ejection period and the rate of firing gradually declined, reaching zero approximately one minute post ejection. The firing rate remained low for another minute before returning to a fast baseline of over 11 Hz.

The slope of the evoked potential decreased to 93% of baseline from 3.9 mV/ms to 3.7 mV/ms. The population spike increased post-ejection from 1.1 mV/ms to 1.4 mV, an increase of 36% over baseline.

The percentage of power present in theta frequencies increased while the percentage of power in gamma frequencies decreased significantly. A decrease in total power was not significant.

*Symmetrical Cells*

There were five symmetrical feedforward interneurons (Fig. 20-24). Four had an average firing rate of 5.2 Hz (range 3.8-7.8 Hz) while one was very slow firing with an average rate of .016 Hz. The higher firing cells exhibited some bursts during spontaneous activity recording; all of these were inhibited by locus coeruleus activation. For the slow firing cell no change was observed possibly due to the paucity of firing.

*Cell JCR 4018B* (see Figure 20)

This cell was isolated 3.1 mm ventral from brain surface. The cell waveform was of the typical peak-valley form with a width of 593 μs and an amplitude of 203 μV. This cell had a moderately high baseline rate of 5.3 Hz with few empty bins and a firing rate of 13 Hz. The cell had a tendency to burst with 5% of the spikes occurring in bursts. The ISI distribution reveals a flat peak from 7-10 ms with no secondary peaks. The cell responded to stimulation of the perforant path at 200 μA which was subthreshold for a population spike, although a deflection was sometimes present in the evoked potential which suggests some principal cells could fire to this stimulus. The latency of the cell firing was 5 ms although this varied substantially from under 4 to over 6 ms. In one instance a

spike followed stimulation by a delay of over 10 ms but it was unclear that this was related to the stimulation.

Following the pressure pulse the average firing rate decreased, largely due to an increase in empty bins. Firing declined reaching 0 at 40 seconds post-ejection and returned to baseline by 123 seconds post-ejection. The ISI showed a primary peak and a broad secondary peak at 400-500 ms following the ejection.

The evoked potential slope declined from 4.1 mV/ms to 3.7 mV/ms. The population spike also decreased from 4.8 mV to 1.3 mV.

The total power of the EEG record decreased significantly following the ejection. In contrast both theta power and gamma power increased significantly.

*Cell JCR 4021C* (see Figure 21)

This cell was isolated 3.2 mm ventral from brain surface. The cell was of the typical peak-valley form with a width of 857 μs and amplitude of 106 μV. The cell fired erratically during baseline recording. Although the peak rate of 13 Hz was reached several times, periods of zero firing longer than thirty seconds occurred twice during the baseline period. The overall baseline rate was 2.6 Hz, although the rate was 4.6 Hz in the minute prior to ejection. The cell burst with approximately 5% of its spikes occurring in bursts. The ISI distribution reveals a broad peak from 7-10 ms. The autocorrelation contains a hint of trailing peak between 400-500 ms. Following the pressure pulse the cell ceased firing for 58 seconds and after that time fired only single spikes interspersed with empty bins

for a further 28 seconds. By three minutes post-ejection the cell had stabilized at a new higher baseline (7.8 Hz) with no empty bins.

The data file for the baseline evoked potential data suffered from irrecoverable damage, although notes suggested the cell fired in a feedforward manner. The values for the post-ejection values were 2.3 mV/ms for the evoked potential slope, and 1.7 mV for the population spike.

The percentage of power present in theta frequencies increased while the percentage of power in gamma frequencies decreased significantly. A decrease in total power was not significant.

*Cell JCR 4019B* (see Figure 22)

This cell was isolated 2.6 mm ventral from brain surface. The cell waveform was of the typical peak-valley form with a width of 1055 μA and amplitude of 393 μV. The cell fired reliably at an average rate of 5.3 Hz during the baseline period. The peak firing rate reached 14 Hz, and there were no empty bins during the baseline period though bins below 4 Hz were not uncommon. The cell did not reliably burst with about 2% of spikes occurring in bursts. The ISI distribution shows a broad peak that stretches from 10-30 ms and skews towards the right. The autocorrelation reveals a slight secondary peak at approximately 200 ms. The cell was driven with 50% efficiency by 150 μA of current and with higher currents fired prior to the population spike. The latency varied approximately 0.5 ms around the mean of 4.2 ms.

Following the pressure pulse firing immediately fell to 0 where it remained for 110 seconds. The cell briefly returned to baseline before it was lost 4 minutes post ejection.

The evoked potential slope decreased to 93% of baseline, from 3 mV/ms to 2.9 mV/ms. The population spike decreased to 91% of its baseline level from 1.9 mV to 1.7 mV.

Total power did not change following the ejection nor did the percentage of power in theta frequencies. The percentage of power in gamma frequencies decreased significantly.

*Cell JCR 4021A* (see Figure 23)

This cell was isolated 3 mm ventral from brain surface. The cell waveform was of the typical peak-valley form with a width of 989 μs and amplitude of 215 μV. The cell fired reliably at an average rate of 3.8 Hz occasionally reaching a peak rate of 10 Hz although these were interspersed with frequent empty bins during the baseline period. The cell frequently burst with over 17% of the spikes in the baseline period occurring in bursts. The ISI plot reveals that the primary peak was centered on 6 ms with a skewness to the right. There were no secondary peaks. The cell fired reliably at 280 μA which was supra-threshold for a population spike. The cell fired with a latency that placed it on the early downward deflection of the population spike, 3.7 ms.

Following the pressure pulse the firing rate immediately declined to zero where it remained for 55 seconds before returning to baseline. For a further three

minutes the rate continued to climb above baseline reaching a peak of 28 Hz before again returning to just slightly above baseline in the 5th minute post ejection. The ISI distribution did not change during this period. The slope of the evoked potential increased to 115% of baseline from 4.0 mV/ms to 4.7 mV/ms. The population spike also increased from 0.7 mV to 1 mV.

All three EEG parameters were significantly altered following the ejection. The percentage of power present in theta frequencies increased, while overall power and the percentage of power in gamma frequencies decreased.

*JCR 4008A* (see Figure 24)

This cell was isolated 2.9 mm ventral to brain surface in the dentate gyrus. The cell was of the typical peak-valley form with an amplitude of 109 μA and a width of 725.3 μs. The cell fired irregularly with a peak rate of 10 Hz although after the first minute of recording the cell only surpassed 5 Hz in a single bin. There were frequent empty bins and the absence of activity could last for over a minute. Overall the baseline rate was 0.016 Hz. The cell could be driven with 60 μA of current, well below the threshold for a population spike. The spiking activity occurred late in the evoked potential however (see Fig 24) at an average of 4.8 ms post stimulation. With higher currents the unit was not visible on the waveform so it's location relative to the population spike could not be determined.

Both the autocorrelation and the ISI distribution were flat due to the paucity of spiking activity. The distributions do show peaks at 5 ms due to the rapid bursting during the first minute of baseline recording.

Following the pressure pulse no change in the activity of the cell was observed. The 60 second silence following the ejection was consistent with the extended periods of silence during baseline recording. In contrast the population spike increased by 96% following the ejection from 1.2 to 2.4 mV. The slope decreased by 5% to 3.5 mV/ms from 3.6 mV/ms.

In the EEG records power in both the theta and gamma bands increased significantly, while overall power decreased.

*Wide Cells*

Eight of the feedforward interneurons were of the wide cell type (see Figures 25-32). Six of these fired with an average rate of 6.7 Hz (2.1-12.9 Hz) while two showed slow firing at an average of 0.3 Hz. Half the cells in this group show evidence of bursts while half did not. Almost all of these cells showed immediate inhibition to locus coeruleus activation..

*Bursting cells*

*Cell JCR 4019A* (see Figure 25)

This cell was isolated 2.8 mm ventral from brain surface. The cell waveform was of the typical peak-valley form with a width of 923 μs and an amplitude of 391 μV. This cell had a moderately high average firing rate of 6.9 Hz with a peak rate of 17 Hz. There were occasional empty bins. The cell burst ,

with 12% of spikes occurring in bursts. The ISI distribution reveals a sharp peak from 6-8 ms with a right skew that flattens by 30 ms. The autocorrelation is largely flat although there is a suggestion of a broad secondary peak that stretches from 100-200 ms. The cell was driven by 100 μA of current which was subthreshold for a population spike. The firing latency varied little from the 3.6 ms mean.

Following the pressure pulse firing immediately ceased for a period of 129 seconds after which the cell rapidly returned to baseline. The evoked potential slope increased to 103% of baseline from 2.1 mV/ms to 2.2 mV/ms. The population spike decreased 9% from 1.9 mV to 1.7 mV.

Total power and gamma frequency power were unchanged following the ejection. Theta power significantly decreased.

*Cell JCR 4022B* (see Figure 26)

This cell was isolated 2.7 mm ventral from brain surface. The cell was of the standard peak-valley form with a width of 923 μs and amplitude of 310 μV. The cell had a fast baseline rate of 7.2 Hz with very few empty bins and a peak rate of 15 Hz. The cell burst with over 10% of spikes occurring in bursts. The ISI distribution for the cell has a broad, largely symmetrical, peak from 7-11 ms with no secondary peaks. The cell responded to 50 μA of current which was subthreshold for a population spike. The cell fired with a latency of 3.2 ms which placed near the peak of the evoked potential.

Immediately following the pressure pulse the firing rate dropped to 0 and remained there for 55 seconds with occasional single spikes interspersed with long periods of silence. The cell quickly returned to baseline rates although there was in increased frequency of empty bins throughout the post-ejection recording period.

The slope of the evoked potential increased approximately 10% from 5.1 mV/ms to 5.6 mV/ms. The population spike also increased almost 30% from 3.9 mV to 5 mV.

All three EEG parameters were significantly altered following the ejection. The percentage of power present in theta frequencies increased, while overall power and the percentage of power in gamma frequencies decreased.

*Cell JCR 4014b* (see Figure 27)

This cell was located 2.7 mm ventral from brain surface. The cell waveform was of the normal peak-valley form with a width of 791.2 μs and amplitude of 233 μA. The cell fired slowly with baseline rate of 0.7 Hz during the baseline period with some empty bins and a peak rate of 8 Hz. The overall baseline rate of 0.66 Hz reflects the patchy firing of this cell. The cell had a propensity to burst with 10% of the baseline spikes occurring in bursts. The ISI distribution shows a peak from 4-8 ms with little change in the pattern beyond 10 ms. The autocorrelogram confirms the lack of a secondary peak at longer ISIs. The cell could be driven by 50 μA of current which produced a small population spike. The cell fired at 4.6 ms in the early stage of the population spike suggesting

that the cell had a threshold similar to granule cells. Following the pressure pulse cell firing decreased to 0 for a period of 85 seconds before returning to baseline. After the ejection the cell entered a period of increased activity with few or no empty bins. The rate for the final minute post-ejection increased to 3.6 Hz. The decrease in rate was significant ($p<0.001$).

The slope of the evoked potential increased marginally from 0.9 mV/ms during baseline to 0.92 mV/ms post-ejection. Following the ejection the population spike decreased over 15% from 1.9 mV to 1.7 mV.

Again there was no significant decrease in overall power, although the decreases in theta and gamma frequencies were both significant.

*Cell JCR 4014a* (see Figure 28)

This cell was located 2.4 mm ventral from brain surface. The cell waveform was of the typical peak-valley form with an amplitude of 317 μA and width of 791 μs. The cell fired at a moderate rate of 2.2 Hz with some empty bins and a peak rate of 10 Hz. The cell burst with 5% of the spikes occurring in bursts. The ISI distribution yielded an unusually broad peak from 5-25 ms. Although there is some peakiness in the autocorrelogram, there are no clearly defined secondary peaks. The cell was driven by 30 μA of current delivered to the perforant path, which was subthreshold for a population spike. The latency showed very little variation from 3.9 ms following stimulation. Following the pressure pulse the cell ceased to fire for a period of 245 seconds before returning to baseline. The decrease in firing was significant ($p<0.001$).

The slope of the evoked potential decreased 10% following the ejection from 3.1 mV/ms to 2.8 mV/ms. The population spike also decreased 10% from 3.3 mV to 3.0 mV.

There was no significant decrease in total EEG power following the ejection, although both theta and gamma frequencies significantly decreased post ejection.

*Nonbursting Cells*

*Cell JCR 4021B* (see Figure 29)

This cell was isolated 3.5 mm ventral from brain surface. The cell waveform was of the typical peak-valley form with a width of 1054 μs and amplitude of 254 μV. The cell fired reliably with a baseline average rate of over 10 Hz. The cell did enter a transient slow cycle during baseline that resulted in a number of empty bins, but outside of this period the cell rarely fell below 4 Hz. The cell rarely burst with <1% of spikes occurring in bursts. The cell responded to 100 μA of current which was below the threshold for a population spike. The latency of 4.6 ms placed the cell just following the peak of the evoked potential although the cell could fire late in the rising phase as well. The ISI plot had a broad peak from 7-13 ms with a pronounced rightward skew. There were no secondary peaks.

Following the pressure pulse the cell immediately ceased firing and remained at 0 Hz for 55 seconds at which point the cell fired at one or two Hertz interspersed with empty bins for a further 20 seconds. The cell returned to

baseline by two minutes post-ejection and there were no further empty bins. The slope of the evoked potential declined slightly from 4.4 mV/ms to 4.2 mV/ms. The population spike doubled in amplitude, from 1.2 mV to 2.4 mV. The ISI distribution was not changed by the ejection.

All three EEG parameters were significantly altered following the ejection. The percentage of power present in theta frequencies increased, while overall power and the percentage of power in gamma frequencies decreased.

*Cell JCR 4023A* (see Figure 30)

This cell was isolated 3.1 mm ventral from brain surface. The cell was of the typical peak-valley form with a width of 989 μs and amplitude of 240 μV. The cell had a fast baseline rate of 5.3 Hz during baseline recording with a peak rate of 15 Hz and very few empty bins. The cell did not burst during baseline. The ISI distribution revealed a primary peak between 8 and 13 ms. The distribution was right skewed with the autocorrelation revealing no secondary peaks. The cell responded to stimulation of the perforant path at 80 μA that was subthreshold for a population spike. The spikes occurred at or near the peak of the evoked potential with a latency of 3.8 ms.

After the pressure pulse the cell continued to fire quickly for several seconds but had ceased firing within 10 seconds. Firing remained at 0 with occasional single spikes for 30 seconds, at which time firing began to gradually increase, returning to baseline within one minute. Following the ejection the cell also burst occasionally with 2% of spike occurring in bursts.

The slope of the evoked potential decreased to 85% of baseline from 2.2 mV/ms to 1.9 mV/ms. The population spike was unchanged from 1.2 mV.

No significant changes were observed in the EEG records following the ejection.

*Cell JCR 4020A* (see Figure 31)

This cell was isolated 3.1 mm ventral from brain surface in the granule cell layer of the upper blade near the crest of the dentate gyrus. The cell waveform was of the typical peak-valley form with a width of 923 μs and amplitude of 588 μV. The cell fired at a moderately rapid rate of 4 Hz during the baseline period. There were occasional empty bins and a peak rate of 15 Hz. The cell did not burst. The ISI distribution had a strong symmetrical peak at 13 ms. The autocorrelation showed minor secondary peaks at approximately 150 and 350 ms. The cell was driven by 100 μA of current, subthreshold for a population spike, which produced spikes one third of the time. The spikes had a latency of 4.1 ms that placed them on the falling phase of the evoked potential.

Following the pressure pulse the firing rate declined to zero where it remained for 76 seconds with the exception of occasional single spikes. The slope of the evoked potential increased 120% from baseline, from 3.3 mV/ms to 4.0 mV/ms. The population spike also increased approximately 120% from 2 mV to 2.4 mV. The ISI distribution shifted rightwards with a weaker primary peak occurring at 20-22 ms. The secondary peaks were unaffected.

All three EEG parameters were significantly altered following the ejection. The percentage of power present in theta frequencies increased, while overall power and the percentage of power in gamma frequencies decreased.

*Cell JCR 4023B* (see Figure 32)

This cell was isolated 3.1 mm ventral from brain surface. The cell was of the standard peak-valley form with a width of 659 μs and amplitude of 139 μV. The cell had an exceptionally slow baseline firing rate of 0.3 Hz or roughly 2 spikes per minute. There was over 3 consecutive minutes of silence during the baseline period. The cell did not burst. Neither the ISI distribution nor autocorrelation was of interest with so few sample points. The cell responded to perforant path stimulation of 100 μA, which was subthreshold for a population spike. The latency of 3.6 ms placed these spikes at the peak of the evoked potential.

After the pressure pulse the cell was silent over two minutes at which time the cell began to slightly increase it's firing rate with some bins containing up to 3 spikes. A peak one minute rate of 0.7 Hz was reached during the third minute post-ejection. A paucity of spikes prevented any conclusion about inhibitory effects of locus coeruleus activation. The slope of the evoked potential was unchanged from 3.1 mV/ms following the ejection, and the population spike decreased by 8% from 1.2 mV to 1.1 mV.

All three EEG parameters were significantly altered following the ejection. The percentage of power present in theta frequencies increased, while overall power and the percentage of power in gamma frequencies decreased.

***Feedback Cells***

The majority (5/7) of the feedback cells had symmetrical waveforms. One was classified as narrow and one as wide. Secondary peaks at the theta frequency were seen in the narrow and wide feedback cells and in 3/5 symmetrical cells. Discrete theta peaks were only evident in the feedback group of cells. Three cells in the feedback group increased their firing rate with glutamate activation of the locus coeruleus.

*Narrow Cells*

*Cell JCR 4003A* (see Figure 33)

This cell was isolated 3.4 mm from brain surface in lower blade of the granule cell layer of dorsal dentate gyrus. The cell waveform was of standard peak-valley form, with amplitude of 110.66 μV, and a width of 327.25 μs. The cell fired reliably at 5.78 Hz and did not generally burst, although there was one doublet in the 5 minute control period (0.5% of all spikes). The firing rate ranged from 0-24 Hz during the baseline period with an average rate of 5.78 Hz. The cell could be driven by high current stimulation of the perforant path. The cell fired in feedback mode, as the current needed to be superthreshold for a population spike, and the cell fired approximately 5.8 ms post stimulation. There was a primary

peak at 24 ms in the autocorrelation, with a slow decay that includes clustering in the theta range. The cell responded to the pressure pulse with an immediate and transient increase in firing rate of 173%, from 6.13 to 10.63 Hz ($p<0.0001$, $t=59$). The firing increase was brief, and the cell returned to the baseline firing rate within 3 minutes.

The evoked potential showed an increase in slope from 0.67 mV/ms to 1.48 mV/ms measured at approximately 8 minutes post ejection. A clear population spike was not seen in this case. Although the population spike had been readily apparent at moderate currents (400 μA) with the low impedance electrode, only a slope deflection was visible with the high impedance electrode, even when current was increased to 1000 μA. The final current for the high stimulation pulse was 800 μa where there was a noticeable deflection in the EPSP.

There was no change in the percentage of theta power in the EEG record (39.92 % pre, 39.39% post, $p=0.99$) and although total power decreased (1172528.714 $mV^2$ pre ejection, 1011161.163 $mV^2$ post ejection) the decrease was not statistically significant ($p=0.37$). The variability of the total power measurement was very high during the pre-ejection period; indeed the standard deviation of the mean was 50% larger than the mean itself.

*Symmetrical Cells*

There were five symmetrical feedback cells (see Figures 34-36) that formed two distinct groups in spontaneous activity. One group of three had an

average baseline firing rate of 11 Hz (4.8-14.9 Hz range). Two of the cells in this group increased their firing rate with locus coeruleus activation. These cells exhibited no bursting. The third cell decreased its firing with locus coeruleus activation. The remaining two cells had low spontaneous firing (.9; .83 Hz). Both decreased their firing further with locus coeruleus activation. Burst events occurred in one cell.

*Cell JCR 4006A* (see Figure 34)

This cell was isolated 2.8 mm from brain surface in the infragranular blade of the CA3 in the hilar region of dorsal dentate gyrus. The cell waveform was of standard peak-valley form, with amplitude of 278.56 μV, and a width of 850.85 μs. The cell fired regularly at 4.82 Hz and did not burst during the entire experiment. The cell rate varied from 0 to 17 Hz during the control period (mean 5.75, stdev 3.45). The cell could be driven by high current stimulation of the perforant path, which was suprathreshold for a population spike. The timing was somewhat variable from 6.2 ms to 8.2 ms post stimulation with a mean of 7.1 ms. The autocorrelation showed a theta-like rhythmicity with an initial peak occurring at 36 ms and a logarithmic-like decay pattern interrupted by minor peaks at approximately 200 and 500 ms.

The cell responded to the pressure pulse with an immediate decrease in firing to 1 Hz from it's baseline rate of 4.82 Hz. This decrease lasted only 15 seconds after which the firing rate rapidly increased to a peak rate of 22 Hz. Overall the average firing rate for one minute pre-ejection vs. one minute post-

ejection increased 263%, from 4.82 to 12.7 Hz ($p<0.0001$, $t=59$). The firing increase was brief, and the cell returned to baseline rate within 1 minute.

The evoked potential decreased in slope from 5.44 mV/ms to 5.03 mV/ms approximately 8 minutes post ejection. There was a similar decrease in the population spike from 1.38 mV to 0.67 mV.

There was a nonsignificant decrease in the percentage of theta power in the EEG record (48.34 % pre, 46.18 % post, $p=0.33$). Total power in the EEG record decreased significantly (166096.994 $mV^2$ pre ejection, 119720.586 $mV^2$ post ejection, $p=0.03$).

*JCR 4011B* (see Figure 35)

This cell was isolated 3.1 mm ventral from brain surface in the subgranular region of zone 3. The cell waveform was of the peak-valley form with a width of 791.2 μs and amplitude of 194.09 μV. The cell fired very rapidly during the free record period with no empty bins and only 10 bins containing fewer than 10 spikes. Overall the average rate was over 14 Hz (range 5 to 31 Hz). The cell could be driven at 50% efficiency by a current level that elicited a substantial pop spike (150 μA). Lower currents were ineffective, even if they elicited a population spike. The latency of the spikes were long, shifting 0.5 ms from the mean of 8.8 ms post stimulation. In at least two cases spikes may have occurred earlier, between 6-7 ms, but the voltage swings at those time points make unit discrimination difficult. The cell did not burst at any time. The ISI

distribution and autocorrelation reveal a strong primary peak at approximately 12 ms and a much weaker secondary peak at approximately 250 ms.

The cell immediately increased its firing rate following the pressure pulse to a peak rate of 35 Hz. The rate remained elevated for the entire 5 minute post-recording period (300 seconds). The change in rate was significant at $p<0.0001$ (14.91 Hz, 24.47 Hz, t59).

The evoked potential slope was essentially unchanged following the ejection, from 5.36 mV/s to 5.34 mV/s at approximately 15 minutes post-ejection. The population spike decreased to 75% of its pre-ejection baseline, from 4.45 mV to 3.16 mV.

EEG analysis revealed a decrease in overall power following the ejection including decreases in power in both the theta and gamma ranges.

*Cell JCR 4019C* (see Figure 36)

This cell was isolated 2.8 mm ventral from brain surface. The cell waveform was of the typical peak-valley form with a width of 857 μs and amplitude of 184 μV. This cell fired rapidly at 13 Hz during the baseline period. The peak firing rate was 19 Hz and there were no empty bins and fewer than 10 bins below 5 Hz. The cell did not burst during the baseline period. The ISI distribution was largely symmetrical and centered at 60 ms. There was a secondary peak at approximately 180 ms. Interestingly there was a total absence of activity below 20 ms. The cell was driven by 150 μA of current delivered to the

perforant path. The latency was very consistent barely varying from 5.2 ms post stimulation.

Following the pressure pulse firing dropped to 0 within 6 seconds. Following this drop a flurry of action potentials lasting 8 seconds (average rate 15.6 Hz) occurred and the rate again dropped to 0 until 166 seconds post-ejection when the cell rapidly returned to baseline rates. The ISI distribution shifted to a new peak at 50 ms although both the symmetry and the secondary peak remained as constant features. Despite a doubling of the peak size there was still a complete absence of activity within 20 ms from a preceding spike. The evoked potential slope was unchanged from 5.6 mV/ms after the ejection. The population spike decreased to 78% of baseline, from 3.0 mV to 2.3 mV.

As with cell 4019 B neither the total power nor the percentage of power in theta frequencies changed following the ejection. The percentage of power in the gamma frequencies did significantly decrease.

*Cell JCR 4015A* (see Figure 37)

This cell was isolated 3.5 mm ventral to brain surface in zone 4 of the hilus proper. The cell waveform was of the typical peak-valley form with a width of 791.2 μs and an amplitude of 86 μV. This cell fired slowly during the baseline period at an average rate of 0.9 Hz although the peak rate of the cell reached 9 Hz. The cell did not burst and both the ISI distribution and the autocorrelogram lack peaks due to the infrequent firing of the cell. The cell fired in response to 400 μA of current which produced a sizable population spike. The cell fired on the down-

slope of the EPSP at a mean latency of 7.9 ms although the times ranged from below 7 to over 9 ms. Following the pressure pulse the firing rate dropped to 0 and remained there until the rate returned to baseline by the 75 second mark.

The evoked potential slope was essentially unchanged at 2.8 mV/ms both pre and post-ejection. Likewise the population spike did not change from 1.3 mV. There were no significant changes in any of the EEG parameters.

*Cell JCR 4013A* (see Figure 38)

This cell was located 2.9 mm ventral from brain surface in the lower blade of the dentate gyrus. The cell waveform was of the valley –peak form with a width of 725 μs and amplitude of 91 μV. The cell had a slow overall firing rate at 0.83 Hz although individual bins could climb as high 9 Hz during the baseline. The cell burst and 10% of the baseline spikes occurred in bursts. The ISI distribution reveals a strong primary peak in the 4-6 ms range confirming the propensity to burst. After glutamate ejection the cell ceased firing for a period of 65 seconds before returning to baseline. The decrease in firing was significant ($p<0.001$). The data files containing the evoked potentials were damaged and could not be retrieved. Notes taken at the time suggest a feed back cell. EEG analysis revealed non-significant changes in gamma frequencies and overall power, with a marginally significant decrease in theta power.

*Wide Cells*

*JCR 4012C* (see Figure 39)

This cell was isolated 3.4 mm ventral from brain surface. This cell waveform was of the standard peak-valley form with a width of 857.14 μs, and amplitude of 127.81 μV. The firing rate of this cell varied during the baseline recording period with periods of silence lasting nearly a minute, to a peak rate of 12 Hz. Eight percent of the spikes occurred in bursts during the baseline period. The cell could be driven by 110 μA of current with a 50% efficiency, which was sufficient to evoke a population spike. The latency of 6 ms placed the spikes on the rising portion of the population spike. Increasing the current level to 150 μA increased the driving efficiency to 100% and shortened the latency. The cell showed a peak in the autocorrelation and ISI distribution plot at 7-8 ms with a much weaker secondary peak at approximately 250 ms.

The cell decreased activity following the pressure pulse. The cell stopped firing action potentials within 5 seconds of the pressure pulse, and remained quiet for over four minutes. A normal pattern appeared to return by the termination of free recording. The decrease in firing rate was significant at $p<0.0001$ (1.17, 0.07, t59).

The population spike decreased by approximately 25% following the ejection, from 1.4 mV to 1.1 mV. There was also a 20% decrease in EPSP slope from 1.3 mV/ms to 1.1 mV/ms.

Over all power decreased following the ejection as did power in both theta and gamma bands.

***Granule Cells***

Two cells were identified as putative granule cells (see Figures 40 and 41). One had a narrow profile while the other had a wide extracellular profile. Their firing rates were uniformly slow < 1 Hz. Both increased firing with locus coeruleus activation,

*Narrow Cells*

*JCR 4010A* (see Figure 40)

This cell was isolated 3.8 mm ventral from brain surface. The cell was of the standard peak-valley form with a width of 527.47 μs and amplitude of 106.57 μV. The cell's firing properties changed substantially during the recording period. During the evoked potential recording the spike was firing somewhat quickly, and every spike occurred in a doublet. The pattern changed when free recording began. The cell slowed substantially and no longer fired in bursts. The baseline firing rate was 0.067 Hz with long periods of silence and only rarely with more than one spike occurring in a one second bin. The cell had an odd response to stimulation of the perforant path. Stimulation subthreshold for a population spike (300 μA) elicited no spikes from the cell. Increasing the stimulation to 500 μa, which produced a small population spike, produced action potentials 66% of the time. The latency of these spikes showed very little variation from 4.5 ms, which

placed the spikes in the downward deflection of the population spike. Increasing stimulation strength to 800 μA produced a reduction in driving efficiency to 22%.

The cell responded to the pressure pulse with an increase in firing rate to a peak of 5 Hz within 5 seconds. The cell maintained an increased spontaneous firing rate for at least 30 seconds following the ejection. The cell was lost 30 seconds after ejection and did not reappear during the remainder of the recording period, nor during the evoked potentials that followed free recording. Because the cell was lost within one minute of the ejection, the rate change was of borderline significance (0.067 Hz, 0.33 Hz, p=0.059, t59)

The population spike increased 170% following the ejection, from 0.44 mV to 0.76 mV when measured approximately 10 minutes following the ejection. EPSP slope was unaffected by the ejection.

EEG records during the free recording period show slight a decrease of power in both the theta and gamma bands following the ejection. Overall power also decreased following the ejection.

*Wide Cells*

*JCR 4007B* (see Figure 41)

This cell was isolated 2.7 mm from brain surface and was located in the crest of the upper blade of the granule cell layer. The cell waveform was of the peak-valley form with an amplitude of 340.48 μV and a width of 726 μs. During baseline recording the cell fired very slowly, only 13 spikes during the entire control period for an overall rate of 0.06 Hz. Firing increased somewhat prior to

the ejection for a rate of 0.3 Hz in the minute prior to ejection. The cell fired to stimulation of the perforant path only at currents that elicited a population spike. The cell fired with a latency of 4.27 ms with a range 4.09-4.63 ms. This latency placed the spike event in the middle of the pop spike suggesting that the cell was being driven directly by PP, and at the same latency as granule cells. The stimulation of the perforant path was at least 75% effective and possibly 100% effective. The latency of the cell increased with repeated stimulation, and eventually the spike waveform moved past the peak of the population spike. Failures may reflect a latency shift of the unit spike to where the positive going portion of the waveform is opposed by the negative going portion of the pop spike, and vice versa. The failure waveforms are somewhat misshapen compared to normal waveforms. The autocorrelation is absolutely flat during the control period. Only twice did the cell fire within a 1000 ms window from a previous spike.

The cell firing pattern changed dramatically following the pressure pulse to locus coeruleus. Although no response occurred for 26 seconds following the ejection (2 spikes during the period) beginning at 27 seconds following the ejection the cell firing rapidly ramped up to a peak rate of 9 Hz 96 seconds post-ejection. The effect was relatively brief and the cell returned to baseline rates by 260 seconds following the ejection.

# Discussion

## *Effect of Locus Coeruleus Activation on EEG*

The data demonstrates that ejection of glutamate in the region the locus coeruleus affects EEG. The total power of EEG decreases but this decrease is not evenly distributed across the range of frequencies as depicted in figure 42. The theta band is relatively protected, and the percentage of power represented by theta is significantly increased in the minute following activation of the locus coeruleus. In contrast the percentage of power represented by the gamma band significantly decreased.

Gamma frequency is believed to represent the coupling of interneurons into a reverberating network that controls the spiking activity of principal cells (Fisahn et al. 1998). The gamma oscillations are thought to be critical for binding together discrete neural patterns into a cohesive representation (Bragin et al. 1995, Buzsaki and Chrobak 1995). The present results suggest that norepinephrine release causes a decrease in the power of gamma frequencies in the EEG, implying an uncoupling of the interneuronal network, although this process may be mediated by acetylcholine. Norepinephrine has been shown to alter EEG in the cortex indirectly via the septum (Berridge and Foote 1996). One interpretation of this data is that norepinephrine assists in updating representations by loosening the associations that form a representation and allowing new sensory information to be incorporated. One example of this process is contextual fear

conditioning, in which a stable contextual representation is required for the context-shock association to be formed. If the animal is shocked immediately after being placed in a novel context no learning occurs (Wiltgen et al. 2001). As little as two minutes exposure to the environment allows a stable contextual representation to be formed and a shock immediately following the animal's placement in the conditioning chamber will then produce fear conditioning. The present data suggest norepinephrine released by shock would permit the modification of the stable contextual representation.

The observed increase in theta power and reduction in gamma power replicate the EEG effects reported by Berridge and Foote (1991). Berridge and Foote infused the cholinergic agonist bethanechol into the peri-locus coeruleus region. Although their theta power increased to 136% of baseline as opposed to 116% in the present study, the difference in activation parameters may account for the difference. Bethanechol depolarizes locus coeruleus neurons and produces an increase in the tonic firing rate of locus coeruleus neurons. The locus coeruleus discharge rate grows to a peak over a period of approximately one minute, maintains that high rate for a further two to three minutes, and then gradually returns to baseline rates over a period of 10-15 minutes. The bethanechol driven increase in tonic firing rates of locus coeruleus unit rates contrasts sharply with the effect of concentrated glutamate. The pressure ejection of small volumes of concentrated glutamate causes an immediate volley of action potentials from locus coeruleus neurons. The burst lasts for approximately 200 ms, and is

followed by cessation of firing for a period of minutes (Harley and Sara 1992). The difference in the activation parameters of locus coeruleus may account for the difference in the magnitude of the theta increase between the two studies, and the difference in the persistence of the theta change. The EEG results in this study are consistent with a brief release of norepinephrine in the dentate gyrus.

### *Effect of Locus Coeruleus Activation on Evoked Potentials*

The effects of glutamate ejection into the brainstem were mixed in comparison to earlier studies that report potentiation of the evoked potential slope and population spike. Only 30% of ejections resulted in an increase in the population spike, and only 40% of animals showed at least one increase in the population spike in response to ejections.

In previous studies utilizing the pressure ejection of glutamate into locus coeruleus a range of effects has been seen including typically both short-term and long-term changes in population spike amplitudes. Cordell Clarke (1995) reported that ten of fifteen animals had population spike potentiations which lasted less than 10 minutes, the average time being 287 seconds, or less than five minutes. Harley and Evans (1988) reported that only 50% of glutamate ejections produced potentiation lasting at least 30 minutes. Harley and Milway (1986) reported that 90% of the norepinephrine induced potentiations induced by glutamate ejections in locus coeruleus lasted less than 30 minutes. The average duration of these ejection effects was 8.4 minutes. Harley and Milway also report that although the

evoked potential slope increased in 65% of the animals, the average duration for the slope increase was only 2 minutes. Short-term increases in population spike are also associated with electrical stimulation of the locus coeruleus, where changes in evoked potential parameters return to baseline within 100 msec after termination of locus coeruleus stimulation (Harley et al. 1989).

In the present study there was a delay of approximately 10 minutes between the glutamate ejection and measurement of the evoked potentials. Transient potentiations, of less than 10 minutes duration, would not be observed in the post-ejection evoked potential records.

It is also possible that norepinephrine must be paired with afferent stimulation in order to stabilize potentiation at the perforant path granule cell synapse. $Ca^{++}$ influx through the NMDA receptor has been shown to be critical in plasticity, and is believed to be the primary mechanism of coincidence detection (Malenka 1991). In LTP $Ca^{++}$ influx is driven by high frequency trains of stimulation which allows both the removal of the magnesium block from NMDA receptor due to post-synaptic depolarization, and to allow $Ca^{++}$ to flow by opening the channel. The binding of norepinephrine to post-synaptic receptors may be sufficient to remove the magnesium blockade from the NMDA receptor (Lacaille and Schwartzkroin 1988) but norepinephrine does not necessarily produce spiking of the post-synaptic cell, which is also believed to be necessary for the strengthening of synaptic connections (Bi and Poo 2001). This study did not drive granule cell afferents for a period of at least 10 minutes following the glutamate

ejection and so it is possible that the lack of afferent activity is responsible for the small percentage of population spike increases. If this were true, differences in population spike size after norepinephrine treatments would be predicted by the amount of afferent activity during the treatments. A similar idea was tested directly by J.C. Lacaille (Lacaille and Harley 1985; see also Dahl and Sarvey 1990) where norepinephrine was or was not paired with afferent stimulation in the in vitro slice. Ten μm norepinephrine was applied for ten minutes either with concurrent afferent stimulation or no stimulation of perforant path. Potentiation was indistinguishable between the conditions. Under those conditions only short-term potentiation was observed.

Short-term actions of norepinephrine have been observed with synaptic activations of locus coeruleus. Babstock and Harley (1992) aimed a stimulating electrode at the paragigantocellularis (PGi, the major glutamatergic input of locus coeruleus) and applied current in order to release glutamate onto the locus coeruleus. Potentiation was very short-lived under these conditions, with the optimal PGi/perforant path interstimulus interval being only 30 ms. The effect was confirmed to be β-adrenergic since propanalol blocked the effect. Short-term enhancements of dentate gyrus population spikes have been shown in awake behaving animals as well (Kitchigina et al. 1997).

### *Effect of Locus Coeruleus Activation on Single Units*

Twenty seven units were recorded, and of these 24 responded to the glutamate ejection. With the four units that did not show significant changes, the population spike and/or the EEG changes provided evidence of noradrenergic modulation of the dentate gyrus for those ejections suggesting a minority of hilar units may be less reactive to norepinephrine than the others. Of the responsive cells 18 decreased their firing rate following the ejection, and 5 increased their firing rate. The units could be further subdivided by their response to perforant path stimulation. Every responsive cell that fired to current below the threshold necessary to evoke a population spike (feedforward) decreased its firing rate. Cells that fired to current above the threshold for a population spike (feedback) could either increase or decrease their firing rates. This finding of differential regulation of feed-forward and feed-back cells by norepinephrine provides a mechanism in addition to that of β-adrenergic receptor activation of principle cells by which norepinephrine can induce potentiation of field potentials in the dentate gyrus.

The magnitude of the disinhibition is substantial. In the combined plot (Figure 11) the activity of the feedforward cells rapidly approaches zero following the glutamate ejection and remains there for approximately one minute. It takes another full minute for the cells to return to their baseline firing rates. During this time period the feed-back cells that increased their firing rate following the ejection are firing at twice their baseline rate and gradually return to baseline over

a period of 2-3 min. The inhibited feedback cells remain inhibited for a similar period of time. Thus a period of disinhibition of 2-3 minutes duration appears to be associated with norepinephrine release in dentate gyrus induced by glutamate activation of the locus coeruleus.

One view of this pattern of effects is that the inhibition of feedforward interneurons permits the rapid firing of granule cells. Granule cell firing in turn activates the feed-back cells they innervate. Since a subpopulation of feedback interneurons is inhibited another mechanism is required for that effect. In addition within this simple model there could be direct differential effects of norepinephrine on subpopulations. This view will be considered in more detail below.

MOPP cells were not recorded in this study. MOPP cells have their cell bodies located in the molecular layer, and their axon appears to associate with perforant path terminal sites (Han et al. 1993). The ultrastructural relationship between the terminals is not presently known.

### *Relation to Previous Dentate Gyrus Interneuron Studies*

While this study has found a differential effect of released norepinephrine on functionally defined subsets of putative interneurons, previous studies have not reported such a difference.

The present results are somewhat at odds with previous reports of norepinephrine's effect on interneurons of dentate gyrus. Pang and Rose (1987)

and Rose and Pang (1989) reported that iontophoretic or pressure application of norepinephrine and norepinephrine-receptor agonists increase the firing rate of interneurons. There are several facts that may account for the difference in results.

Pang and Rose were selective in the interneurons they recorded, but histological verification of recording locations was not available. Specifically they limited their sample to narrow, fast firing cells (rates over 10 Hz). In addition, cells were required to fire multiple action potentials in response to perforant path stimulation below the threshold necessary to evoke a population spike. While this would appear to select for feed-forward cells, this is not necessarily the case. Pang and Rose may have used lower impedance electrodes (values were not given). The use of low impedance electrodes increases the likelihood of recording multiple units. Without the use of cluster cutting techniques to separate events into cells with similar electrophysiological properties, the unit response may be contaminated during norepinephrine application by the appearance of cells that were present but not firing during the baseline period. This is especially true if, as in the case of Pang and Rose, progressively higher currents were not used to test the possibility that high threshold cells are present near the tip, but are silent during the baseline recording period. Notable is the possibility that due to the dense cell packing in the granule cell layer, granule cells may not appear during low current testing, but begin firing during norepinephrine application. Pang and Rose recorded spiking events on a microcomputer with the aid of a window discriminator, but did not appear to have cluster cutting utilities available. The

present results suggest that disinhibited granule cells may have appeared in the post-application record skewing the reported results.

A second possibility is that the pressure ejection or iontophoresis of norepinephrine does not accurately reproduce the effects of endogenously released norepinephrine. Curet and de Montmigny and coworkers have reported differential adrenoceptor activation using iontophoresis and endogenous release. Iontophoresis of norepinephrine in dorsal hippocampus produced predominately an inhibition of pyramidal cell firing that was blocked by the α2 receptor blocker idazoxan (Curet and de Montmigny 1988a). By contrast activation of the locus coeruleus using electrical stimulation produced an early inhibition of pyramidal cell firing that was blocked by prazosin, an α1 receptor antagonist, and a later excitation that was blocked by the β receptor antagonist propranolol (Curet and de Montmigny 1988b). Thus bias towards inhibitory effects does not necessarily imply that inhibition is the typical effect of endogenous norepinephrine. Curet and de Montmigny argue that α1 and β-receptors are concentrated in intra-synaptic locations, and α2 receptors are located in peri- and extra-synaptic locations which makes them more available for exogenous application of norepinephrine or agonists both in vivo and in slice preparations. Further support for the problematic effects of exogenous norepinephrine application is provided by studies (Bijak and Misgeld 1995, Lacaille and Schwartzkroin 1988, Parra et al. 1998), which report that norepinephrine can produce both depolarizing and hyperpolarizing cellular

events in a single hippocampal cell depending upon the location of the iontophoresis pipette in relation to the soma and dendritic tree.

Consistent with these observations, in a much earlier study, Segal and Bloom (1976a, b) recorded cells from the hippocampus in behaving preparations and used locus coeruleus activation to evaluate the effects of norepinephrine. Rats implanted with chronic recording electrodes in hippocampus and stimulating electrodes in the locus coeruleus were trained to self stimulate. Putative stimulation of the locus coeruleus decreased the spontaneous firing rates of cells in the hippocampus. Injection of d-amphetamine increased bar pressing rates and decreased firing rates (Segal and Bloom 1976a). Firing rates were also reduced by a natural tone stimulus, and tone based inhibition was blocked by injections of a blocker of dopamine-β-hydroxylase or by 6-OH-dopamine lesions of norepinephrine terminals (Segal and Bloom 1976b).

In their chronic recordings they report recording from eight cells in the dentate gyrus. The dentate gyrus cells did not differ from the putative pyramidal cells in either their baseline physiology or in their responses to behavioural or noradrenergic manipulations. Segal and Bloom report baseline firing rates ranging from 3-36 Hz for their cells. On this basis we can suggest that Segal and Bloom were recording from interneurons in dentate gyrus rather than granule cells since granule cells fire at a rate of less than 1 Hz. (Jung and McNaughton 1993). Note because in these early studies Segal may have reported inhibition of rapidly firing

interneurons by indirect, likely synaptic, manipulations of hippocampal norepinephrine as observed here for feedforward interneurons.

Finally, the present results reconcile the evoked potential literature with unit behavior. Feedforward disinhibition, in particular, would result in enhanced population spike size as reliably observed with either exogenous or endogenous norepinephrine.

### *Identity of Recorded Cells*

Clustering analysis of the recorded units using the peak to peak cell width and the symmetry ratio produced three clusters of cells. While it is not possible to definitively identify the recorded cells without an intracellular fill, the clustering analysis allows some inferences. The narrowest cells were predominately feed-forward with short firing latencies and may represent HICAP cells which also meet these criteria and are the only interneurons identified as monosynaptically activated from the perforant path (Sik et al. 1997). Another signature for the narrow feedforward cells was an absence of burst patterns in four out of five cells. This is consistent with the intracellular reports for these cells (Sik et al. 1997). However, two of the narrow feedforward cells fired multiple spikes, which is not a signature of HICAP cells. The firing pattern of these two cells was not modified by locus coeruleus activation. There was also a narrow cell that fired in a feed-back fashion which is a pattern that has not been reported for HICAP cells to date.

The remaining two clusters, symmetrical and wide, were also predominately feedforward, and likely contain basket, mossy and HIPP cells. All three of these cell types can fire in a feedback fashion, and both mossy cells and basket cells can fire in a feed-forward manner as well. These remaining two clusters are of identical widths and distinguished by their symmetry ratio. GABAergic neurons tend to be identifiable by their symmetry (Scharfman, personal communication) and the symmetrical cluster may then represent basket cells. As reported in the Introduction both feedforward and feedback subgroups of basket cells have been identified. The feedforward symmetrical cells with short latencies to perforant path stimulation may be parvalbumin basket cells (Buckmaster et al. 2002, Scharfman 1995, Han et al. 1993), while feedback symmetrical cells with longer latencies would correspond to atypical calbindin basket cells (Sik 1997).

Two types of feedback responses were seen in the present study. Feedback cells either increased or decreased their firing with pericoerulear activation by glutamate. Identified basket cells in CA1 have been reported to be depolarized by β-adrenergic stimulation (Freund and Buzsaki 1995), thus there may be a case for the feedback cells that increased responding to be of this type. In addition granule cell activation would be expected to increase feedback activation. The mainly symmetrical feedback cells (but including one narrow and one wide cell) were the only cells to show discrete theta peaks in the autocorrelations. Thus the symmetrical criteria combined with a theta autocorrelation profile might identify

atypical feedback basket cells in extracellular recordings. A second possibility is that some of the symmetrical cells near the wide/symmetrical border in the cluster cut are mossy cells since mossy cells fire in a feedback manner. HIPP cells are rare with only 5000/dentate gyrus (Buckmaster et al., 2002). The cells are located in deep hilus and in the present study only a single placement could be identified in that region. It was a slow firing symmetrical feedback cell with no theta rhythmicity.

The largest cluster of wide asymmetrical waveforms would then consist predominantly of feed-forward mossy cells. Consistent with this idea, mossy cells are the most numerous non-granule cell in dentate gyrus (Patton and McNaughton, 1984), and the wide asymmetrical cluster is a relatively homogenous group of cells. Mossy cells can act in a feedforward mode if a cell has a dendrite that crosses into the molecular layer (Scharfman, 1991). The preparation in the present study is likely biased towards the recording of feed-forward cells due to scaling difficulties discussed elsewhere. Inhibition of mossy cells would serve to increase disinhibition. Mossy cells do provide excitatory inputs onto granule cells, however the connectivity is sparse (Scharfman 1995a). Scharfman, recording in the presence of bicuculline, observed monosynaptic depolarization of granule cells in only 20 of 1, 316 pairs mossy cell/granule cell pairs. In the absence of bicuculline no excitatory responses could be recorded. Interestingly the tentative mossy cell cluster (asymmetric wide) appeared to respond immediately to the glutamate ejection as did some of the symmetrical

feedback cells that were inhibited, while the remaining clusters had slightly delayed effects. This raises the possibility that much of norepinephrine's effect could be to inhibit mossy cells directly, and the resulting loss of afferent input to other feedforward interneurons produces disinhibition of the granule cells.

As discussed elsewhere the number of feed-forward and feed-back cells recorded in this study is likely not indicative of the true proportions of these cells in dentate gyrus. The procedure is biased towards the collection of feed-forward cells due to problems scaling both the evoked potential and the unit with a single gain setting on the A/D board.

Two cells in this study (4007B and 4010A) appear to meet the criteria for granule cells. They have thresholds similar to granule cells, and their latencies place them in the midst of the population spike. In addition they have very low spontaneous firing rates consistent with those observed by Mizumori and McNaughton (1989). The recording site for cell 4007B was recovered and it was in the granule cell layer. Both of these cells showed a sudden and brief period of rapid firing immediately following the glutamate ejection. Their combined rates are depicted in Figure 13.

The non-principal cells in this study displayed a large variation in their extracellular waveform widths and firing rates. The complexity of identifying the heterogeneous population of interneurons seems to preclude simple rules of classification such as those used by Wiebe and Staubli (2001). Caution should be

taken when interpreting the results of studies that have not rigorously examined the pattern of activity of recorded cells including their activation parameters.

A goal of this study had been to identify recorded cells using juxtacellular labeling (Pinault 1995) and to relate the cell's morphological identity with their physiological characteristics as has been done in slice preparations (Parra et al. 1998, Scharfman 1995b). This portion of the study was not completed due to a lack of specificity of the labeling technique. Juxtacellular labeling was developed in thalamus, which has scattered and rather sparse density of cells (Pinault 1995). Adapting the technique to a densely packed layer of cells such as is observed in dentate gyrus proved problematic. Cells could be strongly labelled if their axons were in contact with the region of biocytin iontophoresis (Figure 43a and b) as reported by Pinault and it is possible that this could occur at some distance. The location marked 18x in Figure 9 is an example of a strongly labelled cell (Figure 43a) that may have been the result of an axonal fill. The site is well removed from the clusters of other identified recording sites, although another biocytin ejection occurred several mm medial to 18x in the same animal (Figure 9 labelled 18y, depicted also in Figure 43b). Labelled axons could sometimes be observed in CA3 where no labeling attempts took place. It was not uncommon to observe a patch of reaction product associated with the recording site with several labelled cells surrounding the site (Figure 44a and b). In addition, labelled cortical pyramidal cells could occasionally be observed despite the fact that no specific labeling attempts occurred in cortex (Figure 44c). Small amounts of current were

passed in cortex to balance the bridge on the recording amplifier and this may have been sufficient to label cells. Other researchers report labeling of cortical pyramidal cells merely by passage of the recording electrode (G.Kirouac, personal communication). These problems cast doubt on the reliability of the juxtacellular technique using biocytin. Other markers (such as horse-radish peroxidase) may demonstrate more specificity.

### *Comparison with Disinhibition in CA1*

Noradrenergic disinhibition has previously been reported in CA1. Doze et al. (1991) reported that norepinephrine or the β-receptor agonist isoproterenol increased population spikes in hippocampal slice. The disinhibition appeared to be presynaptic to the interneuron suggesting that norepinephrine reduced the excitatory glutamatergic synaptic drive on interneurons rather than activating post-synaptic receptors on the interneurons themselves. This mechanism may also account for the present results given that double labelling immunohistochemistry has not shown tyrosine hydroxylase positive terminals contacting GABA positive dendrites (Milner and Bacon 1989). GABAergic cells do express adrenergic receptors however, so the possibility exists that norepinephrine released into interstitial space may act directly on these interneurons via volume transmission. Other investigators have confirmed norepinephrine increased the population spike in CA1 either with bath application of isoproterenol in vitro (Heginbotham and

Dunwiddie 1991) or following pressure ejection of glutamate into the locus coeruleus in anesthetized rat (Olpe et al. 1986).

Disinhibition in CA1 by norepinephrine would predict effects on LTP. Multiple papers have reported that tetanic protocols subthreshold for LTP are effective in the presence of norepinephrine or its agonists (Thomas et al. 1996, Katsuki et al. 1997, Lin et al. 2003). In contrast single unit recordings report an increase in chloride conductances (Staley 1994) of principal cells and increases in the firing rates of multiple classes of interneurons (Bergles et al. 1996).

***Comparison with Unit Changes in Dentate Gyrus LTP***

Several studies have examined alterations in unit firing following LTP in both the dentate gyrus and CA1. The comparison is of interest not only because LTP is the predominate model of plasticity, although it is generally only considered with respect to evoked potentials, but also because LTP in dentate gyrus is norepinephrine dependent. Lesion of the locus coeruleus is reported to decrease the probability of LTP induction and reduce the magnitude of LTP in vivo (Bliss et al. 1983 but see Robinson and Racine 1985). Blockade of β-receptors during LTP induction also reduces the probability and magnitude of medial perforant path LTP in vitro (Stanton and Sarvey 1987). LTP of the lateral perforant path is also β-receptor dependent (Bramham et al. 1997). The lesion and pharmacological studies are supported by the finding that tetanus of the perforant

path releases substantial norepinephrine in the dentate gyrus (Bronzino et al. 2001).

Deadwyler et al. (1975) were the first to examine the role of LTP in controlling neuronal firing activity. They recorded intracellular potentials and field potentials in the in vitro slice preparation. They reported increases in the efficacy of perforant path stimulation following tetanus such that granule cells that previously fired single action potentials during the baseline period fired multiple action potentials following the tetanus. The effects lasted from 9 to 90 seconds. Field EPSP potentials also increased.

Kanda et al. (1989) and Maru et al. (1989) examined tetanus induced alterations of GABA function in dentate gyrus. These studies used a paired pulse protocol where commissural stimulation preceded perforant path stimulation at several ISIs. Tetanus of the perforant path decreased inhibition associated with both commissural stimulation and with backfiring of the mossy fibres. Paired pulse evoked potential experiments with elevated norepinephrine had suggested increased feedback inhibition in dentate gyrus (Sara and Bergis 1991), but more recent observations (Knight 2001) suggest the effect may be due to a loss of facilitation rather an increase in inhibition .

Tomasulo and Steward (1996) reported on interneurons of dentate gyrus in response to tetanus of either the perforant path, the commissural pathway, or paired tetani, using either high or low currents. This study was unusual in that firing latency was the dependent measure used throughout the study, with shorter

latencies indicating potentiated responses, and longer latencies suggesting weakened responses. While tetany of the commissural pathway shortened firing latencies of interneurons, tetany of the perforant path, at either intensity, increased the latency of interneuronal firing. Low intensity tetanus of the perforant path also decreased interneuronal firing probability, the only effect on firing probability that was seen in the data set.

The studies with LTP and identified neuronal subtypes are consistent with the effects of released norepinephrine observed here. A paper recording multiple classes of cells reports a mixed set of response with both increases, decreases and no change following tetani (Kimura and Pavlides 2000). Again this can be viewed as consistent with the present pattern of results with norepinephrine.

### *Implications for Signal to Noise Ratio*

Norepinephrine increases signal to noise ratios in several cortical systems in response to sensory input, including somatosensory stimulation (Waterhouse and Woodward 1980), auditory input (Foote et al. 1983), visual stimulation (Kasamutsu and Heggelund 1982) and olfactory input (Linster and Hasselmo 2001). Signal to noise ratios are generated by comparing the activity of a set of cells to repeated presentations of either a sensory stimulus or afferent stimulation (the signal). The evoked activity is then expressed as a ratio of spontaneous background activity (then noise). In this schema a reduction of the

signal can still yield an increase in signal to noise ratios so long as the background activity is decreased by a larger amount.

In the dentate gyrus the background activity of granule cells is very low in anesthetized rats (Mizumori et al. 1989) and awake rats (Jung and McNaughton 1993). In awake rats granule cells behave as 'place' cells firing selectively to appropriate spatial inputs. Under conditions that evoke the release of norepinephrine the present data suggest a large increase in firing to all inputs, reducing the selectivity of normal responses. While this could be interpreted as a decrease in signal to noise, an alternative view is that norepinephrine enhances all signals to permit the binding of new signals to a stable representation in the dentate gyrus. Thus, while norepinephrine promotes sensory detection and sensory selectivity in cortical areas that are primarily sensory in function, in the hippocampus it promotes the updating of stable spatial or contextual representations

### *Significance for Lateral and Medial Perforant Path Input*

Norepinephrine, in vitro, differentially regulates laminar entorhinal inputs to dentate gyrus. Specifically, the EPSP slope and population spike evoked by lateral perforant path stimulation are reduced while the EPSP slope and population spike evoked by medial perforant path stimulation are enhanced (Dahl and Sarvey 1989). Current views of these inputs assign polymodal sensory functions to the lateral perforant path and highly processed cortically generated

representations to the medial perforant path (Sewards and Sewards 2003). In particular the medial perforant path appears to mediate spatial or contextual representations (Sewards and Sewards, 2003). The implication of this effect is that the norepinephrine modulation of dentate gyrus would promote a complex representation of environmental input over less highly processed sensory stimuli.

The present data do not offer any mechanism for a selective modulation of laminar inputs. The robust feedforward disinhibition seen here would suggest all inputs would be nonselectively enhanced. However, no cells in the molecular layer, e.g., MOPP cells, were recorded in the present study as noted earlier. Norepinephrine may excite a set of feedforward interneurons that selectively terminate on lateral perforant path fibers, providing a mechanism, together with the feedforward disinhibition described here, for the observed laminar modulation.

A second possibility is that the norepinephrine effect in vitro is a consequence of differential distribution of norepinephrine receptors such that shunting of lateral perforant path input occurs in the granule cell dendrites or that lateral perforant path input is inhibited presynaptically. This would make the differential medial and lateral responses independent of interneuron activity.

A third possibility is that selective modulation of lateral and medial perforant path input to the dentate gyrus does not occur in vivo. The in vitro effects would then be related to the bath application of norepinephrine producing an anomalous response as seen in studies assessing unit responses under

conditions of exogenous norepinephrine application rather than under conditions of endogenous release (e.g., Curet and de Montigny 1988a, 1988b, 1989).

### *Relation to Locus Coeruleus Activation in Awake Rats*

The locus coeruleus bursts in response to environmental change (Sara and Segal 1991, Vankov et al. 1995). The present results are consistent with the novelty-elicited norepinephrine dependent enhancement of excitability of dentate gyrus reported by Kitchigina et al. 1997. In that study the perforant path evoked dentate gyrus potential was monitored when rats were exploring novel objects in a hole board, an activity that produces transient burst events in the locus coeruleus (Vankov et al. 1995). Associated with these nose poke events, Kitchigina et al observed an enhancement of the population spike lasting ~15 sec. The enhancement rapidly habituates with repeated visits as also seen for locus coeruleus burst events. Pretreatment with the noradrenergic antagonist propranolol prevented the increase in excitability. The duration of evoked potential enhancement was longer when rats were moved from a familiar to an unfamiliar environment. Locus coeruleus induced feed forward disinhibition as seen here readily accounts for this pattern of results. While the duration of disinhibition was briefer with the nose poke events than in the present study, it is likely that duration would be related to the strength and duration of the burst event. The Kitchigina pharmacological result suggests the present observations of disinhibition may be related to β-adrenergic receptor activation.

In an earlier paper Wilson and McNaughton (1993) using stereotrode methodology reported that transfer from a familiar to a novel environment was associated with the massive suppression of interneuron firing in the hippocampus. They speculate that this suppression of interneuron firing allows the encoding of space by a new ensemble through the loosening of prior associations and the promotion of synaptic plasticity. This hypothesis is strongly supported by the present results. Moreover, the present data argue for a specific role of the locus coeruleus in initiating interneuron suppression and promoting new ensemble formation.

### *Conclusions*

The finding that norepinephrine disinhibits the principal cells of the dentate gyrus is of major importance. The ensemble of results points to a new interpretation of the role of interneuron synchronization in the regulation of plasticity in the hippocampus. Previous models have suggested that periods of strong synchronization of the interneuronal network are reflected in a high strength of gamma frequencies. High gamma power shortens the time window for coincidence spiking activity of principle cells in a neuronal ensemble, which is required for both encoding and retrieval. This small window of spiking opportunity binds disparate sensory events that happen close in time into cohesive representations. In this study burst activity of the locus coeruleus which mimics natural release associated with ethologically relevant environmental change

causes a decrease in gamma power implying a decrease in synchronization of the interneuronal network. The decrease in gamma power results in a widening of the time window for the consolidation of coincidence activity in the principle cells. A mechanism such as this would be required where a stable, previously acquired, representation needs to be revised to incorporate new sensory events/information. In initial acquisition of a representation norepinephrine may be less essential given that a number of neuromodulatory influences are active. A role specific to the locus coeruleus appears when expectation mismatches occur associated with an alteration in the environment or in environmental contingencies. Thus the use of an existing representation may be essential to uncover a norepinephrine-specific deficit.

Configuration updating would be much more difficult in a period of high gamma power. The specificity of the encoding would occur in cortical sensory systems where norepinephrine is known to increase the signal to noise ratios. The result of norepinephrine release would be broad integration of sharp sensory events in the hippocampus.

To review the related findings of the present study: First, norepinephrine release produces a reduction of gamma power and an increase in relative theta power. Reduction of gamma power opens stable association to modification. An increase in relative theta power may also contribute to the enhancement of synaptic modification. Direct contributions to enhanced plasticity would occur with the loss of feedforward inhibition. The disinhibition of principle cells would

magnify the direct actions of norepinephrine on principle cells, which include depolarization, an increase in calcium conductances and an increase cAMP level.

At the cellular level there is a suggestion in the data that the loss of feedforward inhibition is largely driven by direct inhibition of mossy cells. Mossy cells are the most numerous nongranule cell type in dentate gyrus. I have tentatively identified these with the largest subgroup recorded here, the wide cluster. These cells tended to be shut off faster than the others suggesting direct action with the resulting changes in other cells being disynaptic. There is some anatomical evidence to support this hypothesis since double labeling studies with tyrosine hydroxylase have not reported such terminals directly innervating GABAergic somas or dendrites (Milner and Bacon 1989). One implication of this would be that the inhibited feedback cells would also be identified with mossy cells that do not have a dendrite in the molecular layer. Feedback interneurons that increase their firing rate may be basket cells that are directly driven by the increased firing rate of the principle cells.

Thus in the network as outlined loss of synchronization and disinhibition could occur either indirectly as a result of the inhibition of mossy cells or alternatively as a direct effect on all interneuron types. The end result of either interpretation would be an uncoupling of the interneuronal network and promotion of the modification of preexisting stable representations. The process as I envisage it can be illustrated through the example of contextual fear conditioning.

Context representations are hippocampal dependent (Kim and Fanselow 1992, Phillips and LeDoux 1992). If an animal is introduced into a context and is *immediately* given a shock no freezing will occur if the animal is reintroduced to the context 24 hours later. If the animal is preexposed to the environment for several minutes 24 hours prior to conditioning a contextual representation is formed and a shock presented immediately upon the animal's re-introduction to the environment will result in a conditioned freezing response (Wiltgen et al. 2001). Contextual conditioning is believed to depend upon on the integrity of the noradrenergic system (Neophytou et al. 2001). Local depletion of norepinephrine in the amygdala blocks the acquisition of hippocampal independent cued conditioning tasks (Selden et al. 2001).

The current framework interprets the contextual representation as a stable preexisting representation, which requires the binding of the shock driven information to produce a conditioned response. An animal that fails to incorporate the new sensory information will display a fear conditioning deficit. The updating of the representation requires a loosening of the contextual association to allow other information to be bound. Norepinephrine allows this process to occur. This conceptualization is testable in a number of ways.

### *Future Directions*

The framework described above makes several clear predictions about the role of gamma in hippocampal-dependent tasks. Tasks which require the

incorporation of new information into stable representations should be facilitated by decreases in gamma (or decreases in interneuron synchronization) as indicated by low gamma power. In contrast deficits should be seen in these tasks if the new information is encountered concomitantly with high gamma power. A pharmacological manipulation that artificially increases gamma power should interfere with pre-exposure rescue of immediate shock deficit as described in the contextual fear paradigm above. In the absence of pharmacological manipulations electrophysiological recording of EEG in hippocampus should reveal low gamma power with the first introduction to a novel environment during the acquisition of the contextual representation. Reintroduction of the animal to the environment should reveal a high gamma power in the EEG record indicative of recall of an existing representation. A subsequent substantial alteration of the environment would produce a decrement in gamma power indicative of the incorporation of new information to the pre-existing representation.

Manipulations that block or attenuate gamma frequencies should interfere with processes of recall of the initial representation. A possible corollary to the consolidation process in this framework may be the development of gamma power following acquisition. Manipulations that interfere with gamma during the consolidation period could prevent consolidation in this view.

In this framework local hippocampal depletion of norepinephrine should result in a failure to update an existing representation. Specifically, in the case of the pre-exposure rescue of immediate shock deficit, the animal would be calling

up the original representation rather than a new representation incorporating the shock information. The behavioral phenotype would be a conditioning deficit.

Global lesions of locus coeruleus should result in a perseverative pattern of behavior in any behavioral paradigm where the animal is required to update existing representations.

At the cellular level the most interesting electrophysiological prediction of the present model is inhibition of morphologically identified mossy cells by release of endogenous norepinephrine.

Although this study describes the activity of the hippocampus under the influence of endogenously released norepinephrine; the norepinephrine release was not confirmed by the use of adrenergic blockers. A study investigating the pharmacology of these responses would be most valuable. It is possible that some of the effects, notably EEG responses, may be mediated by transmitters or modulators other than norepinephrine. Berridge and Foote (1996) have reported that locus coeruleus efferents modulate the activity of the septal nucleus which in turn modulates EEG in cortex via a cholinergic mechanism. Similar mechanisms may be in place in the hippocampus.

Figure 1

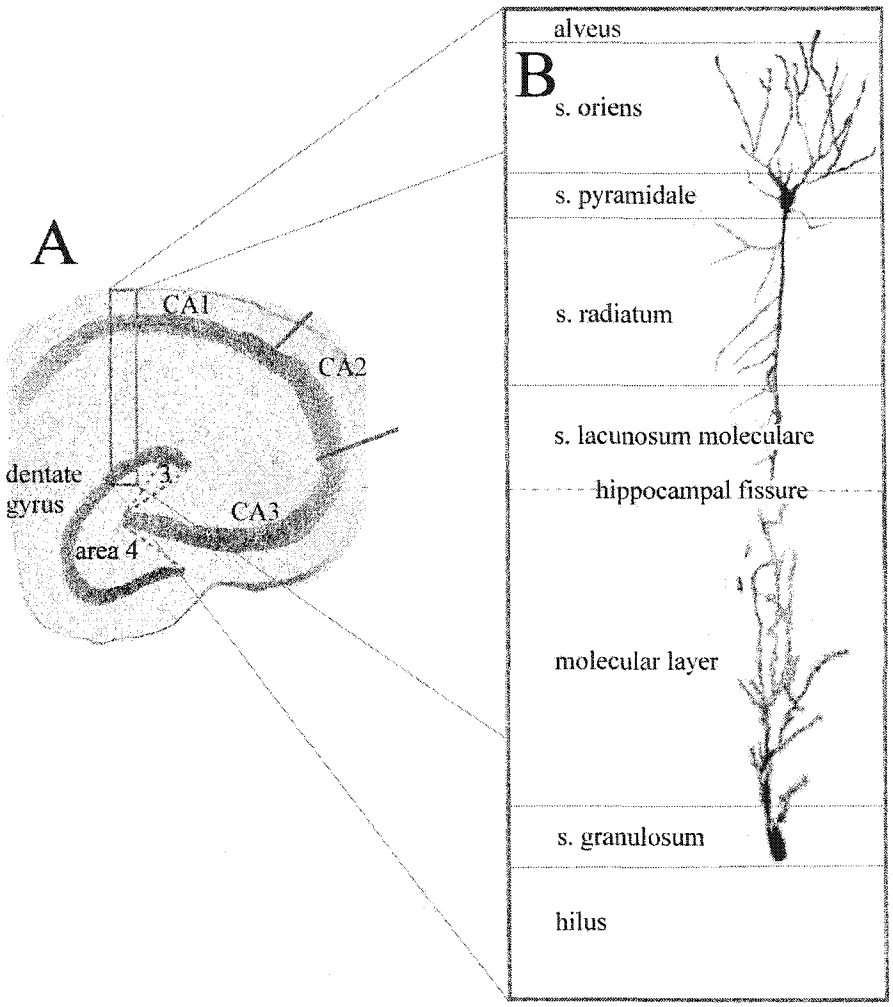


Figure 1: The gross divisions of hippocampus
A: A horizontal section of hippocampus showing the major subdivisions of the hippocampus. Boundaries of CA2 are estimated. B: The major laminar divisions of CA1 and dentate gyrus. Laminar divisions for CA3 are identical to those of CA1.

Figure 2.

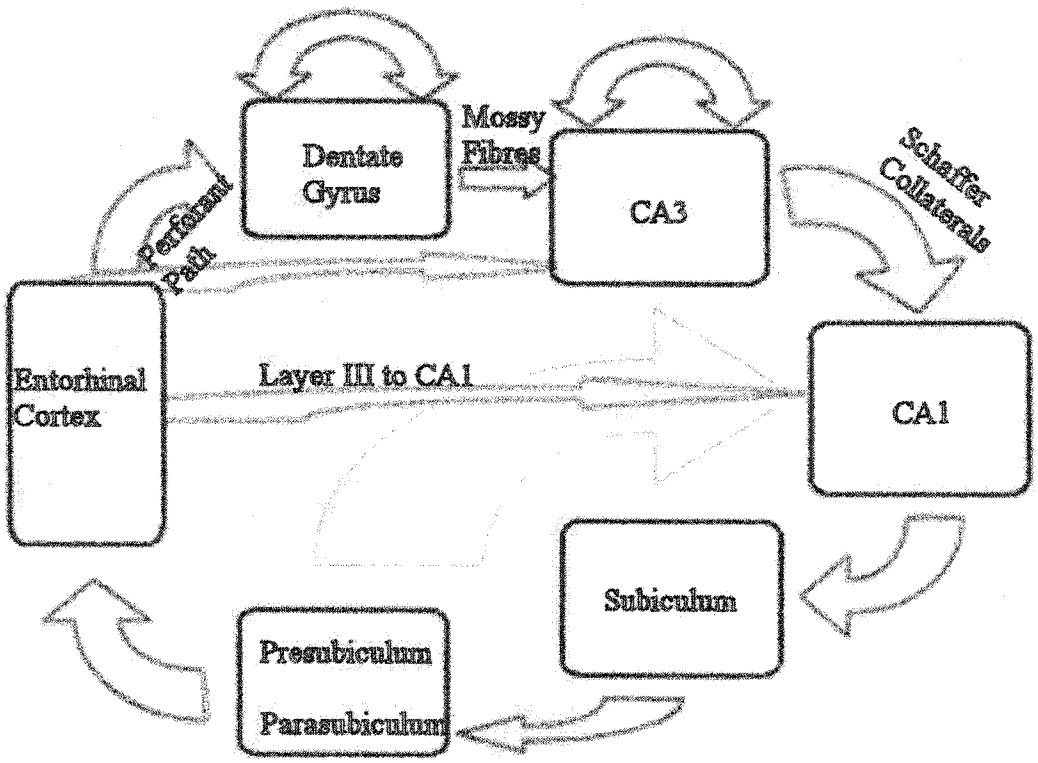


Figure 2: A schematic diagram showing the glutamatergic connections of the hippocampus and associated regions. The recurrent dentate gyral activation occurs via mossy cells, while the recurrent activation in CA3 occurs via recurrent axon collaterals in the basilar dendrites. The arrow indicating the projection from the pre/parasubiculum to CA1 is lighter to indicate the controversy regarding the presence and significance of the projection.

Figure 3.

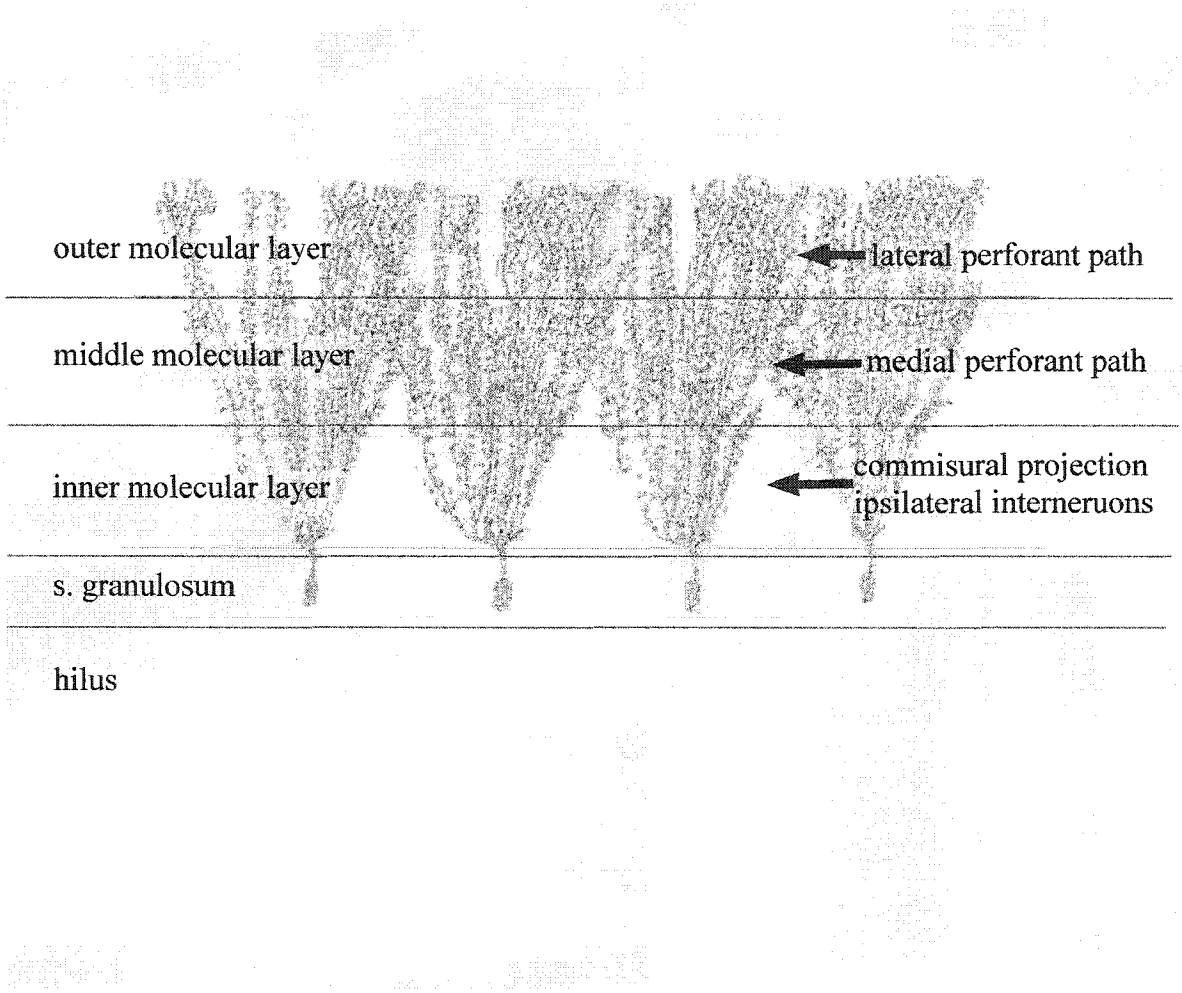


Figure 3: A schematic diagram showing the laminar distribution of glutamatergic inputs to the dentate gyrus.

Figure 4.

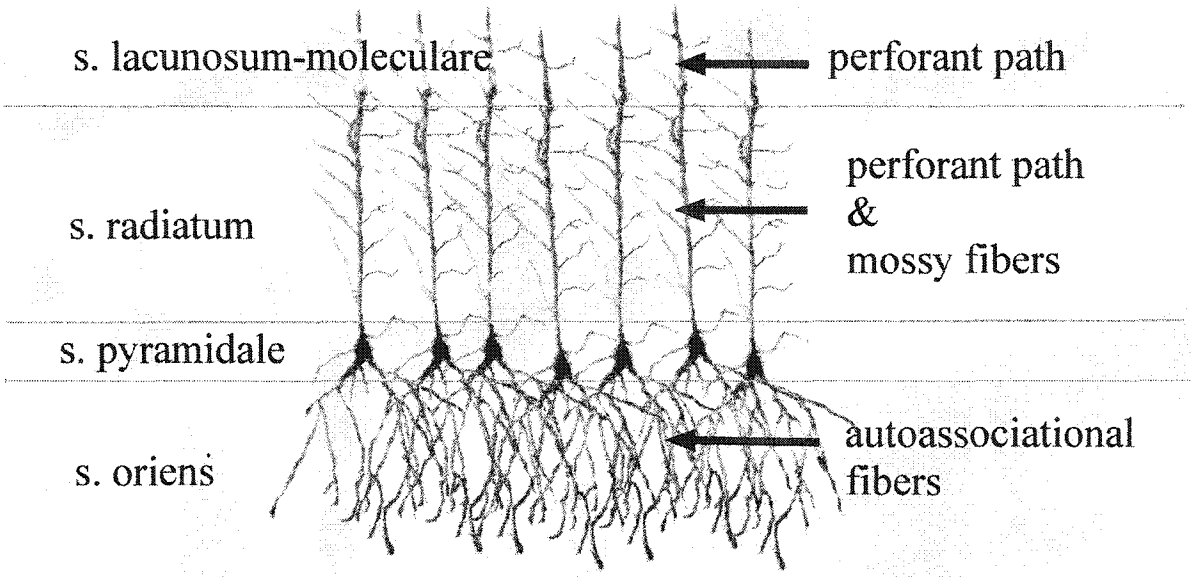


Figure 4: A schematic diagram showing the laminar distribution of glutamatergic afferents to CA3.

Figure 5.

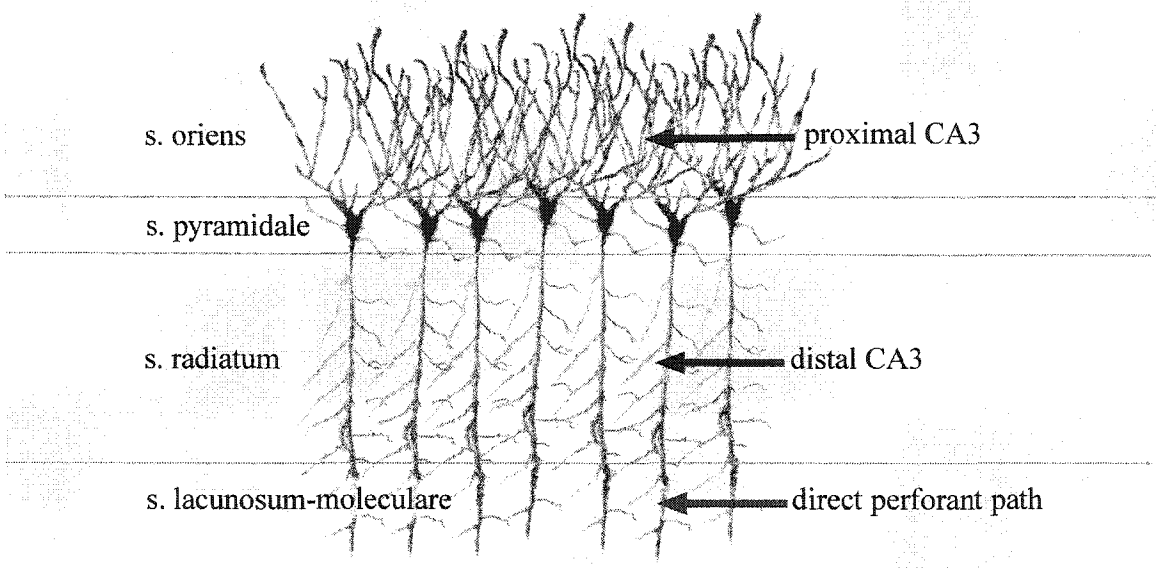


Figure 5: A schematic diagram depicting the laminar distribution of glutamatergic afferents to CA1.

Figure 6.

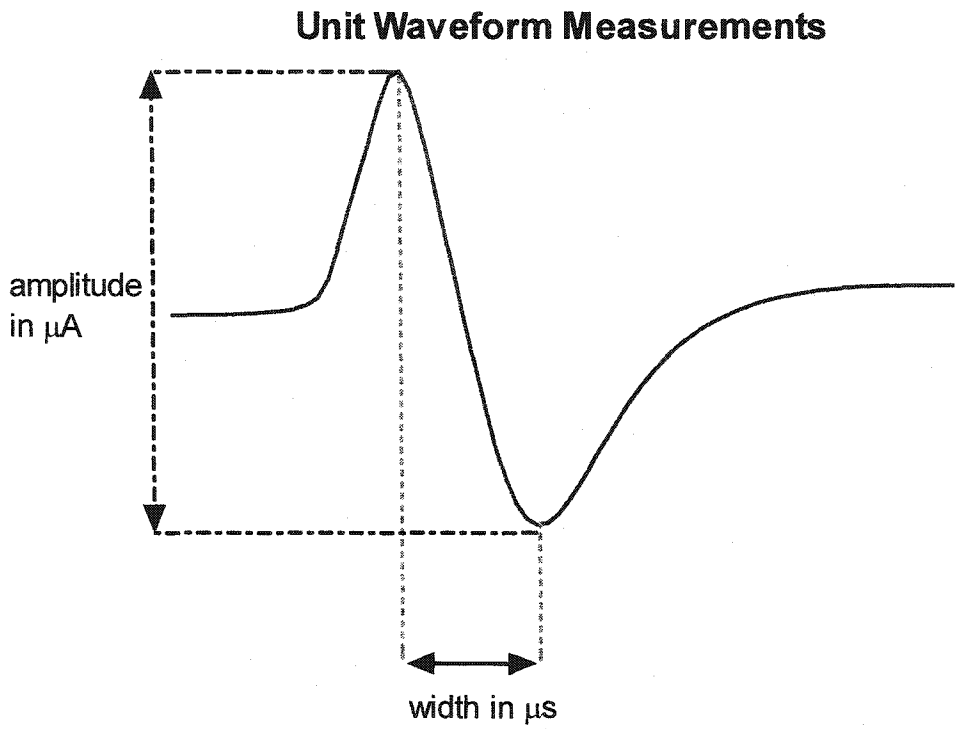


Figure 6: A schematic to show how amplitude and width of individual units were calculated. Amplitude is taken as the maximum voltage difference in the averaged unit waveform. The unit width is the peak-to-peak measurement, the time required for the voltage to swing from the maximum positivity to maximum negativity or vice versa.

Figure 7.

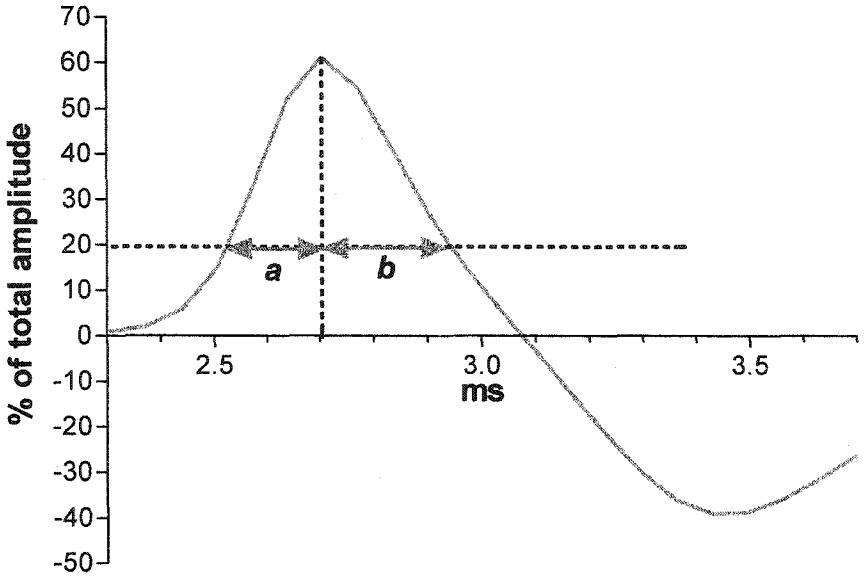


Figure 7: A schematic depicting how wave form asymmetry was calculated. The time from 20% rise to maximum amplitude was divided by the time from maximum to 20% fall. In the case of a unit of the valley-peak form the same procedure was followed using a -20% and minimum amplitude criteria.

Figure 8.

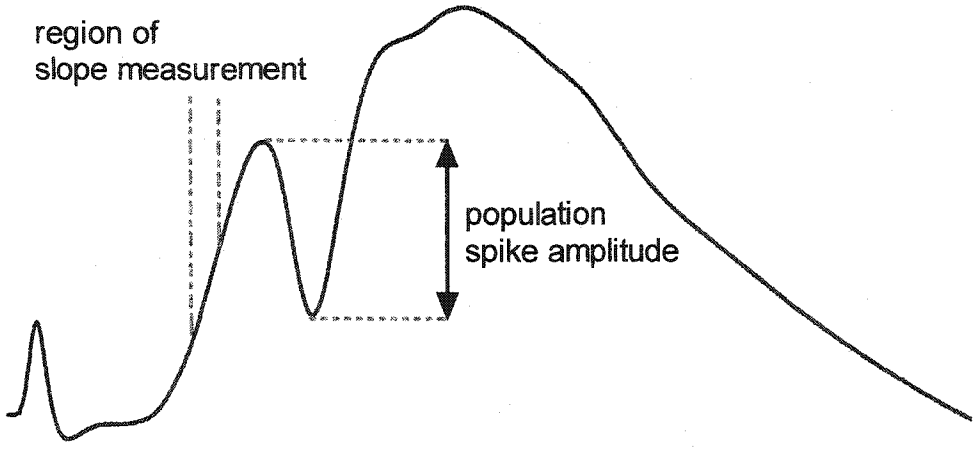


Figure 8: This figure depicts how slope and population spike measurements were calculated. Slope was taken from the initial rise, population spike amplitude was calculated from the top of the initial peak to the depth of the population spike.

Figure 9.

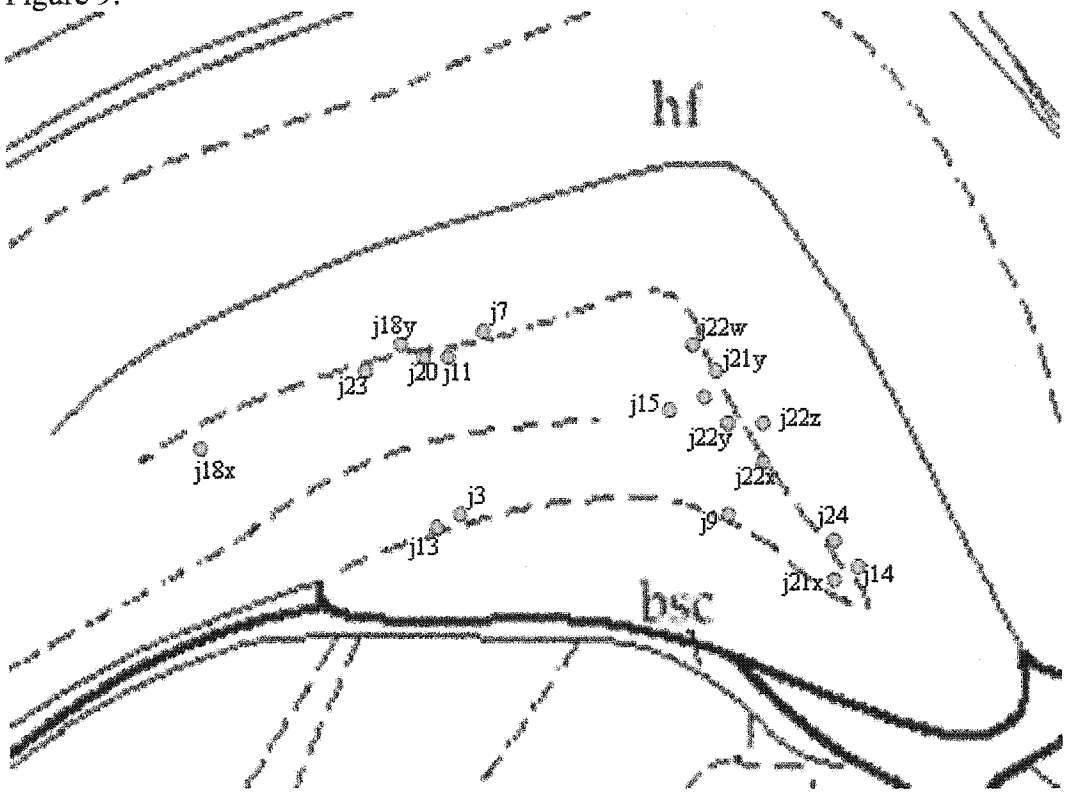


Figure9: Summary of recovered recording placements. All placements were located in dentate gyrus with a cluster located near the crest of the dentate which divides zone 3 from zone 4 of hilus. As discussed in the text j18x is visible as a single site well removed from the other clustered recording sites. Also a cluster of 4 possible recording sites was visible in animal 22 although only 2 sites were marked.

Figure 10.

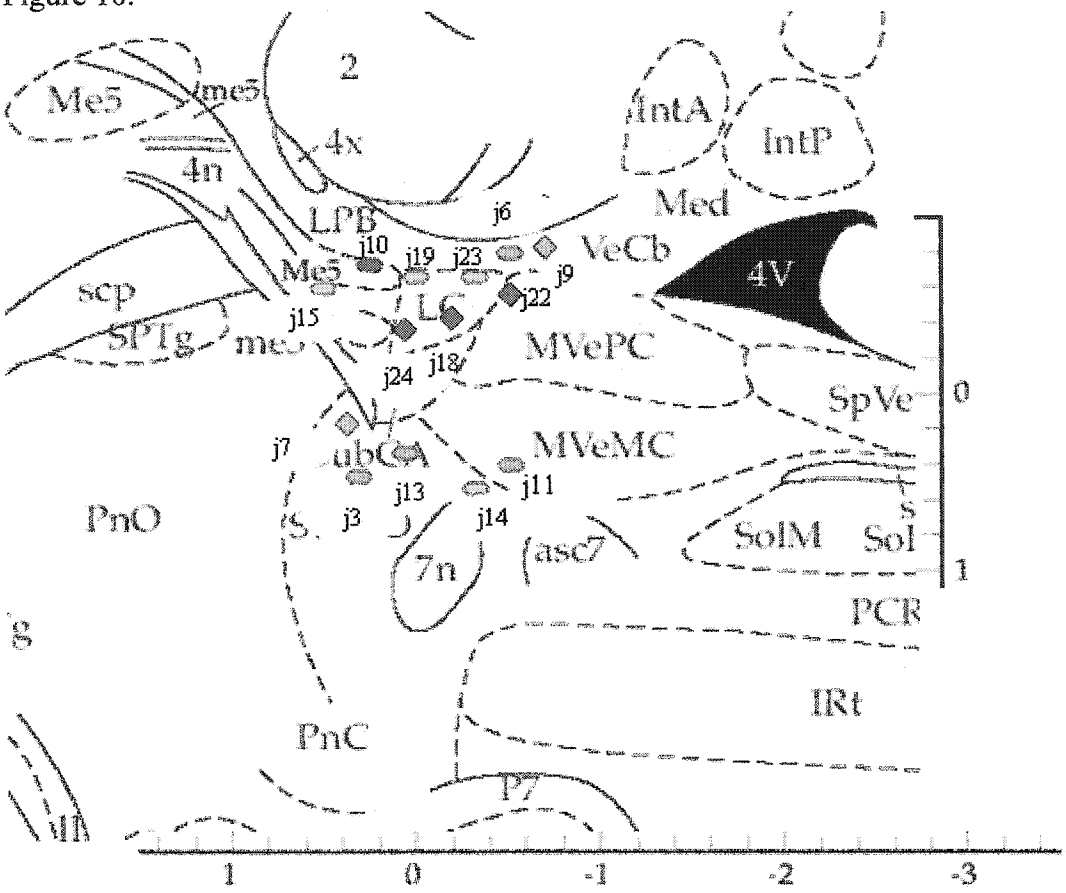


Figure 10: Summary figure of recovered ejection placements. All placements were within 500 μm border of locus coeruleus. Placements that resulted in an increase in the population spike are shown in red; sites with no change are shown in blue; sites associated with a decrease in population spike are shown in green. Changes in theta activity are depicted by shape; sites associated with an increase in theta power are depicted with diamonds, decreases in theta power are depicted with ovals.

Figure 11

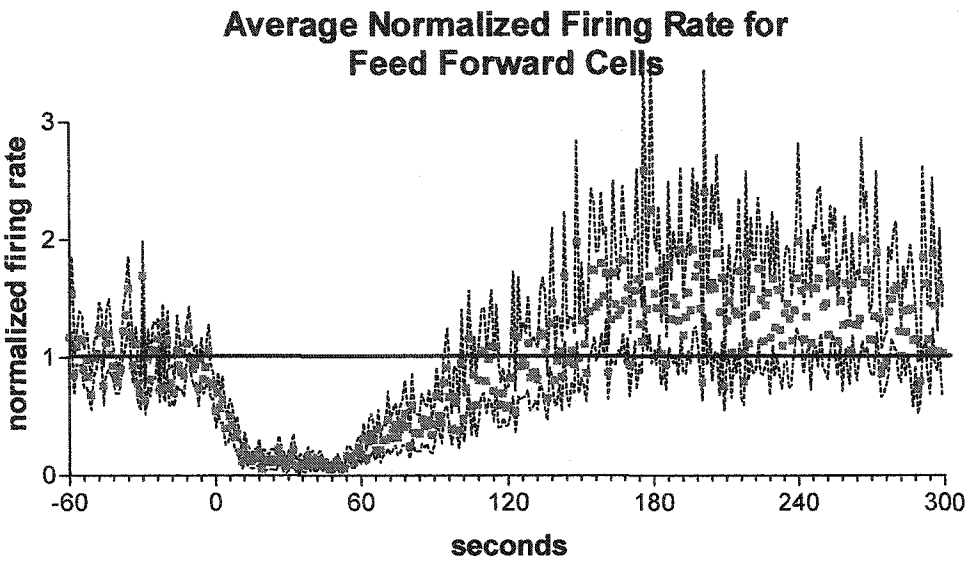


Figure 11: The normalized firing rate for feed-forward cells. The solid bar indicates the average rate of the 60 second baseline prior to the ejection which took place at time 0. Only cells which had a baseline rate over 1 Hz were included to preserve scaling (every spike from a slow firing cell distorted the mean and error for that bin). The dashed lines represent ± 1 standard error.

Figure 12

A

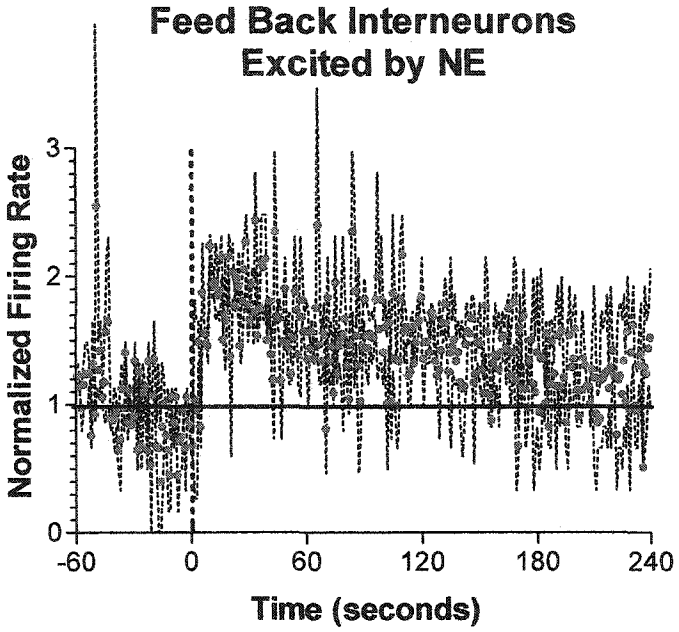


B

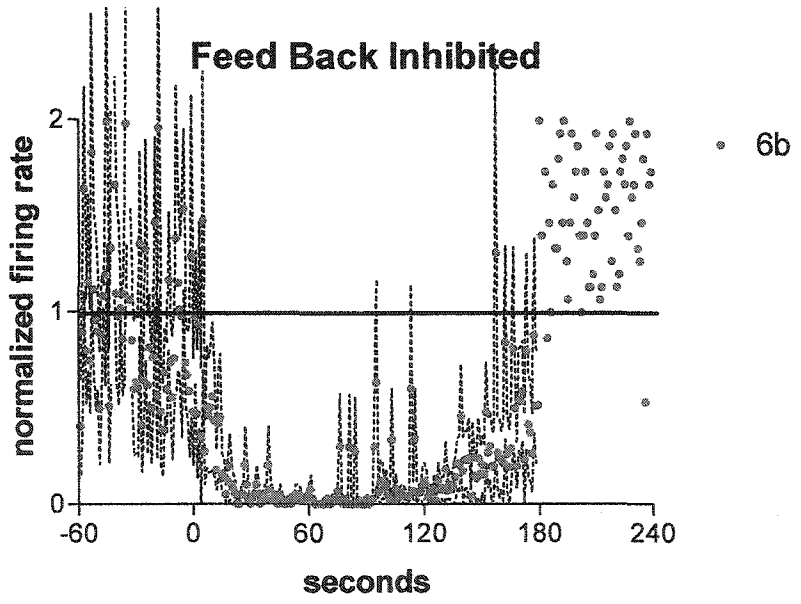


Figure 12: A: Averaged response of feedback cells which were excited following the glutamate ejection. The firing rate roughly doubles and the increase lasts over four minutes. B: Averaged response of feedback cells which were inhibited following the glutamate ejection. Error is large since there were only two of these cells, one of which was lost three minutes following the ejection. The dashed line indicates standard error in both plots.

Figure 13

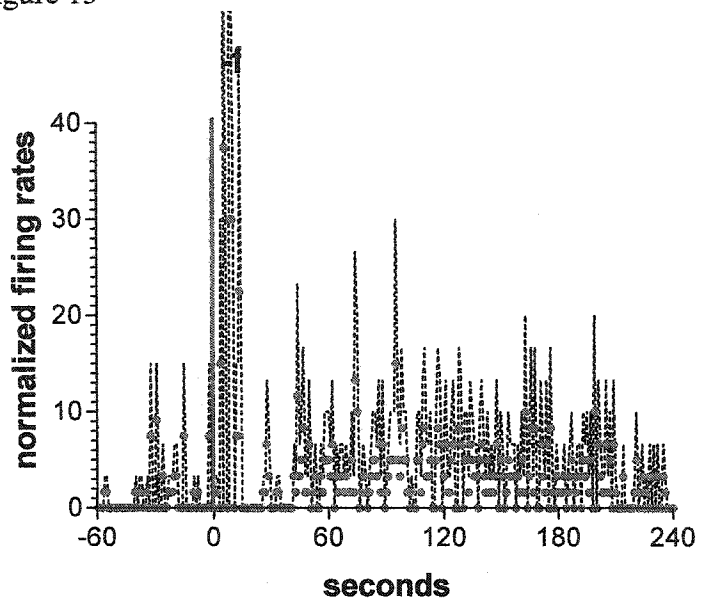


Figure 13: Averaged response of putative granule cells. These cells had a very low firing rate. Individual spikes therefore have a very large impact on firing rate of a given bin. There is a large and transient burst of these cells associated with the glutamate ejection followed by a sustained increase in firing that lasts several minutes. The dashed line indicates standard error.

Figure 14

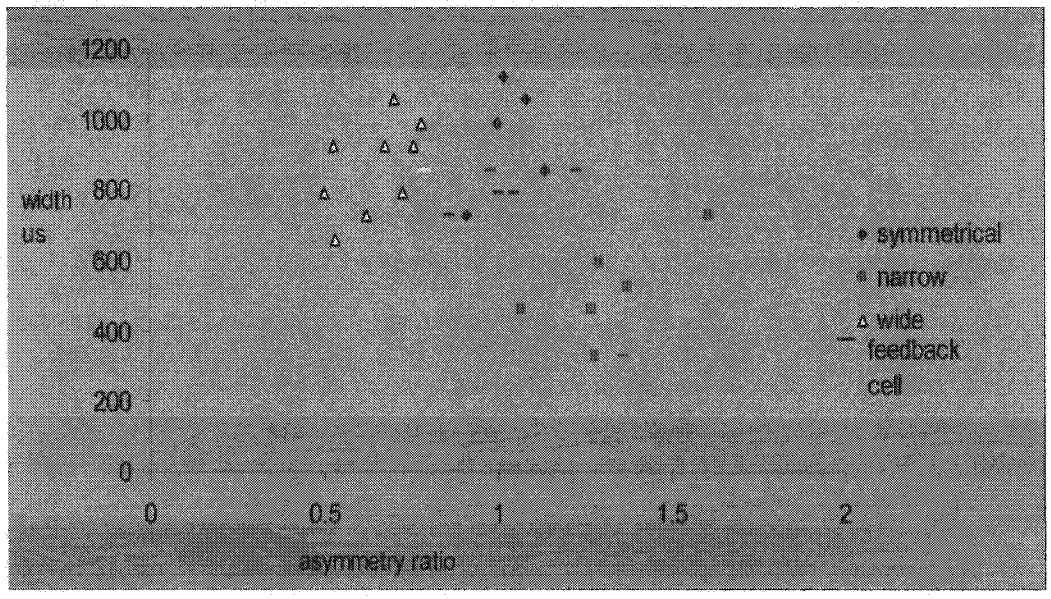


Figure 14: Cluster analysis of all recorded cells. The cells are plotted with width against asymmetry ratio. Three clusters are evident. One cluster is distinguished by narrow cell widths. The remaining two clusters are distinguished by their asymmetry ratios. The majority of feedback cells are wide and symmetrical.

Figure 15

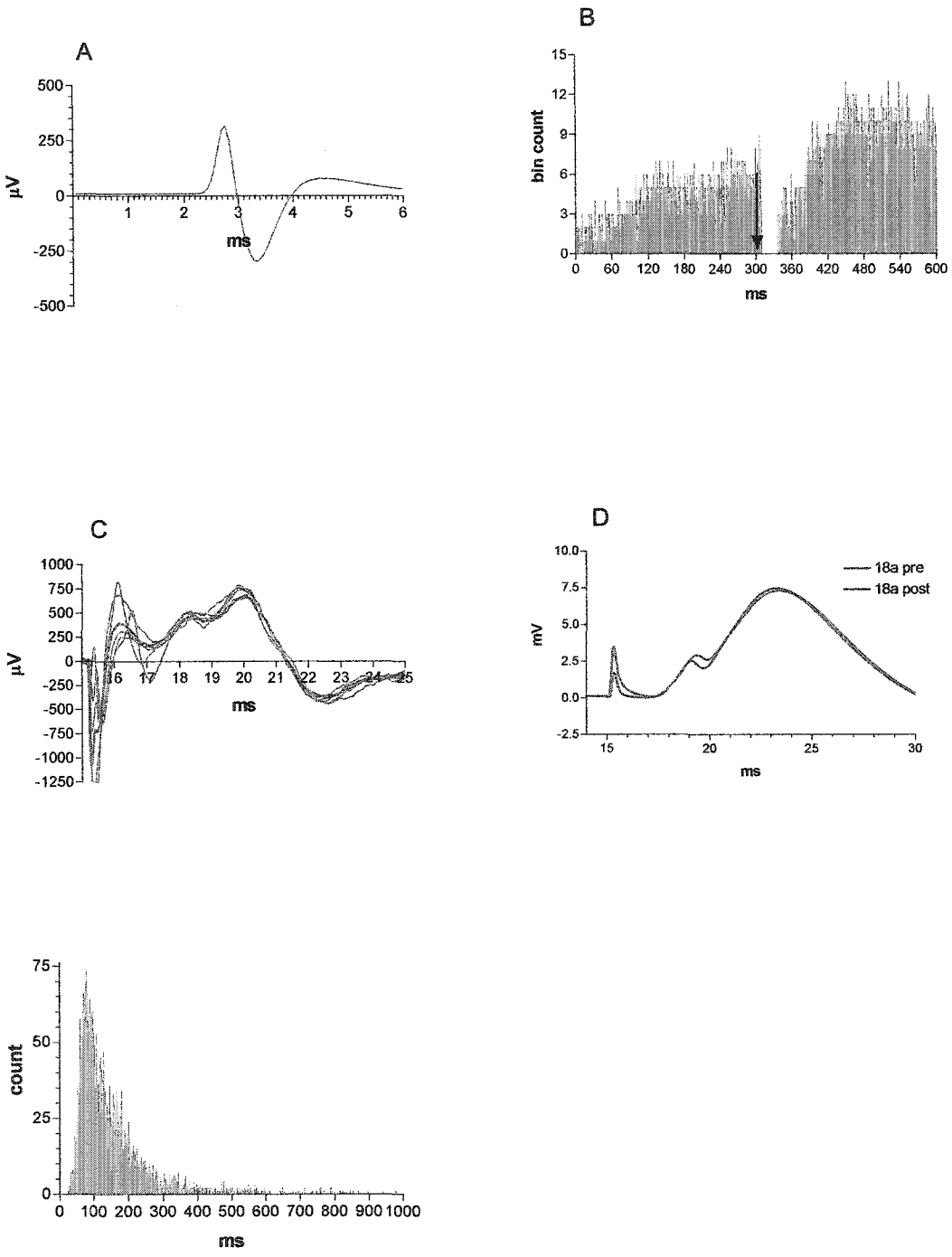
A
500
250
0
-250
-500
µV
1
2
3
4
5
6
ms
B
15
12
9
6
3
0
bin count
0
60
120
180
240
300
360
420
480
540
600
ms
C
1000
750
500
250
0
-250
-500
-750
-1000
-1250
µV
16
17
18
19
20
21
22
23
24
25
ms
D
10.0
7.5
5.0
2.5
0.0
-2.5
mV
18a pre
18a post
15
20
25
30
ms
75
50
25
0
count
0
100
200
300
400
500
600
700
800
900
1000
ms

Figure 15: Record of cell JCR 4018A. A: Averaged waveform for all cell events in the free recording period. B: Rate meter histogram depicting spontaneous activity in one second bins. The glutamate ejection occurred at 300 seconds as indicated by the arrow. C: The unit activity evoked by perforant path activity of 600 μA. The waveforms are noisy but the cell is visible immediately following stimulation. D: Evoked potentials produced by 600 μA stimulation of the perforant path. The baseline waveform is in blue with the post-ejection waveform depicted in red. E: Autocorrelation of spontaneous activity in 1 ms bins. The cell shows a strong primary peak without theta rhythmicity.

Figure 16:

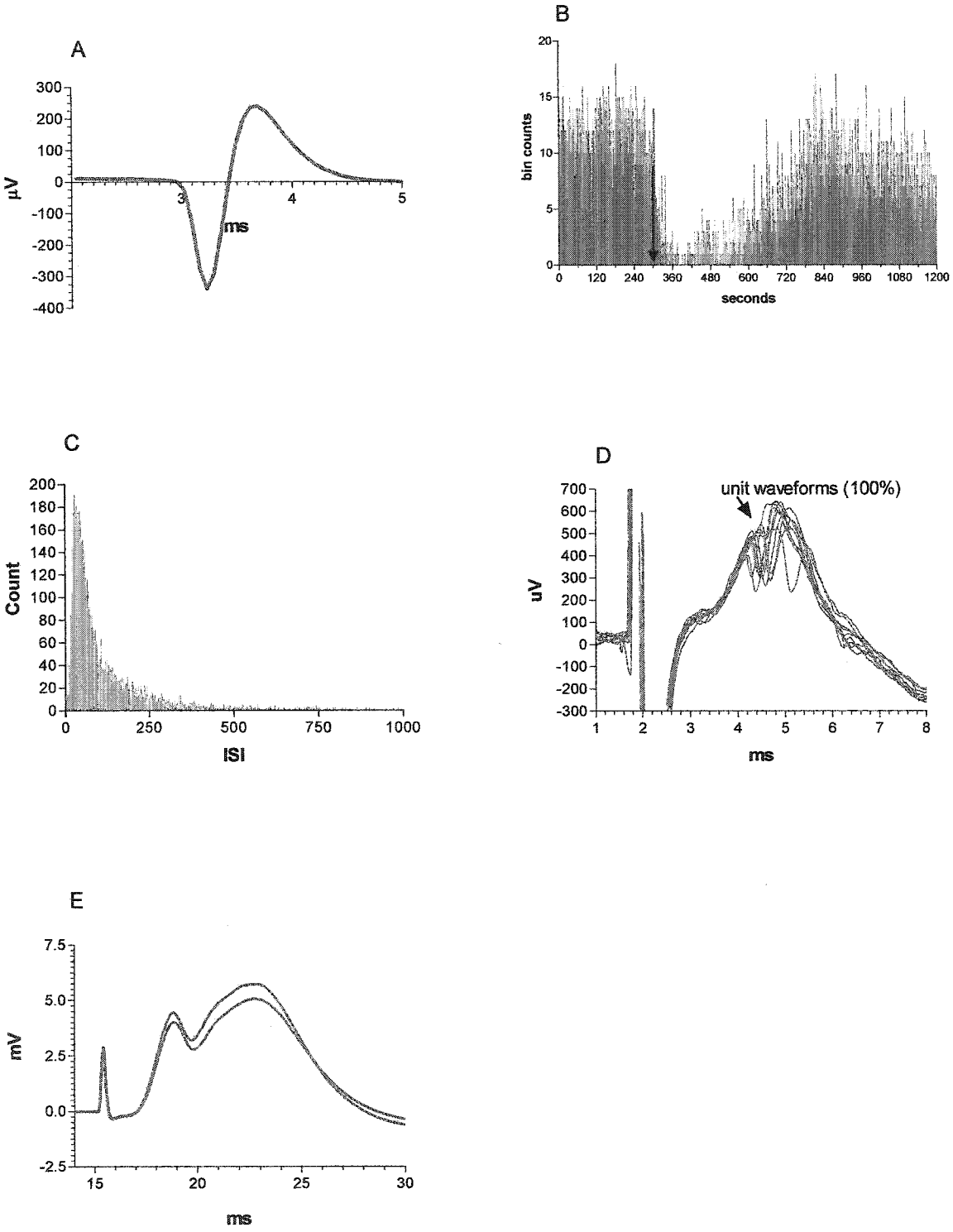
A
300
200
100
0
-100
-200
-300
-400
µV
3
4
5
ms
B
20
15
10
5
0
bin counts
0
120
240
360
480
600
720
840
960
1080
1200
seconds
C
200
180
160
140
120
100
80
60
40
20
0
Count
0
250
500
750
1000
ISI
D
unit waveforms (100%)
700
600
500
400
300
200
100
0
-100
-200
-300
uV
1
2
3
4
5
6
7
8
ms
E
7.5
5.0
2.5
0.0
-2.5
mV
15
20
25
30
ms

Figure 16. Record of cell JCR 4006B. A: Averaged waveform for all cell events in the free recording period. B: Rate meter histogram depicting spontaneous activity in one second bins. The glutamate ejection occurred at 300 seconds as indicated by the black arrow. C: Autocorrelation of spontaneous activity in 1 ms bins. The cell shows a strong primary peak without theta rhythmicity. D: The unit activity evoked by perforant path activity of 200 μA. The cell is visible from four to six ms. The stimulus artifact is at 2 ms. E: Evoked potentials produced by 500 μA stimulation of the perforant path. The baseline waveform is in blue with the post-ejection waveform depicted in red.

Figure 17.

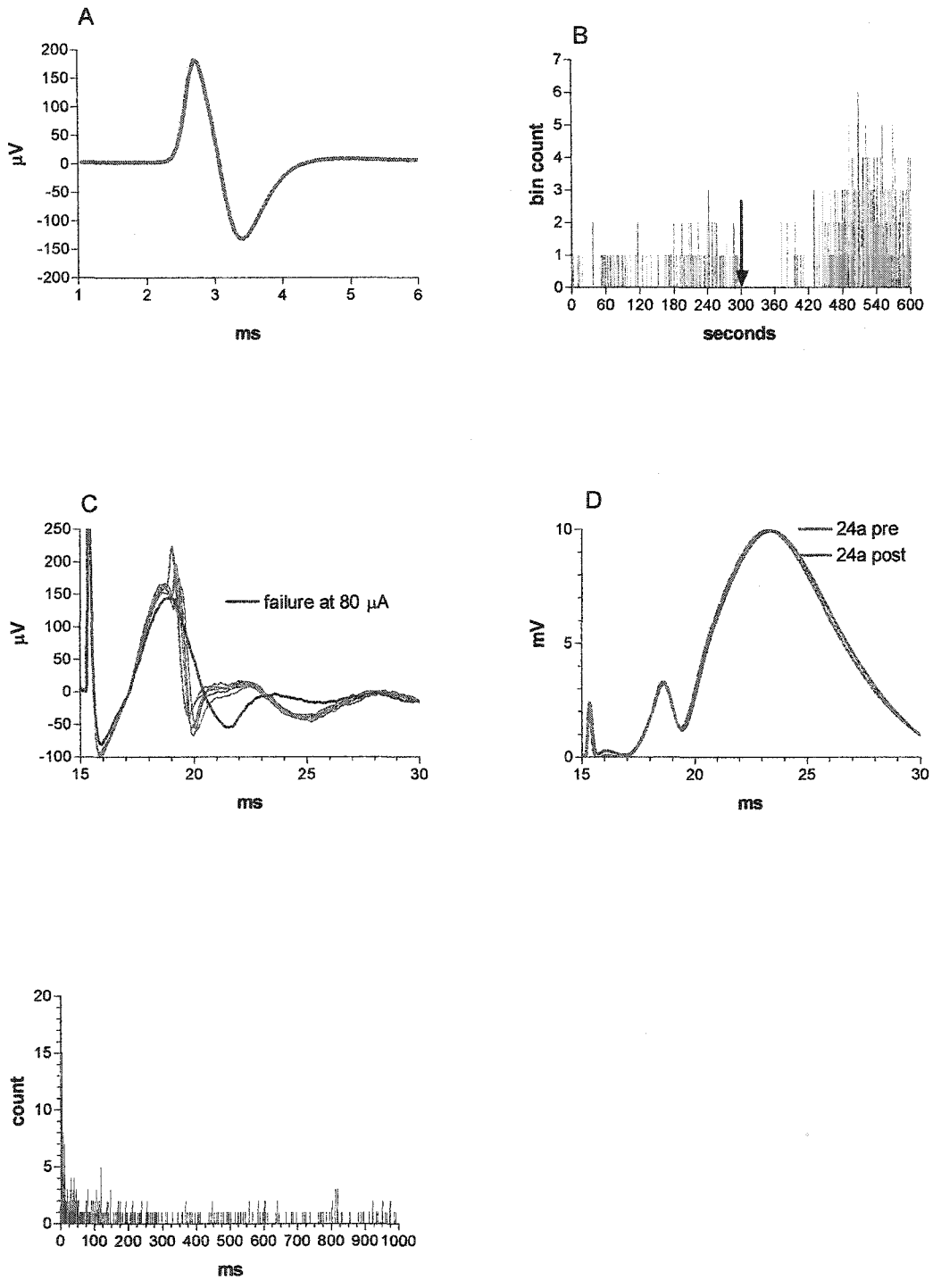
A
200
150
100
50
0
-50
-100
-150
-200
µV
1
2
3
4
5
6
ms
B
bin count
0
1
2
3
4
5
6
7
0 60 120 180 240 300 360 420 480 540 600
seconds
C
250
200
150
100
50
0
-50
-100
µV
failure at 80 µA
15
20
25
30
ms
D
10
5
0
mV
24a pre
24a post
15
20
25
30
ms
20
15
10
5
0
count
0 100 200 300 400 500 600 700 800 900 1000
ms

Figure 17: Record of cell JCR 4024A. A: Averaged waveform for all cell events in the free recording period. B: Rate meter histogram depicting spontaneous activity in one second bins. The glutamate ejection occurred at 300 seconds as indicated by the arrow. C: The unit activity evoked by perforant path activity of 100 μA. D: Evoked potentials produced by 400 μA stimulation of the perforant path. The baseline waveform is in blue with the post-ejection waveform depicted in red. E: Autocorrelation of spontaneous activity in 1 ms bins. The cell shows a suggestion of a sharp early peak.

Figure 18.

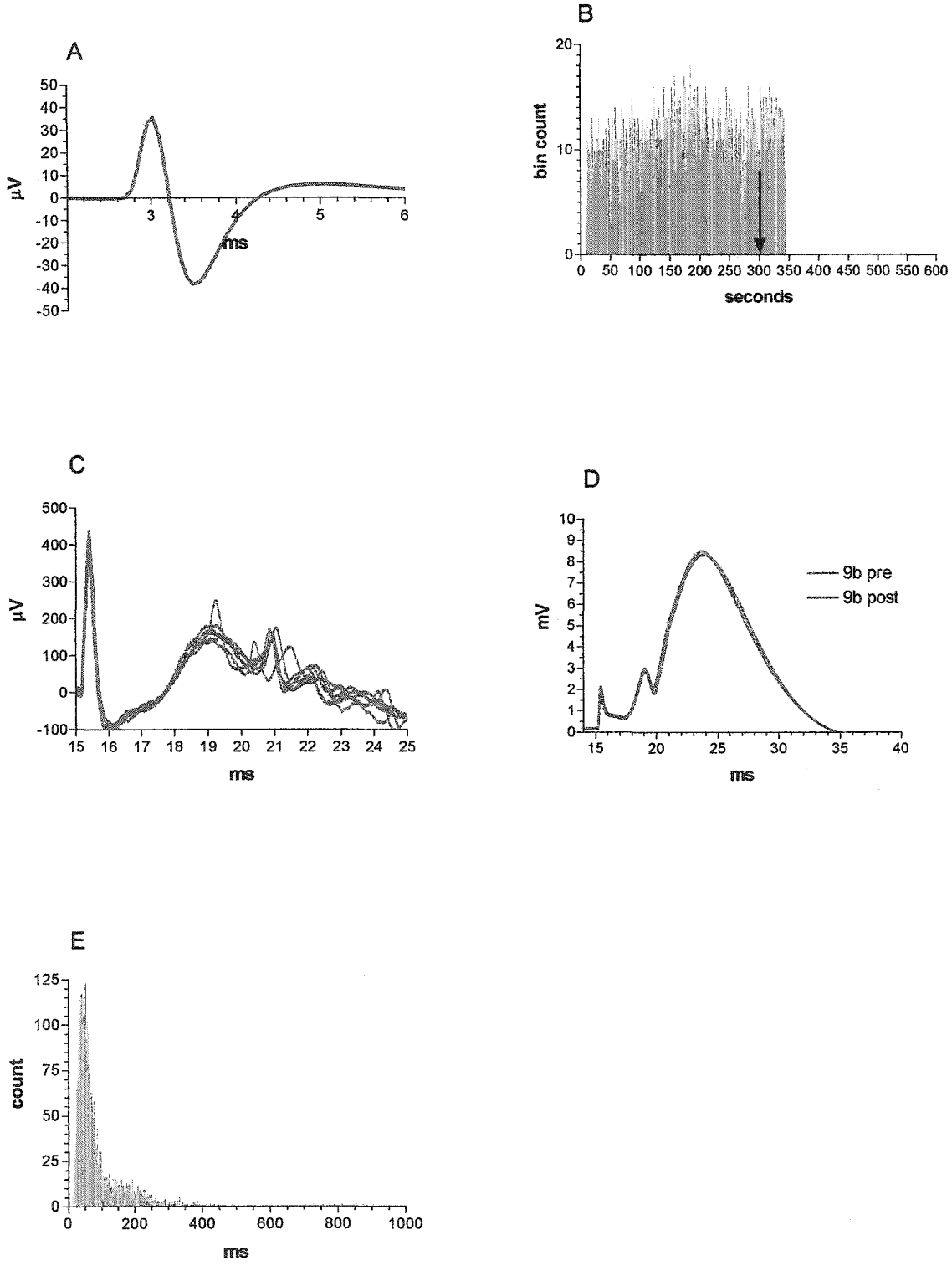
A
μV
ms
B
bin count
seconds
C
μV
ms
D
mV
9b pre
9b post
ms
E
count
ms

Figure 18: Record of cell JCR 4009B. A: Averaged waveform for all cell events in the free recording period. B: Rate meter histogram depicting spontaneous activity in one second bins. The glutamate ejection occurred at 300 seconds as indicated by the black arrow. The cell was lost less than one minute following the ejection. C: The unit activity evoked by perforant path activity of 70 μA. D: Evoked potentials produced by 300 μA stimulation of the perforant path. The baseline waveform is in blue with the post-ejection waveform depicted in red. E: Autocorrelation of spontaneous activity in 1 ms bins. The cell shows a strong primary peak without theta rhythmicity.

Figure 19.

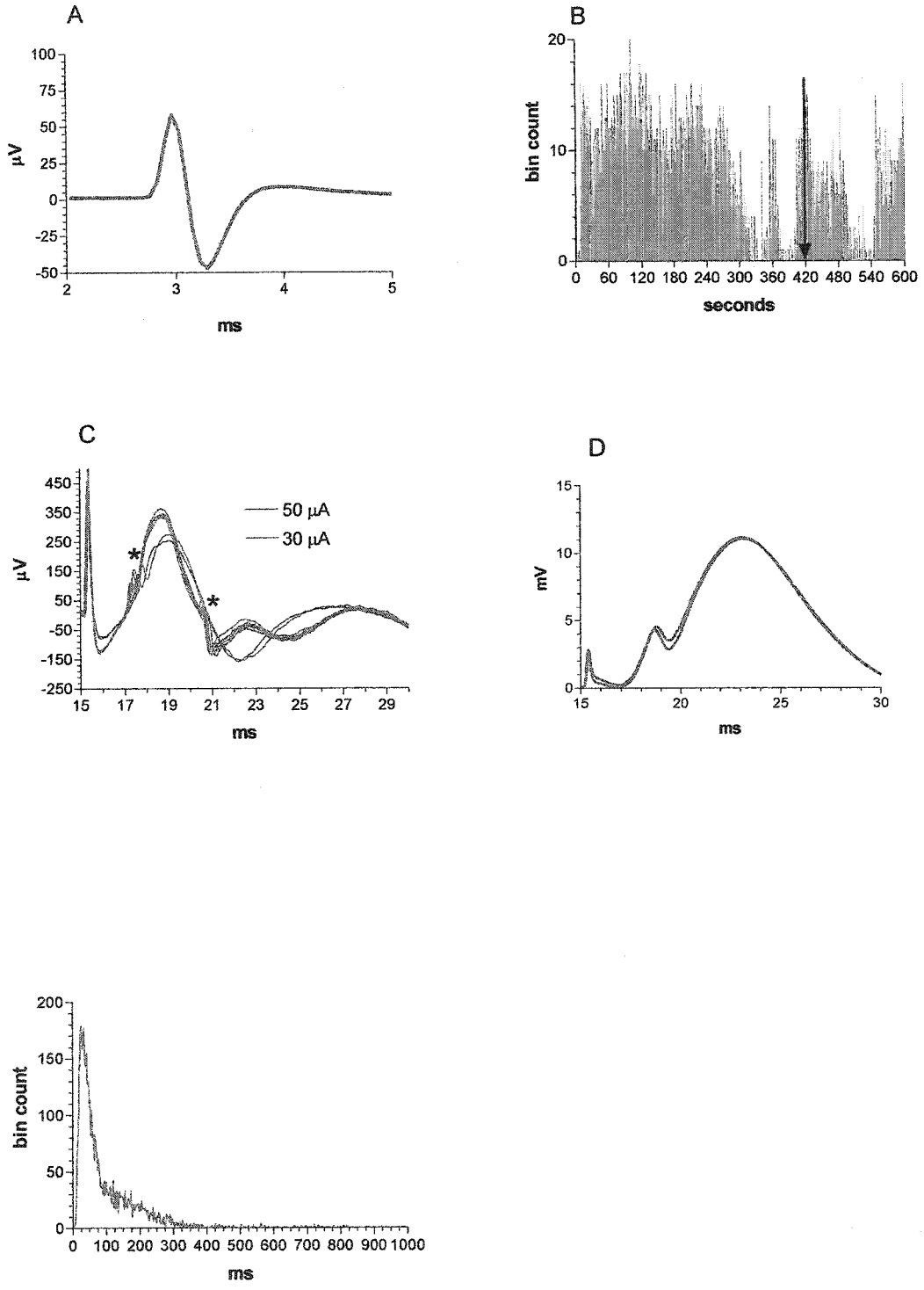
A
100
75
50
25
0
-25
-50
µV
2
3
4
5
ms
B
20
10
0
bin count
0 60 120 180 240 300 360 420 480 540 600
seconds
C
450
350
250
150
50
-50
-150
-250
µV
50 µA
30 µA
*
*
15 17 19 21 23 25 27 29
ms
D
15
10
5
0
mV
15 20 25 30
ms
200
150
100
50
0
bin count
0 100 200 300 400 500 600 700 800 900 1000
ms

Figure 19: Record of cell JCR 4022A. A: Averaged waveform for all cell events in the free recording period. B: Rate meter histogram depicting spontaneous activity in one second bins. The glutamate ejection occurred at 420 seconds as indicated by the arrow. The unit activity was highly variable. C: The unit activity evoked by perforant path activity of 50 μA. The cell displays multiple action potentials as typically discussed in the literature. D: Evoked potentials produced by 250 μA stimulation of the perforant path. The baseline waveform is in blue with the post-ejection waveform depicted in red. E: Autocorrelation of spontaneous activity in 1 ms bins. The cell shows a strong primary peak with no secondary peaks.

Figure 20.

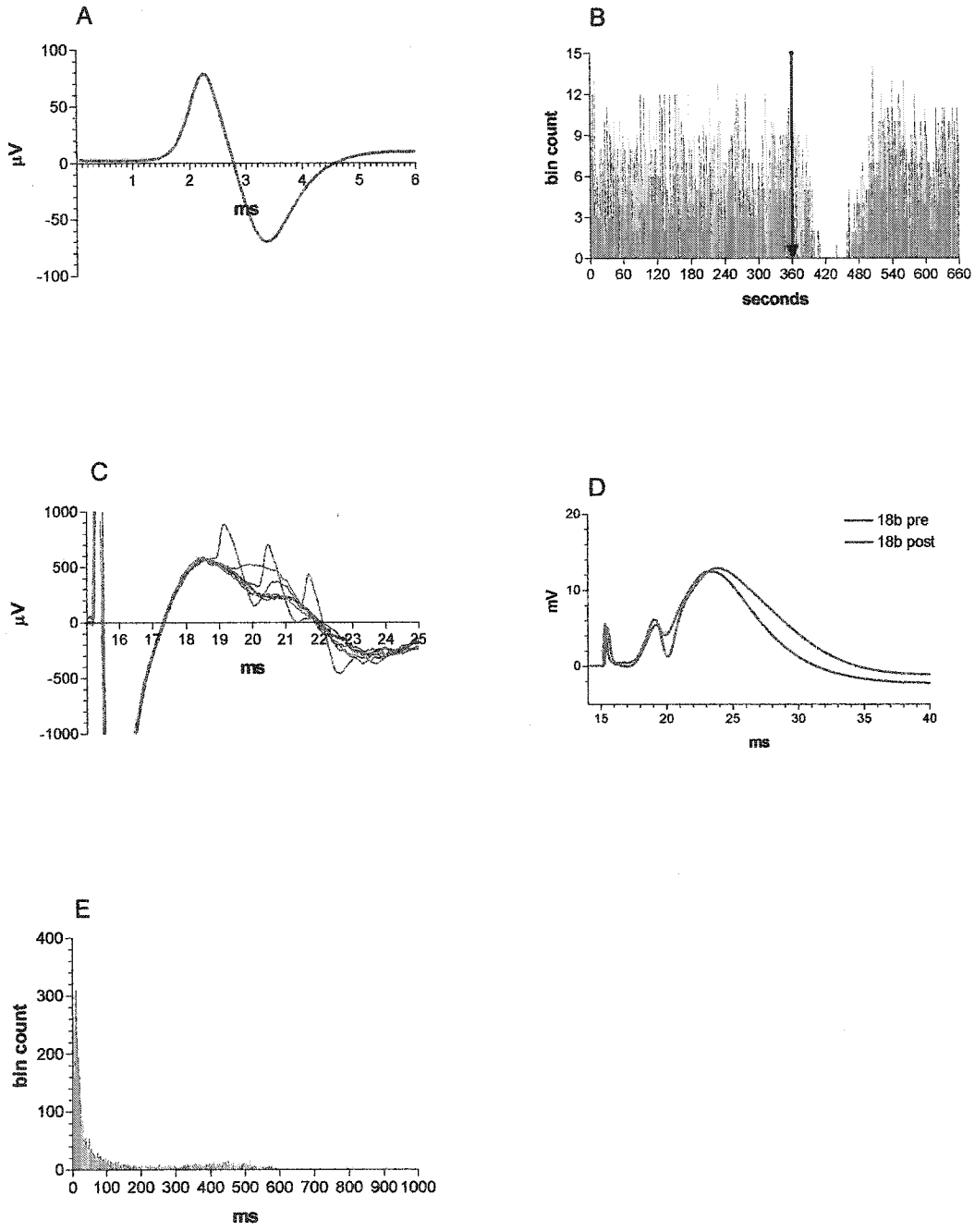
A
100
50
0
-50
-100
µV
1
2
3
4
5
6
ms
B
15
12
9
6
3
0
bin count
0
60
120
180
240
300
360
420
480
540
600
660
seconds
C
1000
500
0
-500
-1000
µV
16
17
18
19
20
21
22
23
24
25
ms
D
20
10
0
mV
18b pre
18b post
15
20
25
30
35
40
ms
E
400
300
200
100
0
bin count
0
100
200
300
400
500
600
700
800
900
1000
ms

Figure 20: Record of cell JCR 4018B. A: Averaged waveform for all cell events in the free recording period. B: Rate meter histogram depicting spontaneous activity in one second bins. The glutamate ejection occurred at 360 seconds as indicated by the arrow. C: The unit activity evoked by perforant path activity of 200 μA. D: Evoked potentials produced by 500 μA stimulation of the perforant path. The baseline waveform is in blue with the post-ejection waveform depicted in red. E: Autocorrelation of spontaneous activity in 1 ms bins. The cell shows a strong primary peak with a broad secondary peak at 450 ms.

Figure 21.

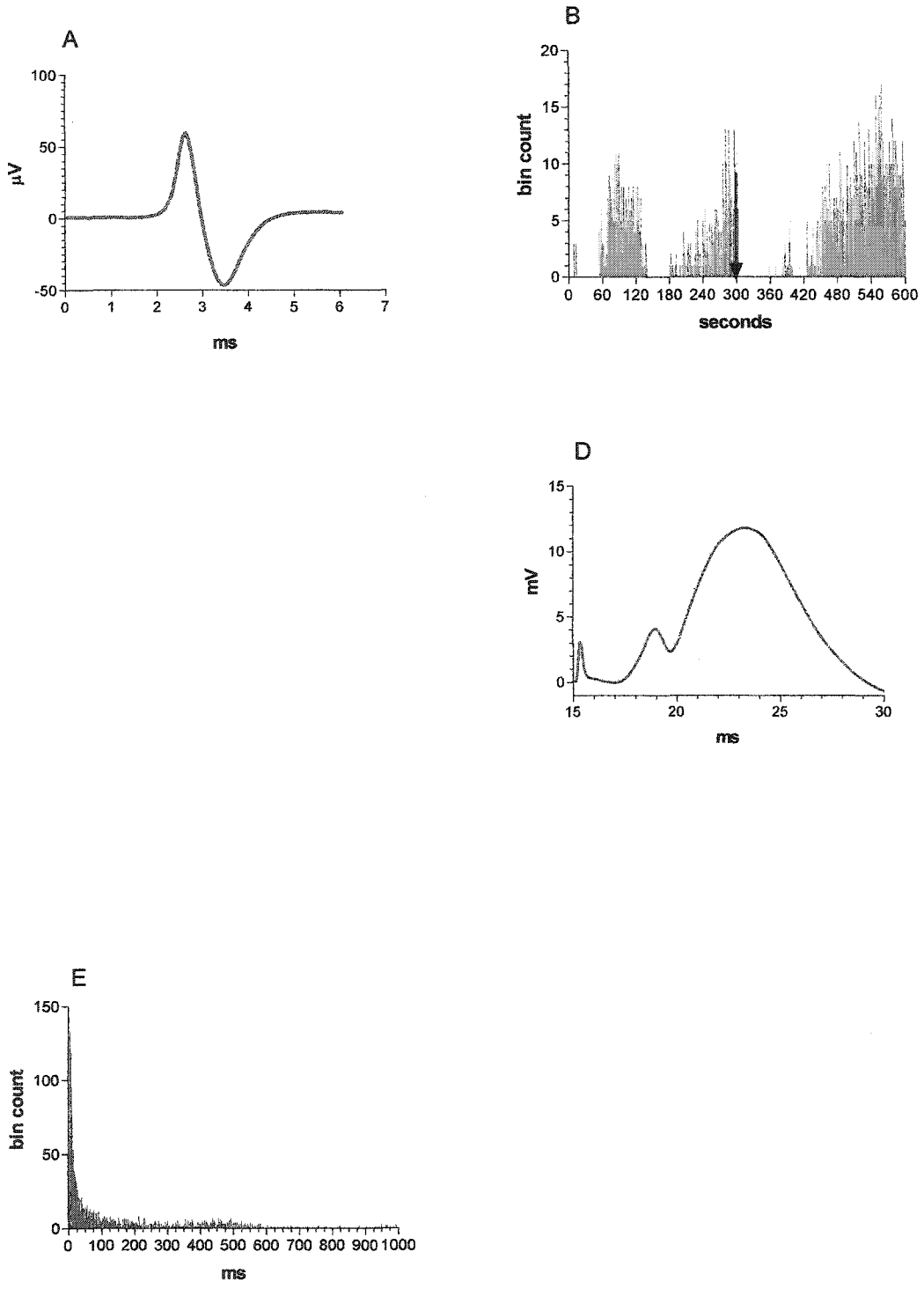
A
100
50
0
-50
µV
0 1 2 3 4 5 6 7
ms
B
20
15
10
5
0
bin count
0 60 120 180 240 300 360 420 480 540 600
seconds
D
15
10
5
0
mV
15 20 25 30
ms
E
150
100
50
0
bin count
0 100 200 300 400 500 600 700 800 900 1000
ms

Figure 21: Record of cell JCR 4021C. A: Averaged waveform for all cell events in the free recording period. B: Rate meter histogram depicting spontaneous activity in one second bins. The glutamate ejection occurred at 300 seconds as indicated by the arrow. D: Evoked potentials produced by 400 μA stimulation of the perforant path. Only the post ejection waveform is depicted since the pre-ejection data files were damaged. E: Autocorrelation of spontaneous activity in 1 ms bins. The cell shows a strong primary peak with a suggestion of a secondary peak at 200 ms.

Figure 22.

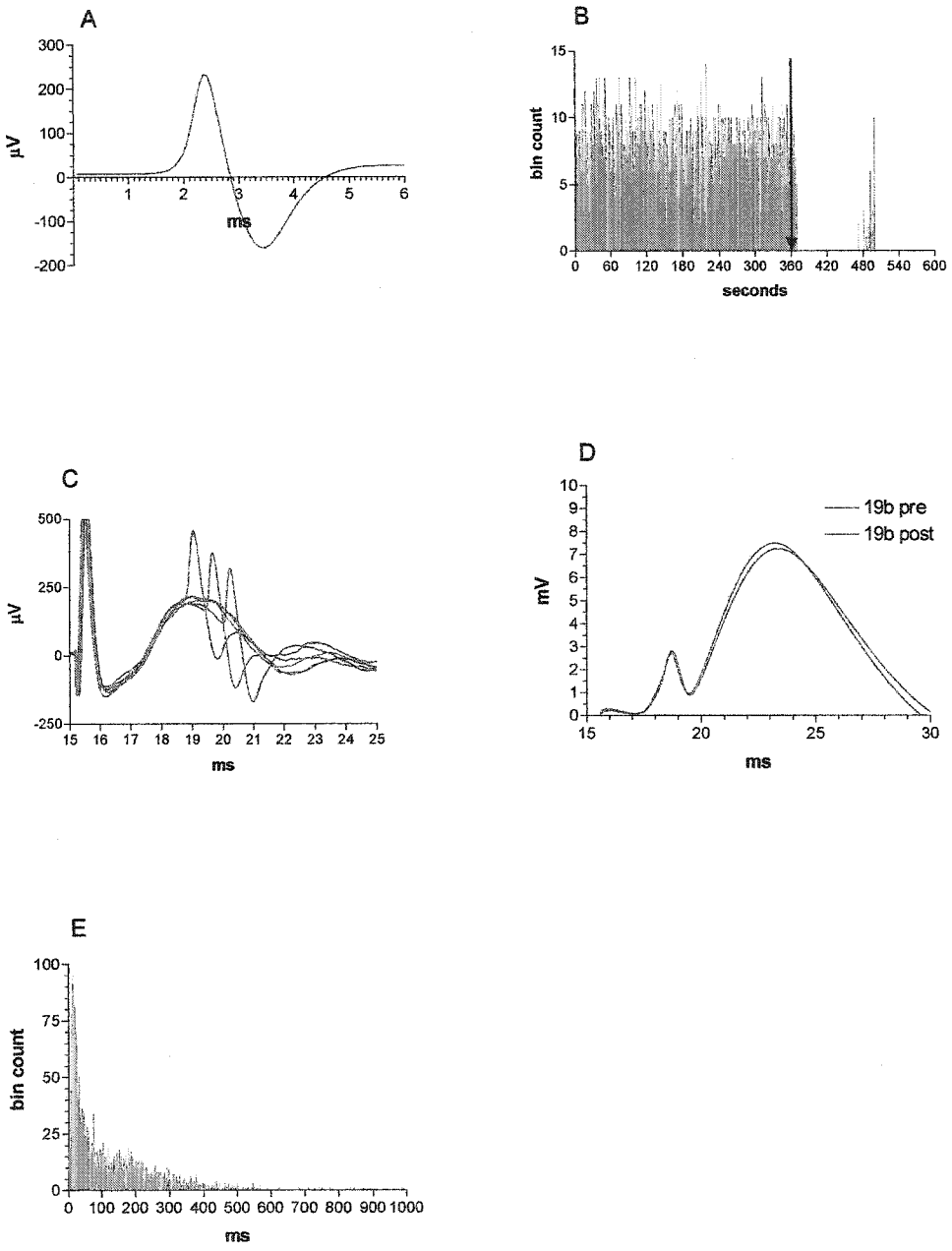
A
300
200
100
0
-100
-200
µV
1
2
3
4
5
6
ms
B
15
10
5
0
bin count
0
60
120
180
240
300
360
420
480
540
600
seconds
C
500
250
0
-250
µV
15
16
17
18
19
20
21
22
23
24
25
ms
D
10
9
8
7
6
5
4
3
2
1
0
mV
19b pre
19b post
15
20
25
30
ms
E
100
75
50
25
0
bin count
0
100
200
300
400
500
600
700
800
900
1000
ms

Figure 22: Record of cell JCR 4019B. A: Averaged waveform for all cell events in the free recording period. B: Rate meter histogram depicting spontaneous activity in one second bins. The glutamate ejection occurred at 360 seconds as indicated by the arrow. C: The unit activity evoked by perforant path activity of 150 μA. The cell is visible at 21 ms while the population spike reaches its maximum at 19.5 ms. D: Evoked potentials produced by 300 μA stimulation of the perforant path. The baseline waveform is in blue with the post-ejection waveform depicted in red. E: Autocorrelation of spontaneous activity in 1 ms bins. The cell shows a sharp primary peak and the suggestion of a secondary peak at 200 ms.

Figure 23.

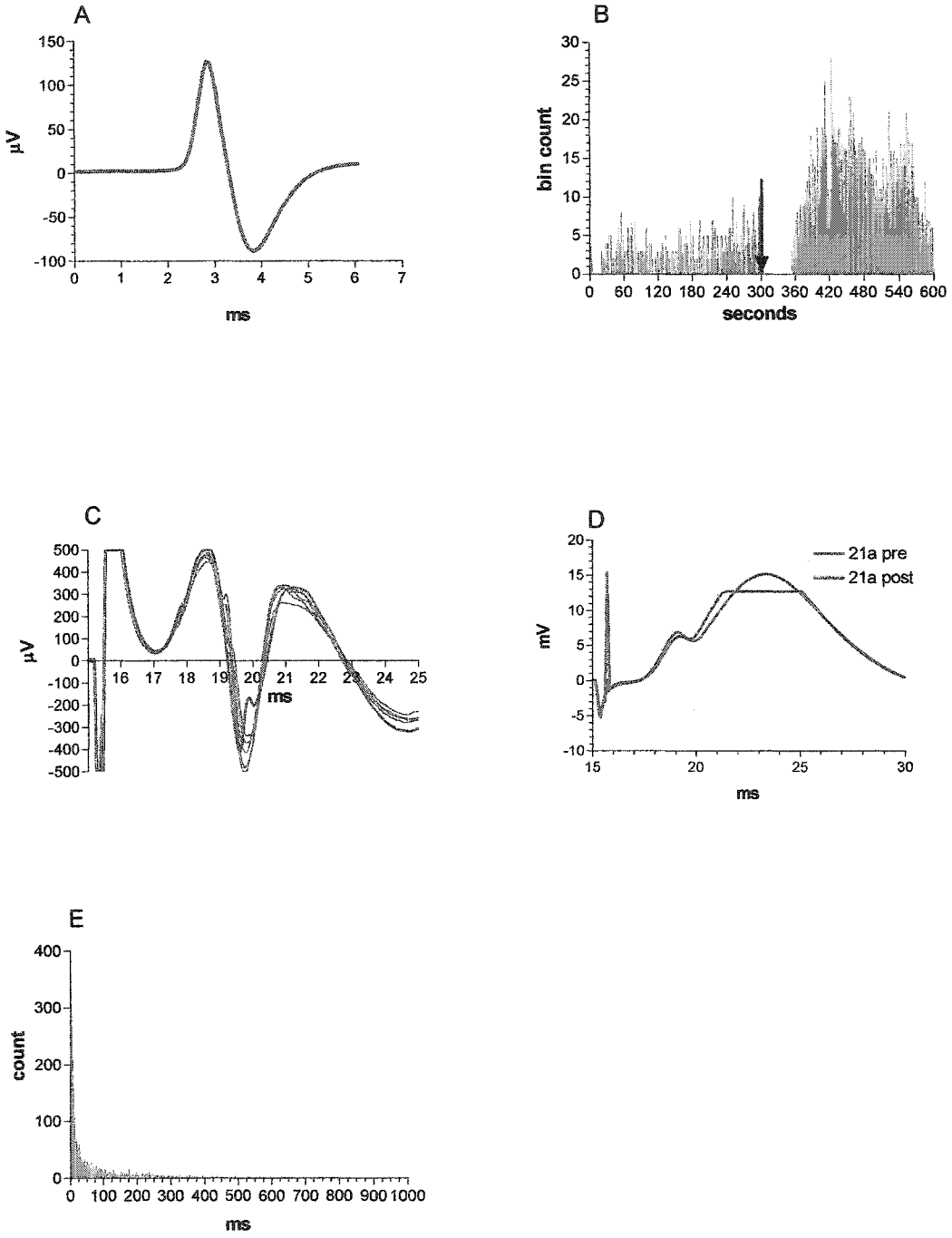
A
150
100
50
0
-50
-100
µV
0 1 2 3 4 5 6 7
ms
B
30
25
20
15
10
5
0
bin count
0 60 120 180 240 300 360 420 480 540 600
seconds
C
500
400
300
200
100
0
-100
-200
-300
-400
-500
µV
16 17 18 19 20 21 22 23 24 25
ms
D
20
15
10
5
0
-5
-10
mV
21a pre
21a post
15 20 25 30
ms
E
400
300
200
100
0
count
0 100 200 300 400 500 600 700 800 900 1000
ms

Figure 23: Record of cell JCR 4021A. A: Averaged waveform for all cell events in the free recording period. B: Rate meter histogram depicting spontaneous activity in one second bins. The glutamate ejection occurred at 300 seconds as indicated by the arrow. C: The unit activity evoked by perforant path activity of 280 μA. The cell fires in the middle of the population spike. D: Evoked potentials produced by 400 μA stimulation of the perforant path. The baseline waveform is in blue with the post-ejection waveform depicted in red. E: Autocorrelation of spontaneous activity in 1 ms bins. The cell shows a very sharp early peak with no suggestion of theta rhythmicity.

Figure 24.

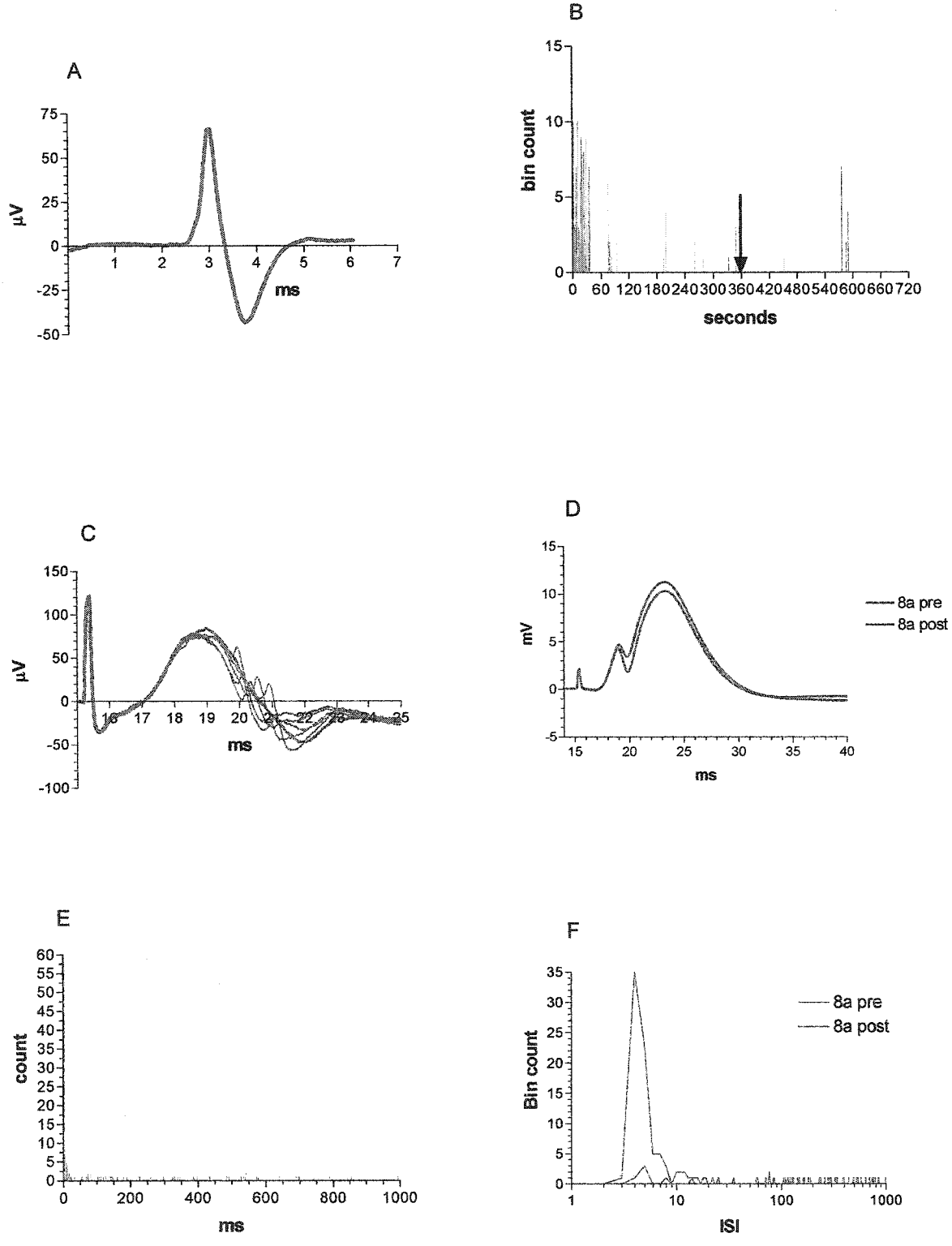
A
μV
ms
B
bin count
seconds
C
μV
ms
D
mV
ms
8a pre
8a post
E
count
ms
F
Bin count
ISI
8a pre
8a post

Figure 24: Record of cell JCR 4008A. A: Averaged waveform for all cell events in the free recording period. B: Rate meter histogram depicting spontaneous activity in one second bins. The glutamate ejection occurred at 360 seconds as indicated by the arrow. C: The unit activity evoked by perforant path activity of 60 μA. D: Evoked potentials produced by 300 μA stimulation of the perforant path. The baseline waveform is in blue with the post-ejection waveform depicted in red. E: Autocorrelation of spontaneous activity in 1 ms bins. The cell shows a strong primary peak without theta rhythmicity.

Figure 25.

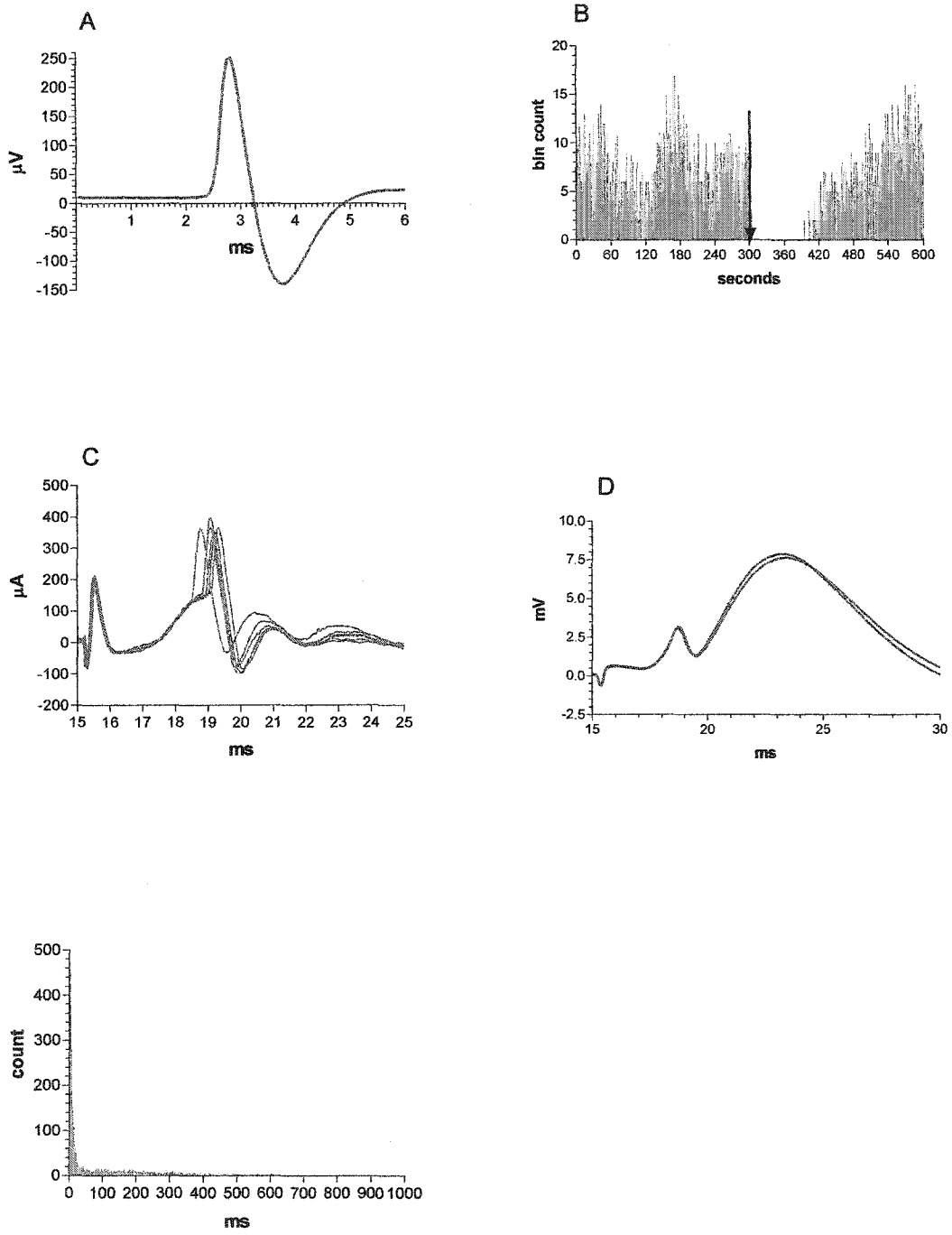

Figure 25: Record of cell JCR 4019A. A: Averaged waveform for all cell events in the free recording period. B: Rate meter histogram depicting spontaneous activity in one second bins. The glutamate ejection occurred at 300 seconds as indicated by the arrow. C: The unit activity evoked by perforant path activity of 100 μA. D: Evoked potentials produced by 400 μA stimulation of the perforant path. The baseline waveform is in blue with the post-ejection waveform depicted in red. E: Autocorrelation of spontaneous activity in 1 ms bins. The cell shows a very sharp primary peak without theta rhythmicity.

Figure 26.

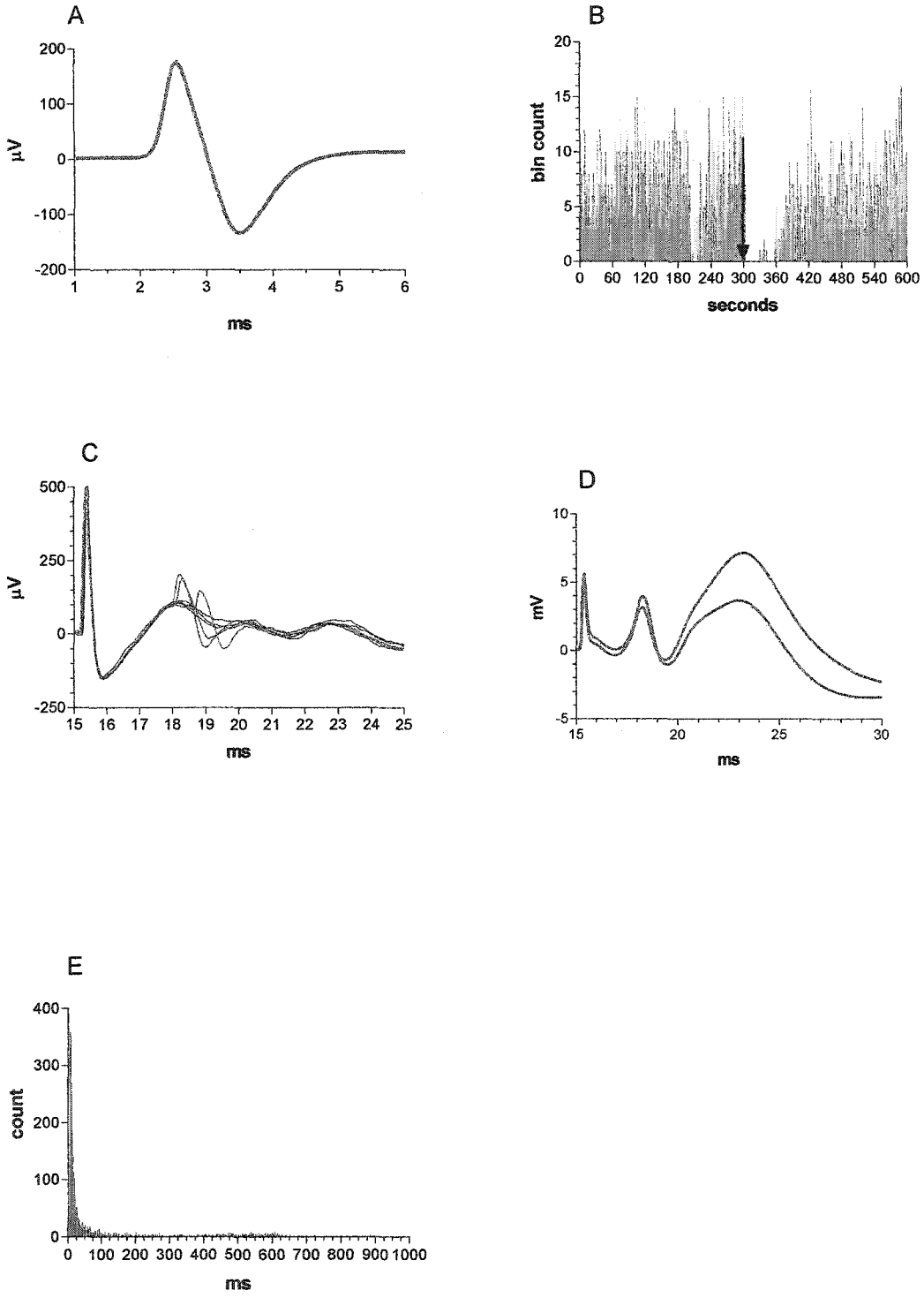
A
200
100
0
-100
-200
µV
1 2 3 4 5 6
ms
B
20
15
10
5
0
bin count
0 60 120 180 240 300 360 420 480 540 600
seconds
C
500
250
0
-250
µV
15 16 17 18 19 20 21 22 23 24 25
ms
D
10
5
0
-5
mV
15 20 25 30
ms
E
400
300
200
100
0
count
0 100 200 300 400 500 600 700 800 900 1000
ms

Figure 26: Record of cell JCR 4022B. A: Averaged waveform for all cell events in the free recording period. B: Rate meter histogram depicting spontaneous activity in one second bins. The glutamate ejection occurred at 300 seconds as indicated by the arrow. C: The unit activity evoked by perforant path activity of 50 μA. D: Evoked potentials produced by 250 μA stimulation of the perforant path. The baseline waveform is in blue with the post-ejection waveform depicted in red. E: Autocorrelation of spontaneous activity in 1 ms bins. The cell shows a strong primary peak with a suggestion of a secondary peak at 600 ms.

Figure 27.

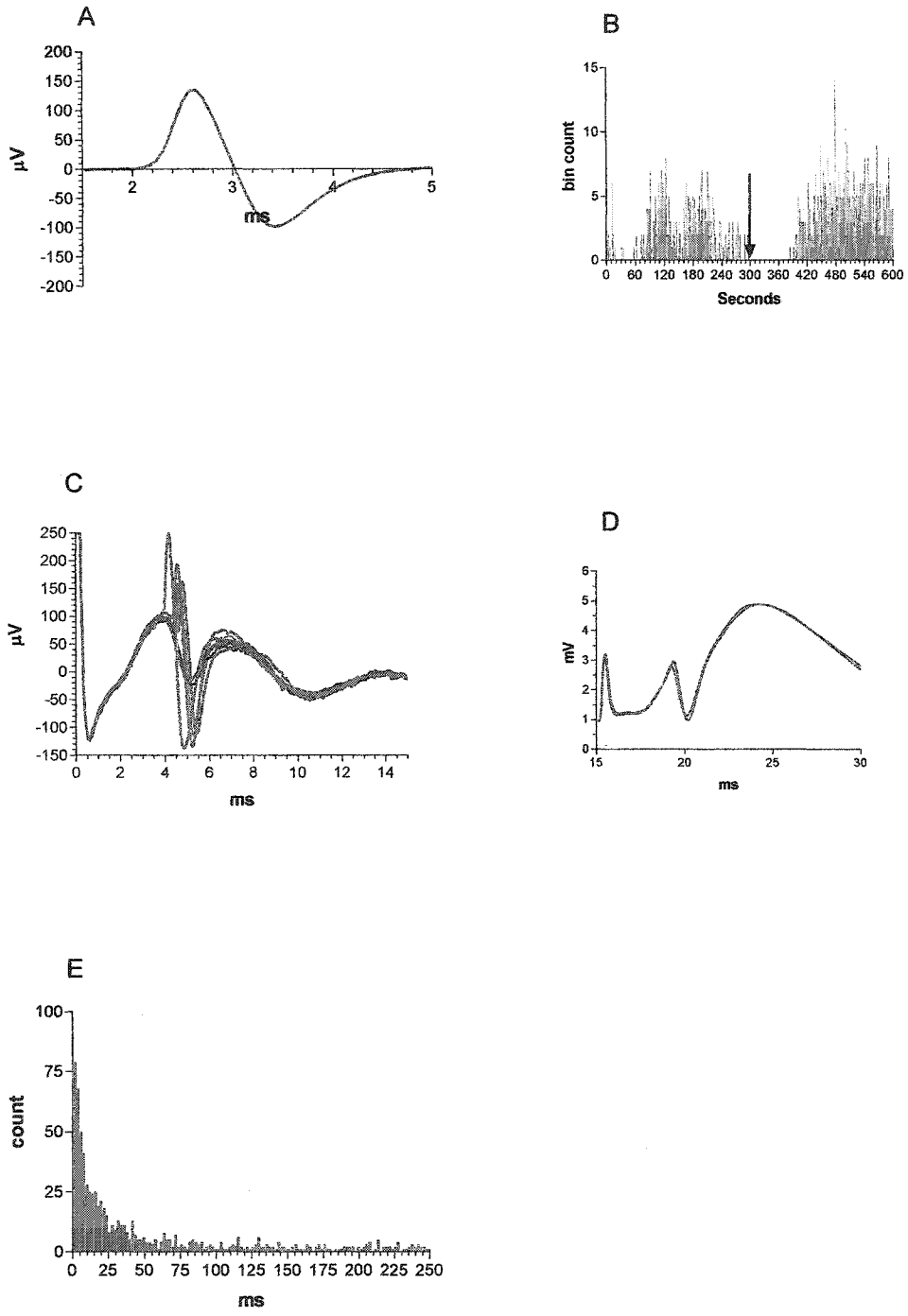
A
200
150
100
50
0
-50
-100
-150
-200
µV
2
3
4
5
ms
B
15
10
5
0
bin count
0 60 120 180 240 300 360 420 480 540 600
Seconds
C
250
200
150
100
50
0
-50
-100
-150
µV
0 2 4 6 8 10 12 14
ms
D
6
5
4
3
2
1
0
mV
15 20 25 30
ms
E
100
75
50
25
0
count
0 25 50 75 100 125 150 175 200 225 250
ms

Figure 27: Record of cell JCR 4014B. A: Averaged waveform for all cell events in the free recording period. B: Rate meter histogram depicting spontaneous activity in one second bins. The glutamate ejection occurred at 300 seconds as indicated by the arrow. C: The unit activity evoked by perforant path activity of 50 μA. D: Evoked potentials produced by 100 μA stimulation of the perforant path. The baseline waveform is in blue with the post-ejection waveform depicted in red. E: Autocorrelation of spontaneous activity in 1 ms bins. The cell shows a strong primary peak without theta rhythmicity.

Figure 28.

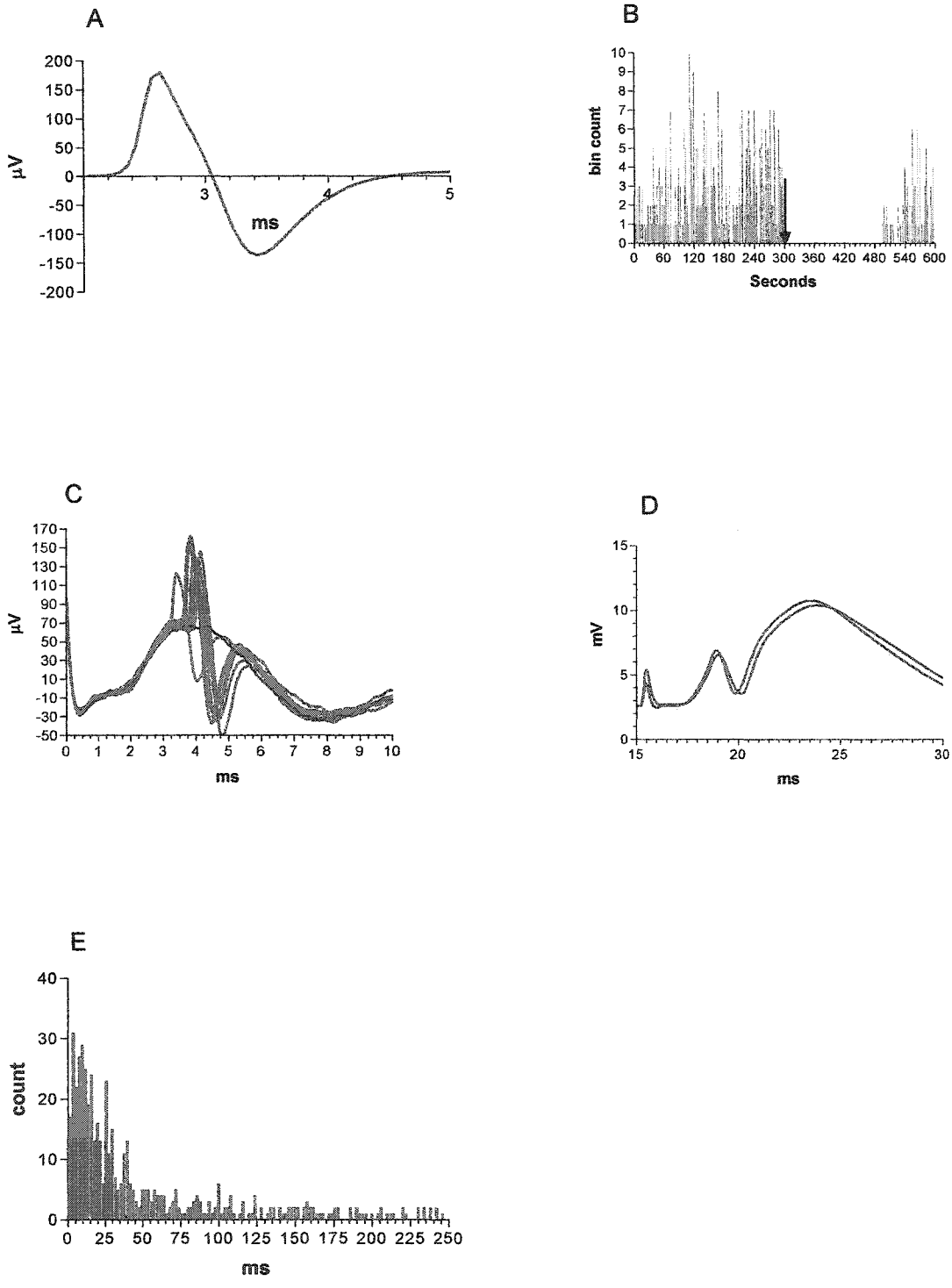
A
200
150
100
50
0
-50
-100
-150
-200
µV
3
4
5
ms
B
10
9
8
7
6
5
4
3
2
1
0
bin count
0 60 120 180 240 300 360 420 480 540 600
Seconds
C
170
150
130
110
90
70
50
30
10
-10
-30
-50
µV
0 1 2 3 4 5 6 7 8 9 10
ms
D
15
10
5
0
mV
15 20 25 30
ms
E
40
30
20
10
0
count
0 25 50 75 100 125 150 175 200 225 250
ms

Figure 28: Record of cell JCR 4014A. A: Averaged waveform for all cell events in the free recording period. B: Rate meter histogram depicting spontaneous activity in one second bins. The glutamate ejection occurred at 300 seconds as indicated by the red bar. C: The unit activity evoked by perforant path activity of 30 μA. D: Evoked potentials produced by 100 μA stimulation of the perforant path. The baseline waveform is in blue with the post-ejection waveform depicted in red. E: Autocorrelation of spontaneous activity in 1 ms bins. The cell shows a strong primary peak without theta rhythmicity.

Figure 29.

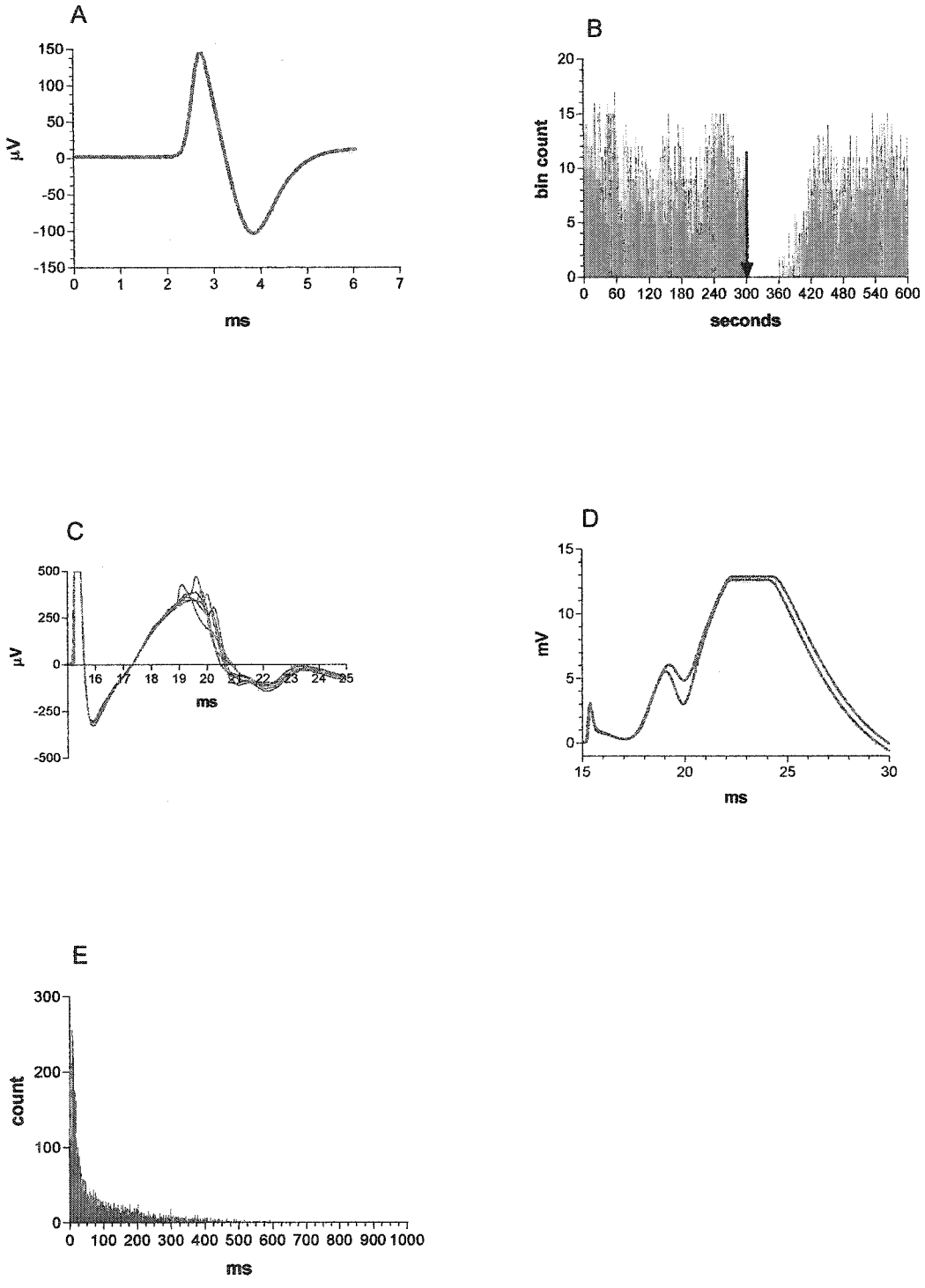
A
150
100
50
0
-50
-100
-150
µV
0 1 2 3 4 5 6 7
ms
B
20
15
10
5
0
bin count
0 60 120 180 240 300 360 420 480 540 600
seconds
C
500
250
0
-250
-500
µV
16 17 18 19 20 21 22 23 24 25
ms
D
15
10
5
0
mV
15 20 25 30
ms
E
300
200
100
0
count
0 100 200 300 400 500 600 700 800 900 1000
ms

Figure 29: Record of cell JCR 4021B. A: Averaged waveform for all cell events in the free recording period. B: Rate meter histogram depicting spontaneous activity in one second bins. The glutamate ejection occurred at 300 seconds as indicated by the arrow. C: The unit activity evoked by perforant path activity of 100 μA. D: Evoked potentials produced by 300 μA stimulation of the perforant path. The baseline waveform is in blue with the post-ejection waveform depicted in red. E: Autocorrelation of spontaneous activity in 1 ms bins. The cell shows a strong early peak with a no suggestion of a secondary peak.

Figure 30.

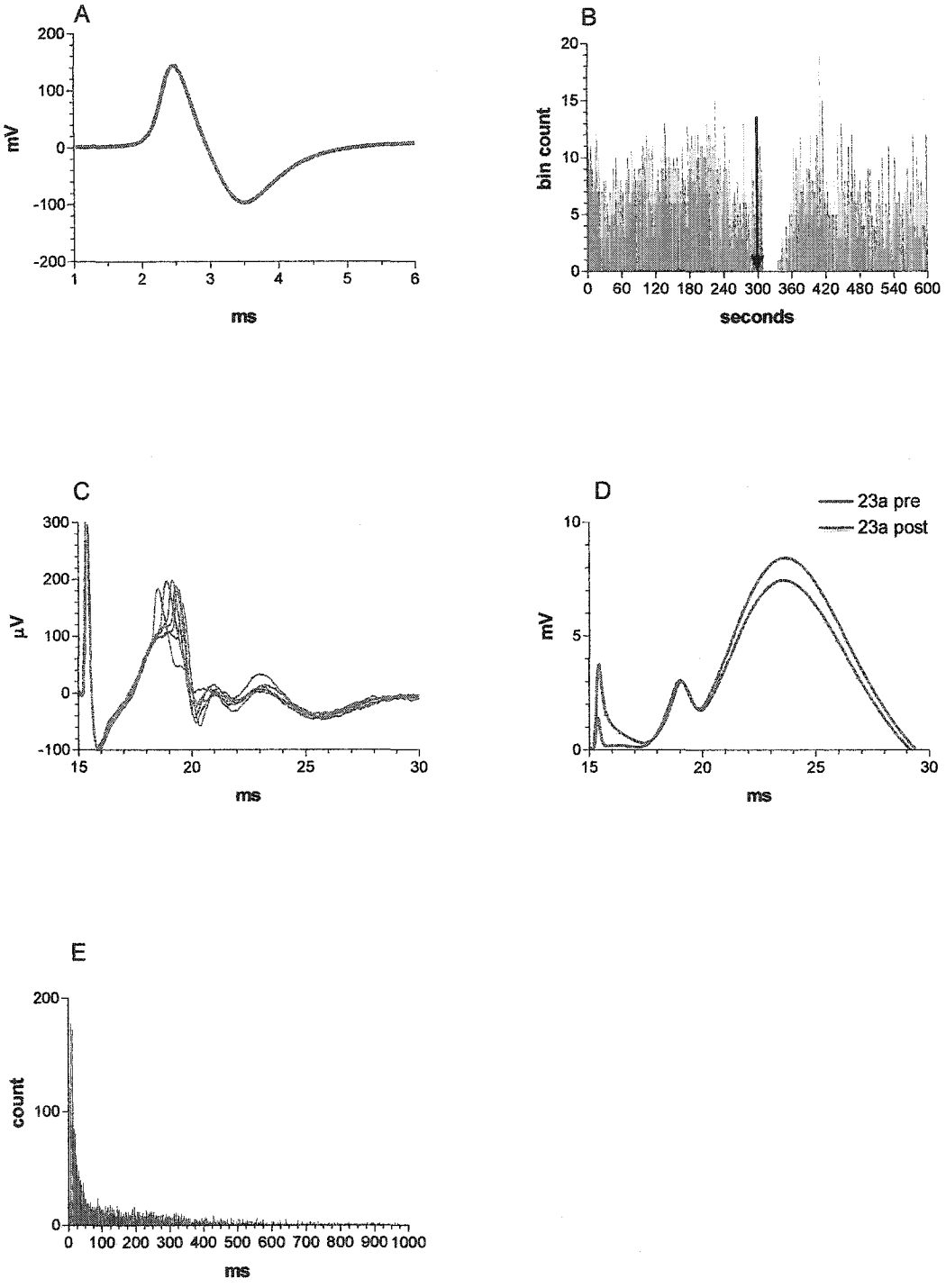
A
200
100
0
-100
-200
mV
1
2
3
4
5
6
ms
B
20
15
10
5
0
bin count
0 60 120 180 240 300 360 420 480 540 600
seconds
C
300
200
100
0
-100
µV
15
20
25
30
ms
D
23a pre
23a post
10
5
0
mV
15
20
25
30
ms
E
200
100
0
count
0 100 200 300 400 500 600 700 800 900 1000
ms

Figure 30. Record of cell JCR 4023A. A: Averaged waveform for all cell events in the free recording period. B: Rate meter histogram depicting spontaneous activity in one second bins. The glutamate ejection occurred at 300 seconds as indicated by the arrow. C: The unit activity evoked by perforant path activity of 80 μA. D: Evoked potentials produced by 300 μA stimulation of the perforant path. The baseline waveform is in blue with the post-ejection waveform depicted in red. E: Autocorrelation of spontaneous activity in 1 ms bins. The cell shows a strong primary peak with no secondary peaks.

Figure 31.

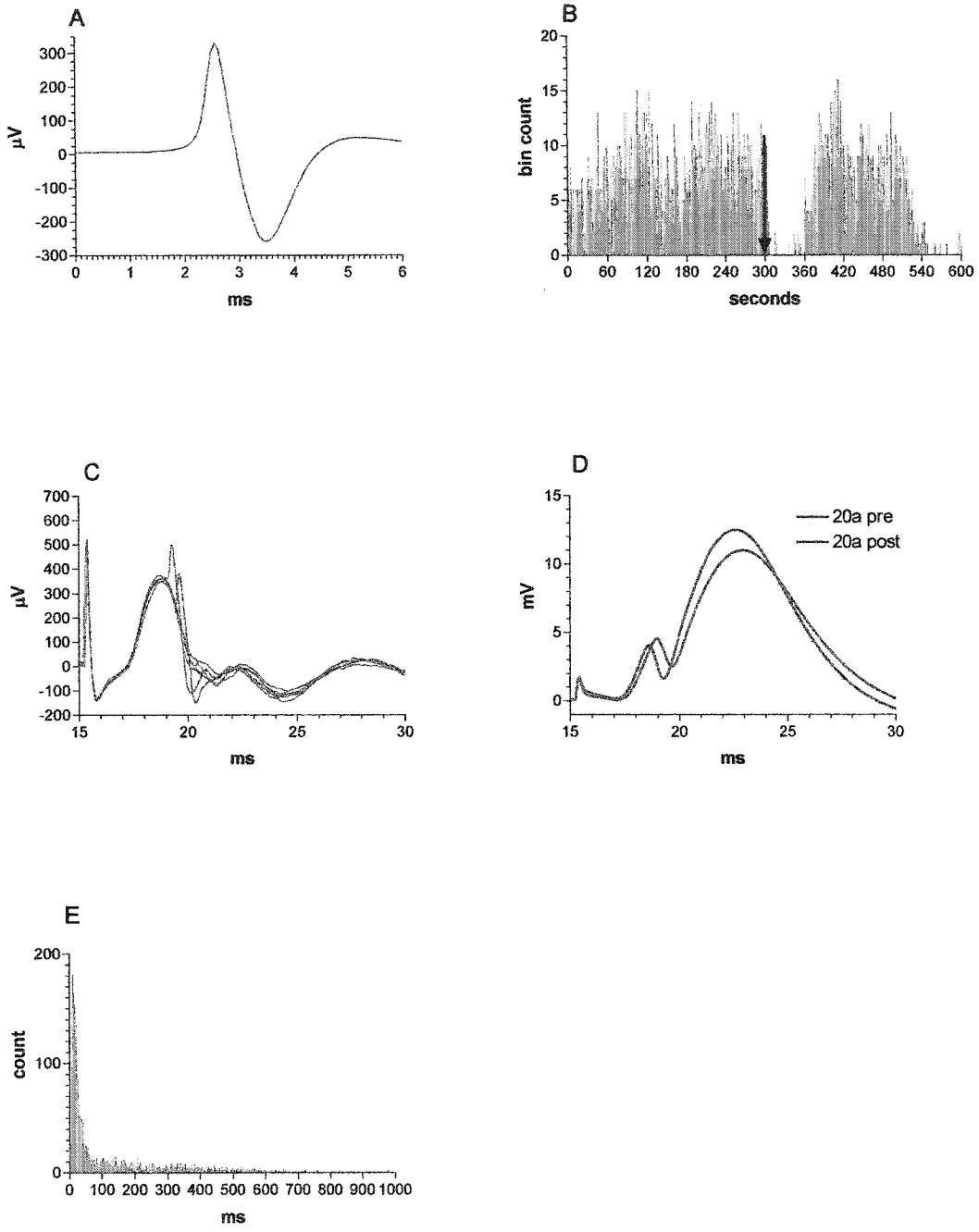
A
μV
ms
B
bin count
seconds
C
μV
ms
D
mV
20a pre
20a post
ms
E
count
ms

Figure 31: Record of cell JCR 4020A. A: Averaged waveform for all cell events in the free recording period. B: Rate meter histogram depicting spontaneous activity in one second bins. The glutamate ejection occurred at 300 seconds as indicated by the arrow. C: The unit activity evoked by perforant path activity of 100 μA. D: Evoked potentials produced by 400 μA stimulation of the perforant path. The baseline waveform is in blue with the post-ejection waveform depicted in red. E: Autocorrelation of spontaneous activity in 1 ms bins. The cell shows a sharp primary peak with no secondary peaks.

Figure 32.

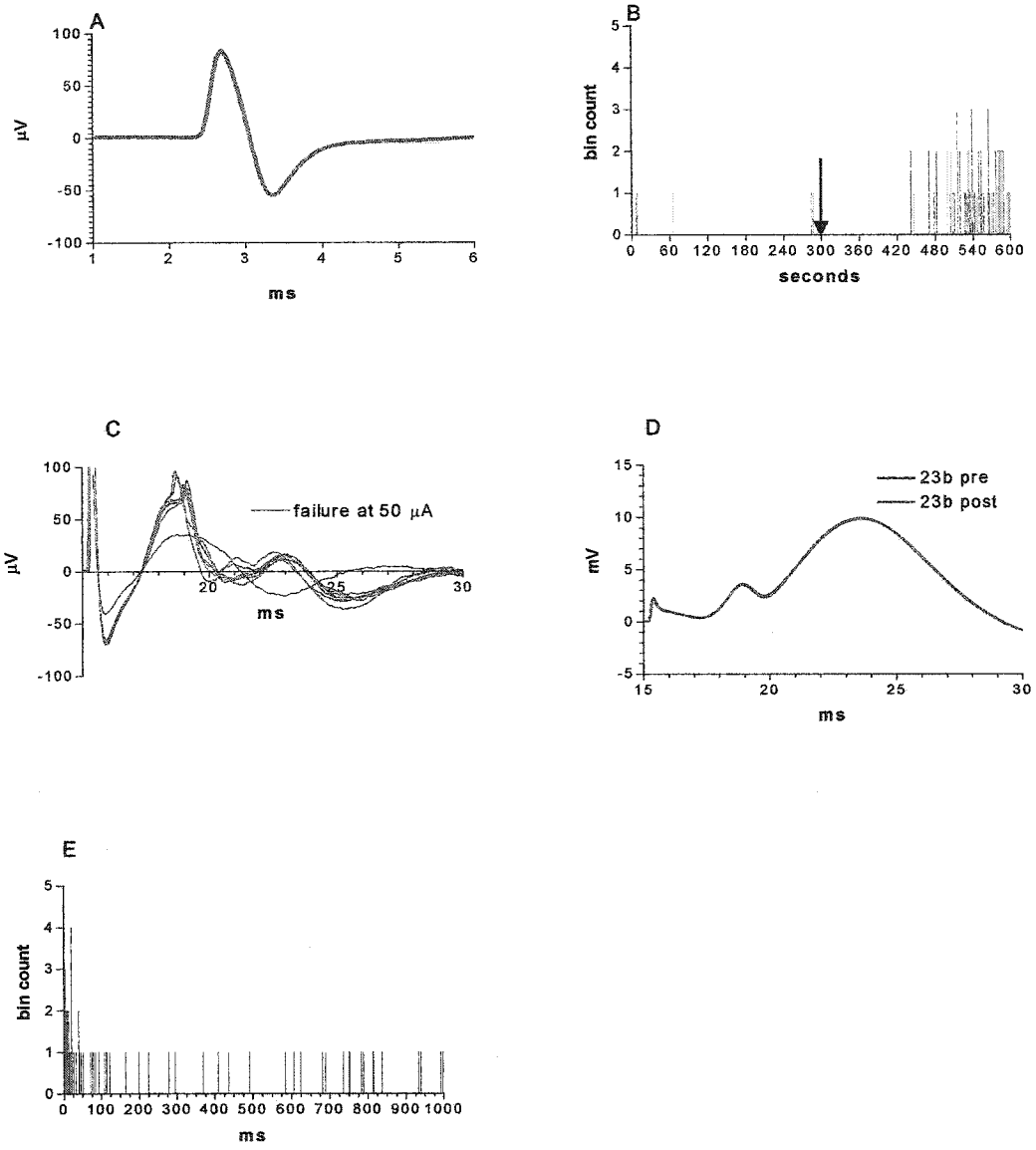
A
100
50
0
-50
-100
µV
1
2
3
4
5
6
ms
B
bin count
0
1
2
3
4
5
0 60 120 180 240 300 360 420 480 540 600
seconds
C
failure at 50 µA
µV
100
50
0
-50
-100
20
25
30
ms
D
23b pre
23b post
mV
15
10
5
0
-5
15
20
25
30
ms
E
bin count
0
1
2
3
4
5
0 100 200 300 400 500 600 700 800 900 1000
ms

Figure 32: Record of cell JCR 4023B. A: Averaged waveform for all cell events in the free recording period. B: Rate meter histogram depicting spontaneous activity in one second bins. The glutamate ejection occurred at 300 seconds as indicated by the arrow. C: The unit activity evoked by perforant path activity of 100 μA. D: Evoked potentials produced by 300 μA stimulation of the perforant path. The baseline waveform is in blue with the post-ejection waveform depicted in red. E: Autocorrelation of spontaneous activity in 1 ms bins. There is a suggestion of an early peak, although there are too few sample points to yield a complete picture.

Figure 33.

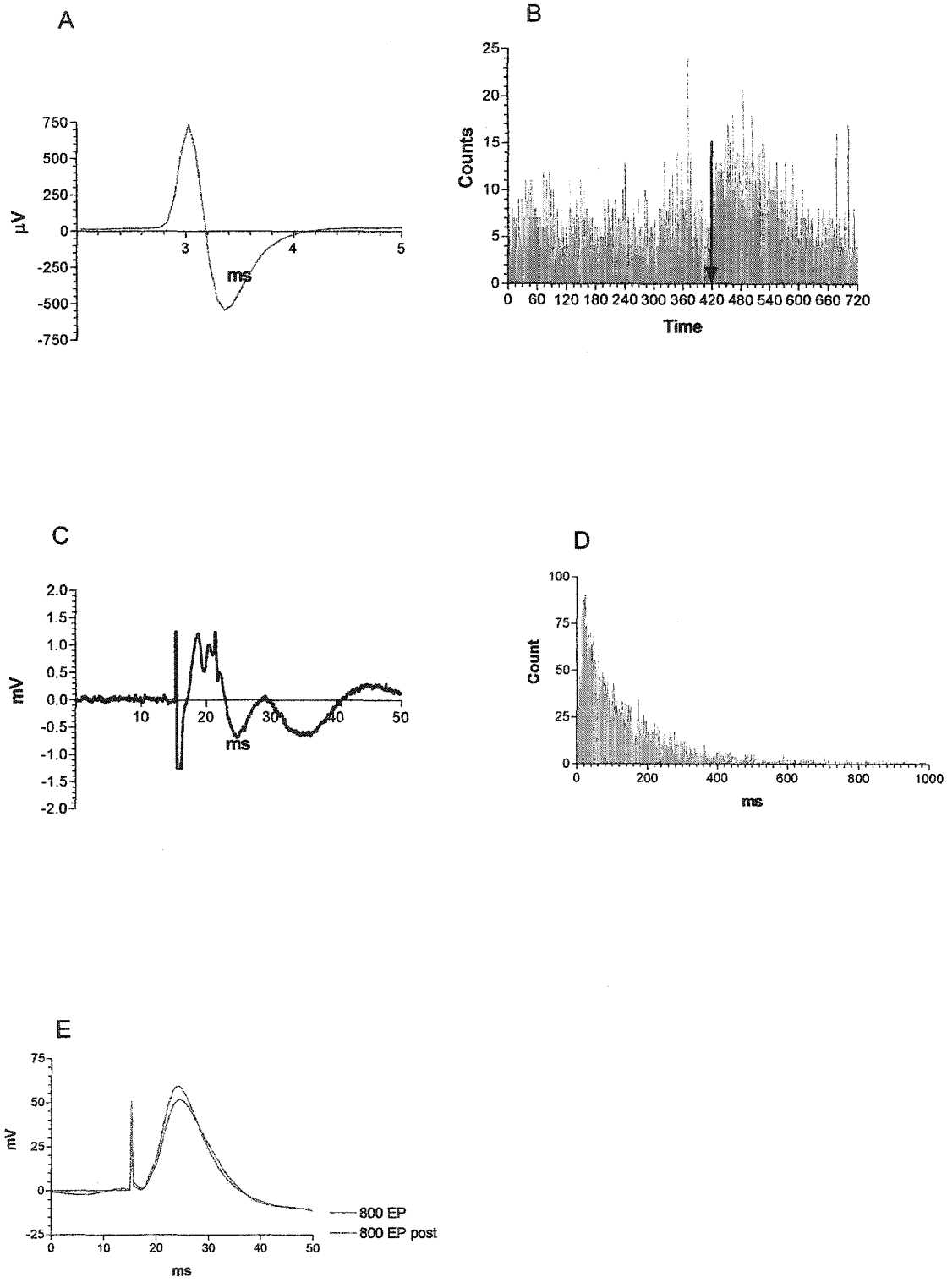
A
750
500
250
0
-250
-500
-750
µV
3
4
5
ms
B
25
20
15
10
5
0
Counts
0 60 120 180 240 300 360 420 480 540 600 660 720
Time
C
2.0
1.5
1.0
0.5
0.0
-0.5
-1.0
-1.5
-2.0
mV
10
20
30
40
50
ms
D
100
75
50
25
0
Count
0
200
400
600
800
1000
ms
E
75
50
25
0
-25
mV
0
10
20
30
40
50
ms
800 EP
800 EP post

Figure 33: Record of cell JCR 4003A. A: Averaged waveform for all cell events in the free recording period. B: Rate meter histogram depicting spontaneous activity in one second bins. The glutamate ejection occurred at 360 seconds as indicated by the red bar. C: The unit activity evoked by perforant path activity of 800 μA. A small population spike is visible in this trace which was not visible in the evoked potential channel due to the different filter settings. The cell is visible at 22 ms following the small population spike at 20 ms. The stimulus artifact is at 15 ms. D: Autocorrelation of spontaneous activity in 1 ms bins. The cell shows a strong primary peak without theta rhythmicity. E: Evoked potentials produced by 800 μA stimulation of the perforant path. The baseline waveform is in blue with the post-ejection waveform depicted in red.

Figure 34.

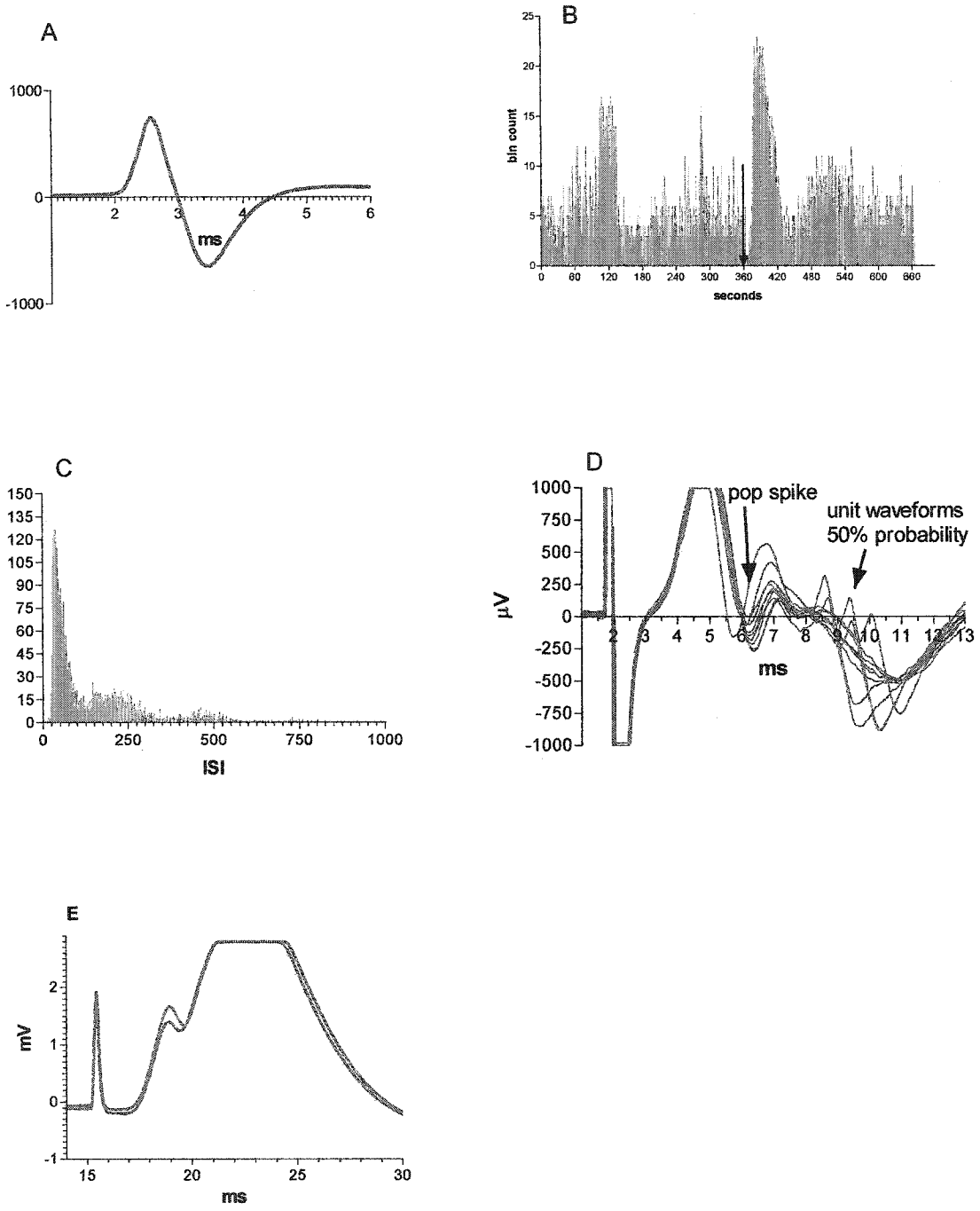
A
1000
0
-1000
2
3
4
5
6
ms
B
bin count
seconds
C
Count
ISI
D
pop spike
unit waveforms
50% probability
μV
ms
E
mV
ms

Figure 34: Record of cell JCR 4006A. A: Averaged waveform for all cell events in the free recording period. B: Rate meter histogram depicting spontaneous activity in one second bins. The glutamate ejection occurred at 360 seconds as indicated by the red bar. C: Autocorrelation of spontaneous activity in 1 ms bins. The cell shows a strong primary peak with theta rhythmicity indicated by the secondary and tertiary peaks at approximately 200 and 500 ms. D: The unit activity evoked by perforant path activity of 500 μA. The cell is visible occurring well after the population spike. E: Evoked potentials produced by 800 μA stimulation of the perforant path. The baseline waveform is in blue with the post-ejection waveform depicted in red. The peak of the evoked potential is clipped.

Figure 35.

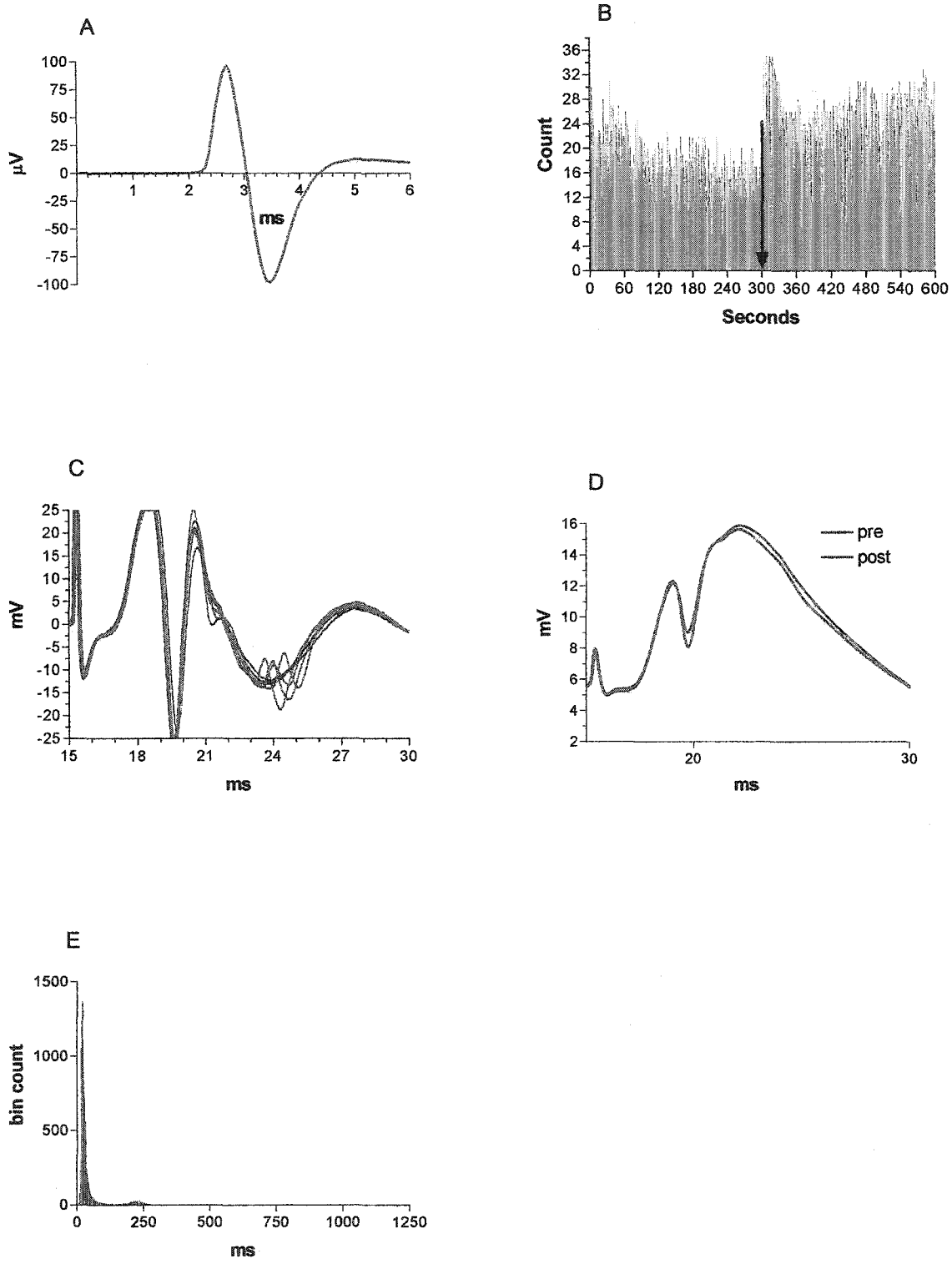
A
100
75
50
25
0
-25
-50
-75
-100
µV
1
2
3
4
5
6
ms
B
36
32
28
24
20
16
12
8
4
0
Count
0
60
120
180
240
300
360
420
480
540
600
Seconds
C
25
20
15
10
5
0
-5
-10
-15
-20
-25
mV
15
18
21
24
27
30
ms
D
16
14
12
10
8
6
4
2
mV
pre
post
20
30
ms
E
1500
1000
500
0
bin count
0
250
500
750
1000
1250
ms

Figure 35: Record of cell JCR 4011B. A: Averaged waveform for all cell events in the free recording period. B: Rate meter histogram depicting spontaneous activity in one second bins. The glutamate ejection occurred at 300 seconds as indicated by the red bar. C: The unit activity evoked by perforant path activity of 150 μA. The cell is visible well after the population spike. D: Evoked potentials produced by 150 μA stimulation of the perforant path. The baseline waveform is in blue with the post-ejection waveform depicted in red. E: Autocorrelation of spontaneous activity in 1 ms bins. The cell shows a strong primary peak with a small secondary peak visible at 200 ms.

Figure 36.

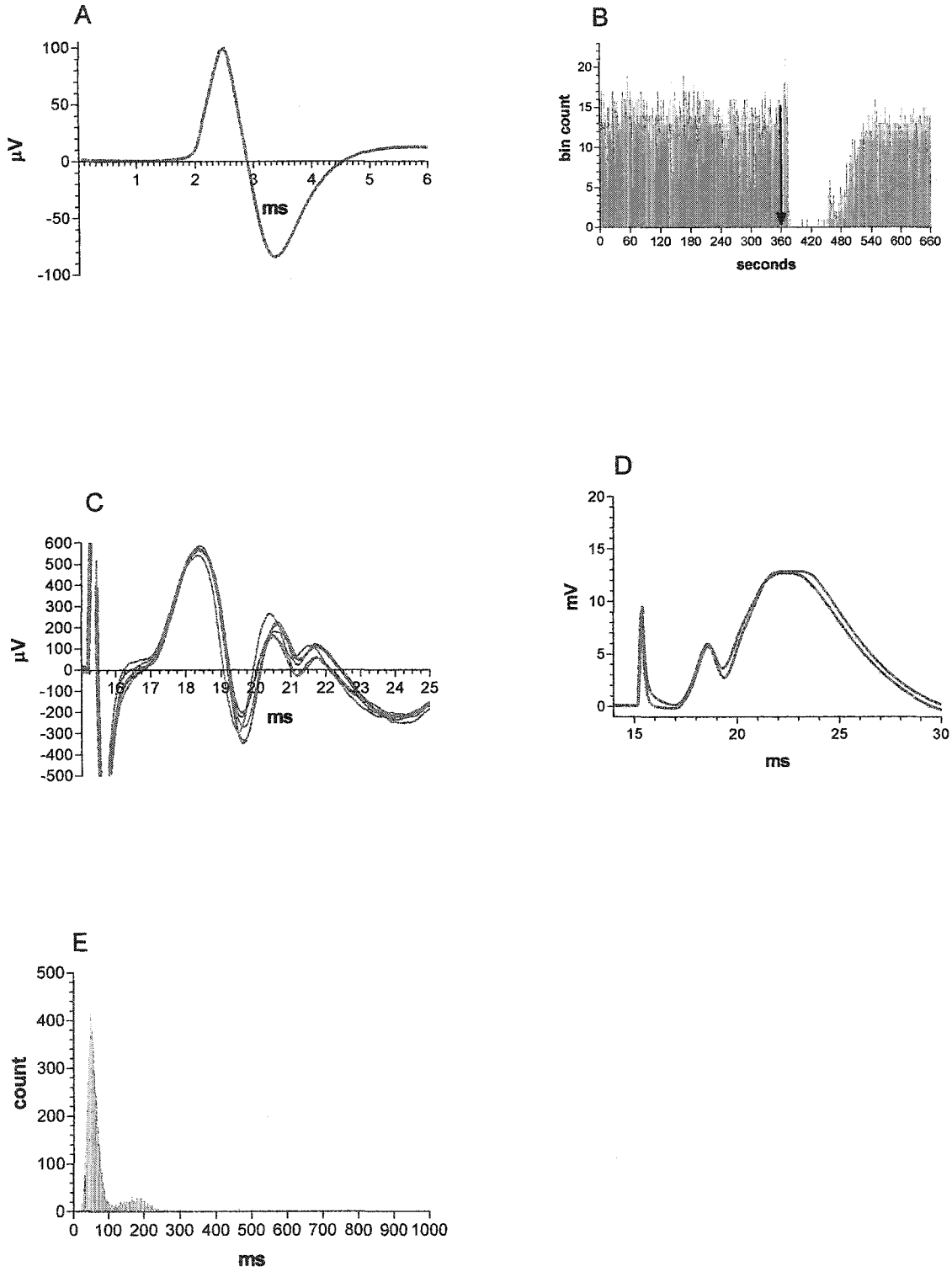
A
100
50
0
-50
-100
µV
1
2
3
4
5
6
ms
B
20
15
10
5
0
bin count
0 60 120 180 240 300 360 420 480 540 600 660
seconds
C
600
500
400
300
200
100
0
-100
-200
-300
-400
-500
µV
16 17 18 19 20 21 22 23 24 25
ms
D
20
15
10
5
0
mV
15 20 25 30
ms
E
500
400
300
200
100
0
count
0 100 200 300 400 500 600 700 800 900 1000
ms

Figure 36: Record of cell JCR 4019C. A: Averaged waveform for all cell events in the free recording period. B: Rate meter histogram depicting spontaneous activity in one second bins. The glutamate ejection occurred at 360 seconds as indicated by the arrow. C: The unit activity evoked by perforant path activity of 150 μA. The cell is visible at 21 ms while the population spike reaches its maximum at 19.5 ms. D: Evoked potentials produced by 300 μA stimulation of the perforant path. The baseline waveform is in blue with the post-ejection waveform depicted in red. E: Autocorrelation of spontaneous activity in 1 ms bins. The cell shows a sharp primary peak and a strong secondary peak at 200 ms.

Figure 37.

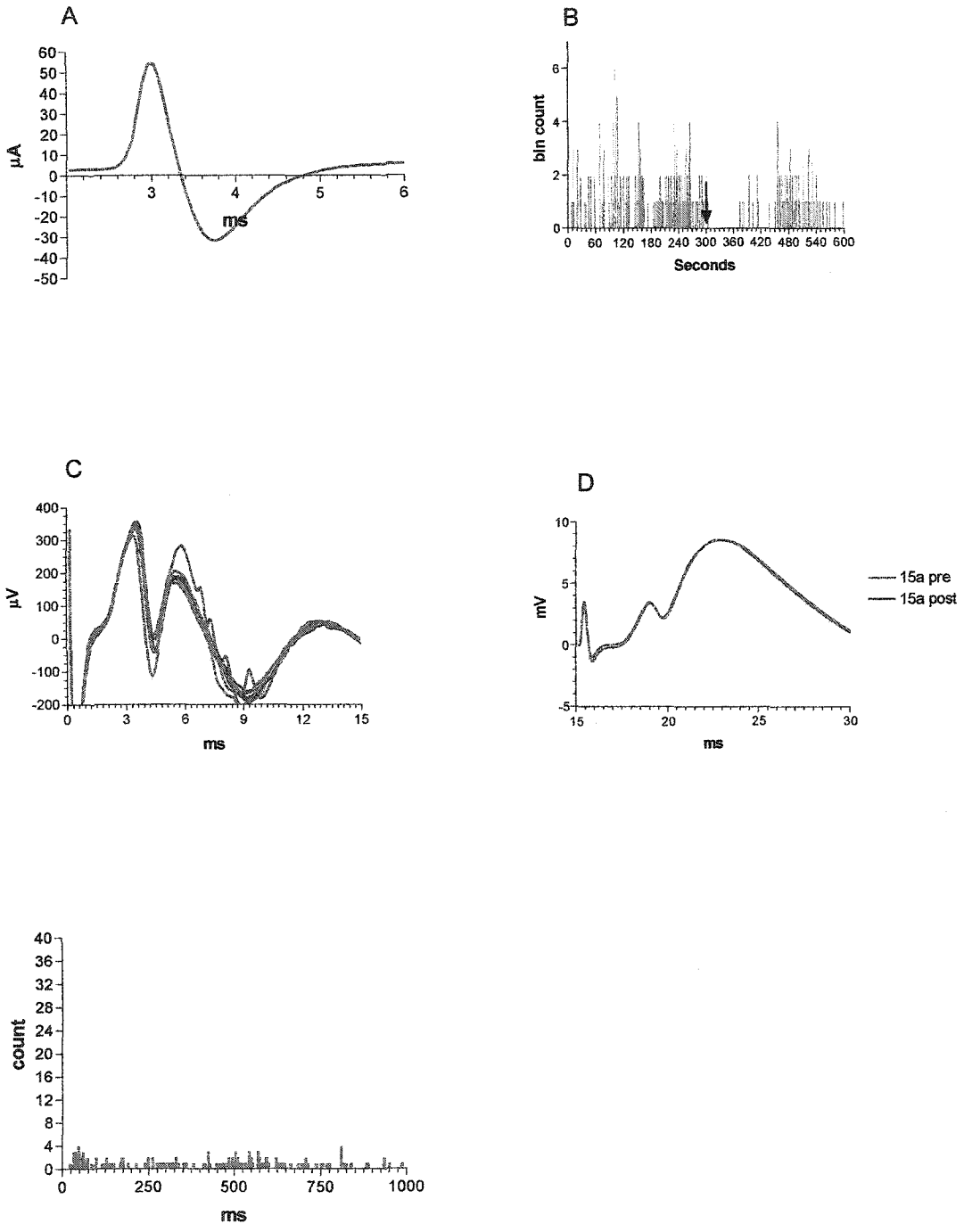
A
µA
ms
B
bin count
Seconds
C
µV
ms
D
mV
ms
15a pre
15a post
count
ms

Figure 37: Record of cell JCR 4015A. A: Averaged waveform for all cell events in the free recording period. B: Rate meter histogram depicting spontaneous activity in one second bins. The glutamate ejection occurred at 300 seconds as indicated by the arrow. C: The unit activity evoked by perforant path activity of 400 μA. The unit appears as small ripples following the population spike. D: Evoked potentials produced by 500 μA stimulation of the perforant path. The baseline waveform is in blue with the post-ejection waveform depicted in red. The evoked potentials overlap to a great extent. E: Autocorrelation of spontaneous activity in 1 ms bins. The cell shows a completely random firing pattern.

Figure 38.

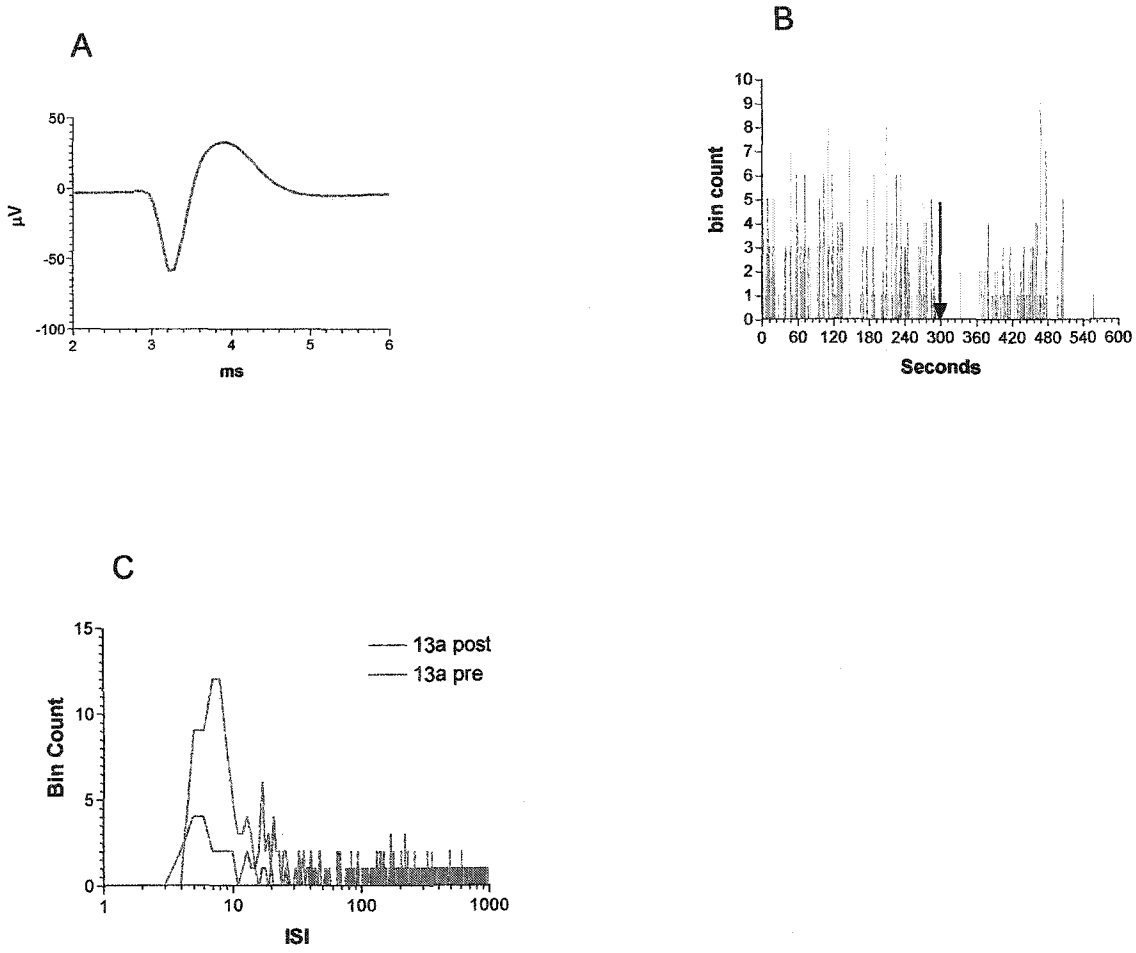
A
50
0
-50
-100
µV
2
3
4
5
6
ms
B
bin count
0
1
2
3
4
5
6
7
8
9
10
0
60
120
180
240
300
360
420
480
540
600
Seconds
C
Bin Count
15
10
5
0
13a post
13a pre
1
10
100
1000
ISI

Figure 38: Record of cell JCR 4013A. A: Averaged waveform for all cell events in the free recording period. B: Rate meter histogram depicting spontaneous activity in one second bins. The glutamate ejection occurred at 300 seconds as indicated by the red bar. C: Autocorrelation of spontaneous activity in 2 ms bins. The cell shows a strong primary peak without theta rhythmicity.

Figure 39.

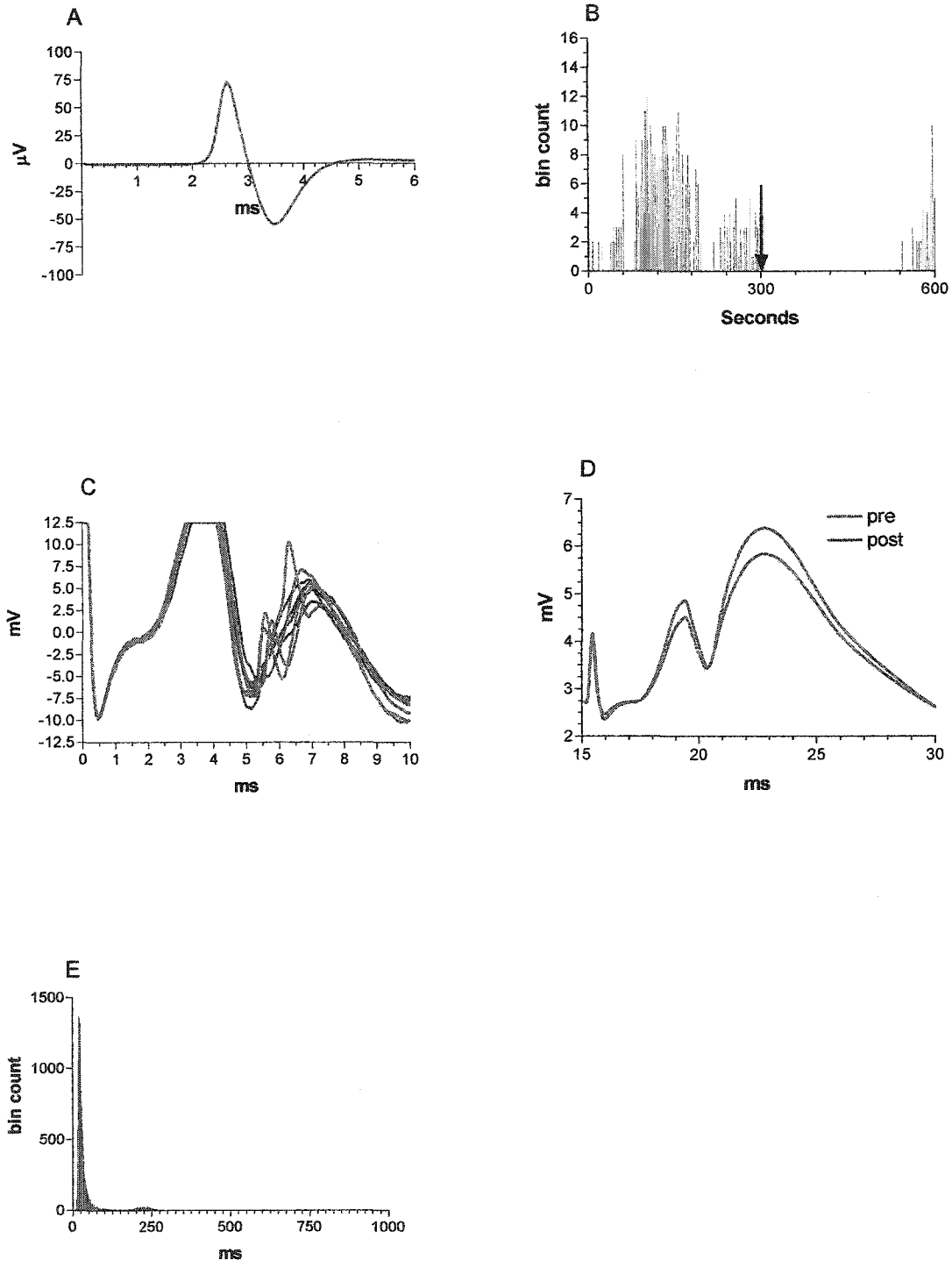
A
100
75
50
25
0
-25
-50
-75
-100
µV
1
2
3
4
5
6
ms
B
16
14
12
10
8
6
4
2
0
bin count
0
300
600
Seconds
C
12.5
10.0
7.5
5.0
2.5
0.0
-2.5
-5.0
-7.5
-10.0
-12.5
mV
0
1
2
3
4
5
6
7
8
9
10
ms
D
7
6
5
4
3
2
mV
pre
post
15
20
25
30
ms
E
1500
1000
500
0
bin count
0
250
500
750
1000
ms

Figure 39: Record of cell JCR 4012C. A: Averaged waveform for all cell events in the free recording period. B: Rate meter histogram depicting spontaneous activity in one second bins. The glutamate ejection occurred at 300 seconds as indicated by the red bar. C: The unit activity evoked by perforant path activity of 110 μA. The population spike is visible in this trace prior to the appearance of the units. The top of the waveform is clipped which was necessary to scale the unit. D: Evoked potentials produced by 150 μA stimulation of the perforant path. The baseline waveform is in blue with the post-ejection waveform depicted in red. E: Autocorrelation of spontaneous activity in 1 ms bins. The cell shows a strong primary peak with a weak secondary peak at 200 ms.

Figure 40.

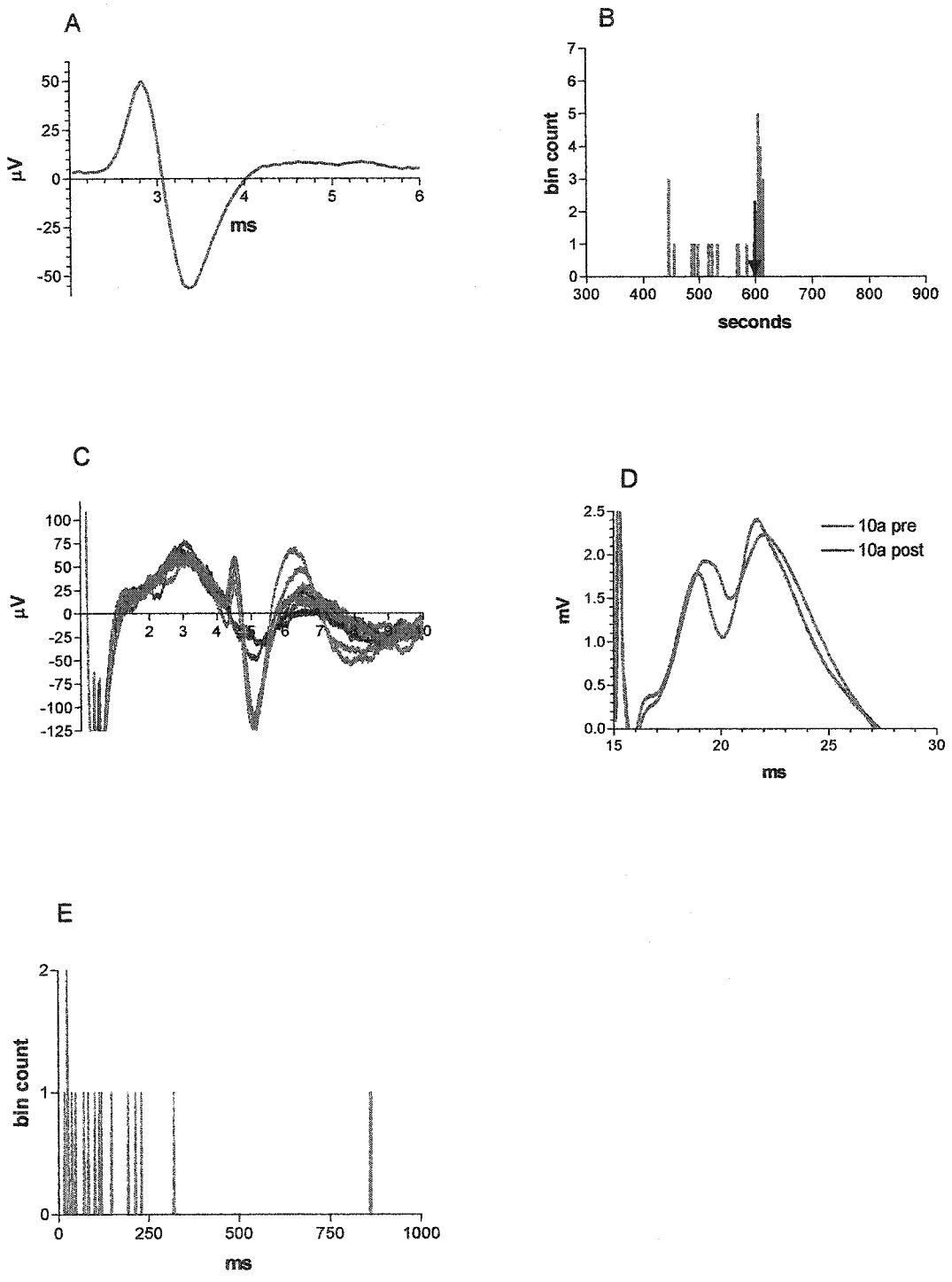
A
μV
ms
B
bin count
seconds
C
μV
D
mV
10a pre
10a post
ms
E
bin count
ms

Figure 40: Composite figure for cell JCR 4010A. A: Averaged waveform for all cell events in the free recording period. B: Rate meter histogram depicting spontaneous activity in one second bins. The glutamate ejection occurred at 600 seconds as indicated by the arrow. C: The unit activity evoked by perforant path activity of 500 μA. The unit would only fire at currents that would produce a population spike. The latency of the unit placed near the peak of the population spike. D: Evoked potentials produced by 800 μA stimulation of the perforant path. The baseline waveform is in blue with the post-ejection waveform depicted in red. E: Autocorrelation of spontaneous activity in 1 ms bins. The cell was very slow firing and did not produce enough spikes to produce a pattern in the autocorrelation.

Figure 41.

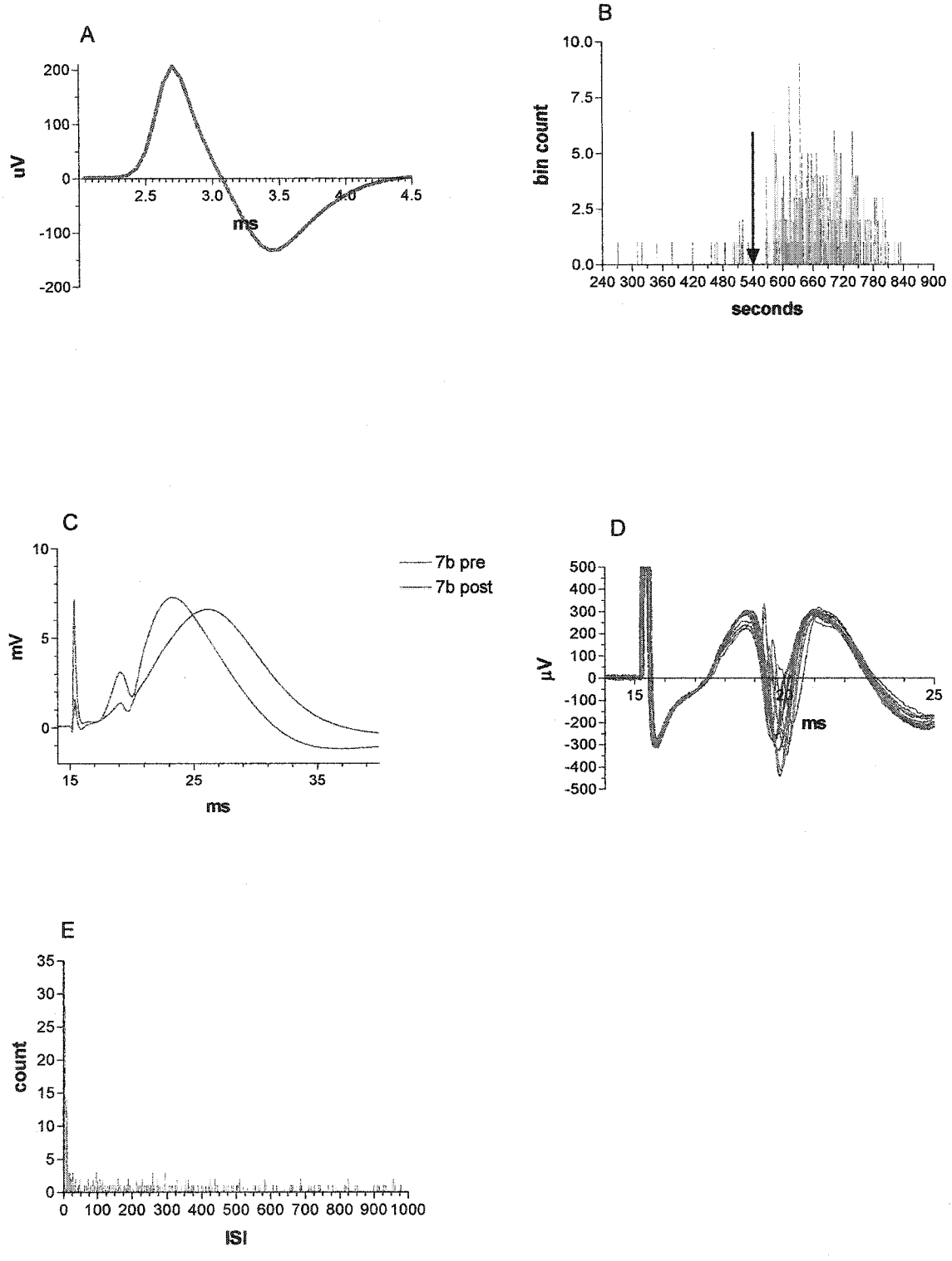
A
uV
200
100
0
-100
-200
2.5
3.0
3.5
4.0
4.5
ms
B
bin count
10.0
7.5
5.0
2.5
0.0
240 300 360 420 480 540 600 660 720 780 840 900
seconds
C
mV
10
5
0
15
25
35
ms
7b pre
7b post
D
µV
500
400
300
200
100
0
-100
-200
-300
-400
-500
15
25
ms
E
count
35
30
25
20
15
10
5
0
0 100 200 300 400 500 600 700 800 900 1000
ISI

Figure 41. Record of cell JCR 4007B. A. Averaged waveform for all cell events in the free recording period. B: Rate meter histogram depicting spontaneous activity in one second bins. The glutamate ejection occurred at 540 seconds as indicated by the red bar. C: Evoked potentials produced by 600 μA stimulation of the perforant path. The baseline waveform is in blue with the post-ejection waveform depicted in red. D: The unit activity evoked by perforant path activity of 600 μA. The unit would only fire at currents that would produce a population spike. The latency of the unit placed near the peak of the population spike. E: Autocorrelation of spontaneous activity in 1 ms bins. The cell was very slow firing and did not produce enough spikes to produce a pattern in the autocorrelation.

Figure 42.

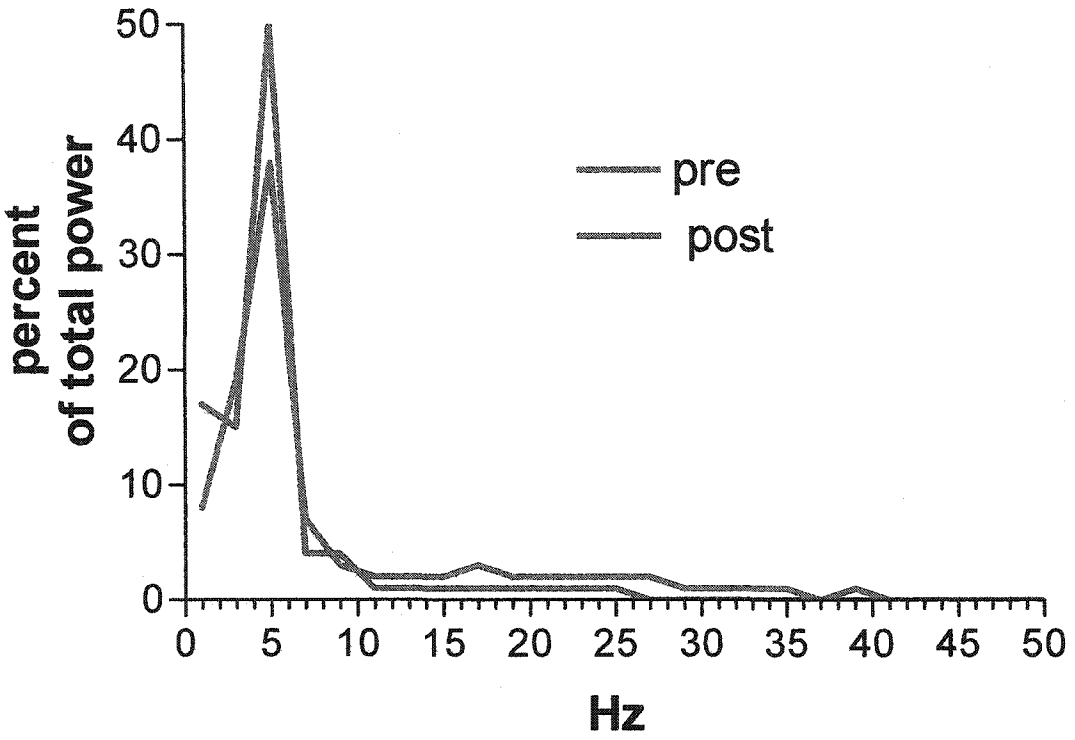


Figure 42. Power spectrum of the hilar EEG. This is a representative figure from a single animal. Fast Fourier transforms were performed on one minute of data prior to (blue) and following (red) the glutamate ejection in locus coeruleus. The resulting power plots were averaged to produce the figure. The majority of power lies below 10 Hz. and the proportion of power in the gamma spectrum is quite low.

Figure 43.

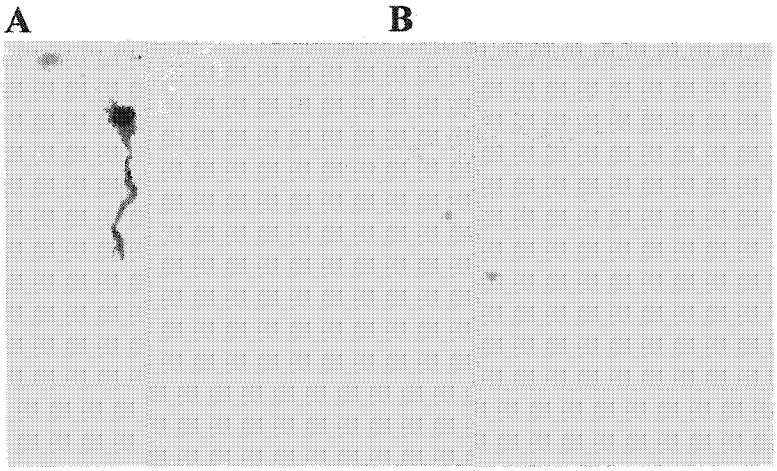


Figure 43: These figures display some of the problems associated with extracellular biocytin labelling. A: A labelled cell from the CA3 dentate border. This location is labelled 18x in figure 9 and is located well away from all other identified recording sites. It is possible that this cell was back filled from the dentate placement depicted in B. B: The recording site labelled 18y in figure 9.

Figure 44

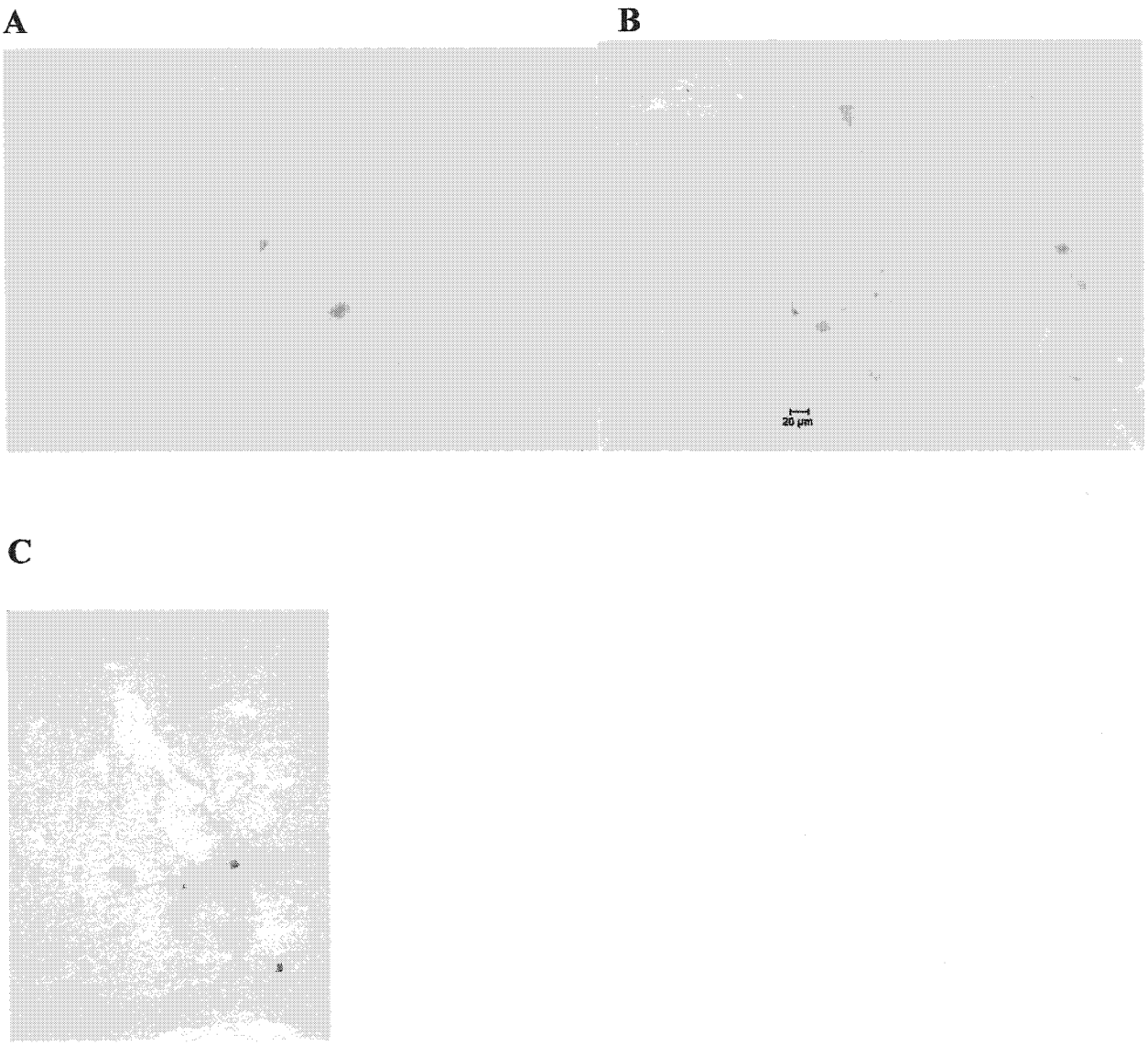


Figure 44: Further examples of difficulties associated with extracellular biocytin fills. A: Recording site J9 in figure 9. A clear ejection mark is visible in the centre of the frame. A mossy cell appears to have been filled by a dendrite while several granule cells have been filled via their axons. B: Recording site J11 in figure 9. Again a clear mark is visible at the recording site which resulted in the axonal filling of several granule cells and a basket cell. C: A cortical pyramidal cell that was filled either during the balancing of the bridge in cortex, or simply by the passage of the electrode.

Table 1.

| | cell amplitude µA | cell width µs | pre rate Hz | post rate Hz | duration seconds | rate t-test p value | % burst 5 min pre | % burst 5 min post | %burst 1 min pre | %burst 1 min post | Cell Profile |
|---|---|---|---|---|---|---|---|---|---|---|---|
| **4018a** | 203.2 | 593.4 | 5.616 | 3.733 | 84 | 0.000 | 0 | 0 | 0 | 0 | N |
| **4006b** | 580.4 | 461.5 | 10.050 | 3.470 | 300 | 0.000 | .06 | 0 | 0 | 0 | N |
| **4024a** | 314.9 | 725.3 | 0.500 | 0.016 | 95 | 0.000 | 1.9 | 8.33 | 6.89 | 0 | N |
| **4009b** | 73.8 | 461.5 | 10.650 | 8.566 | 44 | 0.0054 | 0 | 0 | 0 | 0 | N |
| **4022a** | 105.4 | 329.7 | 4.033 | 7.066 | 10 | 0.000 | 0 | 0 | 0 | 0 | N |
| **4018b** | 148.4 | 1120.9 | 5.316 | 2.516 | 123 | 0.000 | 4.74 | 3.92 | 5.01 | 5.2 | S |
| **4021c** | 106.2 | 857.1 | 4.600 | 0.616 | 138 | 0.000 | 4.94 | 7.73 | 5.69 | 18.75 | S |
| **4019b** | 393.3 | 1054.9 | 7.883 | 0.850 | 122 | 0.000 | 0.54 | 18.39 | 1.48 | 0 | S |
| **4021a** | 215.3 | 989.0 | 3.883 | 0.216 | 59 | 0.000 | 20.84 | 15.87 | 17.16 | 15.38 | S |
| **4008a** | 109.7 | 725.3 | 0.016 | 0.000 | 79 | 0.319 | 50 | 42.85 | 0 | 0 | S |
| **4019a** | 390.9 | 923.1 | 6.850 | 0.233 | 129 | 0.000 | 15.53 | 12.06 | 12.1 | 50 | W |
| **4022b** | 310.1 | 923.1 | 7.233 | 0.783 | 61 | 0.000 | 4.53 | 10.72 | 10.09 | 9.75 | W |
| **4014b** | 233.2 | 791.2 | 0.666 | 0.000 | 85 | 0.000 | 18.07 | 11.01 | 10 | 0 | W |
| **4014a** | 316.7 | 791.2 | 2.133 | 0.000 | 245 | 0.000 | 3.56 | 0 | 4.72 | 0 | W |
| **4021b** | 247.1 | 1054.9 | 10.600 | 0.639 | 125 | 0.000 | 4.27 | 3 | 0.31 | 0 | W |
| **4023a** | 240.4 | 989.0 | 5.333 | 1.683 | 60 | 0.000 | 0.52 | 3.37 | 0 | 2.04 | W |
| **4020a** | 588.1 | 923.1 | 4.000 | 0.750 | 76 | 0.000 | 0.09 | 0.14 | 0 | 0 | W |
| **4023b** | 139.0 | 659.3 | 0.033 | 0.000 | 147 | 0.153 | 0 | 0 | 0 | 0 | W |
| **4003a** | 1276.2 | 329.7 | 6.130 | 10.630 | 190 | 0.000 | .35 | .43 | 0.55 | 0.92 | N |
| **4006a** | 278.6 | 857.1 | 4.820 | 12.700 | 66 | 0.000 | 0 | 0 | 0 | 0 | S |
| **4011b** | 194.1 | 791.2 | 14.910 | 24.470 | 300 | 0.000 | 0 | 0 | 0 | 0 | S |
| **4019c** | 184.2 | 857.1 | 12.867 | 2.50 | 166 | 0.000 | 0 | 1.2 | 0 | 5.3 | S |
| **4015a** | 85.9 | 791.2 | 0.900 | 0.000 | 75 | 0.000 | 0 | 0 | 0 | 0 | S |
| **4013a** | 91.0 | 725.3 | 0.830 | 0.030 | 65 | 0.000 | 8.16 | 7.01 | 10.41 | 0 | S |
| **4012c** | 255.6 | 857.1 | 1.170 | 0.070 | 243 | 0.000 | 8.13 | 20 | 20 | 0 | W |
| **4010a** | 106.6 | 527.5 | 0.067 | 0.330 | 14 | 0.059 | 25 | 8.69 | 0 | 8.69 | N |
| **4007b** | 679.0 | 725.3 | 0.300 | 0.883 | 260 | 0.005 | 0 | 16.3 | 0 | 0 | W |

Table 2

| | slope pre mV/ms | slope post mV/ms | % slope | spike pre mV | spike post mV | % spike |
|---|---|---|---|---|---|---|
| **4018a** | 1.691 | 1.806 | 106.776 | 0.306 | 0.504 | 164.453 |
| **4006b** | 5.907 | 6.482 | 109.740 | 2.454 | 2.476 | 100.909 |
| **4024a** | 3.044 | 3.451 | 113.366 | 1.888 | 2.105 | 111.476 |
| **4009b** | 0.865 | 0.921 | 106.403 | 0.526 | 0.448 | 85.228 |
| **4022a** | 3.933 | 3.682 | 93.630 | 1.055 | 1.440 | 136.548 |
| **4018b** | 4.103 | 3.672 | 89.492 | 4.869 | 1.311 | 26.929 |
| **4021c** | munged | 2.316 | munged | munged | 1.697 | munged |
| **4019b** | 2.975 | 2.788 | 93.702 | 1.919 | 1.749 | 91.145 |
| **4021a** | 4.049 | 4.678 | 115.543 | 0.667 | 1.013 | 151.829 |
| **4008a** | 3.649 | 3.478 | 95.312 | 1.244 | 2.441 | 196.239 |
| **4019a** | 2.077 | 2.159 | 103.922 | 1.919 | 1.752 | 91.304 |
| **4022b** | 5.114 | 5.621 | 109.921 | 3.872 | 5.013 | 129.480 |
| **4014b** | 0.904 | 0.916 | 101.313 | 1.999 | 1.682 | 84.130 |
| **4014a** | 3.113 | 2.827 | 90.824 | 3.330 | 3.012 | 90.447 |
| **4021b** | 4.401 | 4.189 | 95.187 | 1.211 | 2.498 | 206.387 |
| **4023a** | 2.220 | 1.902 | 85.688 | 1.220 | 1.218 | 99.833 |
| **4020a** | 3.328 | 4.020 | 120.808 | 2.024 | 2.394 | 118.241 |
| **4023b** | 3.089 | 3.118 | 100.936 | 1.204 | 1.119 | 92.939 |
| **4003a** | 0.606 | 0.748 | 123.387 | - | - | - |
| **4006a** | 5.608 | 5.154 | 91.902 | 1.298 | 0.607 | 46.755 |
| **4011b** | 5.363 | 5.344 | 99.653 | 4.255 | 3.158 | 74.208 |
| **4019c** | 5.649 | 5.684 | 100.613 | 2.951 | 2.307 | 78.180 |
| **4015a** | 2.788 | 2.772 | 99.426 | 1.283 | 1.290 | 100.601 |
| **4013a** | munged | munged | munged | munged | munged | munged |
| **4012c** | 1.334 | 1.082 | 81.152 | 1.409 | 1.067 | 75.743 |
| **4010a** | 1.025 | 1.039 | 101.377 | 0.446 | 0.762 | 170.804 |
| **4007b** | 1.910 | 0.587 | 30.704 | 1.373 | 0.474 | 34.489 |

Table 3.

| | %theta pre | % theta post | theta t-test P value | % gamma pre | % gamma post | gamma t-test P value | power pre $mV^2$ | power post $mV^2$ | power t-test P value |
|---|---|---|---|---|---|---|---|---|---|
| **4018a** | 41.936 | 60.047 | 0.000 | 3.929 | 2.516 | 0.000 | 570089.915 | 403457.226 | 0.366 |
| **4006b** | 36.807 | 41.991 | 0.018 | 19.400 | 14.036 | 0.000 | 58541.237 | 21109.582 | 0.000 |
| **4024a** | 48.306 | 57.729 | 0.001 | 4.634 | 2.513 | 0.000 | 414717.710 | 185984.715 | 0.000 |
| **4009b** | 43.453 | 52.139 | 0.020 | 1.948 | 1.600 | 0.174 | 0.020 | 4983358.462 | 0.000 |
| **4022a** | 47.106 | 60.602 | 0.000 | 6.910 | 5.324 | 0.001 | 463855.737 | 436630.014 | 0.530 |
| **4018b** | 38.796 | 56.117 | 0.000 | 1.957 | 2.892 | 0.000 | 899414.707 | 505692.421 | 0.000 |
| **4021c** | 44.966 | 55.963 | 0.000 | 4.927 | 1.540 | 0.000 | 162796.051 | 112421.846 | 0.105 |
| **4019b** | 53.612 | 51.893 | 0.692 | 4.881 | 2.500 | 0.000 | 818726.541 | 661585.653 | 0.513 |
| **4021a** | 52.155 | 64.075 | 0.000 | 6.012 | 3.016 | 0.000 | 503248.639 | 357427.836 | 0.000 |
| **4008a** | 16.747 | 22.148 | 0.082 | 13.993 | 21.695 | 0.002 | 6259161.621 | 3714535.686 | 0.000 |
| **4019a** | 59.565 | 46.805 | 0.000 | 3.323 | 3.448 | 0.682 | 687980.571 | 855163.247 | 0.514 |
| **4022b** | 42.681 | 59.514 | 0.000 | 5.081 | 2.339 | 0.000 | 1024563.388 | 422857.728 | 0.000 |
| **4014b** | 1.746 | 0.948 | 0.000 | 0.074 | 0.025 | 0.000 | 1425721.870 | 1397016.308 | 0.263 |
| **4014a** | 6.304 | 1.642 | 0.000 | 0.217 | 0.035 | 0.000 | 1596987.776 | 1465089.244 | 0.041 |
| **4021b** | 33.104 | 59.559 | 0.000 | 9.369 | 1.492 | 0.000 | 301186.744 | 199656.146 | 0.000 |
| **4023a** | 56.395 | 61.015 | 0.051 | 4.188 | 3.612 | 0.063 | 502197.087 | 437434.401 | 0.021 |
| **4020a** | 49.925 | 66.010 | 0.000 | 6.045 | 2.993 | 0.000 | 574808.919 | 373636.702 | 0.002 |
| **4023b** | 55.001 | 65.984 | 0.000 | 6.716 | 2.486 | 0.000 | 480772.301 | 271072.621 | 0.000 |
| **4003a** | 37.955 | 39.554 | 0.596 | 1.864 | 2.149 | 0.227 | 1246061.971 | 981247.231 | 0.199 |
| **4006a** | 49.319 | 45.756 | 0.133 | 15.271 | 14.954 | 0.767 | 171692.429 | 127884.407 | 0.049 |
| **4011b** | 10.945 | 7.645 | 0.007 | 2.214 | 1.409 | 0.000 | 1805002.107 | 1636038.311 | 0.225 |
| **4019c** | 51.461 | 52.619 | 0.665 | 6.983 | 3.516 | 0.000 | 801101.888 | 645710.577 | 0.456 |
| **4015a** | 4.663 | 3.996 | 0.117 | 1.235 | 1.209 | 0.718 | 1823891.346 | 1849795.223 | 0.473 |
| **4013a** | 0.196 | 0.141 | 0.010 | 0.104 | 0.072 | 0.506 | 1288393.519 | 1282480.000 | 0.381 |
| **4012c** | 8.336 | 3.494 | 0.000 | 3.759 | 1.146 | 0.000 | 1799070.392 | 1527226.438 | 0.031 |
| **4010a** | 4.783 | 1.976 | 0.002 | 0.192 | 0.094 | 0.355 | 1669166.427 | 1573907.213 | 0.344 |
| **4007b** | 6.162 | 8.818 | 0.102 | 2.785 | 2.924 | 0.648 | 1719800.143 | 1837842.011 | 0.554 |

References

Abel, T., Martin, K. C., Bartsch, D., and Kandel, E. R. (1998). Memory suppressor genes: inhibitory constraints on the storage of long-term memory. Science 279, 338-341.

Acsády, L., Kamondi, A., Sik, A., Freund, T., and Buzsaki, G. (1998). GABAergic cells are the major postsynaptic targets of mossy fibres in the rat hippocampus. The Journal of Neuroscience 18, 3386-3403.

Ader, J. P., Room, P., Postema, F., and Korf, J. (1980). Bilaterally diverging axon collaterals and contralateral projections from rat locus coeruleus neurons, demonstrated by fluorescent retrograde double labeling and norepinephrine metabolism. Journal of Neural Transmission 49, 207-208.

Al-Zahrani, S. S., Al-Ruwaitea, A. S., Ho, M. Y., Bradshaw, C. M., and Szabadi, E. (1998). Effect of destruction of noradrenergic neurones with DSP4 on performance on a free-operant timing schedule. Psychopharmacology (Berlin) 136, 235-242.

Alexander, R. W., Davis, J. N., and Lefkowitz, R. J. (1975). Direct identification and characterisation of beta-adrenergic receptors in rat brain. Nature 258, 437-440.

Amaral, D. G., and Sinnamon, H. M. (1977). The locus coeruleus: neurobiology of a central noradrenergic nucleus. Progress in Neurobiology 9, 147-196.

Amaral, D. G. (1978). A Golgi study of cell types in the hilar region of the hippocampus in the rat. Journal of Comparative Neurology 182, 851-914.

Amaral, D. G., Ishizuka, N., and Claiborne, B. (1990). Neurons, numbers and the hippocampal network. Progress in Brain Research 83, 1-11.

Andersen, P., Bliss, T. V., and Skrede, K. K. (1971). Unit analysis of hippocampal polulation spikes. Experimental Brain Research 13, 208-221.

Anderson, A. E., Adams, J. P., Qian, Y., Cook, R. G., Pfaffinger, P. J., and Sweatt, J. D. (2000). Kv4.2 phosphorylation by cyclic AMP-dependent protein kinase. Journal of Biological Chemistry 275, 5337-5346.

Agnati, L.F., Bjelke, B., and Fuxe, K. (1992). Volume transmission in the brain: Do brain cells communicate solely through synapses? A new theory proposes that information also flows in the extracellular space. American Scientist 80, 362-373.

Amaral D. G., and Witter M. P. (1989). The three-dimensional organization of the hippocampal formation: a review of anatomical data. Neuroscience 31,571-591

Amaral, D.G. and Witter, M.P. (1995). "Hippocampal Formation" in *The Rat Nervous System*, George Paxinos *ed.* Academic Press, San Diego, CA.

Aoki C., Go C. G., Venkatesan C., and Kurose H. (1994). Perikaryal and synaptic localization of alpha 2A-adrenergic receptor-like immunoreactivity. Brain Research 650, 181-204.

Aston-Jones, G., and Bloom, F. E. (1981a). Activity of norepinephrine-containing locus coeruleus neurons in behaving rats anticipates fluctuations in the sleep-waking cycle. The Journal of Neuroscience 1, 876-886.

Aston-Jones, G., and Bloom, F. E. (1981b). Nonrepinephrine-containing locus coeruleus neurons in behaving rats exhibit pronounced responses to non-noxious environmental stimuli. The Journal of Neuroscience 1, 887-900.

Aston-Jones, G., Ennis, M., Pieribone, V. A., Nickell, W. T., and Shipley, M. T. (1986). The brain nucleus locus coeruleus: restricted afferent control of a broad efferent network. Science 234, 734-737.

Aston-Jones, G., Rajkowski, J., Kubiak, P., and Alexinsky, T. (1994). Locus coeruleus neurons in monkey are selectively activated by attended cues in a vigilance task. The Journal of Neuroscience 14, 4467-4480.

Aston-Jones, G., Shipley, M.T., and Grzanna, R. (1995). "The Locus Coeruleus, A5 and A7 Noradrenergic Cell Groups" in *The Rat Nervous System*, George Paxinos *ed.* Academic Press, San Diego, CA.

Aston-Jones, G., Rajkowski, J., and Kubiak, P. (1997). Conditioned responses of monkey locus coeruleus neurons anticipate acquisition of discriminative behavior in a vigilance task. Neuroscience 80, 697-715.

Aston-Jones, G., Rajkowski, J., Ivanova, S., Usher, M., and Cohen, J. (1998). Neuromodulation and cognitive performance: recent studies of noradrenergic locus ceruleus neurons in behaving monkeys. Advances in Pharmacology 42, 755-759.

Aston-Jones, G., Chen, S., Zhu, Y., and Oshinsky, M. L. (2001). A neural circuit for circadian regulation of arousal. Nature Neuroscience 4, 732-738.

Babstock, D. M., and Harley, C. W. (1992). Paragigantocellularis stimulation induces beta-adrenergic hippocampal potentiation. Brain Research Bulletin 28, 709-714.

Bailey, C. H., Giustetto, M., Huang, Y. Y., Hawkins, R. D., and Kandel, E. R. (2000). Is heterosynaptic modulation essential for stabilizing Hebbian plasticity and memory? Nature Reviews Neuroscience 1, 11-20.

Bergles, D. E., Doze, V. A., Madison, D. V., and Smith, S. J. (1996). Excitatory actions of norepinephrine on multiple classes of hippocampal CA1 interneurons. The Journal of Neuroscience 16, 572-585.

Berridge, C. W., and Foote, S. L. (1991). Effects of locus coeruleus activation on electroencephalographic activity in neocortex and hippocampus. The Journal of Neuroscience 11, 3135-3145.

Berridge, C. W., and Foote, S. L. (1996). Enhancement of behavioral and electroencephalographic indicies of waking following stimulation of noradrenergic beta-receptors within the medial sepatl region of the basal forebrain. The Journal of Neuroscience 16, 6999-7009.

Bi G., and Poo M. (2001). Synaptic modification by correlated activity: Hebb's postulate revisited. Annual Review of Neuroscience 24, 139-166.

Bijak, M., and Misgeld, U. (1995). Adrenergic modulation of hilar neuron activity and granule cell inhibition in the guinea-pig hippocampal slice. Neuroscience 67, 541-550.

Bjorklund, A., and Lindvall, O. (1979). Regeneration of normal terminal innervation patterns by central noradrenergic neurons after 5,7-dihydroxytryptamine-induced axotomy in the adult rat. Brain Research 171, 271-293.

Bjorklund, M., Sirvio, J., Riekkinen, M., Sallinen, J., Scheinin, M., and Riekkinen, P., Jr. (2000). Overexpression of alpha2C-adrenoceptors impairs water maze navigation. Neuroscience 95, 481-487.

Blackstad, T. W., Fuxe, K., and Hokfelt, T. (1967). Noradrenaline nerve terminals in the hippocampal region of the rat and the guinea pig. Zeitschrift Zellforschung Mikroskopiche und Anatomie 78, 463-473.

Blasco-Ibanez, J. M., Martinez-Guijarro, F. J., and Freund, T. F. (2000). Recurrent mossy fibres preferentially innervate parvalbumin-immunoreactive interneurons in the granule cell layer of the rat dentate gyrus. Neuroreport 11, 3219-3225.

Bliss, T. V., and Lomo, T. (1973). Long-lasting potentiation of synaptic transmission in the dentate area of the anaesthetized rabbit following stimulation of the perforant path. Journal of Physiology 232, 331-356.

Bliss, T. V., Goddard, G. V., and Riives, M. (1983). Reduction of long-term potentiation in the dentate gyrus of the rat following selective depletion of monoamines. Journal of Physiology 334, 475-491.

Bragin A., Jando G., Nadasdy Z., Hetke J., Wise K., and Buzsaki G. (1995). Gamma (40-100 Hz) oscillation in the hippocampus of the behaving rat. Journal of Neuroscience 15, 47-60.

Bramham, C. R., Bacher-Svendsen, K., and Sarvey, J. M. (1997). LTP in the lateral perforant path is beta-adrenergic receptor-dependent. Neuroreport 8, 719-724.

Bronzino, J. D., Kehoe, P., Mallinson, K., and Fortin, D. A. (2001). Increased extracellular release of hippocampal NE is associated with tetanization of the medial perforant pathway in the freely moving adult male rat. Hippocampus 11, 423-429.

Buckmaster P. S., and Schwartzkroin P. A. (1995). Interneurons and inhibition in the dentate gyrus of the rat in vivo. The Journal of Neuroscience 15, 774-89.

Buckmaster P. S., and Yamawaki R., and Zhang G. F. (2002). Axon arbors and synaptic connections of a vulnerable population of interneurons in the dentate gyrus in vivo. Journal of Comparative Neurology 445,360-373.

Burgard, E. C., Decker, G., and Sarvey, J. M. (1989). NMDA receptor antagonists block norepinephrine-induced long-lasting potentiation and long-term potentiation in rat dentate gyrus. Brain Research 482, 351-355.

Burwell, R. D. (2000) The parahippocampal region: corticocortical connectivity. Annals of the New York Academy of Sciences 911, 25-42.

Buzsaki G., Leung L. W., and Vanderwolf C. H. (1983). Cellular bases of hippocampal EEG in the behaving rat. Brain Research 287, 139-171.

Buzsaki, G. (1984). Feed-forward inhibition in the hippocampal formation. Progress in Neurobiology 22, 131-153.

Buzsaki G., and Chrobak J. J. (1995). Temporal structure in spatially organized neuronal ensembles: a role for interneuronal networks. Current Opinion in Neurobiology 5, 504-510.

Bylund D. B. (1995). Pharmacological characteristics of alpha-2 adrenergic receptor subtypes. Annals of the New York Academy of Sciences 763, 1-7.

Caffe, A. R., van Leeuwen, F. W., Buijs, R. M., de Vries, G. J., and Geffard, M. (1985). Coexistence of vasopressin, neurophysin and noradrenaline immunoreactivity in medium-sized cells of the locus coeruleus and subcoeruleus in the rat. Brain Research 338, 160-164.

Caffe, A. R., van Leeuwen, F. W., Buijs, R. M., and van der Gugten, J. (1988). Vasopressin and noradrenaline coexistence in the rat locus ceruleus: differential decreases of their levels in distant brain areas after thermal and neurotoxic lesions. Brain Research 459, 386-390.

Cahill, L., Prins, B., Weber, M., and McGaugh, J. L.(1994). Beta-adrenergic activation and memory for emotional events. Nature 371, 702-704.

Canning, K. J., Wu, K., Peloquin, P., Kloosterman, F., and Leung, L. S. (2000). Physiology of the entorhinal and perirhinal projections to the hippocampus studied by current source density analysis. Annals of the New York Academy of Science 911, 55-72.

Carlson, S., Tanila, H., Rama, P., Mecke, E., and Pertovaara, A. (1992). Effects of medetomidine, an alpha-2 adrenoceptor agonist, and atipamezole, an alpha-2 antagonist, on spatial memory performance in adult and aged rats. Behav Neural Biol 58, 113-119.

Chaulk, P. C., and Harley, C. W. (1998). Intracerebroventricular norepinephrine potentiation of the perforant path-evoked potential in dentate gyrus of anesthetized and awake rats: A role for both alpha- and beta-adrenoceptor activation. Brain Research 787, 59-70.

Chrobak, J. J., DeHaven, D. L., and Walsh, T. J. (1985). Depletion of brain norepinephrine with DSP-4 does not alter acquisition or performance of a radial-arm maze task. Behav Neural Biol 44, 144-150.

Cirelli, C., Pompeiano, M., and Tononi, G. (1996). Neuronal gene expression in the waking state: a role for the locus coeruleus. Science 274, 1211-1215.

Clarke, C. G. (1995). Activation of locus coeruleus and concurrent observation of perforant path evoked potential, single unit activity and EEG in the dentate gyrus of the rat . Unpublished Master's thesis, Memorial University of Newfoundland.

Clayton, E. C., and Williams, C. L. (2000). Glutamatergic influences on the nucleus paragigantocellularis: contribution to performance in avoidance and spatial memory tasks. Behavioral Neuroscience 114, 707-712.
Cooper, J. R., Bloom, F. E., and Roth R. H. (1996). *The Biochemical Basis of Neuropharmacology* 6th ed. Oxford University Press, Oxford, UK.

Crutcher, K. A., and Davis, J. N. (1980). Noradrenergic sprouting in response to cholinergic denervation: the sympathohabenular connection. Experimental Neurology 70, 187-191.

Csicsvari, J., Hirase, H., Czurko, A., Mamiya, A., and Buzsaki, G. (1999a). Fast network oscillations in the hippocampal CA1 region of the behaving rat. The Journal of Neuroscience 19, RC20.

Csicsvari, J., Hirase, H., Czurko, A., Mamiya, A., and Buzsaki, G. (1999b). Oscillatory coupling of hippocampal pyramidal cells and interneurons in the behaving rat. The Journal of Neuroscience 19, 274-287.

Curet, O., and de Montigny, C. (1988a). Electrophysiological characterization of adrenoceptors in the rat dorsal hippocampus. I. Receptors mediating the effect of microiontophoretically applied norepinephrine. Brain Research 475, 35-46.

Curet, O., and de Montigny, C. (1988b). Electrophysiological characterization of adrenoceptors in the rat dorsal hippocampus. II. Receptors mediating the effect of synaptically released norepinephrine. Brain Research 475, 47-57.

Curet, O., and de Montigny, C. (1989). Electrophysiological characterization of adrenoceptors in the rat dorsal hippocampus. III. Evidence for the physiological role of terminal alpha 2-adrenergic autoreceptors. Brain Research 499, 18-26.

Dahl, D., and Sarvey, J. M. (1989). Norepinephrine induces pathway-specific long-lasting potentiation and depression in the hippocampal dentate gyrus. Proceedings of the National Academy of Science, USA 86, 4776-4780.

Dahl, D., and Sarvey, J. M. (1990). Beta-adrenergic agonist-induced long-lasting synaptic modifications in hippocampal dentate gyrus require activation of NMDA receptors, but not electrical activation of afferents. Brain Research 526, 347-350.

Dahlstrom A., and Fuxe K. (1964). Localization of monoamines in the lower brain stem. Experientia 20, 398-399.

Dalley, J. W., McGaughy, J., O'Connell, M. T., Cardinal, R. N., Levita, L., and Robbins, T. W. (2001). Distinct changes in cortical acetylcholine and noradrenaline efflux during contingent and noncontingent performance of a visual attentional task. The Journal of Neuroscience 21, 4908-4914.

Davare, M. A., Horne, M. C., and Hell, J. W. (2000). Protein phosphatase 2A is associated with class C L-type calcium channels (Cav1.2) and antagonizes channel phosphorylation by cAMP-dependent protein kinase. Journal of Biological Chemistry 275, 39710-39717.

Deadwyler, S. A., Dudek, F. E., Cotman, C. W., and Lynch, G. (1975). Intracellular responses of rat dentate granule cells in vitro: posttetanic potentiation to perforant path stimulation. Brain Research 88, 80-85.

Deisseroth, K., Bito, H., and Tsien, R.W. (1996). Signaling from synapse to nucleus: postsynaptic CREB phosphorylation during multiple forms of hippocampal synaptic plasticity. Neuron. 16, 89-101.

Deller, T., Martinez, A., Nitsch, R., and Frotscher, M. (1996). A novel entorhinal projection to the rat dentate gyrus: direct innervation of proximal dendrites and cell bodies of granule cells and GABAergic neurons. The Journal of Neuroscience 16, 3322-3333.

Devauges, V., and Sara, S. J. (1991). Memory retrieval enhancement by locus coeruleus stimulation: evidence for mediation by beta-receptors. Behavioural Brain Research 43, 93-97.

Dietrichs, E. (1985). Divergent axon collaterals to cerebellum and amygdala from neurons in the parabrachial nucleus, the nucleus locus coeruleus and some adjacent nuclei. A fluorescent double labelling study using rhodamine labelled latex microspheres and fast blue as retrograde tracers. Anatomy and Embryology (Berlin) 172, 375-382.

Doze, V. A., Cohen, G. A., and Madison, D. V. (1991). Synaptic localization of adrenergic disinhibition in the rat hippocampus. Neuron 6, 889-900.

Dunwiddie, T. V., Taylor, M., Heginbotham, L. R., and Proctor, W. R. (1992). Long-term increases in excitability in the CA1 region of rat hippocampus induced by beta-adrenergic stimulation: possible mediation by cAMP. The Journal of Neuroscience 12, 506-517.

Ennis, M., and Aston-Jones, G. (1987). Two physiologically distinct populations of neurons in the ventrolateral medulla innervate the locus coeruleus. Brain Research 425, 275-282.

Ennis, M., Behbehani, M., Shipley, M. T., Van Bockstaele, E. J., and Aston-Jones, G. (1991). Projections from the periaqueductal gray to the rostromedial pericoerulear region and nucleus locus coeruleus: anatomic and physiologic studies. Journal of Comparative Neurology 306, 480-494.

Everitt, B. J., Hokfelt, T., Terenius, L., Tatemoto, K., Mutt, V., and Goldstein, M. (1984). Differential co-existence of neuropeptide Y (NPY)-like immunoreactivity with catecholamines in the central nervous system of the rat. Neuroscience 11, 443-462.

Fillenz M. (1990). *Noradrenergic Neurons*. Cambridge University Press, Cambridge, UK.

Finley, J. C., Maderdrut, J. L., and Petrusz, P. (1981). The immunocytochemical localization of enkephalin in the central nervous system of the rat. Journal of Comparative Neurology 198, 541-565.

Fisahn A., Pike F. G., Buhl E. H., and Paulsen O. (1998).
Cholinergic induction of network oscillations at 40 Hz in the hippocampus in vitro. Nature 394, 186-189.

Florin-Lechner, S. M., Druhan, J. P., Aston-Jones, G., and Valentino, R. J. (1996). Enhanced norepinephrine release in prefrontal cortex with burst stimulation of the locus coeruleus. Brain Research 742, 89-97.

Foote, S. L., Aston-Jones, G., and Bloom, F. E. (1980a). Impulse activity of locus coeruleus neurons in awake rats and monkeys is a function of sensory stimulation and arousal. Proceedings of the National Academy of Science, USA 77, 3033-3037.

Foote, S. L., Loughlin, S. E., Cohen, P. S., Bloom, F. E., and Livingston, R. B. (1980b). Accurate three-dimensional reconstruction of neuronal distributions in brain:

reconstruction of the rat nucleus locus coeruleus. The Journal of Neuroscience Methods 3, 159-173.

Foote, S. L., Bloom, F. E., and Aston-Jones, G. (1983). Nucleus locus ceruleus: new evidence of anatomical and physiological specificity. Physiological Reviews 63, 844-914.

Forloni, G., Grzanna, R., Blakely, R. D., and Coyle, J. T. (1987). Co-localization of N-acetyl-aspartyl-glutamate in central cholinergic, noradrenergic, and serotonergic neurons. Synapse 1, 455-460.

Fox, S. E., Wolfson, S., and Ranck Jr., J. B. (1986). Hippocampal theta rhythm and the firing of neurons in walking and urethane anesthetized rats. Experimental Brain Research 62, 495-508.

Freund T. F., and Buzsaki G. (1996). Interneurons of the hippocampus. Hippocampus 6, 347-470.

Frey, U., and Morris, R. G. (1997). Synaptic tagging and long-term potentiation. Nature 385, 533-536.

Fung, S. J., Reddy, V. K., Liu, R. H., Wang, Z., and Barnes, C. D. (1994). Existence of glutamate in noradrenergic locus coeruleus neurons of rodents. Brain Researchearch Bulletin 35, 505-512.

Galitzky J., Langin D., Verwaerde P., Montastruc J. L., Lafontan M., and Berlan M. (1997). Lipolytic effects of conventional beta 3-adrenoceptor agonists and of CGP 12,177 in rat and human fat cells: preliminary pharmacological evidence for a putative beta 4-adrenoceptor. British Journal of Pharmacology 122, 1244-1250.

Gray, R., and Johnston, D. (1987). Noradrenaline and beta-adrenoceptor agonists increase activity of voltage-dependent calcium channels in hippocampal neurons. Nature 327, 620-622.

Grzanna R., and Molliver M. E. (1980). The locus coeruleus in the rat: an immunohistochemical delineation. Neuroscience 5, 21-40.

Haas, H. L., and Rose, G. M. (1987). Noradrenaline blocks potassium conductance in rat dentate granule cells in vitro. Neuroscience Letters 78, 171-174.

Haller, J., Makara, G. B., Pinter, I., Gyertyan, I., and Egyed, A. (1997). The mechanism of action of alpha 2 adrenoceptor blockers as revealed by effects on open field locomotion and escape reactions in the shuttle-box. Psychopharmacology (Berlin) 134, 107-114.

Han Z. S., Buhl E. H., Lorinczi Z., and Somogyi P. (1993). A high degree of spatial selectivity in the axonal and dendritic domains of physiologically identified local-circuit

neurons in the dentate gyrus of the rat hippocampus. The European Journal of Neuroscience 5, 395-410.

Han Z. S. (1994). Electrophysiological and morphological differentiation of chandelier and basket cells in the rat hippocampal formation: a study combining intracellular recording and intracellular staining with biocytin. Neuroscience Research 19,101-110.

Haring, J. H., and Davis, J. N. (1983). Topography of locus ceruleus neurons projecting to the area dentata. Experimental Neurology 79, 785-800.

Harley, C.W., Lacaille, J.C., and Galway, M. (1983). Hypothalamic afferents to the dorsal dentate gyrus contain acetylcholinesterase. Brain Research 270, 335-339.

Harley, C. W., and Milway, J. S. (1986). Glutamate ejection in the locus coeruleus enhances the perforant path-evoked population spike in the dentate gyrus. Experimental Brain Research 63, 143-150.

Harley, C. W. (1987). A role for norepinephrine in arousal, emotion and learning?: limbic modulation by norepinephrine and the Kety hypothesis. Progress in Neuropsychopharmacology and Biological Psychiatry 11, 419-458.

Harley, C. W., and Evans, S. (1988). "Locus coeruleus-induced enhancement of the perforant path-evoked potential: Effects of intradentate beta blockers" in *Cellular Mechanisms of Conditioning and Behavioral Plasticity.* Woody,C.D,; Alkon,D.L and McGaugh,J.L. eds. Plenum Publishing, New York.

Harley C., Milway J. S., and Lacaille J. C. (1989). Locus coeruleus potentiation of dentate gyrus responses: evidence for two systems.
Brain Research Bulletin 22, 43-50.

Harley, C. W., and Sara, S. J. (1992). Locus coeruleus bursts induced by glutamate trigger delayed perforant path spike amplitude potentiation in the dentate gyrus. Experimental Brain Research 89, 581-587.

Harley, C. W., Lalies, M. D., and Nutt, D. J. (1996). Estimating the synaptic concentration of norepinephrine in dentate gyrus which produces beta-receptor mediated long-lasting potentiation in vivo using microdialysis and intracerebroventricular norepinephrine. Brain Research 710, 293-298.

Harley, C. W. (1998). Noradrenergic long-term potentiation in the dentate gyrus. Advances in Pharmacology 42, 952-956.

Harris, K. D., Henze, D. A., Csicsvari, J., Hirase, H., and Buzsaki, G. (2000). Accuracy of tetrode spike separation as determined by simultaneous intracellular and extracellular measurements. Journal of Neurophysiology 84, 401-414.

Heginbotham, L. R., and Dunwiddie, T. V. (1991). Long-term increases in the evoked population spike in the CA1 region of rat hippocampus induced by beta-adrenergic receptor activation. The Journal of Neuroscience 11, 2519-2527.

Henze, D. A., Urban, N. N., and Barrionuevo, G. (2000). The multifarious hippocampal mossy fiber pathway: a review. Neuroscience 98, 407-427.

Henze D.A., Wittner L. and Buzsaki G. (2002). Single granule cells reliably discharge targets in the hippocampal CA3 region in vivo. Nature Neuroscience 5, 790-795.

Hirata H., and Aston-Jones G. (1994). A novel long-latency response of locus coeruleus neurons to noxious stimuli: mediation by peripheral C-fibers. Journal of Neurophysiology 71, 1752-61.

Hoffman, D. A., and Johnston, D. (1998). Downregulation of transient K+ channels in dendrites of hippocampal CA1 pyramidal neurons by activation of PKA and PKC. The Journal of Neuroscience 18, 3521-3528.

Izquierdo I., Medina, J.H., Izquierdo, L.A., Barros, D.M., de Souza, M.M., Mello e Souza, T. (1998). Short- and long-term memory are differentially regulated by monoaminergic systems in the rat brain. Neurobiology Learning Memory 69,:219-224.

Jakala, P., Riekkinen, M., Sirvio, J., Koivisto, E., Kejonen, K., Vanhanen, M., and Riekkinen, P., Jr. (1999). Guanfacine, but not clonidine, improves planning and working memory performance in humans. Neuropsychopharmacology 20, 460-470.

Jodo, E., and Aston-Jones, G. (1997). Activation of locus coeruleus by prefrontal cortex is mediated by excitatory amino acid inputs. Brain Research 768, 327-332.

Jodo, E., Chiang, C., and Aston-Jones, G. (1998). Potent excitatory influence of prefrontal cortex activity on noradrenergic locus coeruleus neurons. Neuroscience 83, 63-79.

Jung , M. W. and McNaughton, B. L. (1993). Spatial selectivity of unit activity in the hippocampal granular layer. Hippocampus 3, 165-182.

Kanda, M., Maru, E., Ashida, H., Tatsuno, J., and Takatani, O. (1989). Effects of LTP-inducing tetanic stimulations of the perforant path on the commissural inhibition and facilitation of dentate granule cell discharge. Brain Research 484, 325-332.

Kandel, E.R. (2001). The molecular biology of memory storage: a dialogue between genes and synapses. Science 294, 1030-1038.

Kasamatsu T., and Heggelund P. (1982). Single cell responses in cat visual cortex to visual stimulation during iontophoresis of noradrenaline. Experimental Brain Research 45, 317-27.

Katsuki, H., Izumi, Y. , and Zurumski, C. F. (1997). Noradrenergic regulation of synaptic plasticity in the hippocampal CA1 region. Journal of Neurophysiology 77, 3013-3020.

Kim J. J., and Fanselow M. S. (1992). Modality-specific retrograde amnesia of fear. Science 256, 675-7.

Kimura, A., and Pavlides, C. (2000). Long-term potentiation/depotentiation are accompanied by complex changes in spontaneous unit activity in the hippocampus. Journal of Neurophysiology 84, 1894-1906.

Kitchigina, V., Vankov, A., Harley, C., and Sara, S. J. (1997). Novelty-elicited, noradrenaline-dependent enhancement of excitability in the dentate gyrus. The European Journal of Neuroscience 9, 41-47.

Klukowski, G., and Harley, C. W. (1994). Locus coeruleus activation induces perforant path-evoked population spike potentiation in the dentate gyrus of awake rat. Experimental Brain Research 102, 165-170.

Knight, J. C. (2001). Pharmacological evaluation of idazoxan-induced noradrenergic modulation of excitatory and inhibitory processes in the dentate gyrus of the anaesthetized rat. Unpublished Master's thesis, Memorial University of Newfoundland.

Kobayashi, K., Noda, Y., Matsushita, N., Nishii, K., Sawada, H., Nagatsu, T., Nakahara, D., Fukabori, R., Yasoshima, Y., Yamamoto, T., Miura, M., Kano, M., Mamiya, T., Miyamoto, Y., Nabeshima, T. (2000). Modest neuropsychological deficits caused by reduced noradrenaline metabolism in mice heterozygous for a mutated tyrosine hydroxylase gene. .The Journal of Neuroscience 20, 2418-2426.

Koda, L. Y., and Bloom, F. E. (1977). A light and electron microscopic study of noradrenergic terminals in the rat dentate gyrus. Brain Research 120, 327-335.

Koda, L. Y., Wise, R. A., and Bloom, F. E. (1978). Light and electron microscopic changes in the rat dentate gyrus after lesions or stimulation of the ascending locus coeruleus pathway. Brain Research 144, 363-368.

Lacaille, J. C., and Harley, C. W. (1985). The action of norepinephrine in the dentate gyrus: beta-mediated facilitation of evoked potentials in vitro. Brain Research 358, 210-220.

Lacaille, J. C., and Schwartzkroin, P. A. (1988). Intracellular responses of rat hippocampal granule cells in vitro to discrete applications of norepinephrine. Neuroscience Letters 89, 176-181.

Lapiz, M. D., Mateo, Y., Durkin, S., Parker, T., Marsden, C. A. (2001). Effects of central noradrenaline depletion by the selective neurotoxin DSP-4 on the behaviour of the isolated rat in the elevated plus maze and water maze. Psychopharmacology 155, 251-9.

Leonard, A. S., and Hell, J. W. (1997). Cyclic AMP-dependent protein kinase and protein kinase C phosphorylate N-methyl-D-aspartate receptors at different sites. Journal of Biological Chemistry 272, 12107-12115.

Leung, P. P., and Miller, J. J. (1988). Dual role of norepinephrine in the hippocampal CA1 region of the rat: inhibition and disinhibition. Canadian Journal of Physiology and Pharmacology 66, 814-819.

Li, F., Gangal, M., Jones, J. M., Deich, J., Lovett, K. E., Taylor, S. S., and Johnson, D. A. (2000). Consequences of cAMP and catalytic-subunit binding on the flexibility of the A-kinase regulatory subunit. Biochemistry 39, 15626-15632.

Lin, Y. W., Min, M. Y., Chiu, T. H., and Yang, H. W. (2003). Enhancement of associative long-term potentiation by activation of beta-adrenergic receptors at CA1 synapses in rat hippocampal slices. The Journal of Neuroscience 23, 4173-4181.

Lingenhohl, K., and Finch, D. M. (1991). Morphological characterization of rat entorhinal neurons in vivo: soma-dendritic structure and axonal domains. Experimental Brain Research 84, 57-74.

Linster C., and Hasselmo M. E. (2001). Neuromodulation and the functional dynamics of piriform cortex. Chemical Senses 26, 585-94.

Lorente de No R.(1934). Studies on the structure of the cerebral cortex. II. Continuation of the study of ammonic system. Journal für Psychologie und Neurologie 46, 113-177.

Loughlin, S. E., Foote, S. L., and Grzanna, R. (1986). Efferent projections of nucleus locus coeruleus: morphologic subpopulations have different efferent targets. Neuroscience 18, 307-319.

Loy, R., Koziell, D. A., Lindsey, J. D., and Moore, R. Y. (1980). Noradrenergic innervation of the adult rat hippocampal formation. Journal of Comparative Neurology 189, 699-710.

Luine, V., Bowling, D., and Hearns, M. (1990). Spatial memory deficits in aged rats: contributions of monoaminergic systems. Brain Research 537, 271-278.

Luppi P.-H., Aston-Jones G., Akaoka H., Chouvet G. and Jouvet M. (1995). Afferent projections to the rat locus coeruleus demonstrated by retrograde and anterograde tracing with cholera-toxin B subunit and *phaseolus vulgaris* leucoagglutinin. Neuroscience 65, 119-160.

Madison, D. V., and Nicoll, R. A. (1982). Noradrenaline blocks accommodation of pyramidal cell discharge in the hippocampus. Nature 299, 636-638.

Madison, D. V., and Nicoll, R. A. (1986). Actions of noradrenaline recorded intracellularly in rat hippocampal CA1 pyramidal neurones, in vitro. Journal of Physiology 372, 221-244.

Maeda, T., and Shimizu, N. (1972). [Ascending projections from the locus coeruleus and other aminergic pontine neurons at the level of the rat prosencephalon]. Brain Research 36, 19-35.

Magistretti P. J. (1994). Vasoactive intestinal peptide and noradrenaline regulate energy metabolism in astrocytes: a physiological function in the control of local homeostasis within the CNS. Progress in Brain Research 100, 87-93.

Malenka R. C. (1991). The role of postsynaptic calcium in the induction of long-term potentiation. Molecular Neurobiology 5, 289-95.

Malenka R. C., and Siegalbaum S. A. (2001). "Synaptic Plasticity" in *Synapses,* Cowan, W. M.; Sudhof, T. C., and Stevens C. F. *eds.* The Johns Hopkins University Press, Baltimore, MD.

Martinez A., Lubke J., Del Rio J.A., Soriano E., and Frotscher M. Regional variability and postsynaptic targets of chandelier cells in the hippocampal formation of the rat. Journal of Comparative Neurology 376, 28-44.

Maru E., Ashida H., and Tatsuno J. (1989). Long-lasting reduction of dentate paired-pulse depression following LTP-inducing tetanic stimulations of perforant path. Brain Research 478, 112-20.

Maru, E., Kanda, M., and Ashida, H. (2002). Functional and morphological changes in the hippocampal neuronal circuits associated with epileptic seizures. Epilepsia 43, 44-49.

McBain, C. J., and Fisahn, A. (2001). Interneurons unbound. Nature Reviews: Neuroscience 2, 11-23.

Mermelstein, P. G., Bito, H., Deisseroth, K., and Tsien, R. W. (2000). Critical dependence of cAMP response element-binding protein phosphorylation on L-type calcium channels supports a selective response to EPSPs in preference to action potentials. The Journal of Neuroscience 20, 266-273.

Miettinen, R., and Freund, T. F. (1992). Neuropeptide Y-containing interneurons in the hippocampus receive synaptic input from median raphe and GABAergic septal afferents. Neuropeptides 22, 185-193.

Miettinen, R., Gulyas, A. I., Baimbridge, K. G., Jacobowitz, D. M., and Freund, T. F. (1992). Calretinin is present in non-pyramidal cells of the rat hippocampus--II. Co-existence with other calcium binding proteins and GABA. Neuroscience 48, 29-43.

Milner T. A., and Bacon C. E. (1989). GABAergic neurons in the rat hippocampal formation: ultrastructure and synaptic relationships with catecholaminergic terminals. The Journal of Neuroscience 9, 3410-27.

Milner T.A., and Bacon C.E. (1989). Ultrastructural localization of tyrosine hydroxylase-like immunoreactivity in the rat hippocampal formation. Journal of Comparative Neurology 281, 479-95.

Milner, T. A., Lee, A., Aicher, S. A., and Rosin, D. L. (1998). Hippocampal alpha2a-adrenergic receptors are located predominantly presynaptically but are also found postsynaptically and in selective astrocytes. Journal of Comparative Neurology 395, 310-327.

Milner, T. A., Shah, P., and Pierce, J. P. (2000). Beta-adrenergic receptors primarily are located on the dendrites of granule cells and interneurons but also are found on astrocytes and a few presynaptic profiles in the rat dentate gyrus. Synapse 36, 178-193.

Mizumori, S. J., McNaughton B. L.,and Barnes C. A.(1989). A comparison of supramammillary and medial septal influences on hippocampal field potentials and single-unit activity. Journal of Neurophysiology 61, 15-31.

Moran, P. M., LeMaitre, M. H., Philouze, V., Reymann, J. M., Allain, H., and Leonard, B. E. (1992). Reversal of learning and memory impairments following lesion of the nucleus basalis magnocellularis (NBM) by concurrent noradrenergic depletion using DSP4 in the rat. Brain Research 595, 327-333.

Motro, B., van der Kooy, D., Rossant, J., Reith, A., and Bernstein, A. (1991). Contiguous patterns of c-kit and steel expression: analysis of mutations at the W and Sl loci. Development 113, 1207-1221.

Mott, D. D., Turner, D. A., Okazaki, M. M., and Lewis, D. V. (1997). Interneurons of the dentate-hilus border of the rat dentate gyrus: morphological and electrophysiological heterogeneity. The Journal of Neuroscience 17, 3990-4005.

Naber, P. A., Witter, M. P., and Lopez da Silva, F. H. (1999). Perirhinal cortex input to the hippocampus in the rat: evidence for parallel pathways, both direct and indirect. A combined physiological and anatomical study. The European Journal of Neuroscience 11, 4119-4133.

Nagai, T., Satoh, K., Imamoto, K., and Maeda, T. (1981). Divergent projections of catecholamine neurons of the locus coeruleus as revealed by fluorescent retrograde double labeling technique. Neuroscience Letters 23, 117-123.

Nakamura, S., and Iwama, K. (1975). Antidromic activation of the rat locus coeruleus neurons from hippocampus, cerebral and cerebellar cortices. Brain Research 99, 372-376.

Neophytou, S. I., Aspley, S., Butler, S., Beckett, S., and Marsden, C. A. (2001). Effects of lesioning noradrenergic neurones in the locus coeruleus on conditioned and unconditioned aversive behaviour in the rat. Progress in Neuropsychopharmacology and Biological Psychiatry 25, 1307-1321.

Neuman, R. S., and Harley, C. W. (1983). Long-lasting potentiation of the dentate gyrus population spike by norepinephrine. Brain Research 273, 162-165.

Nielson, K. A.,and Jensen, R. A. (1994). Beta-adrenergic receptor antagonist antihypertensive medications impair arousal-induced modulation of working memory in elderly humans. Behavioral Neural Biology 62, 190-200.

Nowak, L., Bregestovski, P., Ascher, P., Herbet, A., and Prochiantz, A. (1984). Magnesium gates glutamate-activated channels in mouse central neurones. Nature 307, 462-465.

Olpe, H. R., Laszlo, J., Pozza, M. F., De Herdt, P., Waldmeier, P. C. and Jones R. S. (1986). Glutamate-induced activation of rat locus coeruleus increases CA1 pyramidal cell excitability. Neuroscience Letters 65, 11-16.

Oleskevich, S., Descarries, L., and Lacaille, J. C. (1989). Quantified distribution of the noradrenaline innervation in the hippocampus of adult rat. The Journal of Neuroscience 9, 3803-3815.

Olschowka, J. A., Molliver, M. E., Grzanna, R., Rice, F. L., and Coyle, J. T. (1981). Ultrastructural demonstration of noradrenergic synapses in the rat central nervous system by dopamine-beta-hydroxylase immunocytochemistry. J Histochemistry and Cytochemistry 29, 271-280.

Pang, K., and Rose, G. M. (1987). Differential effects of norepinephrine on hippocampal complex-spike and theta-neurons. Brain Research 425, 146-158.

Pang, K., and Rose, G. M. (1989). Differential effects of methionine5-enkephalin on hippocampal pyramidal cells and interneurons. Neuropharmacology 28, 1175-1181.

Papadopoulos, G. C., and Parnavelas, J. G. (1991). Monoamine systems in the cerebral cortex: evidence for anatomical specificity. Progress in Neurobiology 36, 195-200.

Parfitt, K. D., Hoffer, B. J., and Browning, M. D. (1991). Norepinephrine and isoproterenol increase the phosphorylation of synapsin I and synapsin II in dentate slices of young but not aged Fisher 344 rats. Proceedings of the National Academy of Science, USA 88, 2361-2365.

Parra, P., Gulyas, A. I., and Miles, R. (1998). How many subtypes of inhibitory cells in the hippocampus? Neuron 20, 983-993.

Pasquier D.A., and Reinoso-Suarez, F. (1976). Direct projections from hypothalamus to hippocampus in the rat demonstrated by retrograde transport of horseradish peroxidase. Brain Research 108,165-169.

Pasquier, D. A., and Reinoso-Suarez, F. (1978). The topographic organization of hypothalamic and brain stem projections to the hippocampus. Brain Research Bulletin 3, 373-389.

Patton, P. E., and McNaughton, B. (1995). Connection matrix of the hippocampal formation: I. The dentate gyrus. Hippocampus 5, 245-86.

Penttonen, M., Kamondi, A., Acsady, L., and Buzsaki, G. (1998). Gamma frequency oscillation in the hippocampus of the rat: intracellular analysis in vivo. European Journal of Neuroscience 10, 718-728.

Phillips R. G., and LeDoux J. E. (1992). Differential contribution of amygdala and hippocampus to cued and contextual fear conditioning. Behavioral Neuroscience 106, 274-285.

Pike, F. G., Meredith, R. M., Olding, A. W., and Paulsen, O. (1999). Rapid report: postsynaptic bursting is essential for 'Hebbian' induction of associative long-term potentiation at excitatory synapses in rat hippocampus. Journal of Physiology 518, 571-576.

Pinault D. (1996). A novel single-cell staining procedure performed in vivo under electrophysiological control: morpho-functional features of juxtacellularly labeled thalamic cells and other central neurons with biocytin or Neurobiotin. Journal of Neuroscience Methods 65, 113-36.

Pisa, M., Martin-Iverson, M. T., and Fibiger, H. C. (1988). On the role of the dorsal noradrenergic bundle in learning and habituation to novelty. Pharmacol Biochem Behav 30, 835-845.

Rainbow, T. C., Parsons, B., and Wolfe, B. B. (1984). Quantitative autoradiography of beta 1- and beta 2-adrenergic receptors in rat brain. Proceedings of the National Academy of Science, USA 81, 1585-1589.

Rajkowski, J., Kubiak, P., Ivanova, S., and Aston-Jones, G. (1998). State-related activity, reactivity of locus ceruleus neurons in behaving monkeys. Advances in Pharmacology 42, 740-744.

Reid, C. A., Fabian-Fine, R., and Fine, A. (2001). Postsynaptic calcium transients evoked by activation of individual hippocampal mossy fiber synapses. The Journal of Neuroscience 21, 2206-2214.

Richter-Levin, G., Segal, M., and Sara, S. (1991). An alpha 2 antagonist, idazoxan, enhances EPSP-spike coupling in the rat dentate gyrus. Brain Research 540, 291-294.

Robinson, G. B., and Racine, R. J. (1985). Long-term potentiation in the dentate gyrus: effects of noradrenaline depletion in the awake rat. Brain Research 325, 71-78.

Room, P., Postema, F., and Korf, J. (1981). Divergent axon collaterals of rat locus coeruleus neurons: demonstration by a fluorescent double labeling technique. Brain Research 221, 219-230.

Rose, G. M., and Pang, K. C. (1989). Differential effect of norepinephrine upon granule cells and interneurons in the dentate gyrus. Brain Research 488, 353-356.

Salm, A. K., and McCarthy, K. D. (1992). The evidence for astrocytes as a target for central noradrenergic activity: expression of adrenergic receptors. Brain Research Bulletin 29, 265-275.

Sara, S. J., and Devauges, V. (1989). Idazoxan, an alpha-2 antagonist, facilitates memory retrieval in the rat. Behavioral and Neural Biology 51, 401-411.

Sara, S. J., and Bergis, O. (1991). Enhancement of excitability and inhibitory processes in hippocampal dentate gyrus by noradrenaline: a pharmacological study in awake, freely moving rats. Neuroscience Letters 126, 1-5.

Sara, S. J., and Segal, M. (1991). Plasticity of sensory responses of locus coeruleus neurons in the behaving rat: implications for cognition. Progress in Brain Research 88, 571-585.

Sara, S. J., Dyon-Laurent, C., and Herve, A. (1995). Novelty seeking behavior in the rat is dependent upon the integrity of the noradrenergic system. Brain Research; Cognitive Brain Research 2, 181-187.

Scharfman, H. E., and Schwartzkroin, P. A. (1988). Further studies of the effects of somatostatin and related peptides in area CA1 of rabbit hippocampus. Cellular and Molecular Neurobiology 8, 411-429.

Scharfman, H. E., and Schwartzkroin, P. A. (1990). Consequences of prolonged afferent stimulation of the rat fascia dentata: epileptiform activity in area CA3 of hippocampus. Neuroscience 35, 505-517.

Scharfman, H. E., Kunkel, D. D., and Schwartzkroin, P. A. (1990). Synaptic connections of dentate granule cells and hilar neurons: results of paired intracellular recordings and intracellular horseradish peroxidase injections. Neuroscience 37, 693-707.

Scharfman, H.E. (1991). Dentate hilar cells with dendrites in the molecular layer have lower thresholds for synaptic activation by perforant path than granule cells. The Journal of Neuroscience 11, 1660-1673.

Scharfman, H. E. (1993). Spiny neurons of area CA3c in rat hippocampal slices have similar electrophysiological characteristics and synaptic responses despite morphological variation. Hippocampus 3, 9-28.

Scharfman, H. E. (1994). Evidence from simultaneous intracellular recordings in rat hippocampal slices that area CA3 pyramidal cells innervate dentate hilar mossy cells. Journal of Neurophysiology 72, 2167-2180.

Scharfman, H. E. (1995a). Electrophysiological evidence that dentate hilar mossy cells are excitatory and innervate both granule cells and interneurons. Journal of Neurophysiology 74, 179-194.

Scharfman, H. E. (1995b). Electrophysiological diversity of pyramidal-shaped neurons at the granule cell layer/hilus border of the rat dentate gyrus recorded in vitro. Hippocampus 5, 287-305.

Scharfman, H. E., Smith, K. L., Goodman, J. H., and Sollas, A. L. (2001). Survival of dentate hilar mossy cells after pilocarpine-induced seizures and their synchronized burst discharges with area CA3 pyramidal cells. Neuroscience 104, 741-759.

Segal, M., and Bloom, F.E. (1974a). The action of norepinephrine in the rat hippocampus. I. Iontophoretic studies. Brain Research 71, 79-97.

Segal, M., and Bloom, F.E. (1974b). The action of norepinephrine in the rat hippocampus. II. Activation of the input pathway. Brain Research, 99-114.

Segal, M., and Bloom, F.E.(1976a). The action of norepinephrine in the rat hippocampus. III. Hippocampal cellular responses to locus coeruleus stimulation in the awake rat. Brain Research 107, 499-511.

Segal, M., and Bloom, F.E. (1976b). The action of norepinephrine in the rat hippocampus. IV. The effects of locus coeruleus stimulation on evoked hippocampal unit activity. Brain Research 107, 513-25.

Seguela, P., Watkins, K. C., Geffard, M., and Descarries, L. (1990). Noradrenaline axon terminals in adult rat neocortex: an immunocytochemical analysis in serial thin sections. Neuroscience 35, 249-264.

Selden, N. R., Cole, B. J., Everitt, B. J., and Robbins, T. W. (1990). Damage to ceruleo-cortical noradrenergic projections impairs locally cued but enhances spatially cued water maze acquisition. Behavioural Brain Research 39, 29-51.

Sewards, T. V., and Sewards, M. A. (2003). Input and output stations of the entorhinal cortex: superficial vs. deep layers or lateral vs. medial divisions? Brain Research; Brain Research Reviews 42, 243-251.

Shimizu, N., and Imamoto, K. (1970). Fine structure of the locus coeruleus in the rat. Archiv Histologica Japonica 31, 229-246.

Shipley, M. T., Fu, L., Ennis, M., Liu, W. L., and Aston-Jones, G. (1996). Dendrites of locus coeruleus neurons extend preferentially into two pericoerulear zones. Journal of Comparative Neurology 365, 56-68.

Sik, A., Penttonen, M., Buzsaki, G. (1997). Interneurons in the hippocampal dentate gyrus: an in vivo intracellular study.
European Journal of Neuroscience 9, 573-588.

Sirvio, J., Riekkinen, P., Jr., Valjakka, A., Jolkkonen, J., and Riekkinen, P. J. (1991). The effects of noradrenergic neurotoxin, DSP-4, on the performance of young and aged rats in spatial navigation task. Brain Research 563, 297-302.

Sirviö, J., Lukkarinen, K., Riekkinen, P., Jr., Koivisto, E., Virtanen, R., Pennanen, A., Valjakka, A., and Riekkinen, P. J. (1991). The effects of atipamezole, an alpha-2 antagonist, on the performance of young and aged rats in the delayed nonmatching to position task. Pharmacol Biochem Behav 39, 1015-1019.

Sirvio, J., Riekkinen, P., Jr., Ekonsalo, T., Lammintausta, R., and Riekkinen, P. J. (1992). The effects of dexmedetomidine, an alpha 2 agonist, on learning and memory, assessed using passive avoidance and water maze tasks in rats. Neuropharmacology 31, 163-168.

Sirvio, J., Harju, M., Riekkinen, P., Jr., Haapalinna, A., and Riekkinen, P. J. (1992). Comparative effects of alpha-2 receptor agents and THA on the performance of adult and aged rats in the delayed non-matching to position task. Psychopharmacology (Berlin) 109, 127-133.

Sirvio, J., Lahtinen, H., Riekkinen, P., Jr., and Riekkinen, P. J. (1994). Spatial learning and noradrenaline content in the brain and periphery of young and aged rats. Experimental Neurology 125, 312-315.

Skofitsch, G., and Jacobowitz, D. M. (1985). Quantitative distribution of calcitonin gene-related peptide in the rat central nervous system. Peptides 6, 1069-1073.

Smith, G. E. (1896). The fascia dentata. Anatomischer Anzeiger 12, 119-126.

Soriano, E., Del Rio, J. A., Martinez, A., Super, H. (1994). Organization of the embryonic and early postnatal murine hippocampus. I. Immunocytochemical characterization of neuronal populations in the subplate and marginal zone. Journal of Comparative Neurology 342, 571-95.

Staley, K. (1994). The role of an inwardly rectifying chloride conductance in postsynaptic inhibition. Journal of Neurophysiology 72, 273-284.

Stanton, P. K., and Sarvey, J. M. (1984). Blockade of long-term potentiation in rat hippocampal CA1 region by inhibitors of protein synthesis. The Journal of Neuroscience 4, 3080-3088.

Stanton, P. K., and Sarvey, J. M. (1985a). Blockade of norepinephrine-induced long-lasting potentiation in the hippocampal dentate gyrus by an inhibitor of protein synthesis. Brain Research 361, 276-283.

Stanton, P. K., and Sarvey, J. M. (1985b). The effect of high-frequency electrical stimulation and norepinephrine on cyclic AMP levels in normal versus norepinephrine-depleted rat hippocampal slices. Brain Research 358, 343-348.

Stanton, P. K., and Sarvey, J. M. (1985c). Depletion of norepinephrine, but not serotonin, reduces long-term potentiation in the dentate gyrus of rat hippocampal slices. The Journal of Neuroscience 5, 2169-2176.

Stanton, P. K., and Sarvey, J. M. (1987). Norepinephrine regulates long-term potentiation of both the population spike and dendritic EPSP in hippocampal dentate gyrus. Brain Research Bulletin 18, 115-119.

Stanton, P. K., Mody, I., and Heinemann, U. (1989). A role for N-methyl-D-aspartate receptors in norepinephrine-induced long-lasting potentiation in the dentate gyrus. Experimental Brain Research 77, 517-530.

Stephenson, D. T., and Kushner, P. D. (1988). An atlas of a rare neuronal surface antigen in the rat central nervous system. The Journal of Neuroscience 8, 3035-3056.

Sutin, E. L., and Jacobowitz, D. M. (1988). Immunocytochemical localization of peptides and other neurochemicals in the rat laterodorsal tegmental nucleus and adjacent area. Journal of Comparative Neurology 270, 243-270.

Swanson, L. W. (1976). The locus coeruleus: a cytoarchitectonic, Golgi and immunohistochemical study in the albino rat. Brain Research 110, 39-56.

Swanson-Park, J. L., Coussens, C. M., Mason-Parker, S. E., Raymond, C. R., Hargreaves, E. L., Dragunow, M., Cohen, A. S., and Abraham, W. C. (1999). A double dissociation within the hippocampus of dopamine D1/D5 receptor and beta-adrenergic receptor contributions to the persistence of long-term potentiation. Neuroscience 92, 485-497.

Swick, D., Pineda, J. A., Schacher, S., and Foote, S. L. (1994). Locus coeruleus neuronal activity in awake monkeys: relationship to auditory P300-like potentials and spontaneous EEG. Experimental Brain Research 101, 86-92.

Sybirska, E., Davachi, L., and Goldman-Rakic, P. S. (2000). Prominence of direct entorhinal-CA1 pathway activation in sensorimotor and cognitive tasks revealed by 2-dentate gyrus functional mapping in nonhuman primate. The Journal of Neuroscience 20, 5827-5834.

Takayama, N., Iseki, E., Yamamoto, T., and Kosaka, K. (2002). Regional quantitative study of formation process of neurofibrillary tangles in the hippocampus of non-demented elderly brains: comparison with late-onset Alzheimer's disease brains. Neuropathology 22, 147-153.

Takigawa, M., and Mogenson, G. J. (1977). A study of inputs to antidromically identified neurons of the locus coeruleus. Brain Research 135, 217-230.

Talley, E. M., Solorzano, G., Lei, Q., Kim, D., and Bayliss, D. A. (2001). Cns distribution of members of the two-pore-domain (KCNK) potassium channel family. The Journal of Neuroscience 21, 7491-7505.

Tamamaki, N., and Nojyo, Y. (1993). Projection of the entorhinal layer II neurons in the rat as revealed by intracellular pressure-injection of neurobiotin. Hippocampus 3, 471-480.

Tanila, H. (2001). Noradrenergic regulation of hippocampal place cells. Hippocampus 11, 793-808.

Thomas, M. J., Moody T. D., Makihinson M. and O'Dell, T. J. (1996). Activity-dependent β-adrenergic modulation of low frequency stimulation induced LTP in the hippocampal CA1 region. Neuron 17, 475-482.

Tiitinen H., Sinkkonen J., Reinikainen K., Alho K., Lavikainen J., Naatanen R. (1993). Selective attention enhances the auditory 40-Hz transient response in humans. Nature 364, 59-60.

Tiong, A. H., and Richardson, J. S. (1990). The characterization of beta adrenoceptor subtypes in the rat amygdala and hippocampus. Int The Journal of Neuroscience 54, 231-244.

Tomasulo, R. A., and Steward, O. (1996). Homosynaptic and heterosynaptic changes in driving of dentate gyrus interneurons after brief tetanic stimulation in vivo. Hippocampus 6, 62-71.

Traub, R. D., Spruston, N., Soltesz, I., Konnerth, A., Whittington, M. A., and Jefferys, J. G. R.. (1998). Gamma-frequency oscillations: a neuronal population phenomenon, regulated by synaptic and intrinsic cellular processes, and inducing synaptic plasticity. Progress in Neurobiology 55, 563-575.

Umbriaco, D., Garcia, S., Beaulieu, C., and Descarries, L. (1995). Relational features of acetylcholine, noradrenaline, serotonin and GABA axon terminals in the stratum radiatum of adult rat hippocampus (CA1). Hippocampus 5, 605-620.

Usher, M., Cohen, J. D., Servan-Schreiber, D., Rajkowski, J., and Aston-Jones, G. (1999). The role of locus coeruleus in the regulation of cognitive performance. Science 283, 549-554.

Valentino, R. J., Page, M., Van Bockstaele, E., and Aston-Jones, G. (1992). Corticotropin-releasing factor innervation of the locus coeruleus region: distribution of fibres and sources of input. Neuroscience 48, 689-705.

Valjakka, A., Riekkinen, P., Jr., Sirvio, J., Nieminen, S., Airaksinen, M., Miettinen, R., and Riekkinen, P. (1990). The effects of dorsal noradrenergic bundle lesions on spatial learning, locomotor activity, and reaction to novelty. Behavioral and Neural Biology 54, 323-329.

Vanderwolf, C. H. (1969). Hippocampal electrical activity and voluntary movement in the rat. Electroencephalography and Clinical Neurophysiology 26, 401-418.

Vanderwolf C. H., and Leung, L. S. (1982). Effects of entorhinal cingulated, and neocortical lesions on atropine resistant hippocampal RSA. Neuroscience Letters Supplementum 10, 5501.

Vankov, A., Herve-Minvielle, A., and Sara, S. J. (1995). Response to novelty and its rapid habituation in locus coeruleus neurons of the freely exploring rat. The European Journal of Neuroscience 7, 1180-1187.

Wang, J. H., and Kelly, P. T. (1996). The balance between postsynaptic Ca(2+)-dependent protein kinase and phosphatase activities controlling synaptic strength. Learning and Memory 3, 170-181.

Waterhouse, B. D., and Woodward, D. J. (1980) Interaction of norepinephrine with cerebrocortical activity evoked by stimulation of somatosensory afferent pathways in the rat. Experimental Neurology 67, 11-34.

Wenzel, H. J., Buckmaster, P. S., Anderson, N. L., Wenzel, M. E., and Schwartzkroin, P. A. (1997). Ultrastructural localization of neurotransmitter immunoreactivity in mossy cell axons and their synaptic targets in the rat dentate gyrus. Hippocampus 7, 559-570.

Wiebe, S. P., and Staubli, U. V. (2001). Recognition memory correlates of hippocampal theta cells. The Journal of Neuroscience 21, 3955-3967.

Wigstrom, H., and Gustafsson, B. (1983a). Heterosynaptic modulation of homosynaptic long-lasting potentiation in the hippocampal slice. Acta Physiologica Scandinavica 119, 455-458.

Wigstrom, H., and Gustafsson, B. (1983b). Large long-lasting potentiation in the dentate gyrus in vitro during blockade of inhibition. Brain Research 275, 153-158.

Wigstrom, H., and Gustafsson, B. (1983c). Facilitated induction of hippocampal long-lasting potentiation during blockade of inhibition. Nature 301, 603-604.

Wikberg-Matsson, A., Wikberg, J. E., and Uhlen, S. (1995) Identification of drugs subtype-selective for alpha 2A-, alpha 2B-, and alpha2C-adrenoceptors in the pig cerebellum and kidney cortex. European Journal of Pharmacology 284, 271-279.

Wiltgen, B. J., Sanders, M. J., Behne, N. S., and Fanselow, M. S. (2001). Sex differences, context preexposure, and the immediate shock deficit in Pavlovian context conditioning with mice. Behavioral Neuroscience 11, 26-32

Wilson, M. A., and McNaughton, B. L. (1993). Dynamics of the hippocampal ensemble code for space. Science 20, 1055-1058.

Witter, M. P., and Amaral, D. G. (1991). Entorhinal cortex of the monkey: V. Projections to the dentate gyrus, hippocampus, and subicular complex. Journal of Comparative Neurolology 15, 437-459.

Witter, M. P. (1993). Organization of the entorhinal-hippocampal system: a review of current anatomical data. Hippocampus 3, 33-44.

Witter, M. P., Wouterlood, F. G., Naber, P. A., and Van Haeften, T. (2000). Anatomical organization of the parahippocampal-hippocampal network. Annals of the New York Academy of Science 911, 1-24.

Woo, N. H., Abel, T., and Nguyen, P. V. (2002). Genetic and pharmacological demonstration of a role for cyclic AMP-dependent protein kinase-mediated suppression of protein phosphatases in gating the expression of late LTP. The European Journal of Neuroscience 16, 1871-1876.

Wu, K., Canning, K. J., and Leung, L. S. (1998). Functional interconnections between CA3 and the dentate gyrus revealed by current source density analysis. Hippocampus 8, 217-230.

Young, W. S., 3rd, and Kuhar, M. J. (1979). Noradrenergic alpha 1 and alpha 2 receptors: autoradiographic visualization. European Journal of Pharmacology 59, 317-319.

Zappone, C. A., and Sloviter, R. S. (2001). Commissurally projecting inhibitory interneurons of the rat hippocampal dentate gyrus: a colocalization study of neuronal markers and the retrograde tracer Fluoro-gold. Journal of Comparative Neurology 441, 324-344.

Appendix A

*Count-Bursts*

*Count-Bursts* is an awk script written to quantify the number of spikes that occur closely together in time. Input consists of a string of spike timestamps, in 10ths of ms, extracted from the unit cluster using the *Data Editor* function of *Common Processing*. Because the script compiles bursting data for the baseline and post-ejection periods separately, two additional variables are provided at initialization. The first is the time of the ejection in 10ths of ms, and the second is window of time that the script examines (referred to as width). All values reported in this thesis are for 1 minute pre- and post-ejection (600, 000 in the timescale of the script).

The script is called from the command line in the form;
*Count-Bursts* filename period_of_interest time_of_ejection.

The script calculates the range by eject_time ± width. The script next runs the input file through the UNIX utility *dos2unix* to strip/repair non-standard ASCII characters and then calls the function count_bursts for the specified range.

The function count_bursts subtracts the present timestamp from the previous timestamp. If this value is less than or equal to 60 (6 ms), then the counter spikes_this_burst is incremented, and the next timestamp is read. When the value is greater than 60 then the value spikes_this_burst is examined. If this value is less than 1, then the next timestamp is read. If the value is greater than 1, then the value is printed, the spikes_this_burst value is added to the sum counter, the spikes_this_burst counter is reset to 0, the num counter (number of bursts) is incremented, and the next value is read.

At the conclusion of the script the reports the number of bursts (num) and the average spikes per burst (sum/num).

#!/bin/sh

```
count_bursts()
{
gawk '

# given long vector of integers, one per line, THEN
# find instances of two (or more) within 60 (say) units
# of one another. Report first.

BEGIN {
    # inter-spike interval.
    isi=60;
    spikes_this_burst = 0;
    start = 0;
    now = 0;
}

($1 - now) >= isi {
    perhaps_print();

    now = $1;
    start = $1;
    spikes_this_burst = 1;
    next;
}

{
    spikes_this_burst++;
    now = $1;
    next;
}

END {
    perhaps_print();
}

function perhaps_print()
    {
      if (spikes_this_burst > 1) {
          print start " " spikes_this_burst;
          spikes_this_burst = 0;
      }
    }

# awk ends with this apostophe
```

```
'
#function ends
}


find_averages()
{
gawk '
NF >= 2 {
    sum += $2;
    num += 1;
}


END {
    print "num bursts = " num " avg spikes per burst = " sum /
(num+0.00000001)
}
'
}


range()
{
gawk --assign start=$1 --assign upto=$2 '

$1 < start { next }
$1 >= upto { exit }

{print}

'
}


### control


file=$1
width=$2
eject=$3


time1=`expr $eject - $width`
time2=$eject
time3=`expr $eject + $width`


echo $file
echo "    "
echo "=========pre"
cat $file | dos2unix | range $time1 $time2 | count_bursts
echo -n "num events "
cat $file | dos2unix | range $time1 $time2 | wc -l
echo "========="
```

```
cat $file | dos2unix | range $time1 $time2 | count_bursts |
find_averages

echo "=========post"
cat $file | dos2unix | range $time2 $time3 | count_bursts
echo -n "num events "
cat $file | dos2unix | range $time2 $time3 | wc -l
echo "=========="
cat $file | dos2unix | range $time2 $time3 | count_bursts |
find_averages
```

Appendix B.

*Fix-this-mess* is a simple script that bins spike data according to the processing time of the software, rather than the timestamp. The script examines the UFF headers recorded for each event. In the file header of *Workbench* files, spike events are denoted by an initial value of "120", EEG records are denoted by a "98". The exported data file consists of the headers from the final cluster cut written out in ASCII. The script simply examines the initial field of each header, and if the value is 120 increments the unit count (*onetwenties*) and examines the next header. When the value is 98 the script increments the sweep count (*ninetyeights*) and returns the values of *ninetyeights* and *onetwenties*, and zeroes *onetwenties*. The output is then two columns, the first is the data sweep number, and the second is the unit events that were detected during that sweep.

```
BEGIN {
  ninetyeights = 0
  onetwenties = 0
    }

NR==1 {
      print "File" FILEnorepinephrineME
}

NF==1 {
  next
}

$1 == "98," {
  ninetyeights +=  1
  print ninetyeights, onetwenties
  onetwenties = 0
  next
}

$1 == "120," {
  onetwenties +=  1
  next
}
```